The Type-IX Secretion System and Bacterial Outer Membrane Vesicle Biogenesis in Porphyromonas gingivalis

Wang, Sunjun

Awarding institution:
King's College London

The Type-IX Secretion System and Bacterial Outer Membrane Vesicle Biogenesis in *Porphyromonas gingivalis*

Sunjun Wang

Faculty of Dentistry, Oral & Craniofacial Sciences

King's College London

A thesis submitted for the degree of *Doctor of Philosophy* (*Ph.D.*)

September 2022

Declaration

I hereby declare that the results presented in this thesis are generated by my own work except where specifically indicated in the text. The information derived from others has been listed in references.

Sunjun Wang

13/9/2022

Acknowledgements

Firstly, I would like to thank my supervisors Dr. James Garnett and Prof. Mike Curtis for giving me this opportunity to pursue a PhD in their labs. Big thanks to James for his supervision and support for this PhD. With his guidance and support, I have developed my technical lab skills and ability to be an independent researcher. When I faced difficulties in my research, his enthusiasm for scientific research and optimistic attitude always inspired me. Also big thanks to Mike for his supervision and support for this PhD. It was a pleasure to work with such a successful and experienced microbiologist, and his rigorous attitude made a deep impression on me. Mike has been very helpful for my research and always pointed me the right direction when I needed support.

I would like to thank all members in the Garnett lab for assistance with my PhD. I would like to thank Dr. Ben Dorgan for sharing my difficulties in working with the T9SS. We have both worked on the T9SS and he gave me a lot of useful advice for my experiments. I would like to thank Dr. Theo Portlock and Dr. Saima Rehman for giving me knowledgeable suggestions during this project.

I would like to thank all members in the Curtis lab for assistance with my PhD. I would like to give big thanks to Dr. Joe Aduse-Opoku for his support and for sharing his expertise of microbiology. Without Joe's support, my microbiology experiments would not have made so much progress.

I would like to thank Chinese Scholarship Council for the financial support during my PhD.

I would also like to thank my parents for encouraging me to pursue and achieve my aspirations, especially when my life and research were disrupted by the pandemic.

Finally, I would also like to thank everyone supported me during the pandemic. We have never experienced such a tough period, but I believe we will get through this soon.

Covid-19 Impact Statement

Due to the national lockdown and restricted access to laboratories, some research work of the Chapter 4 and Chapter 5 in the thesis was disrupted. Also, some experiments in this thesis were not repeated or not biologically repeated, which are noted in their figure legends.

In the Chapter 4, it was planned to perform MALTI-TOF mass spectrometry for lipid A from the *lpxE* mutant and *lpxE* complements. However, this experiment was disrupted as the MALDI-TOF spectrometer was broken. The repairment for the spectrometer took a long time due to the pandemic and national lockdown. When the MALDI-TOF spectrometer was fixed, I had very limited access to the facility and the technician faced a technical issue to get proper mass of the lipid A samples. For the LpxE co-immunoprecipitation, it was planned to use a more specific tag and more optimizations for this assay were planned. However, because of restricted access to laboratories, these plans were cancelled.

In the Chapter 5, it was planned to express and purify LpxE N-terminal domain using C41 competent cells. It was also planned to express and purify LpxE C-terminal region as an outer membrane protein using pOMPA28 vector. However, these plans were also cancelled due to restricted access to laboratories.

Abstract

Porphyromonas gingivalis is a keystone pathogen of chronic periodontitis. It utilizes the type- IX secretion system (T9SS) to transport cargo proteins (e.g., gingipains) from the periplasm to the outer leaflet of the outer membrane. The secreted proteins can also be delivered long distances via blebbing of outer membrane vesicles (OMVs). However, the functions of T9SS accessory proteins and the mechanism of OMV formation are poorly understood.

In this study, *porU*, *porQ*, *porZ*, *porT*, *porP*, *porG* and *porF* knock-out mutants were created in *P. gingivalis* W50. Electron microscopy results show these mutants produced irregular OMVs compared to W50. MALDI-TOF mass spectrometry of lipid A suggest that W50 possessed phosphorylated and non-phosphorylated lipid A, whereas non-phosphorylated lipid A was absent in all the T9SS mutants. These phenotypes are similar to a *P. gingivalis* lipid A 1-phosphatase *lpxE* mutant, and an interplay between the T9SS and LpxE is therefore proposed.

Sequence alignments show that *P. gingivalis* LpxE is a novel lipid A 1-phosphatase, as it possesses a signal peptide, an N-terminus extension, and an additional C-terminal region (CTR). Electron microscopy and NanoSight data indicate that LpxE is required for normal OMV production. In addition, detergent and antimicrobial peptide inhibition assays suggest that LpxE is required for destabilizing bacteria membrane. Membrane localization data suggest that LpxE may be targeted to the bacterial outer membrane, which would be the first time this localization has been observed for lipid A 1-

phosphatase and may be essential for integrations with the T9SS. Using AlphaFold2, the LpxE CTR was predicted to be a β-barrel domain, which implies that the CTR could interact with one or more secreted T9SS substrate or T9SS outer membrane components. Taken together, I speculate a novel mechanism that the T9SS or one of its secreted substrates may directly regulate the activity of LpxE via interaction with LpxE CTR. The presence of LpxE can result in production of non-phosphorylated lipid A, which is essential to facilitate OMV formation in *P. gingivalis*.

Table of Contents

List of Figures

List of Tables

List of Abbreviations

Å	Angstrom
ABC	ATP-binding cassette
AMP	Antimicrobial peptide
APS	Anionic polysaccharide
Arg	Arginine
BHI	Brain heart infusion
BLAST	Basic local alignment search tool
BAM	β-barrel assembly machine
bp	Base pairs
CD	Catalytic domain
C_8E_4	Tetraethylene glycol monooctyl ether
CFU	Colony forming unit
CMBT	5-chloro-2-mercaptoben-zothiazole
Co-IP	Co-immunoprecipitation
CP	Cytoplasm
CPS	Capsular polysaccharide
Cryo-EM	Cryogenic electron microscopy
CTD	Carboxy-terminal domain
CTR	Carboxy-terminal region
CU	Chaperone-usher

Cys	Cysteine
DAB	3,3’-diaminobenzidine
DDM	n-dodecyl-β-D maltopyranoside
DMS	Dimethyl suberimidate
DNA	Deoxyribonucleic acid
DSP	Dithiobis (succinimidyl propionate)
DTT	Dithiothreitol
E. coli	*Escherichia coli*
ECL	Enhanced chemiluminescence
EDSL	Electron dense surface layer
EDTA	Ethylene diamine tetraacetic acid
EK	Enterokinase
EPB	Electroporation buffer
EV	Extracellular vesicle
FTLA	Finite track length adjustment
Gal	Galactose
GalNAc	N-acetylgalactosamine
Glc	Glucose
GRAVY	Grand average of hydropathicity
GST	Glutathione S-transferase
GuHCl	Guanidinium chloride
HA	Hemagglutinin/adhesion

HA-tag	Human influenza hemagglutinin-tag
HBP35	Hemin-binding protein 35
lDDT	Local distance difference test
IFN-γ	Gamma-interferon
IgSF	Immunoglobulin-superfamily fold
IL	Interleukin
IM	Inner membrane
IPTG	Isopropyl-β-D-1-thiogalactopyranoside
kb	Kilobase
kDa	Kilodalton
Kgp	Lysine-specific gingipain
LB	Lysogeny broth
LDAO	Lauryldimethylamine oxide
LOS	Lipooligosaccharide
LPS	Lipopolysaccharide
Lpt	Lipopolysaccharide transport
Lpp	Braun's lipoprotein
Lys	Lysine
MALDI-TOF MS	Matrix-assisted laser desorption ionization time-of-flight mass spectrometry
m*/*z	Mass-to-charge ratio
MW	Molecular weight

NHS	N-hydroxy succinimide
Ni-NTA	Nickel-nitrilotriacetic acid
NTA	Nanoparticle tracking analysis
NTD	Amino-terminal domain
NTP	N-terminal prodomain
OD	Optical density
OG	Octyl-β-D-glucoside
OMV	Outer membrane vesicle
OPS	O-polysaccharid
ORF	Open reading frame
PAD	Peptidylarginine deiminase
PPAD	*P. gingivalis* peptidylarginine deiminase
PAE	Predicted aligned error
PAMP	Pathogen associated molecular pattern
PAP2	Type-2 phosphatidic acid phosphatase
PCR	Polymerase chain reaction
P. gingivalis	*Porphyromonas gingivalis*
PMF	Protonmotive force
POTRA	Polypeptide transport-associated
PP	Periplasm
PPI	Peptidyl-prolyl cis-trans isomerase
P-pentaacyl	Phosphorylated penta-acylated

P-tetraacyl	Phosphorylated tetra-acylated
qPCR	Quantitative real-time PCR
RA	Rheumatoid arthritis
Rgp	Arginine-specific gingipain
Rha	Rhamnose
SDS	Sodium dodecyl sulfate
SDS-PAGE	Sodium dodecyl sulphate-polyacrylamide gel electrophoresis
S-layer	Surface layer
SMA	Styrene maleic acid
SMALP	Styrene maleic acid lipid particle
SP	Signal peptide
SUMO	Small ubiquitin-related modifier
T1SS	Type-I secretion system
T2SS	Type-II secretion system
T3SS	Type-III secretion system
T4SS	Type-IV secretion system
T5SS	Type-V secretion system
T6SS	Type-VI secretion system
T7SS	Type-VII secretion system
T8SS	Type-VIII secretion system
T9SS	Type-IX secretion system

T10SS	Type-X secretion system
T11SS	Type-XI secretion system
TCS	Two-component system
TEM	Transmission electron microscope
TMH	Transmembrane helix
TLR	Toll-like receptor
TLR2	Toll-like receptor 2
TLR4	Toll-like receptor 4
TPR	Tetratricopeptide repeat

Chapter 1 Introduction

1.1 Periodontal disease

Periodontal disease is highly widespread and can affect up to 90% of the worldwide population[1]. Periodontal disease, also known as gum disease, is an inflammatory process which affects the tissues around the teeth. In the early-stage of gingivitis, the gums become swollen, red, and may bleed (**Figure 1.1A, B**). Gingivitis is the mildest form of periodontal disease, which is very prevalent and easily reversed by simple and effective oral hygiene. Inflammation extending deep into the periodontal tissues and causing loss of supporting connective tissue and alveolar bone, is defined as periodontitis (**Figure 1.1C**). Periodontitis causes the formation of soft tissue pockets or deepened gaps between the gingiva and tooth root. Severe periodontitis can lead to loosening of teeth, pain and discomfort, impaired chewing, and tooth loss[2].

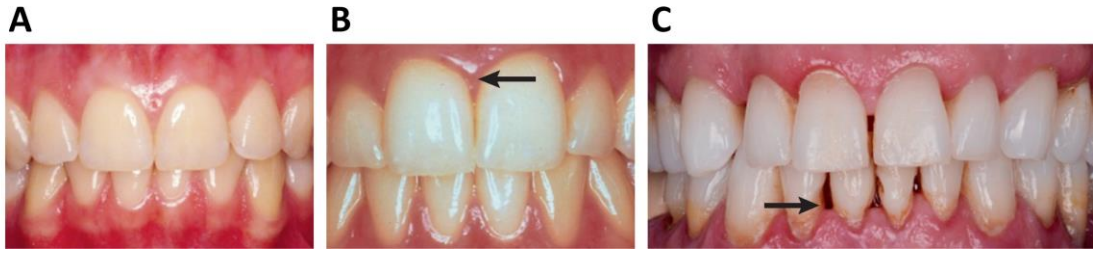

Figure 1.1: Healthy and diseased periodontium. A. Healthy periodontal tissues. **B.** Early gingival inflammation (gingivitis; arrow) can be seen in the gingiva between the central incisor teeth. **C.** Clinical appearance of chronic periodontitis, with tissue loss and deep periodontal 'pockets' that are a hallmark of disease (arrow). This figure was adapted[3].

Many risk factors have been identified that promote periodontal diseases, including smoking[4], diabetes[5], stress[6], genetic predispositions[7] and underlying systemic conditions such as AIDS[8]. In addition, periodontal diseases are also associated with preterm birth[9], cardiovascular disease[10], diabetes[11], arthritis[12] and Alzheimer's disease[13].

However, links between periodontal disease and poor pregnancy outcomes, still needs to be convincingly confirmed and may be instead linked by shared risk factors[14]. Periodontal disease has also been thought to be associated with cardiovascular disease and arthritis, but these associations might again be explained by shared risk factors and comorbidity, rather than direct causality[3]. Nonetheless, strong evidence from longitudinal studies links periodontal disease with diabetes in a two-way relationship, suggesting that chronic periodontitis worsens diabetes and vice versa[5]. Both diseases are thought to adversely influence the patient's metabolic balance and overall inflammatory burden[5]. Based on many studies, it has also been concluded that periodontal disease, through its inflammatory and bacterial burdens, could be a biologically plausible risk factor for Alzheimer's disease[15]. Clinical evidence supports these relationships, but the strength of evidence is still not sufficient to prove causality[16].

Periodontal disease is broadly caused by bacteria in the mouth causing deregulated inflammation in the tissue surrounding the teeth. Biofilm is a thin but robust mucilage adhering to a solid surface and containing a community of bacteria and other micro-organisms. Dental plaque is a microbial biofilm and up to 800 different species have been identified in human dental plaque to date[17]. As dental plaque or biofilm accumulates on the teeth near and below the gums, an inflammatory response develops which in some instances can lead to a change to the microbial population structure of the normal, symbiotic oral microbiome leading to an altered dysbiotic composition with increased pathogenic potential[3]. Chronic gingivitis and chronic periodontitis is then caused and sustained by microbes in the dental plaque[18].

The development of periodontal disease is not caused by a single pathogenic microorganism but by the disordered oral microbiota. Colonization by keystone pathogens (for example, *Porphyromonas gingivalis*) results in impaired innate host defence and promotion of inflammation by subverting complement-Toll-like receptor (TLR) crosstalk in neutrophils and other myeloid cells[19,20,21]. These changes contribute to the emergence of dysbiosis that means quantitative and compositional changes in the periodontal microbiota[19]. Inflammation appears to be an important ecological change that can drive the outgrowth of pathogenic microorganisms through tissue destruction that releases nutrients such as degraded collagen and haem-containing compounds, which are sources of amino acids and iron, respectively[22,23]. These nutrients can be carried via the inflammatory exudate into the gingival crevice to foster the growth of subgingival proteolytic and asaccharolytic bacteria with iron-acquisition ability[24]. In contrast, health-associated species cannot reside in the new environmental conditions and are outcompeted. This imbalance drives dysbiosis, which further worsens inflammation, resulting in periodontitis in susceptible individuals. Alterations in host immune response or diet can affect the oral microbiota composition and the production of virulence factors[24]. Environmental factors such as pH, redox potential and nutrient availability also drive the selection and enrichment of specific pathogenic bacteria[25,26].

1.2 Pathogenesis of *Porphyromonas gingivalis*

Periodontitis results from the interaction between pathogenic microorganisms from the

subgingival biofilms on the tooth surface and an abnormal host response in the periodontal tissues[27]. Extensive microbial compositional analysis has identified potential pathogens which are associated with periodontitis, designated the red complex[28]. The red-complex bacteria *Porphyromonas gingivalis*, *Tannerella forsythia*, and *Treponema denticola*, can disrupt periodontal innate defence functions[18]. The presence of these potential pathogenic species does not directly lead to the development of pathological states, but can switch healthy oral biofilms to pro-inflammatory biofilms[29].

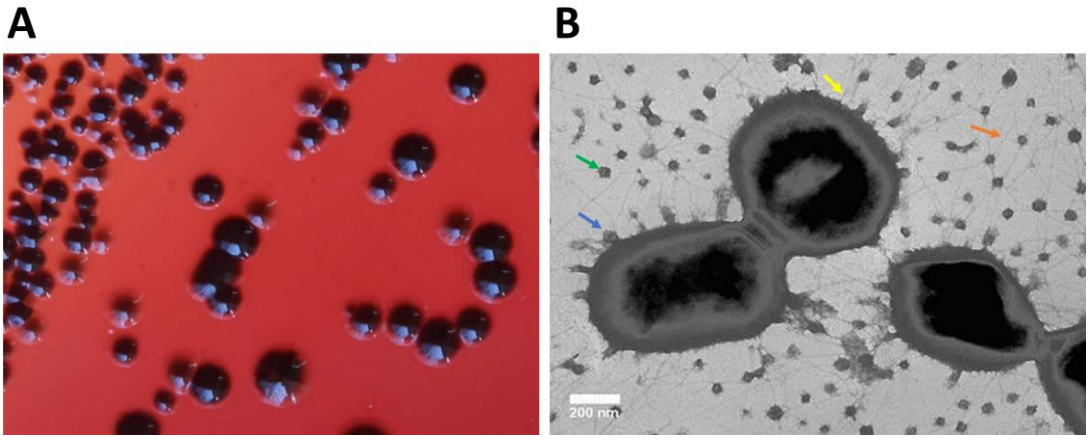

Figure 1.2: *Porphyromonas gingivalis*. A. Colony morphology of *P. gingivalis*. The colonies form black pigmentation on blood agar plate. **B.** Electron microscope image of *P. gingivalis* cells. Bacteria cells form many tiny outer membrane vesicles (OMVs) and filaments named fimbriae surrounding cells or in the milieu. Green arrow: OMV in milieu. Blue arrow: blebbing OMV. Orange arrow: fimbriae attached to the cell. Yellow arrow: fimbriae in milieu. This figure was adapted[30].

P. gingivalis is among the most extensively studied anaerobic bacterial pathogens that contribute to periodontitis, and is thought to play an important role in the pathogenesis of the disease[31]. *P. gingivalis* belongs to the phylum *Bacteroidota* and is a Gram-negative, anaerobic, non-motile bacillus[32] (**Figure 1.2**). In contrast to other members of the genus *Porphyromonas*, many of which can grow on complex carbohydrates, *P.*

gingivalis is asaccharolytic and dependent on nitrogenous substrates such as proteins or peptides as nutrients[33,34]. In order to meet nutritional requirements, *P. gingivalis* is able to produce a large number of proteinases to degrade proteins from the host or other microorganisms[32,35]. These degraded oligopeptides are then acquired by the essential RagAB transport system, and imported into *P. gingivalis* for utilisation[36].

P. gingivalis also relies on exogenous heme for growth because of the lack of a heme biosynthesis pathway[37,38]. *P. gingivalis* is mainly found in bleeding chronic periodontal lesions, as hemoglobin from lysed erythrocytes provides a very convenient and abundant heme source. When growing on blood agar plates, *P. gingivalis* initially presents as white to beige colonies, but these then turn dark red to black after 6-10 days[33]. This black pigmentation has been identified as an accumulation of iron (III) protoporphyrin IX in the form of the μ-oxo dimer $[Fe(III)PPIX]_2O$ on the bacterial cell surface[39].

1.2.1 *P. gingivalis* is keystone pathogen

In recent years, a keystone-pathogen hypothesis has suggested that certain low-abundance microbial pathogens can modulate inflammatory disease by remodelling a normally benign microbiota into a disordered condition[29]. Early bacteriological studies revealed significant differences in the composition of the periodontal microbiota in health versus in disease[40]. *P. gingivalis* may not act directly as a pro-inflammatory bacterium, but it has evolved sophisticated strategies to evade or destroy components

of the host immune system (e.g., Toll-like receptors (TLRs) and complement)[18,41,42]. This evidence supports the keystone-pathogen hypothesis. Accordingly, it was hypothesized that *P. gingivalis* impairs innate immunity by altering the growth and development of the entire biofilm, leading to a destructive change of the homeostatic host-microbiota interaction in the periodontal tissue[29].

The keystone hypothesis is supported by mice model studies where even at very low colonisation levels, *P. gingivalis* can remarkably alter the composition of the periodontal biofilm to cause periodontitis[19]. In addition, colonization of germ-free mice with *P. gingivalis* alone did not lead to the development of periodontitis, suggesting the necessity of commensal microbes in pathogenesis. This hypothesis is consistent with observations that there is low abundance of *P. gingivalis* in periodontitis patients[40,43,44], but the prevalence and association with periodontitis pathogenesis are very high[45,46].

1.2.2 Virulence factors of *P. gingivalis*

The major virulence factors utilized by *P. gingivalis* have been identified and characterized (**Figure 1.3** and **Table 1.1**), including fimbriae, capsule, outer membrane vesicles (OMVs), lipopolysaccharide (LPS), toxic metabolites and proteases[32,34]. *P. gingivalis* is unusual compared with other pathogenic bacteria as it can accumulate cell-surface heme and produce black pigmented colonies, when cultured on blood agar plates. This heme is obtained by degradation of host proteins (e.g., hemoglobin), by lysine-specific (Kgp) and arginine-specific (Rgp) gingipains, which is then captured by

heme-binding proteins such as hemin-binding protein 35 (HBP35)[47]. HBP35 plays an important role in heme acquisition[48]. Besides, HBP35 facilitates binding of *P. gingivalis* to erythrocytes and host epithelial gingival cells[49]. Gingipains and HBP35 are secreted by the type-IX secretion system (T9SS) which is the major determinant of *P. gingivalis* pathogenesis[50]. Additionally, *P. gingivalis* produces other virulence factors such as LPS, capsule and fimbriae. They can perturb host cells, allowing *P. gingivalis* to invade cells and tissues and escaping the immune surveillance (**Figure 1.3** and **Table 1.1**). Once *P. gingivalis* enters the cell, it secretes an ATP-hydrolase enzyme which prevents ATP-dependent apoptosis, contributing its survival into the host[51]. Among the common laboratory strains and clinical isolates of *P. gingivalis*, strains W50, W83 and W12 are found to be more virulent than strains 381, HG66 and ATCC33277[52].

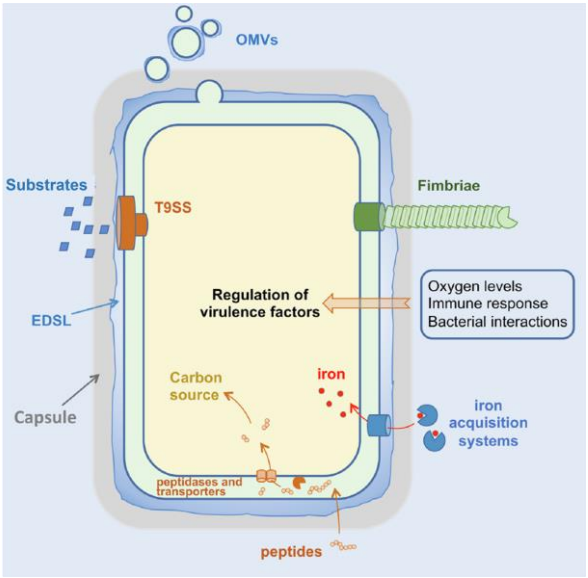

Figure 1.3: Major virulence factors of *P. gingivalis*. Schematic representation of a *P. gingivalis* cell (yellow: cytoplasm, green: periplasm, blue lines: inner and outer membranes). The cell is surrounded by an electron dense surface layer (EDSL, blue) made of gingipains anchored to the cell surface, and by the capsule (grey). Gingipains and other substrates (blue lozenges) are secreted by the type-IX secretion system (T9SS, orange). Other virulence factors include fimbriae (green), outer membrane vesicles (OMVs, blue). Mechanisms of acquisition of essential elements: iron (red circles), acquisition systems (blue), and di- and tri- peptides (peptidases and RagAB oligopeptide transporters, orange) that serve as carbon sources. This figure was adapted[53].

Table 1.1: Major virulence factors of *P. gingivalis*[53].

Virulence factor	Functions
Capsule	– Protection against environmental aggressors
	– Protection against host complement
Fimbriae (Type-V and Mfa pili)	– Adhesion to host cells
	– Bacterial aggregation and biofilms
Lipopolysaccharides	– Protection against detergents and antibiotics
	– Triggers host inflammatory signalling pathways
T9SS	– Virulence factor export
Gingipains	– Degradation of host proteins
	– Processing of fimbriae subunits
Peptidylarginine deiminase (PAD)	– Citrullination of host proteins
OMVs	– Toxin delivery and transport

Capsule

Most strains of *P. gingivalis* are known to produce a capsule that surrounds the cell and shields surface components from the host (**Figure 1.3** and **Table 1.1**). This barrier protects the bacterium from aggressions and killing by the host, and hence encapsulated strains are more virulent in a mouse model of infection[54,55]. The capsule of *P. gingivalis* is mainly composed of capsular polysaccharide (CPS) which protects cells from engulfment by eukaryotic cells, such as macrophages[55]. CPSs are highly hydrated molecules[56] and they are often linked to the cell surface of the bacterium via covalent

attachments to either phospholipid or lipid A molecules, although some CPS may be associated with the cell in the absence of a membrane anchor[57,58].

Fimbriae

Fimbriae are a series of adhesive hair-like structures on the cell surface of bacteria (**Figure 1.3**). In pathogenic species, fimbriae are often crucial virulence factors, which are involved in attachment and invasion of target cells, evasion of the host immune system, and biofilm formation[59]. *P. gingivalis* produces short (Mfa pili) and long (Type-V pili) fimbriae. Due to their adhesive properties, these fimbriae participate in the formation of multispecies biofilms, colonization of host cells, and development of periodontitis[60,61]. Type V pili are composed of the major FimA fimbrillin. FimA are first transported to the cell surface as lipoproteins, which are then hydrolysed by the RgpB gingipain before being polymerized into fimbria structures by a strand exchange mechanism[62,63]. In addition to promoting adhesion to host tissues, Type-V pili bind α5β1-integrins[64] and inhibit the Toll-like receptor (TLR)-mediated proinflammatory response[65], which allows *P. gingivalis* to invade host cells. Besides, Type-V pili can mediate coaggregation with other oral pathogens such as *T. denticola*, *Streptococcus oralis* and *Streptococcus gordonii*[64,66]. Similar to Type V pili FimA, Mfa1 which is the major fimbrillin of the Mfa short pili, is also processed by gingipains before being polymerized[67].

Gingipains

Gingipains are cysteine proteinases that belong to the peptidase family C25[68], and represent the major virulence factors of *P. gingivalis*[69]. In *P. gingivalis*, there are three types of gingipains: lysine-specific gingipain (Kgp), arginine-specific gingipain A (RgpA) and arginine-specific gingipain B (RgpB)[70]. Gingipains are abundantly expressed and after translocation across both the inner membrane and outer membrane, gingipains are attached on the bacterial cell surface or secreted into the extracellular milieu[71].

Gingipains share a similar multidomain organization (**Figure 1.4**): from N- to C-terminus, the signal peptide is followed by a prodomain that functions as a chaperone and maintains the protease in an inactive state to prevent cleavage of cellular proteins[72], a catalytic domain, an immunoglobulin-superfamily fold (IgSF), and a globular C-terminal domain (CTD) involved in gingipain secretion[73]. Additionally, RgpA and Kgp have several copies of hemagglutinin/adhesion (HA) domains located between the IgSF and CTD domains[71,74]. Gingipains are involved in the erosion of periodontal tissues and the degradation of iron-binding proteins. To disrupt the epithelial barrier function and allow *P. gingivalis* to penetrate into subepithelial tissues, gingipains can target important extracellular matrix components, such as tight-junction associated protein JAM1[75]. Furthermore, via cleaving T-cell surface proteins such as CD4 and CD8[76], the IL-6, IL-8, IL-12 cytokines[77] and the gamma-interferon (IFN-γ)[78], gingipains interfere with the host immune response and hence promote evasion of host defence.

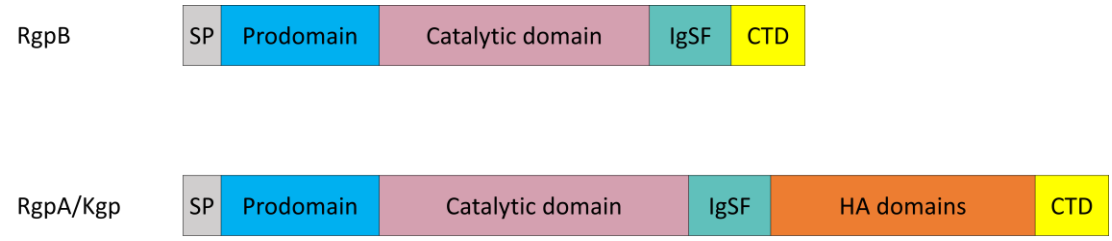

Figure 1.4: Schematic diagram of the gingipain domain structures. All three gingipains possess a Sec signal peptide (SP), pro-peptide (prodomain), catalytic domain, immunoglobulin-superfamily fold (lgSF) and C-terminal domain. RgpA and Kgp also possess hemagglutinin/adhesin (HA) domains which are extensively processed by autolytic cleavage. Regions of sequence conservation are given the same colouring.

Peptidylarginine deiminase

Peptidylarginine deiminase (PAD) is an enzyme involved in the citrullination of proteins, which is only produced and secreted by members of the *Porphyromonas* genus[79]. Citrullination is an enzymatic reaction that converts arginine to citrulline, a neutral, non-natural amino acid. By neutralizing positively-charged residues, this post-translational modification increases the overall hydrophobicity of target proteins and results in protein unfolding and dysfunction[80]. Citrullinated proteins are targeted by the immune system, and lead to autoimmune diseases such as rheumatoid arthritis (RA). In fact, a relation between the development of RA and severe periodontitis was noticed[81] and further results indicated that *Porphyromonas* PAD (PPAD) is a key factor in the development of periodontitis and RA in mice[82].

The other major virulence factors including the LPS, T9SS and OMVs, will be clarified in detail in the following sections.

1.3 Lipopolysaccharide

LPS is the major macromolecule on the outer leaflet of Gram-negative bacteria (**Figure 1.5**). The cell envelope of gram-negative bacteria consists of an outer membrane (OM), an inner membrane (IM) and a periplasmic space. Each membrane is a lipid bilayer consisting of two leaflets. Both leaflets of the IM are composed of phospholipids. The OM is an asymmetric bilayer that consists of phospholipids on the inner leaflet and LPS on the outer leaflet. LPS is essential to the bacterium for maintaining its structural integrity, as well as establishing a selective permeability barrier that limits entry of hydrophobic molecules and toxic chemicals such as detergents and antibiotics[83]. Also, LPS is required for the proper folding and insertion of many OM proteins. Due to many important functions, LPS is essential for the survival of all Gram-negative bacteria[84].

LPS is composed of three domains: lipid A; a core oligosaccharide; and a long polysaccharide chain named O-antigen (**Figure 1.5**). Lipid A is the innermost component of LPS and is conserved in structure. O-antigen is the outermost component of LPS and forms the external surface of bacteria. The structure of O-antigen is highly variable and immunogenic[85]. In *P. gingivalis*, two forms of LPS, O-LPS and A-LPS have been identified. The O-antigen of O-LPS is neutral O-polysaccharide (OPS) and the O-antigen of A-LPS is anionic polysaccharide (APS)[86]. Although the structure of the O-antigen has not been elucidated, both O-LPS and A-LPS consist of the same lipid A and core oligosaccharides[87,88,89]. The structure of OPS has been found to possess tetrasaccharide units of N-acetylgalactosamine (GalNAc), rhamnose (Rha), glucose (Glc) and galactose (Gal)[90], while APS units are formed of branched phosphomannan

containing eight mannose sugars[91]. Only A-LPS has been found to be involved in the attachment of T9SS substrates to the cell surface. However, the biosynthesis mechanisms of O-LPS and A-LPS are not clear.

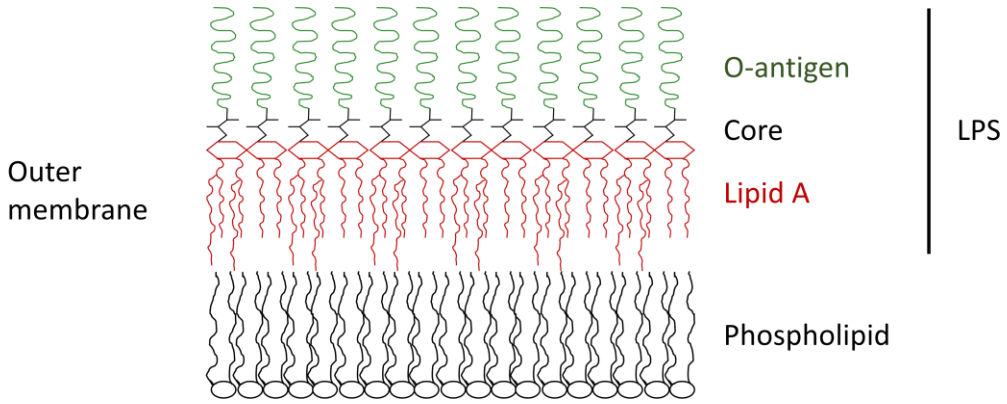

Figure 1.5: Schematic of Gram-negative bacteria outer membrane. Lipopolysaccharide (LPS) forms the outer leaflet of the outer membrane. It is composed of three domains, namely the lipid A anchor (red), the core oligosaccharide (black) and the outermost O-antigen (green), which is variable in structure and immunogenic.

1.3.1 Pathogenicity of *P. gingivalis* LPS

In hosts, LPS results in a strong innate immune response in a tissue or cell specific manner[92]. This was found in bone, epithelial cell barrier breakdown, and keratinocytes[93,94]. Lipid A, also named endotoxin, is the bioactive region of LPS and is recognized by the innate immune system[95]. Lipid A from either commensal *Escherichia coli* (*E. coli*) or pathogenic *E. coli*, is highly immunostimulatory even at a low concentration. Immune detection of lipid A is extremely sensitive since a bloodstream infection can lead to a severe complication called endotoxic shock. This is a major clinical issue that results in around 200,000 deaths in the USA every year[96].

LPS can activate a wide range of host immune cells in periodontal tissues, triggering a local immune response, allowing the defence cells to release numerous inflammatory mediators and leading to secondary damage to the periodontal tissue. Regarding pathogenesis, Toll-like receptors (TLRs), as the recognition receptors of pathogen associated molecular patterns (PAMPs)[97], can mediate the inherent immunological reactions of the host to *P. gingivalis*, which plays a vital role during the occurrence and development of periodontitis[98]. LPS of *E. coli* was found to be able to activate the host inflammatory response by stimulating Toll-like receptor 4 (TLR4)[99,100]. However, the TLR activations that triggered by *P. gingivalis* LPS are much more complicated, and the main signalling pathways remains controversial[101]. Some research has shown that TLR4 exerts a dominant function, whereas others suggested that Toll-like receptor 2 (TLR2) is the major receptor[102]. It has been thought that TLR2 is required for alveolar bone loss caused by *P. gingivalis* infection in animal models, as *P. gingivalis* causes the up-regulation of TLR2 expression and pro-inflammatory cytokine production *in vitro*[103]. However, LPS was found to act as an agonist for TLR2 or as an antagonist and/or agonist for TLR4 activation, which leads to further contradiction[104,105,106,107]. Although *P. gingivalis* LPS likely activates TLR2, the difference lies in the form of LPS presented to the host. For instance, the protein-free LPS is unable to activate TLR2, whereas the protein bound LPS on the live bacterium can mediate TLR2 activation via a novel class of lipoprotein lipase-sensitive molecules, which highlights the importance of active infection[108]. In essence, the tightly associated or covalently attached protein to LPS on live *P. gingivalis* contributes to the TLR2 activation[109].

1.3.2 LPS biogenesis in *P. gingivalis*

Bacterial LPS biogenesis has been extensively studied in *E. coli*. More than 100 genes are involved in the biosynthesis of LPS and much is known about the molecular mechanisms of the biosynthetic enzymes[110,111,112]. The lipooligosaccharide (LOS) containing lipid A and core oligosaccharide is synthesized on the cytoplasmic side of the inner membrane and flipped to the periplasmic side by an ATP-binding cassette (ABC) transporter named MsbA[113,114,115,116,117] (**Figure 1.6**). The O-antigen is ligated to the LOS by an O-antigen ligase named WaaL, following its independent synthesis in the cytoplasm and transport to the periplasm[118,119,120,121]. *P. gingivalis* genes have been characterised that produce O-antigen, A-antigen and lipooligosaccharide (LOS) precursors[122] and function as an O-antigen flippase (PorS) and ligase (WaaL) (**Figure 1.6**). Based on sequence homology, several candidate genes also exist for an A-antigen flippase and ligase, but these still need confirming experimentally.

Recent studies have shown that the products of 15 genes *vimA*, *vimE*, *vimF*[123,124], *wbpB*[125], *waaL*[87], *ugdA*, *rfa*[126], *wzy*[88], *gtfB*[127], PGN_0242, PGN_0663[128], *wbaP*, *wzx*, *wzzP*[129] and *porR*, are involved in the biosynthesis of A-LPS. Of these, the *wzy*, *waaL*, *gtfB* and *wzzP* gene products are involved in the biosynthesis of both A-LPS and O-LPS, as mutations in these genes result in immature or semi-mature LPS[88,129,127]. In contrast, *porR*, *vimA*, *vimE*, *wbpB*, *ugdA* and *wbaP* mutants produce O-LPS but lack A-LPS, suggesting that some of these genes may be required for A-LPS synthesis. A-LPS is composed of a LOS and anionic polysaccharide (APS) repeating units that contain phosphorylated branched mannan[87,91]. The APS is predicted to be synthesized by

mannosyltransferases, but the genes encoding the mannosyltransferases have not been identified[91]. Recently, VimF has been found to be one of the proteins necessary for A-LPS biosynthesis, and has been demonstrated to possess galactosyltransferase activity[130]. More recently, a Wbp pathway has been discovered in *P. gingivalis*. The Wbp pathway including four enzymes: WbpA, WbpB, WbpD and PorR, which are essential for A-LPS synthesis[131]. WbaP, GtfC, GtfF, and VimF are predicted to be A-LPS-specific glycosyltransferases[132]. VimA and VimE are reported to be a putative acetyl-coenzyme A transferase and a carbohydrate esterase, respectively. But their roles in A-LPS biosynthesis have not been elucidated[133].

In *E. coli*, seven essential proteins, LptA, LptB, LptC, LptD, LptE, LptF and LptG are required for the transport of LPS from the outer leaflet of the inner membrane (IM) to the outer leaflet of the outer membrane (OM)[134,135,136,137]. The ABC transporter, $LptB_2FG$ complex, in association with LptC, is thought to extract LPS from the IM[138]. The soluble protein LptA mediates the transport of LPS across the aqueous periplasmic compartment[139,140]. Finally, the β-barrel OM protein LptD and the OM lipoprotein LptE form a large translocon in the OM that extracts LPS from LptA and delivers it to the cell surface[141,142]. *P. gingivalis* is likely to possess the general LPS transport (Lpt) pathway as homologues have been identified. It has been found that PGN_1553 contains LptA-, LptC-, or LptD-like domains. PGN_0669, PGN_1512, PGN_0884 and PGN_0260 are the best-matched *P. gingivalis* equivalents of LptB, LptC, LptD and LptE, respectively. PGN_0642 contains LptF- or LptG-like domains[129]. However, only one copy of a Lpt assembly complex has been detected in *P. gingivalis* and this suggests

that this is functional for both the transport of O- and A-LPS[143].

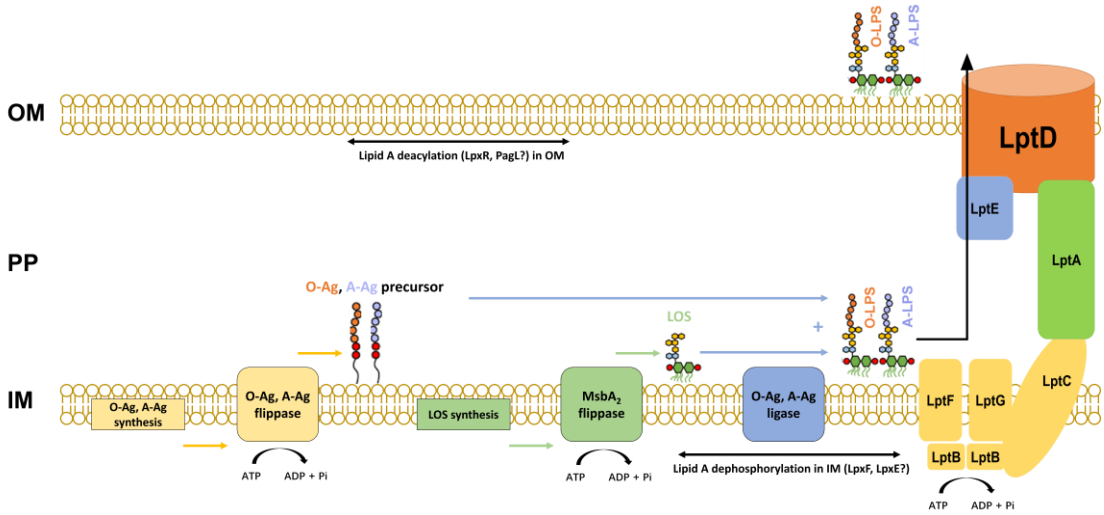

Figure 1.6: Schematic of *P. gingivalis* LPS biogenesis. Synthesis of the lipid A and core domains of LPS occurs in the cytoplasm and at the cytoplasmic interface of the inner membrane (IM). O-antigen is synthesized separately and attached to the carrier lipid. $MsbA_2$ flips lipooligosaccharide (LOS) and O-antigen flippases flip O-antigen precursors across the IM. O-antigen is attached to LOS on the periplasmic (PP) side of the IM. Finally , the Lpt complex transports LPS from the IM to the surface of the outer membrane (OM). This pathway is composed of seven essential proteins: LptA, LptB, LptC, LptD, LptE, LptF and LptG. LPS is extracted from the IM in an ATP-dependent manner by the ABC transporter $LptB_2FG$ and transferred to LptC, which forms a complex with $LptB_2FG$[138]. LptC consists of a single membrane-spanning domain and a large periplasmic domain, which forms a periplasmic bridge with the soluble protein LptA and the N-terminal region of LptD[144]. LPS crosses the aqueous periplasmic space through this protein bridge and reaches the cell surface with the presence of the C-terminal domain of LptD, which forms a β-barrel structure that is plugged by the OM lipoprotein LptE[141,142].

During LOS synthesis bacteria can generate species-specific lipid A structures which differ in their sugars and acyl chains[145]. Further downstream modifications that alter acyl chains, phosphorylation and sugar structure are also common, and function to help bacteria evade host immunity and alter the properties of their OM[145]. For example, some bacteria express the IM localised enzymes LpxE (lipid A 1-phosphatase) and LpxF (lipid A 4'-phosphatase)[146,147] (**Figure 1.6**), which can modify the phosphorylation status of Lipid A. Likewise, if bacteria possess the OM localised β-barrel deacylases

LpxR and PagL[148,149]**,** they can remove the 3'-acyl chains from the first and second glucosamine moiety of lipid A, respectively.

1.3.3 Heterogeneity of lipid A

In *P. gingivalis*, the heterogeneity of A-LPS represents the major virulence factors that promote inflammation and bone loss. The heterogeneous forms of A-LPS interact with the host as pathogen associated molecular patterns (PAMPs) and have been extensively studied for their role in the pathogenesis of periodontitis[97]. As the variant domain of A-LPS, a variety of different lipid A structures have been reported[150,151] (**Figure 1.7**). These lipid A structures are referred as phosphorylated tetra-acylated (P-tetraacyl) and phosphorylated penta-acylated (P-pentaacyl) portions. The tetra-acylated form of LPS has non-P-tetraacyl (*m/z* 1,368) and mono-P-tetraacyl (*m/z* 1,448) species. The penta-acylated form of LPS has non-P-pentaacyl (*m/z* 1,608), mono-P-pentaacyl (*m/z* 1,688) and di-P-pentaacyl (*m/z* 1,768) species[152] (Figure 1.10). It has been demonstrated that *P. gingivalis* uses lipid A 1-phosphatase (LpxE), lipid A 4′-phosphatase (LpxF) and lipid A deacylase (PGN_1123) to generate unique non-phosphorylated lipid A[153,154] (**Figure 1.7**). Although this may appear to be energetically wasteful to add a phosphate group and subsequently remove it, it provides a mechanism to modify the phosphorylation status of lipid A. These non-phosphorylated forms of lipid A can then help *P. gingivalis* evade TLR4 activation and resist killing by cationic antimicrobial peptides[153]. In addition, an additional PagL-like deacylase appears to be present, which creates triacyl

forms of lipid A that were only detected in OMVs[152]. However, this PagL-like deacylase still has not been identified in *P. gingivalis*.

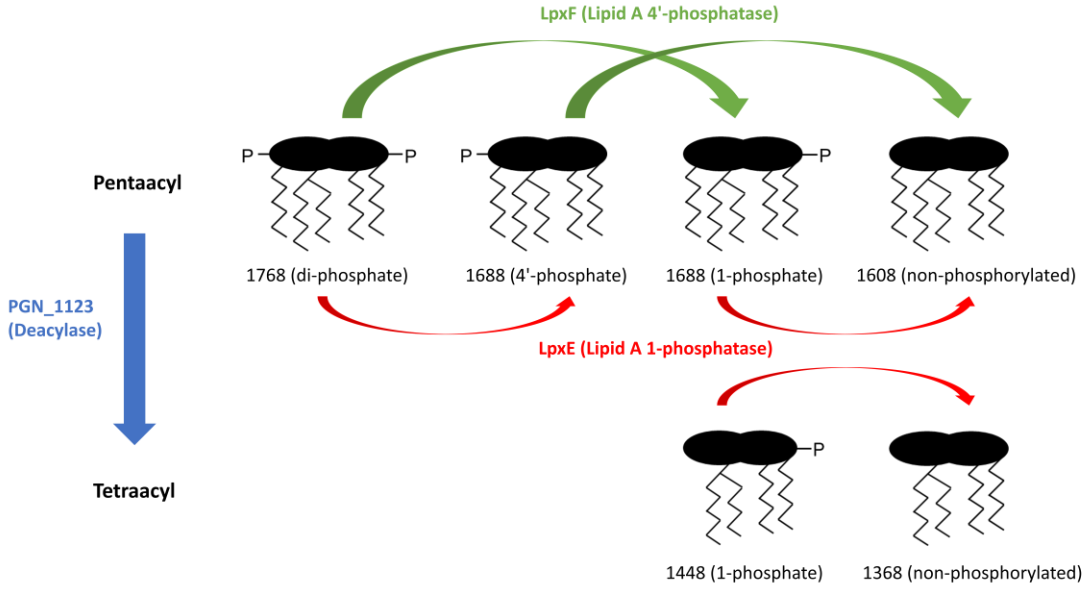

Figure 1.7: The major lipid A structures identified in *P. gingivalis*. The major forms of lipid A were examined by matrix-assisted laser desorption ionization time-of-flight mass spectrometry (MALDI-TOF MS) and MALDI-TOF tandem MS[153]. The arrows suggest the dephosphorylation and deacylation modifications between different lipid A species.

Two studies have suggested that the T9SS outer membrane protein PorV is involved in lipid A modification. The first research only found the penta-acylated forms of mono-phosphorylated lipid A in the *porV* mutant, indicating a specific role of PorV in the O-deacylation of mono-phosphorylated lipid A[155]. However, other research has demonstrated that PorV is required for lipid A dephosphorylation as non-phosphorylated lipid A were absent in *porV* mutant[152]. Although the conclusions are contradictory, both observed that *porV* mutant forms large and abnormal OMVs. And compared with W50, there was a significant reduction of OMV yields in the *porV* mutant[152]. Because the main component of the outer leaflet of OMVs is LPS, there could be a novel mechanism within PorV, lipid A modification and OMV production.

1.4 Type-IX secretion system

To interact with host and environment, bacteria have evolved a wide variety of highly specialized macromolecular transport nanomachines[156] to secrete a wide range of substrates, including small molecules, proteins and DNA from their cytoplasm to extracellular environment. One major category of substrates transported out of the bacteria cell are proteins. To secrete proteins, bacteria have evolved numerous secretion systems[157,158] and several of them have been designated as general secretion systems. Ten such general secretion systems (type-I to type-IX and the chaperone-usher system)[158] have been well studied so far and two more (type-X and type-XI)[159,160] have recently been discovered.

In Gram-negative bacteria, the type-I secretion system (T1SS), type-III secretion system (T3SS), type-IV secretion system (T4SS), and type-VI secretion system (T6SS) are all one-step secretion systems, where the substrate protein is transported directly from the cytoplasm to the extracellular environment, usually in a partially unfolded state[161,162,163,164]. In Gram-negative bacteria, the type-II secretion system (T2SS), type-V secretion system (T5SS), type-VIII secretion system (T8SS), type-IX secretion system (T9SS), and chaperone-usher (CU) system are two-step secretion systems, where a substrate is transported across the IM by the Sec or Tat system into the periplasm and then across the OM by the secretion system machinery[165,166,167,168,169]. The type-VII secretion system (T7SS) has only been identified in Gram-positive but not in Gram-negative bacteria. The type-X secretion system (T10SS) and type-XI secretion system (T11SS) have only been recently described and their mechanisms are

at present unclear[159,160].

Over the last two decades, a novel Gram-negative bacterial secretion system has been discovered in the Fibrobacteres-Chlorobi-Bacteroidota (FCB) superphylum[50]. As this was the ninth protein secretion system to be identified in bacteria, it was named the type-IX secretion system (T9SS)[170,171]. The T9SS has mostly been studied in the oral pathogen *P. gingivalis* and the gliding bacterium *Flavobacterium johnsoniae*. In *P. gingivalis*, the T9SS is an essential determinant of pathogenicity in severe periodontal disease, because many virulence factors (for example, gingipains) are secreted by the T9SS[172].

During transport through the T9SS, a conserved C-terminal domain (CTD) of substrates has been shown to be the secretion signal. In addition, CTD-like sequences have also been observed in other Gram-negative bacteria: *T. forsythia*, *Prevotella intermedia*, and *Parabacteroides distasonis*[173], and T9SS homologs were also found in these species[174]. Moreover, the fish pathogens *Flavobacterium columnare* and *Flavobacterium psychrophilum* also utilize the T9SS to cause columnaris disease and bacterial cold-water disease[175,176]. This evidence implies that T9SSs are present and have diverse functions in *Bacteroidota*.

1.4.1 T9SS architecture

Currently, 22 T9SS protein components have been identified (**Table 1.2**). Deletion of any of these genes causes defects in secretion, highlighted by white pigmentation of *P.*

gingivalis colonies and accumulation of cargo proteins (e.g., gingipains) in the periplasm. Some of these proteins build the core structures in the inner membrane (IM) and outer membrane (OM) of the secretion apparatus, some play regulatory or accessory roles, and others are involved in post-translational modification of cargo proteins (**Figure 1.8**)[172]. However, many aspects of their functions have yet to be discovered, and potentially other components are still to be identified.

Table 1.2: Components of the T9SS in *P. gingivalis*.

W50/W83 Logus Tag	Protein Name	Description	Localization	Interaction	References
PG0026	PorU	Contains uncleaved T9SS CTD; Cargo protein sortase	OM	PorV	177,178,179
PG0027	PorV (LptO)	β-Barrel; PorU anchoring and cargo protein shuttling; Interacts with Sov	OM	PorU; Substrates	152,155,179,180,168
PG0052	PorY	Sensor histidine kinase	IM	PorX	50,181,182
PG0162	SigP	T9SS sigma factor	CP	PorX	181
PG0189	PorG	β-Barrel; Binds to the PorK/N rings	OM	PorK/N	183
PG0192	Omp17	Skp-like chaperone	PP	-	184
PG0287	PorP	β-Barrel	OM	PorE/K/N/; PG1035	50,185
PG0288	PorK	Lipoprotein; Forms ring complex with PorN	PP	PorG/M/N /P/T/W; Sov	50,183,185,186
PG0289	PorL	Pentameric inner membrane protein;	IM	PorM/X	50,183,185,187

		Motor stator			
PG0290	PorM	Dimeric inner membrane protein; Rotor and shaft	IM	PorL/K/N	[50,185,187,188]
PG0291	PorN	Forms ring complex with PorK	PP	PorG/K/M/T/W; Sov	[50,183,185]
PG0534	PorF	β-Barrel; Predicted to be TonB dependent receptor	OM	-	[189]
PG0602	PorQ	β-Barrel; Anchors PorZ to surface	OM	PorZ	[50,179]
PG0751	PorT	β-Barrel	OM	PorK/N	[50,155,190,191]
PG0809	Sov (SprA)	β-Barrel; Translocon	OM	PorK/N/V/W	[168,192,193,194]
PG0928	PorX	Chemotaxis protein	CP	PorL/Y; SigP	[50,181,182,195]
PG1058	PorE	Lipoprotein; Cell wall anchoring	PP	PorP; Peptidoglycan	[196,197]
PG1604	PorZ	β-Propeller; A-LPS attachment	OM	PorQ; A-LPS	[179,109,198]
PG1850	-	Periplasmic protein	PP	PorW	[186,196]
PG1947	PorW	Lipoprotein	PP	Sov; PG1850	[50,199]
PG2092	Plug	Sov channel plug	OM	Sov	[168]
PG2172	PorA	Possesses a floating CTD	OM	PorV; Sov	[186,200]*

OM: outer membrane. PP: periplasm. IM: inner membrane. CP: cytoplasm.

*Original citations for protein identification and key citations with novel data pertaining to protein function, structure and/or interactions are listed.

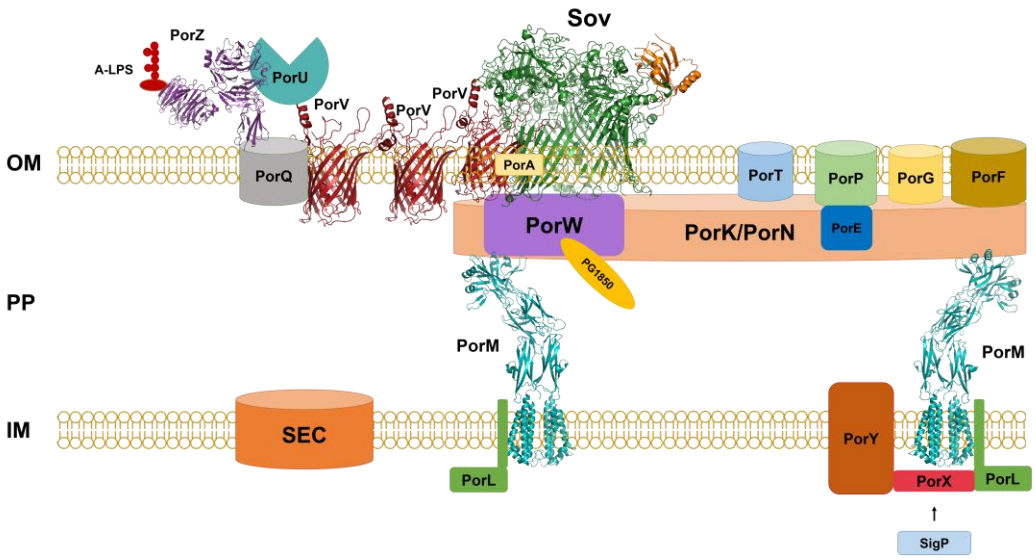

Figure 1.8: Speculative model of the *P. gingivalis* T9SS. The different subunits of the T9SS are shown in different colours, with their localizations. The overall translocon structure and the proteins form a pore in the outer membrane (OM). Interacting proteins are situated in proximity. The known atomic structures of PorM, Sov's homologue SprA, PorV and PorZ are shown. IM protein PorY binds to cytoplasmic protein PorX to form a two-component regulatory system. SigP is a ECF sigma factor that acts on PorX. PorL and PorM form an inner membrane (IM) complex that arrange as a ring structure, composed of 12 copies of a $PorL_5PorM_2$ sub-complex. PorK, PorW, and PorE are lipoproteins anchored into the inner surface of the OM. PorK interacts with PorN to form a large ring which spans both the OM and periplasm (PP). PorP, PorT, PorG, PorF and PorQ are β-barrel proteins that locate in the OM. Structural models are shown for proteins that have an experimentally determined atomic structural model available. The PDB entries (www.rcsb.org) for the structures shown are: SprA-PorV-PPI (6H3I), SprA-Plug-PPI (6H3J), PorZ (5M11) and PorM (6EY0, 6EY5).

Cytoplasmic and inner membrane components of the T9SS

PorX and SigP are the only two known T9SS-related protein residing entirely in the cytoplasm (**Figure 1.8**). PorX and IM protein PorY form a two-component system (TCS) to regulate the expression of several T9SS genes. In this complex, PorX acts as a response regulator and PorY works as a histidine kinase. PorY contains two transmembrane helices (TMHs) and a large cytoplasmic domain[195]. PorXY TCS regulates T9SS-mediated protein secretion via the SigP ECF sigma factor[181].

Two other essential components of the T9SS, PorL and PorM are also located in the IM

(**Figure 1.8**). PorL carries two TMHs and a cytoplasmic domain[185]. PorM is anchored into the IM by a single TMH and presents a large periplasmic C-terminal domain. PorM forms dimers and interacts with PorL via their TMHs, and with PorN in the periplasm[185]. The crystal structures of the periplasmic domains PorM and its homologue GldM from *F. johnsoniae* suggest they are both composed of four domains: an N-terminal α-helical domain, and three Ig-like domains[188,201]. Recently, it has been reported that the PorLM sub-complex acts as motor by converting electrochemical energy into mechanical energy to drive the T9SS[187]. In *F. johnsoniae*, gliding motility is dependent on the protonmotive force (PMF) and a functional GldLM module. It is supposed that electrochemical energy is converted to mechanical movement via the rotation of the GldM TMH, and subsequent conformation changes within the GldM periplasmic domains[187]. Due to sequence and structural conservation between GldLM and PorLM, the T9SS motors more than likely share the same mechanism of action.

Periplasmic components of the T9SS

Six T9SS proteins PorK, PorN, PorW, PorE and PG1850 are in the periplasm (**Figure 1.8**). PorN forms dimers *in vitro* and interacts with IM protein PorM and periplasmic lipoprotein PorK[183,185]. PorK and PorN interact to form a 50 nm diameter ring-shaped complex containing around 32-36 subunits of each protein, and the ring structure is anchored into the OM through the fatty acids of PorK[183]. The trans-envelope core complex PorKLMNP has been discovered and suggests that the PorKLMN proteins assemble a large complex of over 1.2 MDa[185]. PorL and PorM form a ring structure that

is composed of 12 copies of a $PorL_5PorM_2$ sub-complex at the IM which spans the periplasm to interact with the large ~50 nm PorKN ring via the periplasmic portion of PorM[186,202]. The OM barrel protein PorP was also found to form part of this complex by binding to PorK and PorN[185].

PorW is an OM lipoprotein that interacts with the Sov translocon and an unknown T9SS protein PG1850[186]. It is proposed that PorW has the function of linking the PorKN ring to the Sov translocon[186]. The periplasmic lipoprotein PorE was found to interact with PorP and the CTD containing protein PG1035. PorE is predicted to comprise four domains: a tetratricopeptide repeat (TPR) domain, a β-propeller domain, a carboxypeptidase regulatory domain-like fold and an OmpA-like C-terminus peptidoglycan binding domain[196]. The crystal structure of the OmpA-like C-terminus domain has been solved[197]. This structure possesses a protein cleft which is similar to other peptidoglycan binding proteins. As PorE is the only T9SS component that is associated with the peptidoglycan, it has been suggested that PorE may have the role of anchoring the T9SS to the peptidoglycan and acting as a template for the assembly of the translocon[186].

Outer membrane and surface components of the T9SS

The majority of T9SS components are located in the OM (**Figure 1.8**). PorT, PorG, PorP, PorF and PorQ are predicted to be integral OM β-barrel proteins. The structures of Sov's homologue SprA, and PorV have been solved in *F. johnsoniae*. PorU and PorZ, are associated with the bacterial cell surface. Omp17 was thought to contribute to the

processing and modification of CTD cargo proteins [184], it has been therefore proposed to be a molecular chaperone.

PorT and Sov were the first proteins found to be essential for *P. gingivalis* protein secretion, and the discovery led to intense research on T9SS[50,190,192]. The predicted structure of PorT has eight anti-parallel, transmembrane β-strands, with four large loops facing the extracellular environment[191]. Recently, the Sov homologue SprA in *F. johnsoniae* was isolated in complex with a peptidyl-prolyl cis-trans isomerase (PPI), and either PorV or the Fjoh_1759 plug protein that is *P. gingivalis* PG2092's homologue[168]. The role of the PPI is unclear. Cryogenic electron microscopy (Cryo-EM) analyses showed that SprA is a giant 36-strand β-barrel with a lateral opening and a 70-Å internal channel that is large enough to allow the transit of folded substrates (**Figure 1.8**). SprA interacts with PorV or the plug protein to form two states of translocon complexes: SprA-PorV and SprA-plug. Recently, a binding partner of PorV, named PorA, was identified in *P. gingivalis* and proposed to be a component of the translocon complex. However, PorA is absent in most T9SS bacteria, suggesting it might be specific to gingipains[186]. Additionally, PorA was found to be involved in a signalling pathway between the translocon and the PorXY-SigP transcriptional regulatory system[200].

PorG and PorP were detected in association with the PorKLMN complex. Cross-linking experiments showed that a periplasmic loop of PorG interacts with both PorK and PorN. Due to its low abundance, PorG may play an accessory role in secretion[183]. The nature of the interaction of PorP with PorK and PorM is still inconclusive. Although these

proteins co-precipitate *in vitro*, all tested proteins were produced recombinantly in *E. coli* cells. So far, PorP has not been detected in the native complex[185]. Furthermore, PorP binds to a T9SS cargo protein PG1035[186]. As an essential protein for T9SS function, PorF is predicted to be a TonB dependent receptor that is associated with the uptake and transport of large substrates such as iron siderophore complexes and vitamin B12[203]. PorF is also upregulated in human gingival epithelial cells, suggesting it contributes to eukaryotic cell invasion and/or intracellular survival[204].

PorV, also named LptO, is the most studied protein in the T9SS. It is a 14-strand β-barrel OM protein and a member of the fatty acid FadL transporters family[168]. The *porV* mutant strain retains immature, unprocessed gingipains in the periplasm[180]. PorV interacts with PorU *in vivo*, and it was proposed that PorV anchors PorU to the outer membrane[205]. PorU localizes to the surface of *P. gingivalis* cells and utilize a sortase-like mechanism to process T9SS cargo proteins[177,178]. PorV binds to multiple CTD proteins[179] and this has been supported by the Cryo-EM structure of SprA-PorV complex, where a loop on the surface of the PorV barrel penetrates inside of SprA via its lateral opening[168]. It is suggested that this loop mediates recognition of T9SS substrates in the translocon and shuttles them to the attachment complex. Although the function of the cell surface protein PorZ is not well defined, its crystal structure suggests PorZ could bind to anionic lipopolysaccharide (A-LPS)[109]. Recent data demonstrated that PorZ specifically binds to A-LPS and provides PorU with A-LPS[198]. PorQ is also a FadL-like OM β-barrel protein that binds to PorZ[179]. It has been experimentally shown that PorV binds to PorU and PorQ binds to PorZ. PorU, PorV, PorQ and PorZ form a

440 kDa T9SS attachment complex and mass spectrometry suggested the molar ratio of these proteins is 1:3:1:1, respectively[179].

1.4.2 Biogenesis of bacteria outer membrane proteins

After synthesis in the cytoplasm, all the outer membrane (OM) proteins must cross through both the inner membrane (IM) and the periplasmic space before reaching the OM, where folding and insertion takes place. This process is composed of multiple stages (**Figure 1.9**). The nascent β-barrel outer membrane proteins (OMPs) containing an N-terminal signal peptide (SP) are first synthesized in the cytoplasm and then are translocated across the cytoplasmic membrane by the Sec translocon[206], which is a process dependent on ATP and the proton motive force[207]. When entering the periplasm, the N-terminal SP is cleaved off by a signal peptidase[208], and the nascent OMP associates with periplasmic chaperones, such as survival protein A (SurA), seventeen kilodalton protein (Skp) and DegP. Chaperones are generally soluble proteins that prevent unfolded proteins from misfolding or aggregating before they adopt their native state. These chaperones are thought to form two pathways, the SurA pathway and the Skp-DegP pathway, which transport nascent OMPs across the periplasm to the OM[209].

SurA was first identified for its essential role in cell survival during stationary phase. It has then been shown to have general chaperone activity in the biogenesis of OMPs[210] and has been shown to contact BamA directly *in vivo*[209]. SurA has therefore been thought to transport the most of OMPs to the OM. Skp and DegP, have been shown to

compensate for the absence of SurA and may be more important for handling proteins that are not properly folded and inserted into OM[209]. Skp has been shown to bind very tightly to unfolded OMPs[211]. A trimer of Skp was shown to bind and form complexes with various OMPs[212], the formation of which prevents their aggregation[213], suggesting a chaperone role in the periplasm. OMPs which misfold during their transport are thought to be degraded by the protease DegP to prevent aggregation[214].

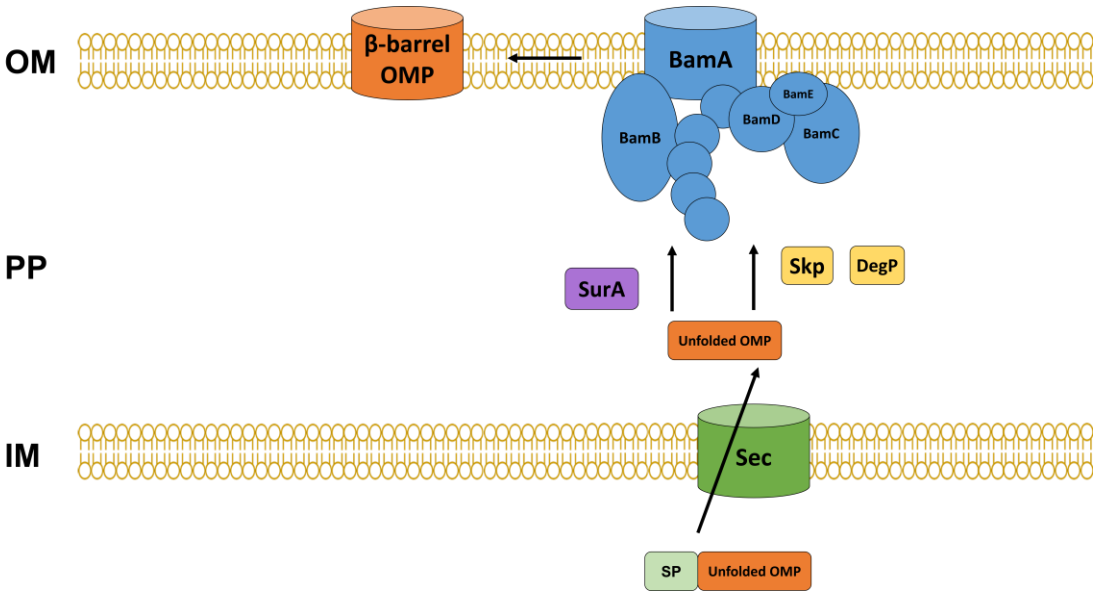

Figure 1.9: Schematic of outer membrane protein biogenesis in *E. coli*. Outer membrane proteins (OMPs) destined for the BAM complex are first targeted to the Sec translocon. Following export through Sec, the nascent OMPs are recruited by two proposed chaperone pathways, the SurA and the Skp-DegP pathway, and are transported through the periplasm to the outer membrane. Unfolded OMPs are thought to be recognized as β-barrels at the OM and are subsequently assembled into their folded structures and inserted into the membrane. IM: Inner membrane; PP: Periplasm; OM: Outer membrane.

Unlike the actively driven Sec translocon, the OM uses the passive β-barrel assembly machine (BAM) complex (**Figure 1.9**). In *E. coli*, the BAM complex is composed of five proteins BamA, BamB, BamC, BamD and BamE[215]. The core of the complex is BamA which belongs to the Omp85 superfamily of OMPs that function as protein translocation or assembly factors[216] and is conserved in all Gram-negative bacteria[217].

BamA has five N-terminal soluble periplasmic polypeptide transport-associated (POTRA) domains and a C-terminal β-barrel transmembrane domain. The POTRA domains act as a scaffold that mediates interaction with four lipoproteins BamB, BamC, BamD, and BamE[218]. Although the folding and insertion mechanism is not clear, unfolded OMPs are thought to be recognized as β-barrels at the OM and are subsequently assembled into their folded structures and inserted into the membrane[219].

1.4.3 Proposed mechanism of secretion

A common feature of all T9SS cargo proteins is the conserved CTD that targets T9SS cargo proteins to the OM translocon and associates with surface proteins. Sequence alignments of proteins identified as T9SS substrates showed that in *F. johnsoniae* there are two families of CTDs, named type-A and type-B CTDs[220]. However, type-A CTD is the main form of T9SS signals in both *F. johnsoniae*[220] and *P. gingivalis*[128].

Type-A CTDs are the most common and have been studied in different *Bacteroidota* species. As deletion of these domains results in accumulation of the substrates in the periplasm, type-A CTDs are necessary for secretion via the T9SS[170]. The structures of type-A CTDs from three *P. gingivalis* T9SS substrates (PorZ, RgpB and HBP35) have been solved and their β-sandwich fold structures are highly conserved[109,221,222]. Sequence alignment of type-A CTDs showed that five motifs (A, B, C, D and E) are conserved and three of them (B, D and E) are highly conserved[173,223]. Motif D (G(I/L/V)Y) and motif E (K(VIL)(VIA)(VI)) are located at the extreme C-terminus,

which have the highest level of conservation and are sufficient for T9SS dependent secretion[173,223,224]. A recent study showed that motif D is required to interact with PorM[225].

Type-B CTDs are not similar in sequence to type-A CTDs, and they have not been studied in detail. In *P. gingivalis*, only one cargo protein PG1035 has been found to possess a type-B CTD[226]. In *F. johnsoniae*, type-B CTDs are quite different in sequence, and there is little know the function of the motifs. Most genes encoding proteins with type-B CTDs are in the same operon with porP/sprF-type genes, suggesting that each type-B CTD interacts with a specific PorP family protein. In *F. johnsoniae*, a fusion protein containing sfGFP and a type-B CTD was not secreted when over-expressed alone, but was secreted when the PorP family protein associated with the type-B CTD was over-expressed at the same time[220,226].

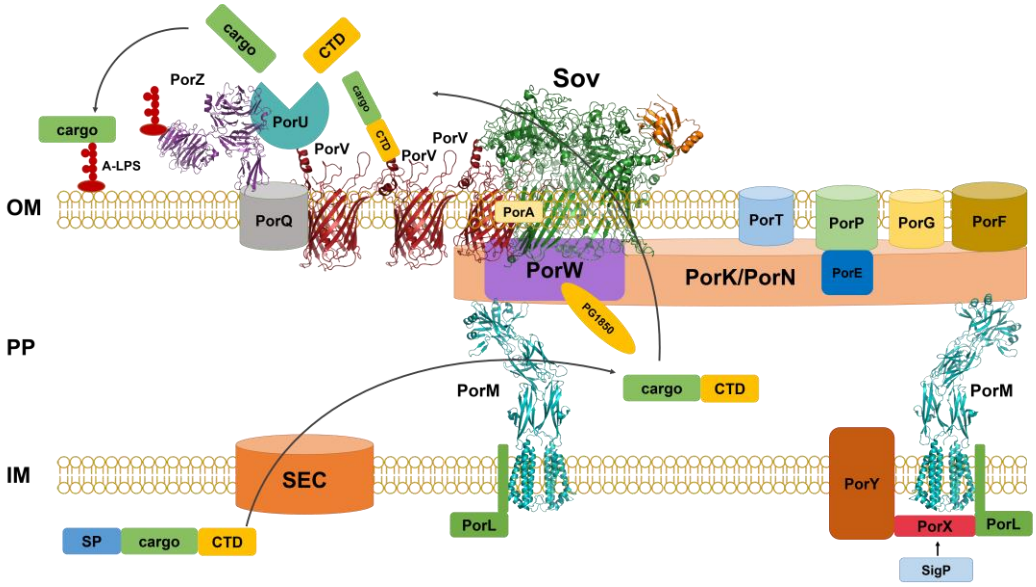

Figure 1.10: Proposed mechanism of secretion. A T9SS cargo protein possesses two sorting signals: N-terminal signal peptide (SP) directing the protein to the general secretion system SecYEG and conserved C-terminal domain (CTD) recognized by T9SS. In inner membrane (IM), Two-component system PorX/PorY is involved in regulation of the system via interaction with the sigma factor SigP and PorL. The PorLM complex is believed to power export of cargo protein across the OM using proton motive force (PMF). In periplasm (PP), The PorKN ring complex forms an anchor for folded cargo

proteins to bind and delivers them to the outer membrane (OM) translocon Sov. The cargo protein is then transferred to PorV which then shuttles the cargo protein to the attachment complex that is comprised of PorV, PorU, PorQ and PorZ. Finally, CTD is cleaved off by PorU sortase and a secreted protein is modified by attachment of A-LPS and anchored to the cell surface. PorE interacts with the PorP in the OM and anchors the system to the peptidoglycan layer. The PDB entries (www.rcsb.org) for the structures shown are: SprA-PorV-PPI (6H3I), SprA-Plug-PPI (6H3J), PorZ (5M11) and PorM (6EY0, 6EY5).

Protein secretion through the T9SS includes at least three steps (**Figure 1.10**). Firstly, the cargo proteins are directed by a general signal peptide (SP) to the Sec machinery in the IM[206]. During translocation, the SP is cleaved off by type I signal peptidase[208], and the cargo is released into the periplasm. Although the Sec pathway has not been experimentally analysed in *P. gingivalis*, genomic analyses confirmed that the system is conserved in *Bacteroidota*[171]. The PorKLMN complex spans both the inner and outer membranes and has been proposed to recognise the CTDs of cargo in the periplasm through interactions with PorM and PorN[225]. A pentamer of PorL generates proton motive force (PMF) across the IM resulting in the rotation of dimeric PorM, which extends across the periplasm[185,187,188,201]. This provides energy to drive cargo secretion and assembly on the bacterial surface, although this precise mechanism is still unclear[183,185,188,227].

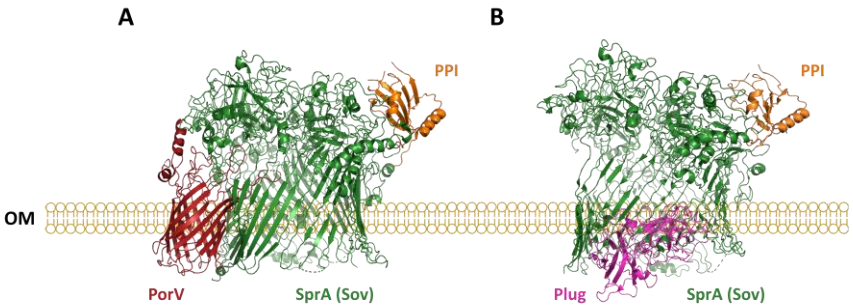

Figure 1.11: Cryo-EM structures of SprA complexes. SprA is the *F. johnsoniae* protein which is a homologue of *P. gingivalis* Sov. **A.** SprA-PorV complex: SprA binds to PorV at the lateral opening. **B.** SprA-Plug complex: SprA binds to the Plug at the periplasmic opening. The PDB entries (www.rcsb.org) for the structures shown are: SprA-PorV-PPI (6H3I) and SprA-Plug-PPI (6H3J).

Next, cargo proteins fold into a stable conformation in the periplasm, and the CTD guides them to the T9SS translocon complex (**Figure 1.10**). This translocation model is thought to be dependent on the transformation between the two states of translocon complexes: SprA-PorV and SprA-Plug (**Figure 1.11**)[168]. In the SprA-PorV complex (**Figure 1.11A**), SprA displays a lateral opening that is filled by a loop of PorV. This loop penetrates inside the lumen of the SprA pore[168]. In the SprA-Plug complex (**Figure 1.11B**), PorV is absent and the lateral opening of SprA is open, but the pore is occluded at the periplasmic entrance by the plug protein[168]. As PorV has been shown to associate with the T9SS substrates on the cell surface[179], it has been suggested that PorV binds to the substrates in the interior of the SprA barrel and triggers the release of substrates from the SprA channel. The Plug protein then binds to SprA on the periplasmic face to seal the channel.

Finally, PorV likely acts as a shuttle protein and delivers cargo proteins to the T9SS attachment complex (PorVUQZ)[179], where a sortase-like reaction leads to removal of

the CTD and simultaneous linkage to A-LPS[198]. The location of the attachment complex is unclear, and it may be inside the T9SS translocon ring or somewhere outside in the OM. In the attachment complex, one or more PorV molecules work as shuttle proteins to transport cargo proteins to PorU. The role of PorQ is to anchor PorZ on the cell surface[179]. PorU is the sortase that is responsible for CTD cleavage[178]. PorZ is a carbohydrate-binding protein and recombinant PorZ specifically binds to A-LPS *in vitro*. Moreover, PorZ provides PorU with A-LPS for cargo modification[198]. The substrates are finally anchored covalently to A-LPS on the cell surface and the CTD signal is released into the culture fluid. These secreted substrates are mainly attached to the surface of the OM, but are also partially released in a soluble form into the extracellular milieu[71,228]. The secreted substrates can also be attached to the surface of OMVs[229].

1.4.4 The T9SS is linked to LPS transport

Two forms of LPS, neutral charged O-LPS and negatively charged A-LPS have been identified in *P. gingivalis*[86]. The evidence used to show that *P. gingivalis* T9SS substrates are modified with LPS, is to detect them with MAb-1B5 antibody in Western blots. The epitope of this monoclonal antibody includes the Manα1-2Manα1-phosphate portion of APS, which confirms T9SS substrates are modified with A-LPS but not O-LPS[91]. In *porV*, *porT* and *porU* mutants, a small amount of MAb-1B5-reactive material accumulates in the periplasm but is not attached to T9SS substrates, suggesting a link

between the secretion and A-LPS modification[155,177]. An electron-dense surface layer (EDSL) was observed to be surrounding *P. gingivalis* cells, and it was formed from A-LPS attached gingipains and other substrates. However, this EDSL was absent in *porV*, *porT* and *porU* mutants[155,177,]. It has been demonstrated that disruption of A-LPS synthesis prevents the formation of the EDSL[91]. Therefore, the secretion of T9SS substrates and A-LPS biosynthesis could be co-ordinated, and disruption of either process could cause blockage of the entire system.

1.4.5 Adaptations to the T9SS

In *F. johnsoniae*, the T9SS is involved in gliding motility and chitin utilization[50]. Most of T9SS components in *P. gingivalis* are also present in *F. johnsoniae*, but *F. johnsoniae* possesses additional motility proteins (**Figure 1.12**). *F. johnsoniae* secretes the motility adhesins SprB and RemA via the T9SS to enable the bacteria to glide over surfaces[230]. SprB is a 669 kDa highly repetitive protein, which forms long filaments that extend from the OM and move along the cell surface in a helical track[231]. RemA is a much smaller protein of 152 kDa, but also was shown to move along a helical track[232]. However, it is not clear how these motility adhesins of *F. johnsoniae* are attached to the cell surface to allow their movement along a track.

The *F. johnsoniae* T9SS and gliding motility machines appear to be associated, since many mutations disrupt gliding and secretion[233]. Similar to PorL and PorM in *P. gingivalis*, GldL and GldM in *F. johnsoniae* have been suggested to be part of the proton

motive force (PMF)-driven rotary gliding motor, and they are also thought to energize secretion[185,231,232]. Other core components of the T9SS (GldK, GldN, SprA, SprE, and SprT) are also essential for gliding, suggesting the possibility that a transmembrane complex of these T9SS proteins may be central to gliding and secretion. Loss of some other motility proteins, GldA, GldB, GldD, GldF, GldG, GldH, GldI, and GldJ, also results in defects in motility and secretion[233]. It has been discovered that GldJ is required to stabilize the T9SS protein GldK[233], and GldA, GldB, GldD, GldF, GldG, GldH, and GldI are needed to stabilize GldJ[234]. Therefore, the T9SS and gliding motility appear to be connected in *F. johnsoniae*.

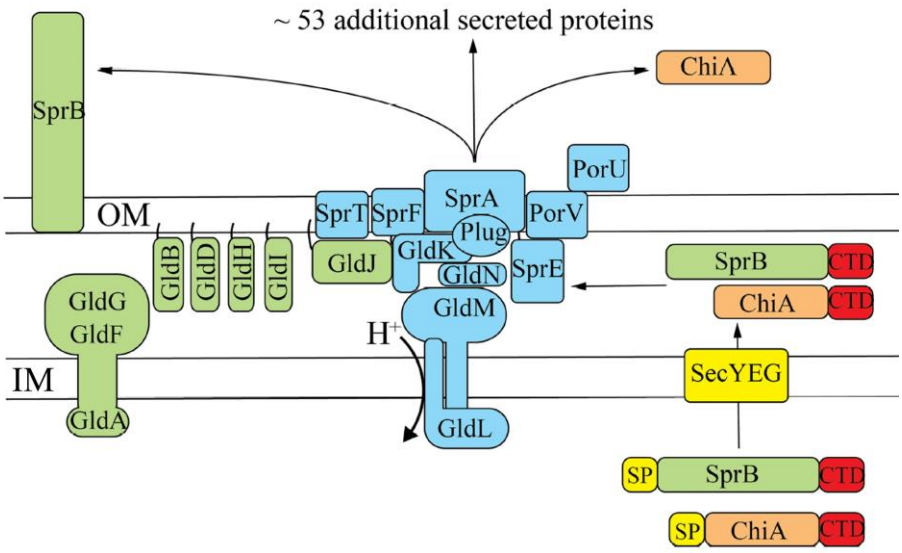

Figure 1.12: *F. johnsoniae* T9SS and gliding motility proteins.
Proteins in blue are associated with the T9SS, and proteins in green are motility proteins that are not directly associated with the T9SS. *F. johnsoniae* GldK, GldL, GldM, GldN, SprA, SprE, and SprT are homologues of *P. gingivalis* PorK, PorL, PorM, PorN, Sov, PorW, and PorT, respectively. Black lines are lipid tails on lipoproteins. Proteins secreted by the T9SS have predicted N-terminal signal peptides (yellow) that target them to the Sec system for export across the inner membrane (IM) and CTDs (red) that target them to the T9SS for secretion across the outer membrane (OM). SprB is a motility adhesin that is propelled by some of the other proteins shown. SprF is required for secretion of SprB but not for secretion of other proteins. SprF and nine other *F. johnsoniae* proteins are related to *P. gingivalis* PorP. *F. johnsoniae* PorV is required for secretion of ChiA and many other proteins, but not for secretion of SprB. This figure was adapted[235].

Unlike *P. gingivalis* that possesses an amorphous surface layer composed of T9SS substrates, *T. forsythia* exhibits a true surface layer (S-layer) composed of two homologous glycoproteins TfsA and TfsB that are important for various virulence traits[236]. The *T. forsythia* S-layer proteins TfsA and TfsB have been confirmed to be secreted by the T9SS because the S-layer was absent in T9SS deficient *porK*, *porT*, *porU* and *Sov* mutants[237,238]. Although some T9SS homologues have been found in *T. forsythia*, the *T. forsythia* T9SS model has not been established and there is very little known about it.

In *P. gingivalis*, the T9SS has also been linked to OMV biogenesis, as mutations of T9SS components *porT*, *porU* and *porV* result in irregular OMV formation[152,155,177]. This could be an additional adaption of the T9SS, specifically in *P. gingivalis*, as the effect of mutated T9SS component on OMVs has not been reported in *F. johnsoniae*, *T. forsythia* or other bacteria carrying T9SS.

1.5 Outer membrane vesicles

OMVs, which are derived from the cell envelope of Gram-negative bacteria, have been observed and studied for decades. Many species of Gram-negative bacteria have been seen to produce OMVs in a variety of environments[239], and it is believed to be a common mechanism. Although many studies have documented the production of OMVs, their importance has been underestimated and previously OMVs were simply regarded as cell debris or microscopy artifacts[240]. Until recently, it has been recognized

that OMVs produced via blebbing of the outer membranes (OM) of bacteria have multiple functional roles[241]. In *P. gingivalis*, OMVs range in size from 50 to 300 nm in diameter, are relatively small, discrete, spherical membranous structures[239]. OMVs consist of a single bilayer membrane that is derived from the OM. The inner layer comprises phospholipids whereas the outer layer is composed of LPS. OM proteins make up the other major component of the OMVs[239,242]. As secreted complexes of insoluble and soluble bacterial envelope components, OMVs play a variety of biological roles (**Figure 1.13**). OMVs can deliver a range of molecular effectors which are responsible for cell-cell interactions, nutrient acquisition, host immune dysregulation and modulation, host-cell interaction and biofilm formation[243]. Furthermore, the capacity of OMVs to disseminate far from the cell enables biofilm-associated bacteria to extend their sphere of influence[243]. Therefore, OMVs are major contributors to bacterial survival, virulence and pathogenicity.

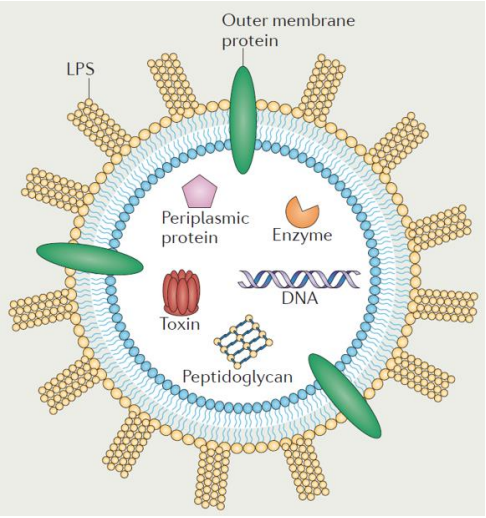

Figure 1.13: A schematic of bacterial outer membrane vesicle. Outer membrane vesicles (OMVs) are bilayer lipid membrane nanostructures that are produced by Gram-negative bacteria. OMVs are proposed to provide an advantage to the parent bacterium by facilitating bacterial communication and the transfer of DNA, proteins and enzymes, and they promote the survival and maintenance of bacterial communities. This figure was adapted[244].

1.5.1 Pathogenicity of OMVs

OMVs are major virulence determinant of *P. gingivalis*, and can induce inflammatory responses, impair host cells and transmit other virulence factors into host cells[245,246]. Several membrane proteins which are involved in *P. gingivalis* attachment to, and invasion of, host cells have been identified in vesicles, including fimbrillin (FimA), hemagglutinin A (HagA) and heat-stress protein (HtrA)[247,248,249,250]. Additionally, vesicles derived from *P. gingivalis* are able to invade human primary oral epithelial cells, gingival fibroblasts and human umbilical vein endothelial cells[251,252,253]. However, the effect of OMV invasion on host cells has not yet been fully elucidated.

P. gingivalis OMVs also play a role in the induction of inflammatory responses. It has been shown that stimulation of human gingival epithelial cells with vesicles caused an increased expression of cyclooxygenase-2 (Cox-2), interleukin (IL-6 and IL-8) and matrix metalloproteinases (MMP-1 and MMP-3)[254]. This may be the result of enriched virulence factors in OMVs, as a recent study demonstrated the existence of a specific cargo selection process that only virulence factors (e.g., gingipains) were enriched in *P. gingivalis* OMVs[229]. Production of IL-8 is known for its role in innate immune responses of periodontal tissues, as this chemokine participates in the recruitment of neutrophils from the vascularized gingival tissue to the gingival crevice[18]. Unexpectedly, *P. gingivalis* OMVs appeared to inhibit immune responses induced by gamma interferon (IFN-γ)[255]. These studies suggest that *P. gingivalis* OMVs have multiple and complicated effects on the human immune response system.

1.5.2 OMV biogenesis

The biogenesis of OMVs is a complicated process, as the outer membrane (OM) of Gram-negative bacteria is a dynamic region of the cell. Although many aspects of Gram-negative bacterial envelopes have been well studied, understanding OMV production has only recently been given attention[239]. Current evidence indicates that OMV biogenesis is a tightly controlled and regulated process, although the biogenesis pathways are yet to be elucidated[243]. Key stages of OMV biogenesis are thought to include breaking the contacts between the OM and the peptidoglycan wall, inducing localized membrane curvature, enrichment or exclusion of particular proteins, and release of OMVs[239].

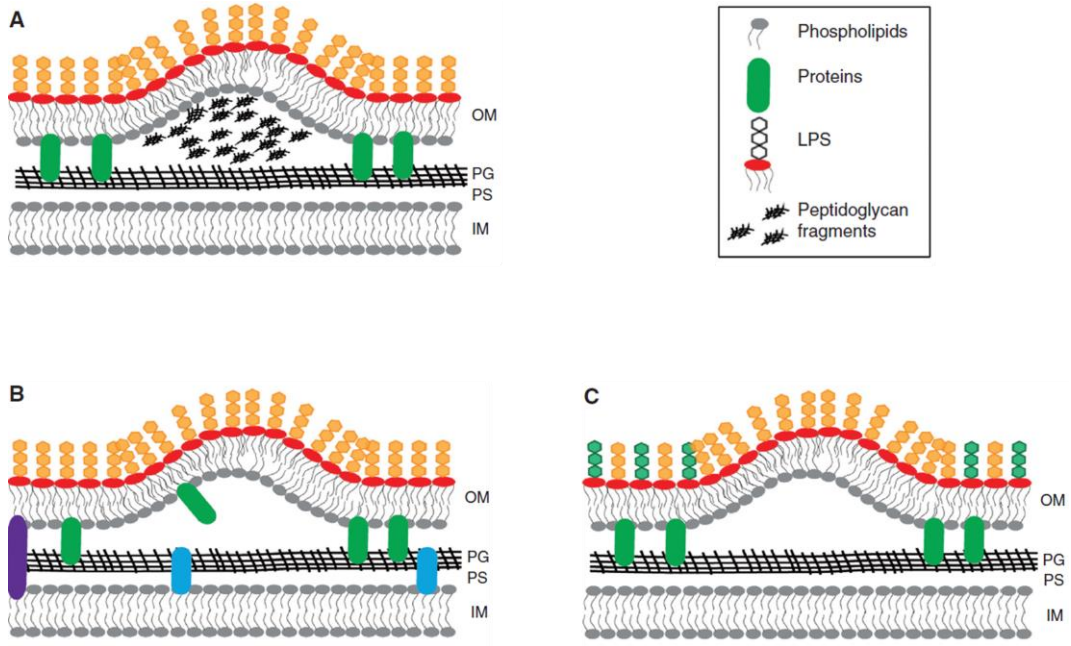

Figure 1.14: Models for outer membrane vesicle (OMV) formation. A. Peptidoglycan fragment accumulation model. Peptidoglycan fragments accumulate in the periplasm and generate enough turgor pressure to bend the outer membrane (OM). **B.** OM-peptidoglycan interaction model. OMVs are formed in regions with relaxed OM-peptidoglycan interactions. Lipoproteins that favour peptidoglycan interaction are excluded from the region where OMV formation is initiated. **C.** O antigen charge repulsion model. OMVs are generated in regions where the negatively charged O antigen (orange) is more abundant and the neutral O antigen (green) is excluded. OM, outer membrane. PG, peptidoglycan layer. PS, periplasmic space. IM, inner membrane. This figure was adapted[256].

Three different models have been proposed for the biogenesis of OMVs in different bacteria, involving peptidoglycan, lipoproteins and LPS (**Figure 1.14**).

Peptidoglycan fragment accumulation model

The first one was based on the presence of peptidoglycan fragments with autolysins in the OMVs of *P. gingivalis* (**Figure 1.14A**). This model proposes that during synthesis of the peptidoglycan layer, sites exist where the concentration of peptidoglycan is higher, causing protrusions in the outer membrane and indicating the beginning of vesicle formation. An important finding that supported this model was the presence of muramic acid, a known peptidoglycan layer precursor, in OMVs purified from *P. gingivalis*[257]. Furthermore, an increase in OMV production was observed when peptidoglycan fragments accumulated because of the incomplete degradation of the peptidoglycan in a *P. gingivalis* autolysin mutant[258]. These findings suggest that the accumulation of peptidoglycan fragments increases outer membrane bulging, triggering the release of OMVs[257,258].

OM-peptidoglycan interaction model

Bacterial lipoproteins are a subset of membrane proteins localized on either leaflet of the lipid bilayer. These proteins are anchored to membranes through their N-terminal lipid moiety covalently attached to a conserved cysteine residue. The second model explains the formation of OMVs due to the low number of lipoproteins attached to the peptidoglycan layer, which results in OM bulging and vesicle production (**Figure 1.14B**). Hoekstra *et al.* found fewer lipoproteins in the vesicles than in the OM of *E.*

coli[259]. Based on these results, they proposed that vesicles are released from OM sites with few lipoprotein linkages[241,259].

Braun's lipoprotein (Lpp) and the OM protein OmpA are also involved in OMV biogenesis in *E. coli*. Peptidoglycan is bound to proteins in the outer and inner membranes through covalent and noncovalent bonds[260]. Lpp, is the major lipoprotein in *E. coli* and is the only lipoprotein that is covalently linked to the peptidoglycan layer and plays a unique role in the envelope architecture. The N-terminal domain of Lpp is acylated and inserted into the outer membrane, while the C-terminal domain is covalently linked to the peptidoglycan layer[261]. OmpA in *E. coli* is a β-barrel, and its C-terminal domain interacts with peptidoglycan through a 20-aa residue linker region[262]. Recently, Samsudin *et al*. have shown that Lpp aids in the interaction of OmpA with the peptidoglycan layer, which is essential in maintaining the integrity of the cellular envelopes[263].

O-antigen charge repulsion model

The third model involves the electric charge of LPS in OMV formation (**Figure 1.14C**). *Pseudomonas aeruginosa* produces two types of LPS: neutrally charged O-LPS and negatively charged A-LPS, the latter being enriched in OMVs[264,265]. Therefore, an increase in A-LPS within the cell envelope was proposed to support the release of OMVs because of the O-antigen repulsion caused by negative charges in the OM[266,267]. *P. aeruginosa* cells that express only O-LPS produce smaller OMVs than cells that express only A-LPS[265]. Likewise, predominant A-LPS has been found in *P. gingivalis* OMVs. It has been therefore suggested that an interaction between negatively charged

O-antigen chains contributes to OMV formation[266].

These models highlighted the importance of peptidoglycan, lipoproteins and LPS during OMV formation. However, it remains unknown whether these mechanisms act in tandem or alone. Furthermore, other factors have been identified that also have a major role in membrane stabilisation and OMV formation.

Additional factors affecting OMV biogenesis

Phospholipids are the major components of OMVs. Gram-negative bacteria maintain asymmetric distribution of phospholipids in their membranes through the translocation of phospholipids from the IM to the inner leaflet of the OM (phospholipid anterograde transport) and inversely (phospholipid retrograde transport)[268]. The molecular mechanism of anterograde transport is still not fully understood. Regarding retrograde transport, two systems Tol-Pal system and OmpC-Mla system have been described in *E. coli*. The Tol-Pal system is involved in the movement of phospholipids from the inner leaflet of the OM to the IM[269]. The OmpC-Mla system is responsible for OM asymmetry by transporting misplaced phospholipids found in the outer leaflet of the OM to the IM[270]. The MlaA lipoprotein interacts with OmpC, which is embedded in the OM and removes phospholipids in the outer leaflet of the OM to another component of the system the MlaC protein. Subsequently, MlaC delivers these phospholipids to the MlaFEDB complex located in the IM. This complex can then reintegrate these phospholipids to the IM[270,271]. Mutation of *mla* in *E. coli* induces vesicle production and promotes cell death[272]. Moreover, mutations of the homologs of *mlaA* and *mlaE*, which are associated with phospholipid transport in *Vibrio cholerae* and *Campylobacter*

jejuni, increased OMV production, confirming the hypothesis that phospholipid asymmetry plays a role in OMV biogenesis[273,274].

OMV production is also associated with the bacterial flagellum. The flagellum is composed of a basal body, a flexible linker known as the hook, and a filament that drives the bacterium's movement. The filament of the bacterial flagellum comprises the flagellin protein[275]. Using proteomics, Flagellin (FliC) was identified in purified OMVs from *E. coli*[276]. Manabe *et al.* created a *fliC* mutant in *E. coli* and observed a decline of OMV production in this mutant[277]. In another study in *Vibrio fischeri*, OMV production was analysed in the *motB1* mutant (MotB1 is a sodium pump and the main motor protein for the flagellum machinery), non-flagellated *flrA* mutant (FlrA is a transcriptional activator), hyper-flagellated swarmer strain that expresses 3- to 4-fold more flagella, and wild-type strain[278]. The number of vesicles decreased in the *V. fischeri flrA* mutant that lacks flagella. OMV production increased in the hyperflagellated strain. The addition of phenamil that is a sodium pump blocking reagent to the *V. fischeri* hyper-flagellated strain decreased OMV production, suggesting that flagellum rotation improves OMV release[278]. To better understand the relationship between flagella and OMV production, more flagellated strains along with their corresponding non-flagellated mutants and hyper-flagellated strains should be studied.

LPS contains negatively charged phosphate groups in the lipid A and it is known that divalent cations such as Ca^{2+} and Mg^{2+} are important in forming salt bridges with the negative charges of LPS. The generation of these salt bridges helps to stabilize the OM.

Several compounds can sequester these divalent cations and destabilize the OM, contributing to the generation of OMVs to release the charge repulsion[279]. Furthermore, molecules that can change OM fluidity were found to stimulate vesiculation. For example, a quorum-sensing molecule PQS found in the OMVs, interacts with lipid A and induces the OMV production[280,281].

Recently, A few studies demonstrated that lipid A modification has effects on OMV production (**Figure 1.15**). In *P. gingivalis*, mutation of PorV was found to cause the inactivation of lipid A 1-phophatase LpxE which is responsible for dephosphorylation of lipid A at 1 position, and led to budding of abnormally large OMVs[152]. Another study suggested lipid A deacylation triggers formation of OMVs in *Salmonella enterica*, since expression of the lipid A deacylase PagL resulted in increased vesiculation[282]. Moreover, lipid A 1-phophatase LpxE from *Aquifex aeolicus* was discovered to be a multifunctional regulatory enzyme that is responsible for lipid A modification, O-antigen production, and peptidoglycan biogenesis to remodel multiple layers of the Gram-negative bacterial envelope[283].

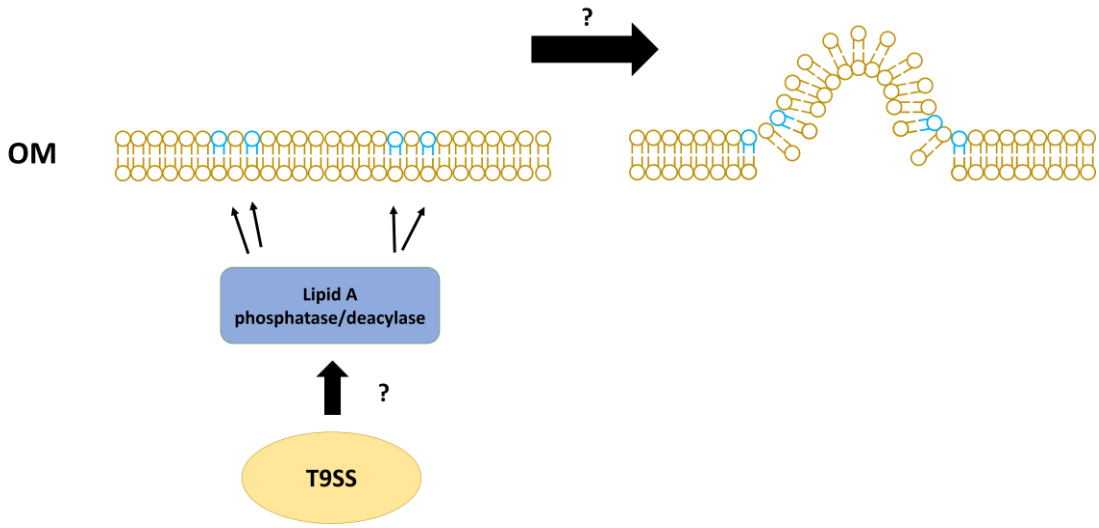

Figure 1.15: A putative schematic of OMV biogenesis in *P. gingivalis*. In *P. gingivalis*, it has been suggested that T9SS regulates lipid A modification via T9SS outer membrane (OM) component PorV. However, the correlation between the T9SS and lipid A modification is still unclear. Dephosphorylation and deacylation of lipid A can result in unique LPS species that may destabilize membrane and therefore facilitate OMV production, although the mechanism has not been elucidated. Dephosphorylated and deacylated lipid A are shown in blue colour.

1.6 Project aims

The overall aim of this PhD was to understand how the T9SS is able to regulate OMV biogenesis. The specific aims were to: understand how the T9SS affects OMV formation, examine the interplay between the T9SS and lipid A modification and decipher how the interplay is achieved.

1.6.1 Aim 1: Understand how the T9SS affects OMV formation

Our understanding of how the type-IX secretion system functions is still unclear, and the roles of many T9SS accessory proteins remain to be elucidated. Furthermore, how

type-IX dependent secretion is coupled with OMV enrichment is also unknown. The first aim of this project was to create knockout mutants of *porV*, *porU*, *porQ*, *porZ*, *porP*, *porT*, *porG* and *porF* in *P. gingivalis*. Next, it was planned to determine the phenotypes of these mutants using *in vivo* assays. Characterization of these T9SS accessory proteins would provide insight into the correlation between the T9SS and OMV biogenesis.

1.6.2 Aim 2: Decipher how the interplay between T9SS and lipid A modification is achieved

By analysing the lipid A status of these T9SS mutants and carrying out bacterial pull-down experiments, the aim was to discover partner proteins which may be involved in lipid A modification. Identification of candidate proteins may reveal unknown interplay between the T9SS and lipid A modification. Furthermore, it was planned to create knockout mutants of any identified candidate proteins and determine their location, function and interaction profile *in vivo*.

1.6.3 Aim 3: Recombinant expression and purification of the T9SS outer membrane accessory proteins

The final aim of this project was to get molecular insight into any identified proteins and their complexes. The aim was to produce recombinant proteins in *E. coli* or isolate

them from *P. gingivalis* and determine the function of these proteins *in vitro*. These were then to be studied further using X-ray crystallography and transmission electron microscopy.

Chapter 2　Materials and Methods

2.1 Materials

2.1.1 Strains, plasmids, oligonucleotides

Strains and plasmids used in this study are shown in **Table 2.1**.

Table 2.1: Strains and plasmids[284].

Strains and plasmids		Relative characteristics	Reference or source
P. gingivalis	W50	Wild type, no resistance.	[285]
	Δ*porV*	W50 *porV* (PG0027, PGN_0023) knock-out mutant, Cm^r.	[152]
	Δ*porU*	W50 *porU* (PG0026, PGN_0022) knock-out mutant, Cm^r.	This study
	Δ*porQ*	W50 *porQ* (PG0602, PGN_0645) knock-out mutant, Cm^r.	This study
	Δ*porZ*	W50 *porZ* (PG1604, PGN_0509) knock-out mutant, Cm^r.	This study
	Δ*porP*	W50 *porP* (PG0287, PGN_1677) knock-out mutant, Cm^r.	This study
	Δ*porT*	W50 *porT* (PG0751, PGN_0778) knock-out mutant, Cm^r.	This study
	Δ*porG*	W50 *porG* (PG0189, PGN_0297) knock-out mutant, Cm^r.	This study
	Δ*porF*	W50 *porF* (PG0534, PGN_1437) knock-out mutant, Cm^r.	This study
	Δ*kgp*	W50 *kgp* (PGN_1728) knock-out mutant, Cm^r.	[286]
	Δ*lpxE*	W50 *lpxE* (PG1773, PGN_1713) knock-out mutant, Cm^r.	This study

	lpxE/N-HA	W50 *lpxE* knock-out mutant, complemented with an expressible N-terminal HA-tagged *lpxE* gene, Tet^r.	This study
	lpxE/C-HA	W50 *lpxE* knock-out mutant, complemented with an expressible C-terminal HA-tagged *lpxE* gene, Tet^r.	This study
E.coli	BL21 (DE3)	Competent cells for protein expression, routine T7 expression.	New England Biolabs
	Lemo21 (DE3)	Competent cells for protein expression, BL21 (DE3) containing the Lemo System. Tuneable T7 expression for difficult targets: membrane proteins, toxic proteins and proteins prone to insoluble expression.	New England Biolabs
	C41 (DE3)	Competent cells for toxic protein expression. The strain was derived from BL21 (DE3). This strain has a mutation that reduces the level of T7 RNAP activity, thereby preventing cell death associated with overexpression of many recombinant toxic proteins.	Cambridge Bioscience
Plasmids	pET28b	Bacterial expression vector with T7 promoter for recombinant expression of proteins.	Novagen®
	pOMPA28	pET28b vector modified with OmpA signal sequence for recombinant expression of membrane proteins.	This study

	pET46 Ek/LIC	pET46 Ek/LIC is a LIC-compatible derivative of pET45b containing a strong T7 lac promoter and an N-terminal His-tag coding sequence immediately followed by an Ek/LIC cloning site.	Novagen®
	pUCET1	Complementation vector for *P. gingivalis* knock-out mutants.	[287]
	pVA2198	Source of *erm* cassette. The erm cassette is used to generate linear DNA for *P. gingivalis* mutagenesis.	[288]
	p*lpxE*/N-HA	pUCET1 carrying an expressible N-terminal HA-tagged *lpxE* gene to generate *lpxE*/N-HA complement.	This study
	p*lpxE*/C-HA	pUCET1 carrying an expressible C-terminal HA-tagged *lpxE* gene to generate *lpxE*/C-HA complement.	This study
	pET28b-PorV$_{1\text{-}391}$	pET28b carrying an expressible PorV$_{1\text{-}391}$ gene for recombinant expression.	This study
	pET28b-PorV$_{28\text{-}391}$	pET28b carrying an expressible PorV$_{28\text{-}391}$ gene for expression in inclusion bodies.	This study
	pOMPA28-PorV$_{28\text{-}391}$	pOMPA28 carrying an expressible PorV$_{28\text{-}391}$ gene for recombinant expression.	This study
	pOMPA28-PorU$_{24\text{-}1158}$	pOMPA28 carrying an expressible PorU$_{24\text{-}1158}$ gene for recombinant expression.	This study

	pOMPA28-PorQ$_{38-346}$	pOMPA28 carrying an expressible PorQ$_{38-346}$ gene for recombinant expression.	This study
	pOMPA28-PorP$_{20-294}$	pOMPA28 carrying an expressible PorP$_{20-294}$ gene for recombinant expression.	This study
	pOMPA28-PorT$_{29-244}$	pOMPA28 carrying an expressible PorT$_{29-244}$ gene for recombinant expression.	This study
	pOMPA28-PorF$_{37-827}$	pOMPA28 carrying an expressible PorF$_{37-827}$ gene for recombinant expression.	This study
	pOMPA28-LpxE$_{23-445}$	pOMPA28 carrying an expressible LpxE$_{23-445}$ gene for recombinant expression.	This study
	pOMPA28-LpxE$_{23-241}$	pOMPA28 carrying an expressible LpxE$_{23-241}$ gene for recombinant expression.	This study
	pET46-LpxE$_{242-445}$	pET46 carrying an expressible LpxE$_{242-445}$ gene for recombinant expression.	This study

*Cm^r: Clindamycin resistance. Tet^r: tetracycline resistance. Locus numbers in *P. gingivalis* W50, W83 (PG) and ATCC33277 (PGN) are labelled.

Oligonucleotide primers used in this study are shown in **Table 2.2**. The start italics are protection bases. The restriction site is bold and underlined.

Table 2.2: Oligonucleotides used in this study.

Names	Sequences 5′-3′	Used for:
porUF1	ATGAAACGAATACTTCCAATAGTCGCA	Mutagenesis of *porU*. Amplification of *porU* 5′ flanking region (500 bp).
porUR1	*ATATAT***GAGCTC**TCATCGTAGTAGT	Mutagenesis of *porU*. Amplification

	CGATCAAA	of *porU* 5′ flanking region (500 bp). Restriction site SacI is underlined.
porUF2	*ATATAT***TCTAGA**CCGACCTGACCTACAACCTCA	Mutagenesis of *porU*. Amplification of *porU* 3′ flanking region (500 bp). Restriction site XbaI is underlined.
porUR2	CTATTGTCCTACCACGATCATTTTCTT	Mutagenesis of *porU*. Amplification of *porU* 3′ flanking region (500 bp).
porQF1	ATGATGGAAAAATGTATCTTTGCTCACT	Mutagenesis of *porQ*. Amplification of *porQ* 5′ flanking region (300 bp).
porQR1	*ATATAT***GAGCTC**ATGCGAACCACTCATATAAT	Mutagenesis of *porQ*. Amplification of *porQ* 5′ flanking region (300 bp). Restriction site SacI is underlined.
porQF2	*ATATAT***TCTAGA**CACTATTTCAAGCGTCTTGTACC	Mutagenesis of *porQ*. Amplification of *porQ* 3′ flanking region (300 bp). Restriction site XbaI is underlined.
porQR2	TTAGAAGATGCTCTTATCGTCCAA	Mutagenesis of *porQ*. Amplification of *porQ* 3′ flanking region (300 bp).
porZF1	ATGTGCAAAATAAGATTCAGCCTCTTGC	Mutagenesis of *porZ*. Amplification of *porZ* 5′ flanking region (500 bp).
porZR1	*ATATAT***GAGCTC**TTAGTTCCCTTGGCGTAGG	Mutagenesis of *porZ*. Amplification of *porZ* 5′ flanking region (500 bp). Restriction site SacI is underlined.
porZF2	*ATATAT***TCTAGA**TCGTCGTGGACAAACTCAATCA	Mutagenesis of *porZ*. Amplification of *porZ* 3′ flanking region (500 bp). Restriction site XbaI is underlined.
porZR2	TCAGCGAATCACTGCGAAGCG	Mutagenesis of *porZ*. Amplification of *porZ* 3′ flanking region (500 bp).
porPF1	TTGCATAAATCTTTCCGTTCGCTCA	Mutagenesis of *porP*. Amplification of *porP* 5′ flanking region (300 bp).
porPR1	*ATATAT***GAGCTC**AAAGAGTCCTCTCGTTTCGG	Mutagenesis of *porP*. Amplification of *porP* 5′ flanking region (300 bp). Restriction site SacI is underlined.
porPF2	*ATATAT***TCTAGA**GCATGGCATCCTTCTATCTTTGC	Mutagenesis of *porP*. Amplification of *porP* 3′ flanking region (300 bp). Restriction site XbaI is underlined.
porPR2	TCAGAGGAAACGAATGCTTTT	Mutagenesis of *porP*. Amplification of *porP* 3′ flanking region (300 bp).
porTF1	ATGCAATTCTTATATAATTCACGTTTTTCG	Mutagenesis of *porT*. Amplification of *porT* 5′ flanking region (300 bp).
porTR1	*ATATAT***GAGCTC**CAGATTGGGCAGAAGG	Mutagenesis of *porT*. Amplification of *porT* 5′ flanking region (300 bp). Restriction site SacI is underlined.
porTF2	*ATATAT***TCTAGA**CGCCTGAACAATATGCG	Mutagenesis of *porT*. Amplification of *porT* 3′ flanking region (300 bp).

		Restriction site XbaI is underlined.
porTR2	CTACTCGAAATTGAACGTAAGCAT	Mutagenesis of *porT*. Amplification of *porT* 3′ flanking region (300 bp).
porGF1	ATGAAAACAATTAGTAAGAACCATGCGGC	Mutagenesis of *porG*. Amplification of *porG* 5′ flanking region (300 bp).
porGR1	*ATATAT***GAGCTC**CGCTTGAGCAAAATCGG	Mutagenesis of *porG*. Amplification of *porG* 5′ flanking region (300 bp). Restriction site SacI is underlined.
porGF2	*ATATAT***TCTAGA**GCGGCCGGGTTGTCTTT	Mutagenesis of *porG*. Amplification of *porG* 3′ flanking region (300 bp). Restriction site XbaI is underlined.
porGR2	CTATTGTTTATTACAAAAAGTCTTACGCAG	Mutagenesis of *porG*. Amplification of *porG* 3′ flanking region (300 bp).
porFF1	ATGAAGGAAGCTATTCCCCGAA	Mutagenesis of *porF*. Amplification of *porF* 5′ flanking region (500 bp).
porFR1	*ATATAT***GAGCTC**TGCGTTACTCCTGCGTA	Mutagenesis of *porF*. Amplification of *porF* 5′ flanking region (500 bp). Restriction site SacI is underlined.
porFF2	*ATATAT***TCTAGA**TCAAGCTCTTCGGCGAACT	Mutagenesis of *porF*. Amplification of *porF* 3′ flanking region (500 bp). Restriction site XbaI is underlined.
porFR2	TTAGAATTCGACGAGGAGACGCA	Mutagenesis of *porF*. Amplification of *porF* 3′ flanking region (500 bp).
lpxEF1	ATGAATCGAGAAAGCTTTTTACTCCTGC	Mutagenesis of *lpxE*. Amplification of *lpxE* 5′ flanking region (500 bp).
lpxER1	*ATATAT***GAGCTC**AAAGCTGTTGCCGTATGT	Mutagenesis of *lpxE*. Amplification of *lpxE* 5′ flanking region (500 bp). Restriction site SacI is underlined.
lpxEF2	*ATATAT***TCTAGA**CTTTCGGCATGAACCTGAA	Mutagenesis of *lpxE*. Amplification of *lpxE* 3′ flanking region (500 bp). Restriction site XbaI is underlined.
lpxER2	TCAGCGGAAAGGATAGAATTGTAGT	Mutagenesis of *lpxE*. Amplification of *lpxE* 3′ flanking region (500 bp).
lpxENHAF1	*GA***AGATCT**TCAGCTATCCGAACAGCAAAGCG	Construction of N-terminal HA-tagged *lpxE* complement. Restriction site BglII is underlined.
lpxENHAR1	CTGGAACATCGTATGGGTATGCTTGCAGATGGAGCGG	Construction of N-terminal HA-tagged *lpxE* complement.
lpxENHAF2	GCATACCCATACGATGTTCCAGATTACGCTGGCAGCACCTCGTCTCCATGCAACAACATG	Construction of N-terminal HA-tagged *lpxE* complement.

lpxENHAR2	*GGT***GCGGCCGC**TCAGCGGAAAGGATAGAATTGTAGTCC	Construction of N-terminal HA-tagged *lpxE* complement. Restriction site NotI is underlined.
lpxECHAF	*GA***AGATCT**TCAGCTATCCGAACAGCAAAGCG	Construction of C-terminal HA-tagged *lpxE* complement. Restriction site BglII is underlined.
lpxECHAR	*ATATAT***GCGGCCGC**TCAAGCATAATCTGGAACATCATATGGATAGCGGAAAGGATAGAATTGTAGT	Construction of C-terminal HA-tagged *lpxE* complement. Restriction site NotI is underlined.
pET28porVF1	*GC***TCTAGA**AATAATTTTGTTTAACTTTAAGAAGGAGATATACCATGATTATCAAGAAAATGCTGAAAAATAAATTGG	Construction of pET28b-PorV$_{1\text{-}391}$. Restriction site XbaI is underlined.
pET28porVF2	*GC***TCTAGA**AATAATTTTGTTTAACTTTAAGAAGGAGATATACCATGGCTCAGGAGCAACTGAATGTG	Construction of pET28b-PorV$_{28\text{-}391}$. Restriction site XbaI is underlined.
pET28porVR	*CCG***CTCGAG**GTGGAACAAATTGCGCAATCCATC	Construction of pET28b-PorV$_{1\text{-}391}$ and pET28b-PorV$_{28\text{-}391}$. Restriction site XhoI is underlined.
pOMPAporVF	*CCC***AAGCTT**GCTCAGGAGCAACTGAATGT	Construction of pOMPA28-PorV$_{28\text{-}391}$. Restriction site HindIII is underlined.
pOMPAporVR	*ATTT***GCGGCCGC**TTAGTGGAACAAATTGCGCA	Construction of pOMPA28-PorV$_{28\text{-}391}$. Restriction site NotI is underlined.
pOMPAporUF	*CCC***AAGCTT**CAACGAGCTATGGGGAAGAC	Construction of pOMPA28-PorU$_{24\text{-}1158}$. Restriction site HindIII is underlined.
pOMPAporUR	*ATTT***GCGGCCGC**CTATTGTCCTACCACGATCA	Construction of pOMPA28-PorU$_{24\text{-}1158}$. Restriction site NotI is underlined.
pOMPAporQF	*CCC***AAGCTT**CAACAAGAGAAGCAGGTGTT	Construction of pOMPA28-PorQ$_{38\text{-}346}$. Restriction site HindIII is underlined.
pOMPAporQR	*ATTT***GCGGCCGC**TTAGAAGATGCTCTTATCGT	Construction of pOMPA28-PorQ$_{38\text{-}346}$. Restriction site NotI is underlined.
pOMPAporPF	*CCC***AAGCTT**GAGGATATTTTCGCT	Construction of pOMPA28-PorP$_{20\text{-}294}$. Restriction site HindIII is

	CAGGG	underlined.
pOMPAporPR	*ATTT***GCGGCCGC**TCAGAGGAAAC GAATGCTTT	Construction of pOMPA28-PorP$_{20-294}$. Restriction site NotI is underlined.
pOMPAporTF	*CCC***AAGCTT**GCGCAAACGGAAAA AGTACAAAATC	Construction of pOMPA28-PorT$_{29-244}$. Restriction site HindIII is underlined.
pOMPAporTR	*ATTT***GCGGCCGC**CTACTCGAAATT GAACGTAAGCATAAT	Construction of pOMPA28-PorT$_{29-244}$. Restriction site NotI is underlined.
pOMPAporFF	*CCC***AAGCTT**CAAGGCGTCAGGGT ATCGGG	Construction of pOMPA28-PorF$_{37-827}$. Restriction site HindIII is underlined.
pOMPAporFR	*ATTT***GCGGCCGC**TTAGAATTCGAC GAGGAGAC	Construction of pOMPA28-PorF$_{37-827}$. Restriction site NotI is underlined.
pOMPAlpxEF	*CCC***AAGCTT**TCGTCTCCATGCAAC AACATGGC	Construction of pOMPA28-LpxE$_{23-445}$ and pOMPA28-LpxE$_{23-241}$. Restriction site HindIII is underlined.
pOMPAlpxER	*ATTT***GCGGCCGC**TCAGCGGAAAG GATAGAATTG	Construction of pOMPA28-LpxE$_{23-445}$. Restriction site NotI is underlined.
pOMPAlpxENR	*ATTT***GCGGCCGC**TCACTTGTAGTT GTAGCCCGTAGGA	Construction of pOMPA28-LpxE$_{23-241}$. Restriction site NotI is underlined.
pET46lpxECF	GACGACGACAAGATCACGGGCTAC AACTACAAGC	Construction of pET46-LpxE$_{242-445}$.
pET46lpxECR	GAGGAGAAGCCCGGTCAGCGGAA AGGATAGAATTGTA	Construction of pET46-LpxE$_{242-445}$.

2.1.2 Media and growth conditions

P. gingivalis W50 and mutant strains from -80°C glycerol stocks were grown on blood agar plates containing 5% (vol/vol) defibrinated horse blood or in brain heart infusion (BHI) broth supplemented with hemin (5 μg/ml) in an anaerobic atmosphere of 80%

N_2, 10% H_2, and 10% CO_2 (Don Whitely Scientific). Clindamycin (5 μg/ml) or tetracycline (1 μg/ml) was added when required. Antibiotics were added for cell selection (tetracycline HCl, 20 μg/ml) and plasmid selection (ampicillin, 100 μg/ml).

E. coli cells were grown in lysogeny broth (LB; Sigma-Aldrich) or on LB agar plates (Sigma-Aldrich) at 37°C and with 225 rpm agitation for liquid cultures.

2.1.3 Chemicals

All chemicals and reagents were from Sigma-Aldrich unless otherwise stated.

2.2 Methods

2.2.1 Genetic techniques

2.2.1.1 Genomic DNA purification

P. gingivalis W50 genomic DNA was extracted from a 10 ml culture grown overnight at 37°C. The DNeasy UltraClean Microbial kit (Qiagen) was used according to manufacturer instructions. Genomic DNA samples were stored at -20°C.

2.2.1.2 Plasmid DNA purification

Plasmid DNA was extracted from cell culture samples using Monarch® Plasmid Miniprep Kit (New England Biolabs) according to manufacturer instructions. Purified

plasmid DNA was eluted in dH_2O and stored at -20°C.

2.2.1.3 Agarose gel electrophoresis

DNA samples were separated via agarose gel electrophoresis using 1-1.5% (wt/vol) agarose gels prepared with TAE buffer (40 mM Tris, pH 7.6, 20 mM acetic acid, 1 mM EDTA) and SYBR safe stain. Samples were mixed with 6×loading dye (New England Biolabs) and Gels were ran using a PowerPac™ basic power supply (BioRad) at 90 V for 30 min. 2-log DNA ladder (New England Biolabs) was used as a marker to determine DNA base pairs (bp).

2.2.1.4 Agarose gel band extraction

DNA bands of the appropriate size were excised from agarose gels using a sterile scalpel. The sample was then purified using Monarch® DNA gel extraction kit (New England Biolabs) according to manufacturer instructions. Purified DNA was eluted in dH_2O and stored at -20°C.

2.2.1.5 Polymerase chain reaction

DNA fragments for use in molecular cloning were amplified via polymerase chain reaction (PCR). Q5 High-Fidelity DNA polymerase (New England Biolabs) was used

in all PCR reactions following the 50 µl reaction protocol (**Table 2.3**). Reactions were performed in a CFXConnect™ or a Techne 312™ (BioRad) thermocycler using the settings shown in **Table 2.4**.

Table 2.3: PCR reaction recipe.

Component	50 µl Reaction
5×Q5 Reaction buffer	10 µl
10 mM dNTPs	1 µl
10 µM Forward primer	2.5 µl
10 µM Reverse primer	2.5 µl
Template DNA	100 ng
Q5 High-Fidelity DNA polymerase	0.5 µl
Nuclease-free water	to 50 µl

Table 2.4: PCR thermocycler settings.

Temperature (°C)	Time (seconds)	Cycles
98	30	1
98	10	×30
×*	30	×30
72	30 (per 1000 bp)	×30
72	180	1
4	Hold	-

* Annealing temperatures were determined by NEB Tm Calculator: www.tmcalculator.neb.com.

2.2.1.6 PCR product purification

PCR amplified products were purified using Monarch® PCR & DNA clean up kit (New England Biolabs) according to manufacturer's instructions. This purification was used to remove reagents, unwanted buffers and impurities from the sample prior to restriction endonuclease digestion or ligation.

2.2.1.7 Restriction enzyme digestion

All digestions were performed using CutSmart buffer and restriction endonucleases (New England Biolabs) following the 50 µl reaction protocol (10 units enzyme, 1 µg DNA). Reactions were incubated at 37°C for 1 hour, immediately followed by agarose gel electrophoresis.

2.2.1.8 DNA ligation

Plasmid and DNA fragment ligations were performed using T4 DNA ligase (New England Biolabs) according to manufacturer instructions, followed by heat-shock transformation.

2.2.1.9 *P. gingivalis* mutagenesis

Single isogenic mutants defective in *porU*, *porQ*, *porZ*, *porP*, *porT*, *porG* and *porF*

were generated using primer pairs designed to separately amplify the 5′ and 3′ ends of each open reading frame (ORF) by PCR[287] (**Table 2.2**). The strategy also incorporated SacI and XbaI restriction sites at the 5′ and 3′ ends of the amplicons respectively to facilitate subsequent cloning. Following purification and digestion with SacI and XbaI, these amplicons were ligated to the SacI-XbaI *erm* cassette, retrieved from pVA2198[288] by T4-DNA ligase. The mixture was purified and used as a template in PCR to generate linear chimeric amplicons that comprise *erm* cassette flanked by the 5′ and 3′ regions of the ORF (**Figure 2.1**). The linear chimeric amplicons were electroporated into exponential cells of *P. gingivalis* W50 to generate clindamycin resistant mutants by allelic exchange. As the *erm* cassette encodes macrolide-lincosamide resistance, it can be selected on either erythromycin (macrolide) or clindamycin (lincosamide). Clindamycin was selected for resistance screening because it is soluble in water and can be filter sterilized and stored for a long time at -20°C. Erythromycin, on the other hand, is only soluble in 100% ethanol and crystallizes after two weeks at -20°C. *P. gingivalis* mutant colonies were then screened by PCR that showed that the erm cassette had been inserted in the correct, predicted position. Details of generated mutants are in **Table 2.1**.

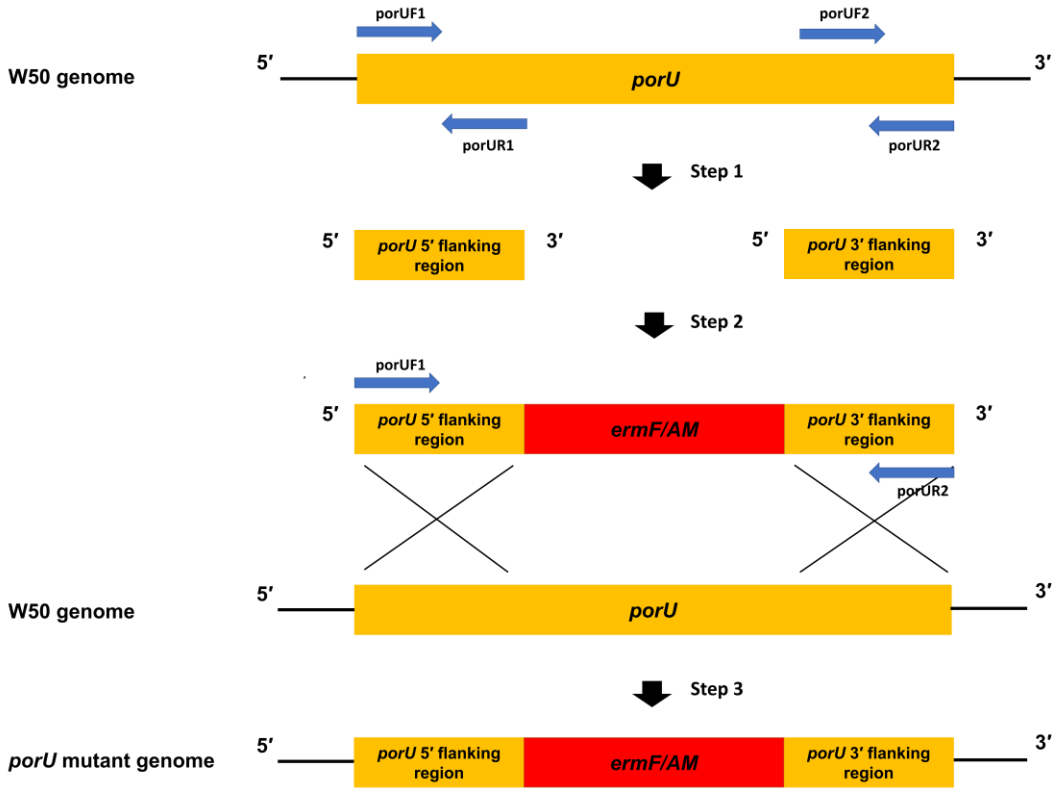

Figure 2.1: Construction of *P. gingivalis* T9SS mutant. The method used for mutagenesis includes three steps. The generation of *porU* mutant is given as an example. The other mutations were constructed analogously. Step 1: The 5′ and 3′ ends of *porU* were amplified. Step 2: The 5′ and 3′ regions of *porU* were ligated to the *erm* cassette (*ermF/AM*), respectively. The generated erm cassette flanked by the 5′ and 3′ region of the ORF was amplified. Step 3: The linear chimeric amplicon was targeted to *porU* ORF on the genome by homologous recombination via electroporation, which resulted in replacement of internal fragments at 5′ region and 3′ region of the target gene with the *erm* cassette possessing stop codons and rho-independent transcription terminators to avoid read through. Blue arrows: primers used for PCR amplification and their details are in **Table 2.2**.

2.2.1.10 Complementation

The complementation plasmid was generated by Rangarajan *et al*[287] (**Figure 2.2A**). Adjacent BglII and NotI sites upstream of the coding region for *tetQ* were used to insert a gene expressed from its own promoter into pUCET1. Thus, the new gene tagged with *tetQ* and flanked by *erm* sequences was used in homologous recombination to a site already possessing an *erm* cassette for integration of a single copy of a defined gene to

replace the existing *erm* with *tetQ*[229]. An amplicon corresponding to the *lpxE* ORF, further manipulated to include an N-terminal human influenza hemagglutinin-tag (HA-tag) and preceded by an additional 500 bp regulatory upstream sequence was amplified from W50 genome by PCR to generate p*lpxE*/N-HA (**Figure 2.2B**). Another amplicon corresponding to the *lpxE* ORF, again further manipulated to include a C-terminal HA-tag and preceded by an additional 500 bp regulatory upstream sequence was amplified from W50 genome by PCR to generate p*lpxE*/C-HA (**Figure 2.2B**). All constructs were generated by cloning the chimeric amplicons in corresponding restriction sites in pUCET1. The recombinant plasmid was linearized with XbaI and the flanking *erm* cassette was then used to target the homologous regions in *lpxE* mutant via electroporation and allelic exchange with selection for the tagged *tetQ* on blood agar plates[87] (**Figure 2.2C**). PCR was used to confirm chromosomal integration of the *tetQ*-tagged amplicon. Details of generated plasmids and complemented strains are in **Table 2.1**.

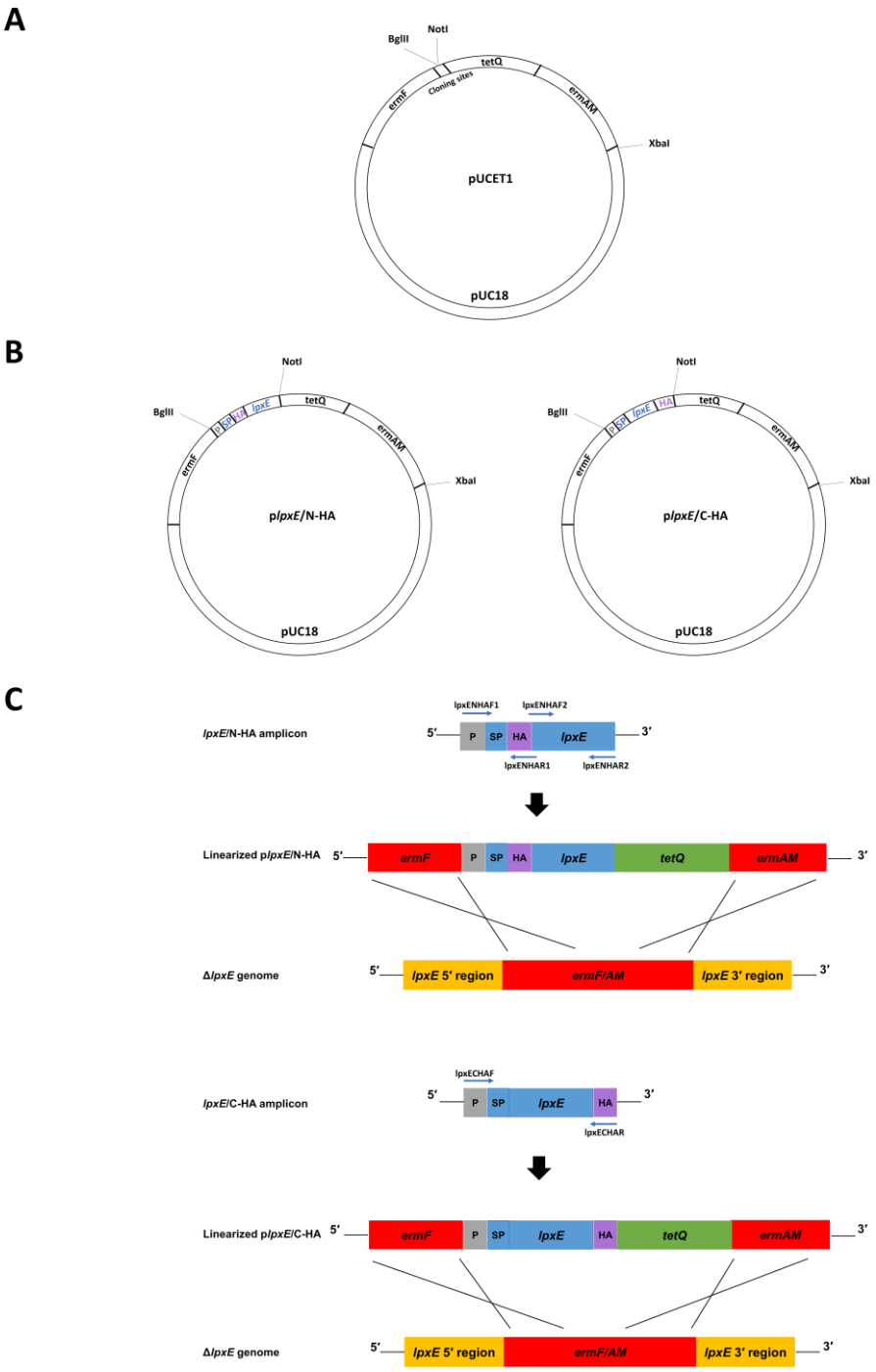

Figure 2.2: Complementation of *P. gingivalis lpxE* mutant. A. The plasmid map of pUCET1[287]. **B.** The plasmids for *lpxE* N-terminal HA-tagged complement and *lpxE* C-terminal HA-tagged complement. P: promotor, a 500 bp regulatory upstream sequence. SP: the gene of *lpxE* signal peptide. HA: the gene of HA-tag. *lpxE*: *lpxE* ORF excluding the sequence of signal peptide. BglII and NotI are cloning sites. XbaI is for plasmid linearization. **C.** Generation of HA-tagged complement strains. Two amplicons were amplified from W50 genome by PCR using designated primers. The linearized p*lpxE*/N-HA and p*lpxE*/C-HA were targeted to the *erm* cassette in the *lpxE* mutant by homologous recombination as well as introducing *tetQ* marker into the genome of the complemented strain. Blue arrows: primers used for PCR amplification and their details are in **Table 2.2**.

2.2.1.11 Electroporation

For electroporation, all procedures were performed at 4°C. A 6-hour culture of *P. gingivalis* (30 ml) grown at 37°C anaerobically was harvested by centrifugation at 10,000 g for 10 min and then resuspended thoroughly with 1 ml electroporation buffer (EPB: 10% glycerol-1 mM $MgCl_2$). This was washed twice in EPB and then the pellet was resuspended in 600 µl EPB. Approximately 200 ng of DNA in 5 µl dH_2O, was then added to 200 µl cells in a 0.2 cm-path length cuvette and electroporated using a Bio-Rad Gene Pulser with the parameter's set at 2.5 kV for the potential difference, 200 Ω for the resistance and 25 µF for the capacitance. *P. gingivalis* cells were then immediately diluted in 1 ml BHI-haemin broth, allowed to recover for 16 hours in an anaerobic cabinet and then plated out onto blood agar plates containing appropriate antibiotics.

2.2.1.12 Plasmid construction for recombinant expression of membrane proteins

In this thesis, three plasmids, pET28b, pOMPA28 and pET46, were used for recombinant expression of *P. gingivalis* proteins in *E. coli*.

pET28b

The gene sequences of membrane protein $PorV_{1\text{-}391}$ (containing native signal peptide) and $PorV_{28\text{-}391}$ (native signal peptide removed) were cloned into pET28b at XbaI and XhoI by molecular cloning techniques which are mentioned in section 2.2.1.1-2.2.1.8.

Primers used for PCR amplification and their details are in **Table 2.2**. Details of generated plasmids are in **Table 2.1**.

pOMPA28

To express membrane proteins, using a pET28b vector, I created a synthetic insert (Genscript) containing an OmpA signal peptide and a 6×His sequence, which was cloned into pET28b using NcoI and NotI restriction sites to create vector pOMPA28 (**Figure 2.3A**). This modified vector contains sequences of OmpA signal peptide, a 6×His-tag with enterokinase (EK) site and followed by the cloning sites (**Figure 2.3B**). The gene sequences of membrane protein $PorV_{28\text{-}391}$, $PorU_{24\text{-}1158}$, $PorQ_{38\text{-}346}$, $PorP_{20\text{-}294}$, $PorT_{29\text{-}244}$, $PorF_{37\text{-}827}$, $LpxE_{23\text{-}445}$ and $LpxE_{23\text{-}241}$ were cloned into pOMPA28 at HindIII and NotI by molecular cloning techniques which are mentioned in section 2.2.1.1-2.2.1.8. Primers used for PCR amplification and their details are in **Table 2.2**. Details of generated plasmids are in **Table 2.1**.

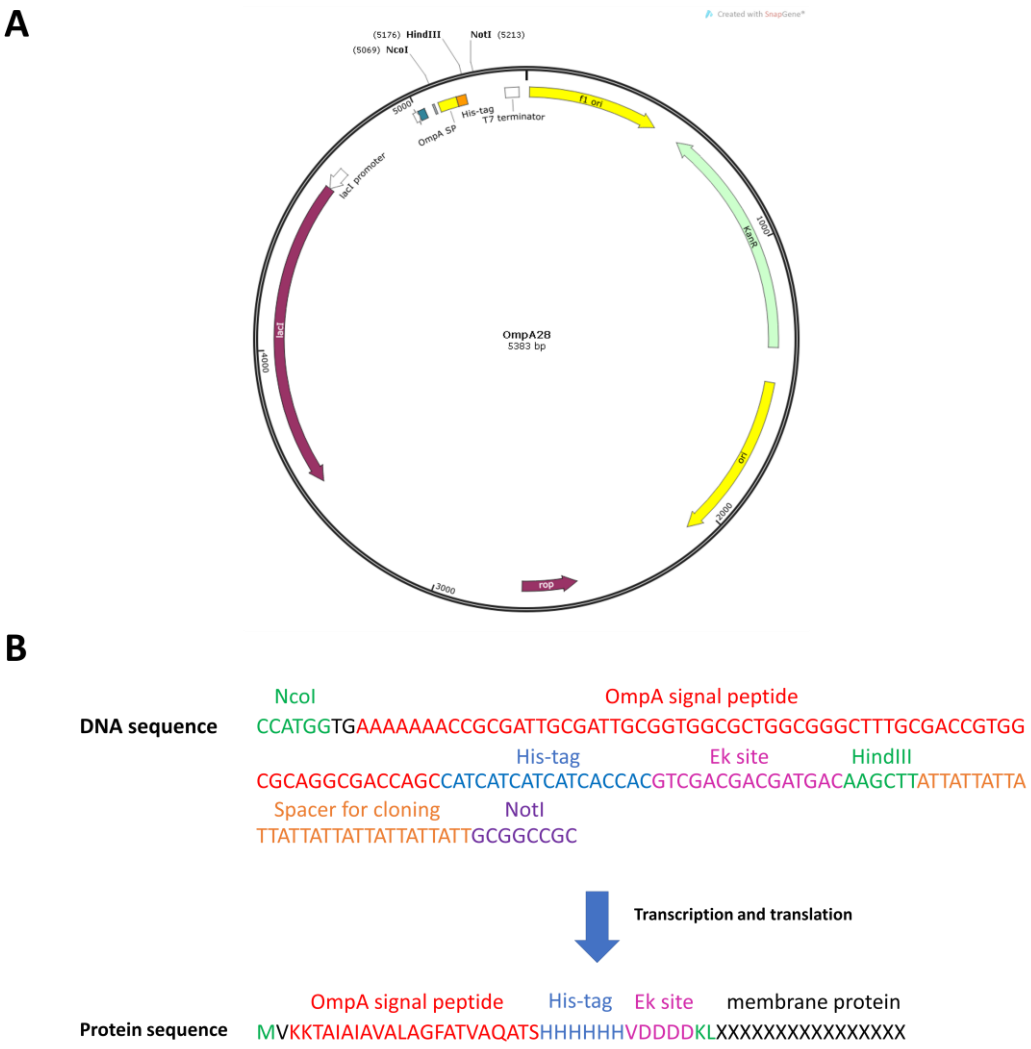

Figure 2.3: Strategies for recombinant expression of membrane proteins. A. The plasmid map of pOMPA28. The pET28b original sequence between NcoI and NotI was replaced with a sequence of OmpA signal peptide, a 6×His-tag with enterokinase (EK) site and followed by the cloning sites. **B.** The features of pOMPA28 expression region. Membrane proteins are cloned into pOMPA28 using HindIII and NotI restriction enzyme sites.

pET46 Ek/LIC

With pET46 Ek/LIC, inserts could be cloned without the need for restriction digestion and ligation. The gene sequence of $LpxE_{242\text{-}445}$ was cloned into pET46 Ek/LIC by ligation-independent cloning, with N-terminal His-tag sequence. Primers used for PCR amplification and their details are in **Table 2.2**. Details of generated plasmids are in **Table 2.1**.

2.2.1.13 Heat-shock transformation

20 µl chemically competent cells (New England Biolabs) were incubated on ice with plasmid for 20 min. Cells were then heat shocked for 30 sec using a 42°C water bath then incubated on ice for 2 min. Outgrowth of transformed cells was achieved using 400 µl LB with 1 hour of 37°C incubation. 50-200 µl culture was then taken and plated on LB agar plates with appropriate antibiotics for selection. BL21(DE3), Lemo21(DE3) and C41(DE3) competent cells were used in this study and their details are in **Table 2.1**.

2.2.2 Microbiology techniques

2.2.2.1 Enzyme assays

P. gingivalis W50 and mutant strains were grown in BHI broth supplemented with hemin (5 µg/ml) in an anaerobic cabinet overnight. The whole cells were obtained by collecting the cell pellet fraction after centrifugation at 9000 g, 4°C for 25 min. The supernatant samples were obtained by collecting the supernatant fraction after centrifugation at 9000 g, 4°C for 25 min.

Arg-specific and Lys-specific protease activities of whole cells and culture supernatants were measured in duplicates[285]. 100 ml of assay buffer was prepared (10 mM L-cysteine, 10 mM calcium chloride and 100 mM Tris-HCl buffer, pH 8.0) along with 10 ml of 0.5 mM DL-BRpNA, dissolved in 10 ml 10% (vol/vol) DMSO and 10 ml of 0.5 mM L-AcLyspNA, dissolved in 10 ml 10% DMSO. Here DL-BRpNA and AcLyspNA act as

substrates which are colourless amide derivatives of nitroanilide, but on hydrolysis a yellow free nitroanilide is released which absorbs at 405 nm. 800 µl of assay buffer and 90 µl of each substrate was then transferred into a microtitre-plate at 30°C and incubated for at least 30 min. 20 µl of culture or supernatant was then added and absorbance was measured at 405 nm. Protease activity was measured over several time points (24, 48, 72 hours).

2.2.2.2 Bacterial growth curves

W50 and mutant strains were inoculated into 10 ml BHI broth supplemented with hemin (5 µg/ml) in an anaerobic cabinet overnight at 37°C. 200 µl of cultures were removed and diluted to the same OD_{600}. These were then grown in an anaerobic cabinet at 37°C. 0.5 ml cultures were removed at different time points and their OD_{600} were measured.

2.2.2.3 Bacterial membrane fractionation

For the preparation of membrane fractions, washed cells from 20 ml of culture were resuspended in 5 ml of TC50 buffer (50 mM Tris-HCl, pH 8, 50 mM NaCl, 5 mM $CaCl_2$), sonicated, and centrifuged at 900 g, 4°C for 10 min to remove unbroken cells. The supernatant was then centrifuged at 48,400 g, 4°C for 30 min to pellet membranes[177].

The membrane pellet containing both inner and outer membranes was resuspended in

TC50 buffer with 0.5% sarcosine, stirring at room temperature for 30 min. A second spin at 48,400 g for 30 min, the supernatant was saved as inner membrane fraction and the pellet was resuspended in 0.72 ml of TC50 buffer containing 1% (vol/vol) Triton X-114 and saved as the outer membrane fraction.

2.2.2.4 Purification of LPS and lipid A

Bacteria were cultured for 48 hours in BHI medium containing hemin at a concentration of 5 μg/ml. LPS was isolated using a modified version of the Tri-Reagent protocol for LPS isolation[289]. To generate lipid A, dried LPS samples were resuspended in 10 mM sodium acetate (pH 4.5) containing 1% (wt/vol) sodium dodecyl sulphate (SDS). The solution was heated at 100°C for 1 hour, followed by lyophilization overnight. The resulting lipid A pellets were washed once in ice-cold 95% ethanol containing 0.02 N HCl and then three times in 95% ethanol, followed by a final extraction with 1,160 μl of chloroform-methanol-water (1:1:0.9 = vol/vol/vol) to remove residual carbohydrate contaminants. The chloroform layer containing the lipid A was dried and used for matrix-assisted laser desorption ionization-time of flight mass spectrometry (MALDI-TOF MS) or MALDI-TOF/TOF tandem MS analyses.

2.2.2.5 MALDI-TOF mass spectrometry

For MALDI-TOF MS analyses, lipid A samples were dissolved in 10 μl of a mixture of

5-chloro-2-mercaptoben-zothiazole (20 mg/ml) in chloroform-methanol at 1:1 (vol/vol), and 0.5 µl of each sample was analysed in both positive- and negative-ion modes on an AutoFlex Analyzer (Bruker Daltonics)[290]. The data were acquired with a 50 Hz repletion rate and up to 3,000 shots were accumulated for each spectrum. Instrument calibration and all other tuning parameters were optimized using HP Calmix (Sigma-Aldrich). The data were acquired and processed using FlexAnalysis software (Bruker Daltonics)[290].

2.2.2.6 Transmission electron microscope

10 ml cultures of *P. gingivalis* W50 and mutant strains were grown in BHI broth containing hemin for 24 hours and the cultures were then used for transmission electron microscope (TEM) imaging.

Formaldehyde fixation

Cells were fixed for 2 hours at room temperature in 100 mM phosphate buffer pH 7.0 containing 3% (wt/vol) glutaraldehyde, 1% (wt/vol) formaldehyde and 0.5% (wt/vol) tannic acid, washed with phosphate buffer, and incubated in 2% (wt/vol) OsO_4 in phosphate buffer overnight. Bacterial cells (10 µl) were then applied to mesh copper grids, prepared with glow discharged carbon support films, and incubated for 2 min. The grids were then washed five times with 50 µl of 1% aqueous uranyl acetate. Grids were left to dry for 5 min before being viewed. Micrographs were taken with a JEOL JEM 1230 transmission electron microscope (JEOL, Japan) operated at 80 kV at a

magnification of 80,000 x to 100,000 x. Digital images were recorded using a Morada CCD camera (EMSIS, Germany) and processed via iTEM (EMSIS).

Flash-freeze fixation

Bacteria cultures were concentrated by centrifugation for 5 min at 2000 rpm. They were loaded in gold plated carriers and high-pressure frozen in a Leica EM ICE high-pressure freezer (Leica Microsystems). For ultrastructural analysis, the samples were freeze substituted in a solution of acetone containing 2% (vol/vol) osmium tetroxide, 0.1% (vol/vol) uranyl acetate, and 5% (vol/vol) distilled water in the Leica AFS. The samples remained at -90°C for 10 hours, and subsequently warmed to -20°C over a period of 12 hours. Samples were transferred to 4°C for 30 min, followed by washing with anhydrous acetone at room temperature. The samples were infiltrated and embedded in Spurr resin. Sections of 70 nm were collected using a Leica UC7 ultramictrome, followed by post staining with lead citrate. Image acquisition was done automatically, using the "Limitless Panorama" (LLP) feature in a JEM 1400 Flash running at 80 kV (JEOL).

2.2.2.7 NanoSight analysis

5 ml cultures of *P. gingivalis* W50 and mutant strains were grown in BHI broth overnight (OD_{600} = 2) and then centrifuged at 26,000 g and 4°C for 30 min. The supernatant was filtered with a 0.22-µm filtration apparatus. The filtrate containing OMVs was diluted 10-fold and subjected to Malvern NanoSight LM10 nanoparticle

characterisation. Using a laser light source with a wavelength of 405 nm (blue), 532 nm (green), or 638 nm (red), the particles in each sample were illuminated, and the scattered light captured by the camera and displayed on the connected personal computer running nanoparticle tracking analysis (NTA) software. This then allowed the particles to be automatically tracked and sized, with results displayed as a frequency size distribution graph.

2.2.2.8 Quantification of OMVs

200 ml cultures of *P. gingivalis* W50 and mutant strains grown in BHI broth for 24 hours were centrifuged at 26,000 g and 4°C for 40 min. The supernatant was filtered with a 0.22-µm filtration apparatus. The filtrate was subjected to ultracentrifugation at 180,000 g and 8°C for 1 hour. The pellet was resuspended in sterile phosphate-buffered saline, and the ultracentrifugation step was repeated, followed by resuspension of the pellet in water and freeze-drying. The yield of OMVs was taken as the dry weight in milligrams per 200 ml of culture.

2.2.2.9 Colony inhibition assay

Cecropin B, LL-37, SDS and Triton X-100 was added to blood agar medium, at final concentration of 10 mM, 10 mM, 8 µg/ml and 35 µg/ml, respectively. A *P. gingivalis* culture at OD_{600} = 0.5 was then diluted 10^1, 10^2, 10^3, 10^4 and 10^5-fold. 5 µl of each

dilution was then spotted onto the blood agar containing antimicrobial peptide or detergent. The plates were cultured at 37°C anaerobically for 5 days.

2.2.2.10 *In vivo* cross-linking

20 ml cultures of *P. gingivalis* grown in BHI-H broth for 24 hours were centrifuged at 26,000 g and 4°C for 30 min. Cells were then washed twice with PBS and resuspended in 5 ml PBS.

For dithiobis (succinimidyl propionate) (DSP) cross-linking, DSP was added to cells at a final concentration of 2 mM and incubated at room temperature for 30 min. Stop solution (1 M Tris, pH 7.5) was then added to a final concentration of 50 mM and incubated for 15 min.

For formaldehyde cross-linking, formaldehyde was added at 1% and incubated at room temperature for 30 min. Stop solution (1 M Tris, pH 7.5) was then added at a final concentration of 50 mM and incubated for 15 min.

2.2.2.11 Co-immunoprecipitation

Co-immunoprecipitation (Co-IP) reactions were performed using the BioVision immunoprecipitation kit according to manufacturer's instructions.

Non-cross-linked and cross-linked cells were collected by centrifugation. For reactions in which no chemical cross-linking was performed the non-denaturing lysis buffer,

supplemented with protease inhibitor, was used for protein extraction. For reactions involving chemical cross-linking the denaturing RIPA lysis buffer was used. 5 µl of anti-HA mouse immunoglobulin (Thermo) was added to each sample and left to incubate overnight at 4°C with gentle mixing.

For target protein capture, 30 µl of pre-equilibrated Protein A/G beads were used per sample for antibody capture and suspensions incubated at 4°C for 1 hour. Beads were washed three times using 1 ml of kit wash buffer and all samples were eluted using a denaturing method via the addition of 40 ml 2×SDS-PAGE loading buffer. Target protein capture was also tried with Pierce® anti-HA agarose, according to the manufacturer's instructions.

2.2.3 Protein techniques

2.2.3.1 SDS-PAGE

Protein samples were mixed with 4×LDS sample buffer containing reducing agent (Invitrogen) and then heated up to 100°C for 5 min. Samples were then loaded into a NuPAGE Bis-Tris gel mini gel (Invitrogen) with a mini tank (Invitrogen) and ran at 180 V for 40 min in MES SDS running buffer (Invitrogen). Protein colour standard (New England Biolabs) was used as a marker to determine the size of protein bands.

2.2.3.2 Western blot

Following SDS-PAGE, gels were removed from their cassette and transferred to an iBlot®2 PVDF transfer stack (Invitrogen). The stack was prepared according to the manufacturer's instructions and ran using the pre-set P0 method for 7 min. The PVDF membrane was then transferred to 10 ml blocking buffer (3% BSA in TBST buffer (150 mM NaCl, 20 mM Tris-HCl, 0.1% Tween 20, pH 7.4)) and left to block in the cold room overnight. The membrane was then washed three times with TBST and then left to incubate with the primary antibody diluted in blocking buffer for 2 hours at room temperature (anti-CTD, 1B5, 3158, 1A1 and Rb7 antibodies diluted 1:1000). The membrane was then washed three times with TBST for 10 min and then incubated with the secondary antibody at room temperature for 2 hours (anti-mouse or anti-rabbit diluted to 1:2000). The membrane was then washed a further three times with TBST before development with either 3,3'-diaminobenzidine (DAB) or enhanced chemiluminescence (ECL). The DAB solution was prepared by adding 25 mg of DAB to 50 ml of PBS and 33 µl of hydrogen peroxide was added immediately prior to use. 10 ml was added to the membrane and the reaction allowed to develop for 5 min or until protein bands were visible. The reaction was stopped by the remove of DAB solution and resuspension of 10 ml H_2O. Alternatively, ECL was prepared using the ClarityTM western ECL substrate kit (Biorad). 7 ml substrate mix was prepared by mixing the two substrate solutions at a 1:1 ratio. The solution was added to the blot and incubated for 5 min before imaging with a ChemiDocTM MP imaging system (Biorad).

2.2.3.3 Membrane protein expression

Prior to large-scale expression of recombinant membrane proteins, small scale protein expression trials were performed. The relevant plasmids were transformed into BL21, Lemo21 or C41 cells by heat-shock transformation. The transformants were grown overnight on LB agar plates at 37°C with appropriate antibiotic selection. Single colonies were then transferred to 10 ml LB in 30 ml universal bottles containing the appropriate antibiotic. In addition, Lemo21 cultures were supplemented with 0, 100, 250, 500, 750, 1000 and 2000 µM L-rhamnose. Cultures were grown at 37°C with 240 rpm shaking to an OD_{600} of ~0.4 and then induced with 0 or 0.4 mM IPTG. Cells were grown post-induction at 20°C for 16 hours with 200 rpm shaking.

0.5 ml samples from each culture were taken and centrifuged at 13, 000 g for 1 min. The cell pellet was resuspended in 50 µl of 1×BugBuster® protein extraction reagent, prepared from a 10×stock solution diluted in phosphate buffered saline (PBS; 137 mM NaCl, 2.7 mM KCl, 10 mM Na_2HPO_4 and KH_2PO_4, pH 7.4). Cells were incubated at room temperature for 15 min with gentle mixing and then centrifuged again at 16, 000 g for 20 min at 4°C to remove insoluble material. The supernatant was then mixed with 50 µl of 2×SDS-loading buffer. Additional 0.5 ml samples were taken from each culture and resuspended in 100 µl 1×SDS-loading buffer. Samples were then analysed by SDS-PAGE and Western blot.

2.2.3.4 Optimization of membrane protein purification

Membrane protein solubilisation efficiency was tested using a series of detergents. Purified membranes containing the target protein was suspended in buffer containing 20 mM Tris, pH 8 and 200 mM NaCl. The buffer was supplemented with 1% octyl-β-D-glucoside (OG; Sigma Aldrich), 1% n-dodecyl-β-D maltopyranoside (DDM; Sigma Aldrich), 1% lauryldimethylamine oxide (LDAO; Sigma Aldrich) or 1% tetraethylene glycol monooctyl ether (C_8E_4; Sigma Aldrich). The suspension was left to slowly mix at room temperature on a rolling-mixer for one hour. Samples were then centrifuged at 100, 000 g, 4°C for 30 min and the supernatant retained as the solubilised protein fraction. The pellet was resuspended in buffer containing 20 mM Tris, pH 8, 200 mM NaCl and 2% SDS. Soluble vs insoluble fractions for each solubilising agent were then analysed by Western blot.

For extraction of bacterial membranes containing folded membrane protein large-scale cultures were collected after 16 hours of protein expression by centrifugation at 5000 g for 15 min at 4°C. The pellet was resuspended in ice-cold lysis buffer (20 mM Tris-HCl pH 8.0, 200 mM NaCl, 10% Glycerol, 0.1% Triton X-100 and 1×cOmplete™ EDTA-free protease inhibitor cocktail (Sigma Aldrich)) at approximately 5 g/ml of wet cell weight. Samples were then sonicated on ice for 3 min at 70% power with 3 sec pulses. Sonicated samples were centrifuged at 20, 000 g for 30 min at 4°C to remove cellular debris. The supernatant was collected and centrifuged at 100,000 g, 4°C for 1 hour to pellet bacterial membranes. The pellet was resuspended in buffer containing 20 mM

Tris pH 8, 200 mM NaCl and 1% LDAO. The suspension was left to mix for 45 min at room temperature on a rolling mixer. The suspension was centrifuged again at 100,000 g for 1 hour at 4°C to remove insoluble material. The supernatant was retained as the solubilised membrane fraction and then analysed by SDS-PAGE or Western blot.

2.2.3.5 Large scale membrane protein purification

E. coli BL21 (DE3), Lemo21 (DE3) or C41 (DE3) cells transformed with a relevant expression vector were grow to an OD_{600} of 0.6-0.8 at 37°C in LB medium before overnight induction at 20°C with 0.4 mM IPTG. Cells were harvested and resuspended in 20 mM Tris-HCl pH 8, 1 μg/ml DNaseI, 1 μM PMSF and lysed by sonication followed by centrifugation at 23,000 g for 20 min. The OM fraction was prepared by centrifugation of the supernatant at 100,000 g for 2 hours. The pellet was then resuspended in 20 mM Tris-HCl pH 8, 0.5% sarcosine, while stirring at room temperature for 30 min. This was followed by a second spin at 100,000 g for 1.5-2 hours and then the pellet was resuspended for overnight extraction at 4°C with 20 mM Tris-HCl pH 8, 200 mM NaCl, 1% detergent. Protein was then purified from the solubilized outer membrane fraction by nickel-affinity chromatography. The column was washed with 30 ml 20 mM Tris-HCl pH 8.0, 200 mM NaCl, 0.1% detergent, 20 mM imidazole, washed again with 30 ml 20 mM Tris-HCl pH 8.0, 200 mM NaCl, 0.1% detergent, 20 mM imidazole and eluted with 20 mM Tris-HCl pH 8.0, 200 mM NaCl, 0.1% detergent, 500 mM imidazole. The protein samples were concentrated to 1-3 ml and then applied

to a Superdex 200 column at a flow rate of 1 ml/min and 3 ml fractions were collected over 120 ml.

2.2.3.6 Protein refolding

Cells containing PorV were resuspended in 20 mM Tris-HCl pH 8, 8 M urea, lysed by sonication and purified using nickel affinity chromatography. PorV was then refolded by dialysis against 20 mM Tris-HCl pH 8, 4 M urea, 200 mM NaCl, 1% LDAO followed by 20 mM Tris-HCl pH 8, 200 mM NaCl, 1% LDAO. Samples were then gel filtered using a Superdex 200 column (GE Healthcare) equilibrated in 20 mM Tris-HCl pH 8, 200 mM NaCl, 1% LDAO.

2.2.3.7 Far Western blot

Serial dilutions of bait protein PorV were applied to a pre-cut, dry membrane leaving at least 1 cm of space between the centres of each dot of the series. BSA which does not bind the prey protein RgpB-CTD was applied to the membrane as a negative control. RgpB-CTD antibody which binds the prey protein RgpB-CTD was applied to the membrane as a positive control. The membrane was dried before the next step. The membrane was placed in blocking buffer for 1 hour at room temperature on an orbital shaker with gentle agitation to block the membrane. Blocking buffer was removed and replaced with protein binding buffer containing the prey protein RgpB-CTD for at least

6 hours of incubation at 4ºC with gentle agitation. The membrane was washed 3 times in blocking buffer for 15 min each with gentle rotation. The membrane was incubated in blocking buffer containing RgpB-CTD antibody (1:1000 dilution) overnight at 4°C with gentle agitation. The primary antibody solution was removed and washed 3 times with blocking buffer for 5 min each. The blot was placed in secondary antibody HRP-conjugated anti-rabbit solution diluted 1:2000 in blocking buffer for 2-3 hours gentle rotation. The membrane was washed 3 times in blocking buffer for 15 min each with gentle rotation. ECL was prepared using the ClarityTM western ECL substrate kit (Biorad). 7 ml substrate mix was prepared by mixing the two substrate solutions at a 1:1 ratio. The solution was added to the blot and incubated for 5 min before imaging with a ChemiDocTM MP imaging system (Biorad).

Chapter 3 Characterization of Outer Membrane Accessory Proteins from the *P. gingivalis* Type-IX Secretion System

3.1 Chapter aims

This chapter seeks to understand how the *P. gingivalis* type-IX secretion system (T9SS) affects outer membrane vesicle (OMV) formation. In previous studies, an electron-dense surface layer (EDSL) surrounding the outer membrane (OM) had been seen in *P. gingivalis* wild-type strain[155]. This layer is composed of fully processed T9SS cargo proteins that are attached to the cell surface by A-LPS. However, the EDSL was absent in *porV* and *porT* mutants[155]. This EDSL was also not present in a *porU* mutant, which produced irregular large OMVs that were similar in size to those of a *porT* mutant[177]. Furthermore, a *porV* (*lptO*) mutant has again been observed to form abnormally large OMVs and *porV* was shown to be required for lipid A 1-phosphatase activity in *P. gingivalis* W50[152]. Although these studies suggest that knocking out the T9SS components *porV*, *porU* and *porT* have an influence on OMV formation, the interplay between the T9SS and OMV biogenesis has yet to be elucidated.

In *P. gingivalis*, the protein compositions of whole cells and OMVs are different. It has been suggested that outer membrane proteins (OMPs) and T9SS substrates account for only 21.6% of proteins in *P. gingivalis* whole cell lysates but account for 98% of proteins in OMVs, reflecting their considerable enrichment in OMVs. These enriched OMPs include most of the T9SS outer membrane components[291]. According to the above evidence, it has been speculated that the T9SS OM accessory proteins may have important roles in OMV biogenesis. When starting this research project, the protein Sov had been identified as the main porin in the *P. gingivalis* T9SS, but the functions of the other components was still unclear. Therefore, the other OM components of the T9SS

are referred to here as OM accessory proteins. Thus, the first aim was to create knock-out mutants of *porV*, *porU*, *porQ*, *porZ*, *porP*, *porT*, *porG* and *porF* in *P. gingivalis* and determine the phenotypes of these mutants using *in vivo* assays.

3.2 Mutagenesis of T9SS outer membrane accessory proteins

Genes encoding T9SS outer membrane components are located in separate operons in the *P. gingivalis* genome (**Figure 3.1**). An operon contains one or more structural genes which are generally transcribed into one polycistronic mRNA (a single mRNA molecule that codes for more than one protein). To create T9SS knock-out mutants, the mutagenesis strategy aimed to insert an *erm* cassette to inactivate the target gene. However, this can lead to polar effects which affect the expression of downstream genes transcribed within the same polycistronic mRNA.

Although *porU* and *porV* are adjacent, the fact that both *porU* and *porV* mutants can be complemented separately[152,177] implies that their expression is independent. Both *porG* and *porZ* are at the 3′ end of their operons, suggesting that their mutations would not influence transcription of upstream genes. *porF* and *porT* are in single gene operons, thus the mutagenesis would not cause any polar issues. *porQ* is in an operon containing two unidentified genes *PG0603* and *PG0604*, indicating that mutation of *porQ* may affect the expression of these two uncharacterized genes. Five genes *porP*, *porK*, *porL*, *porM* and *porN* are in the same operon and they have been experimentally shown to be co-transcribed[185]. This suggests that mutation of *porP* may affect the expression of

porK, *porL*, *porM* and *porN*. Nevertheless, PorK is detected in a *porP* mutant[50], indicating the mutation in *porP* is independent on *porK* expression. Taken together, except *porQ* and *porP*, mutations of these T9SS outer membrane components theoretically would not cause polar issues.

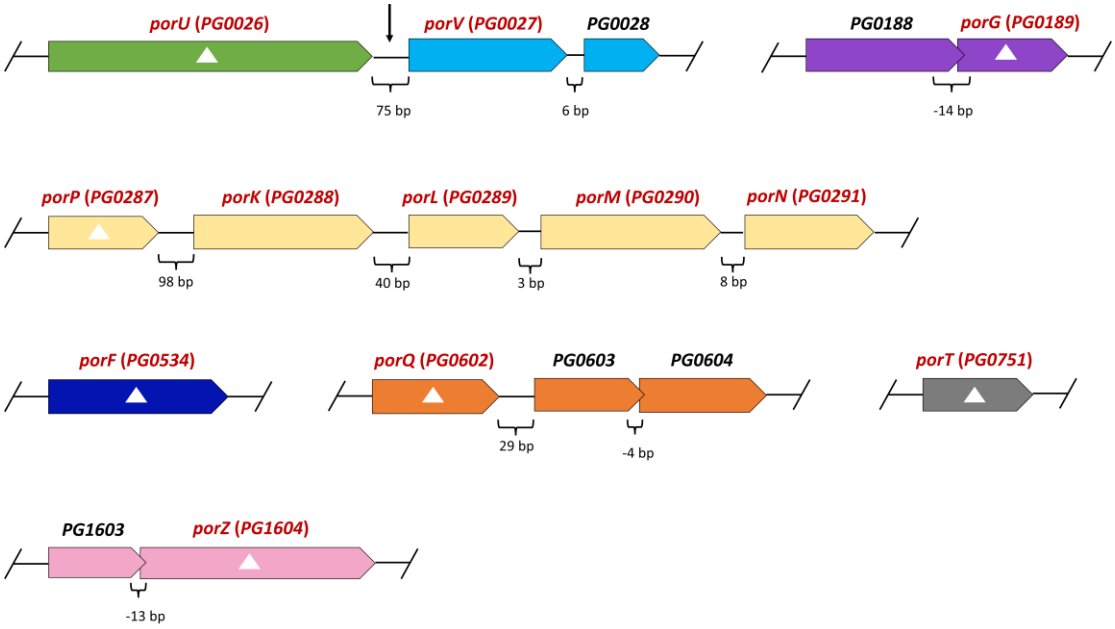

Figure 3.1: Arrangement of *P. gingivalis* W50 genes encoding T9SS outer membrane components. Genes are divided into groups according to *in silico* operon predictions, reflecting direction of transcripts[292,293,294,295]. Gaps in the genome are indicated by the slashes. Intervals between adjacent genes or overlapping regions (in base pairs-bp) are marked below each section. None of the adjacent genes encode T9SS cargo proteins. Each transcription unit is shown in a different colour. Genes encoding T9SS components are depicted in red font. The genes to be mutated are marked with white triangles. The black vertical arrow shows a continuous region (75 bp) between *porU* (*PG0026*) and *porV* (PG0027) but the two genes are predicted to be transcribed independently.

To evaluate the effects of T9SS outer membrane accessory proteins on OMV production, the knock-out mutants were produced in *P. gingivalis*. The Δ*porV* strain had already been created in our lab from a previous study[152]. Thus, the plan in this study was to generate additional Δ*porU*, Δ*porQ*, Δ*porZ*, Δ*porP*, Δ*porT*, Δ*porG* and Δ*porF* knock-out mutants in *P. gingivalis* W50 strains. An *erm* (*ermF-ermAM*) cassette was used as

the positive selector. Flanking regions of the gene were designed and tagged to the cassette at 5′ and 3′ ends by PCR. The construct was then targeted to the genomic gene to be modified by electroporation, and then positive colonies on blood agar plates were selected by clindamycin resistance. Finally, correct insertions of the cassette into the required coding regions of these genes were confirmed by colony PCR (**Figure 3.2**). As this is a well-established method in our lab and most of these mutants have been reported using similar methods (e.g. Δ*porV*[152], Δ*porU*[177], Δ*porQ*[179], Δ*porZ*[109], Δ*porP*[50], Δ*porT*[155], Δ*porG*[296] and Δ*porF*[189]), quantitative real-time PCR (qPCR) was not performed to verify gene expression. However, complementation of these mutants and mRNA analysis[87] would be needed to confirm that these mutations do not cause any polar issues.

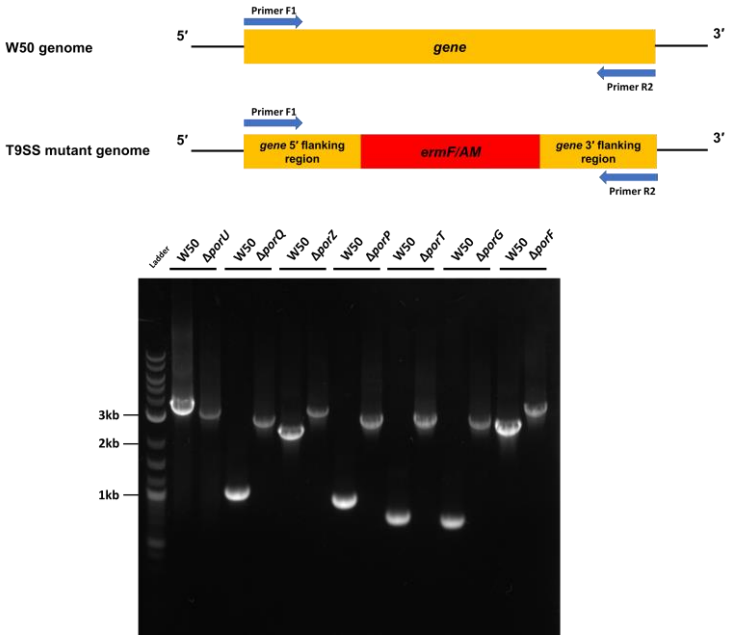

Figure 3.2: Colony PCR of *P. gingivalis* W50 and T9SS mutants. Primers at the ends of 5′-region and 3′-region of target gene were used to amplify target DNA fragment. Genomic DNA of W50, Δ*porU*, Δ*porQ*, Δ*porZ*, Δ*porP*, Δ*porT*, Δ*porG* and Δ*porF* were used as colony PCR templates. A distinct band shift was seen between W50 and mutants, suggesting Erm cassette was successfully inserted into the coding regions of *porU*, *porQ*, *porZ*, *porP*, *porT*, *porG* and *porF*. Number ladders on the left-hand side represent the size of marker DNA in kb.

3.3 Characterization of type-IX knock-out mutants

3.3.1 Pigmentation

Colonies of wild-type *P. gingivalis* W50 were grown anaerobically on blood agar plates and presented the expected black pigmentation (**Figure 3.3**). This black pigment is composed of μ-oxo-bisheme $[Fe(III)PPIX]_2O$, and requires both Arg- and Lys-gingipains for its production[297,298,299]. RgpA first promotes the formation of methemoglobin from oxyhemoglobin, which is then degraded by Kgp to form the black pigment μ-oxo-bisheme[300]. Therefore, a lack of pigmentation indicates a defect in gingipain expression, maturation and/or secretion. The T9SS mutant strains created here were not able to form black pigment. Δ*porU*, Δ*porQ*, Δ*porZ* and Δ*porF* displayed light brown colonies after 7 days of incubation, which turned darker after 14 days. Whether grown for 7 days or 14 days, the colours of Δ*porQ* and Δ*porZ* were consistent and were darker than Δ*porU* and Δ*porF* (**Figure 3.3**). More significant phenotypes were observed in Δ*porV*, Δ*porP*, Δ*porT* and Δ*porG*, as these mutants presented a non-pigmented colony phenotype on blood agar (**Figure 3.3**). These results suggest these T9SS outer membrane accessory proteins are required for the secretion of Kgp and RgpA, but they may have different roles during T9SS dependent secretion.

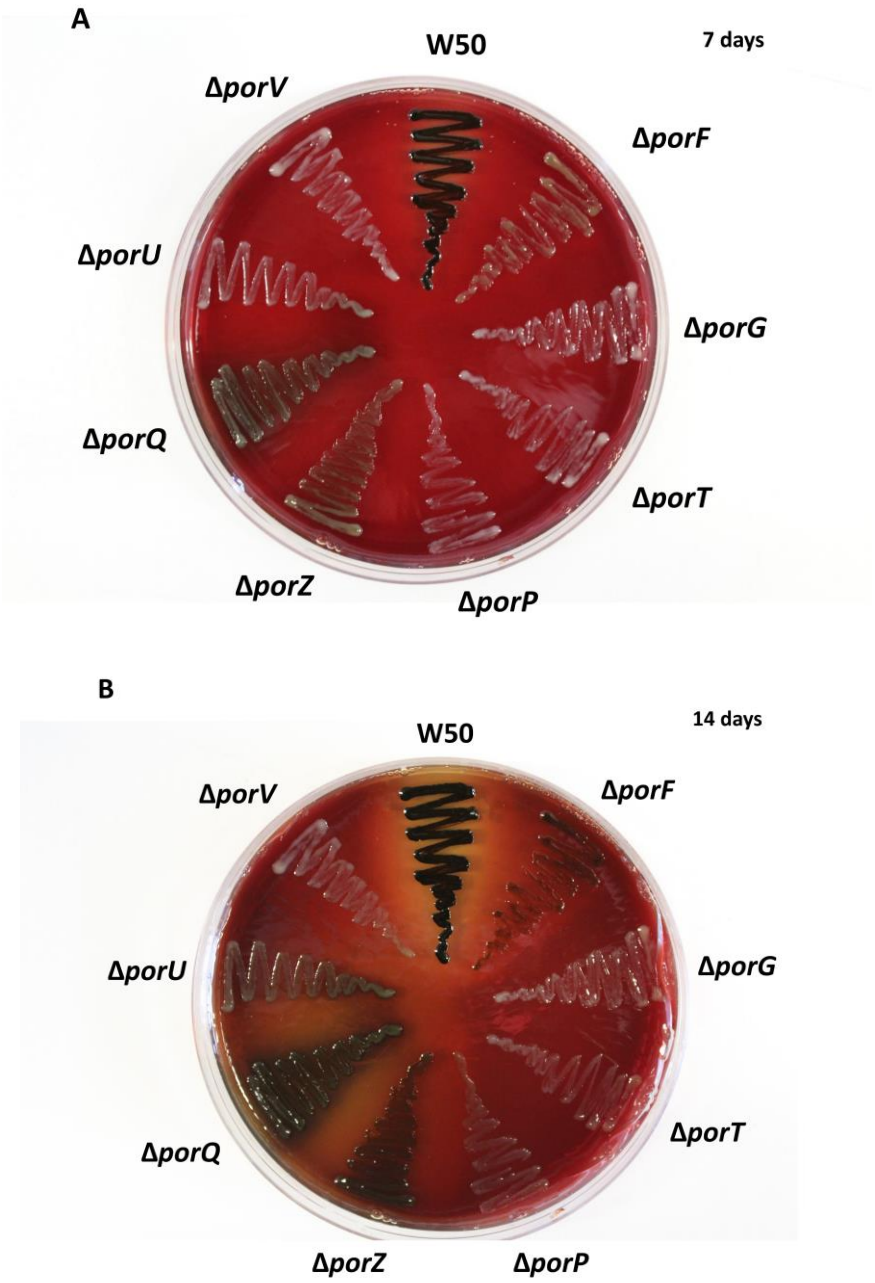

Figure 3.3: Colony morphology of *P. gingivalis* W50 and T9SS mutants. The *P. gingivalis* W50, Δ*porV*, Δ*porU*, Δ*porQ*, Δ*porZ*, Δ*porP*, Δ*porT*, Δ*porG* and Δ*porF* strains grew anaerobically on blood agar plates for **A.** 7 days. **B.** 14 days. The W50 presented black pigmentation. Δ*porU*, Δ*porQ*, Δ*porZ* and Δ*porF* presented light brown colonies, and the colours of colonies turned darker after 14 days of incubation. Δ*porV*, Δ*porP*, Δ*porT* and Δ*porG* displayed a non-pigmented colony phenotype on blood agar. This assay was biologically repeated three times, and this is a typical representation.

It has previously been shown that *P. gingivalis* W50 *rgpA/rgpB* and *kgp* mutants have pigmentation defects when grown on blood agar plates[299]. However, pigmentation of

these mutants is restored after cross-streaking on plates where *P. gingivalis* W50 has previously grown, although this is not seen in mutants that affect A-LPS production or T9SS dependent secretion (e.g., Δ*porR*, Δ*waaL*, Δ*wzy* and Δ*PG0129*)[299]. This is thought to be because *rgpA/rgpB* and *kgp* mutants can still pigment if hemin is supplied externally, while mutants affecting T9SS dependent secretion cannot. A cross-streaking assay was therefore performed to confirm that the non-pigmentation of T9SS mutants was caused by the disruption of the T9SS.

P. gingivalis W50 was first vertically streaked on a blood agar plate and followed by the formation of a zone of hemolysis (3 days), the cells were removed with a swab containing clindamycin to suppress regrowth of the wild-type strain. The plates were then horizontally cross-streaked with the T9SS mutants and *kgp* mutant (Δ*kgp*) and grown for a further 6 days (**Figure 3.4**). As anticipated, Δ*kgp* formed non-pigmenting colonies when grown alone on blood agar plates, but it pigmented when cross-streaked on plates where *P. gingivalis* W50 had been previously grown. However, cross-streaking of T9SS mutants on blood agar plates as above did not lead to any pigment. This indicates that these mutants cannot harness environmental hemin and retain it on their cell surfaces, and also confirms that the non-pigmentation of T9SS mutants was caused by the disruption of the T9SS.

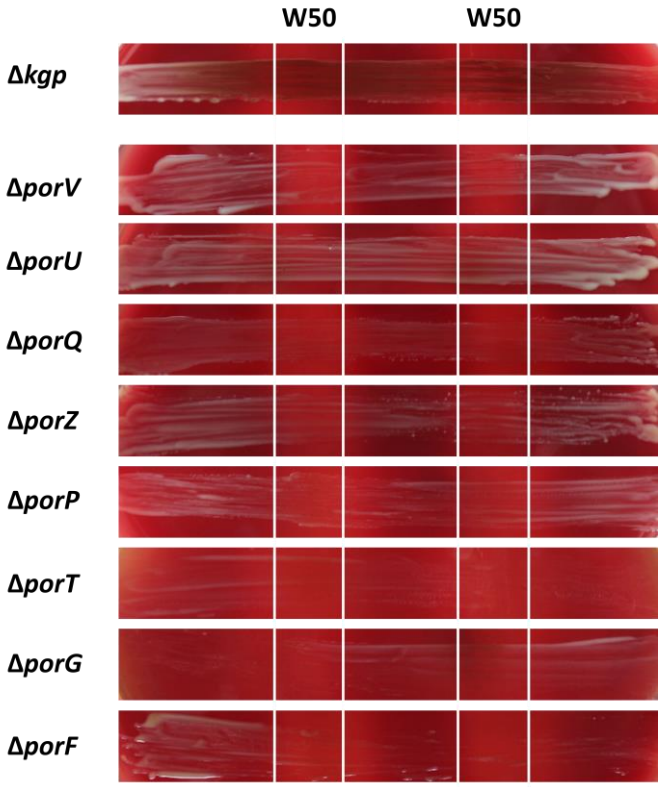

Figure 3.4: Cross-streaking of *P. gingivalis* T9SS mutants and *kgp* mutant. Cross-streaking of *P. gingivalis* Δ*kgp*, Δ*porV*, Δ*porU*, Δ*porQ*, Δ*porZ*, Δ*porP*, Δ*porT*, Δ*porG* and Δ*porF* strains on blood agar. *P. gingivalis* W50 was initially streaked on a blood agar plate and following the formation of a zone of hemolysis (3 d), the cells were removed with a swab containing clindamycin to suppress regrowth of the wild-type strain and the plates were cross-streaked with Δ*kgp* and T9SS mutant strains. Pigmentation of Δ*kgp* took place on the zone of hemolysis whereas Δ*porV*, Δ*porU*, Δ*porQ*, Δ*porZ*, Δ*porP*, Δ*porT*, Δ*porG* and Δ*porF* did not pigment even after 6 d of growth. This experiment was not repeated due to time restriction.

3.3.2 Growth rate analysis

To determine the effects of *porV*, *porU*, *porQ*, *porZ*, *porP*, *porT*, *porG* and *porF* deficiency on the growth of *P. gingivalis* W50, the growth rates of these T9SS mutants were next assessed using a typical growth curve method. Bacterial density (OD_{600}) was monitored over 3 days and significant difference in growth between the W50 and mutant strains was observed during the late logarithmic, stationery and death phases (**Figure 3.5**). Besides, these T9SS mutants also presented different growth

characteristics. For example, at logarithmic phase, the growth rates Δ*porV*, Δ*porG*, Δ*porQ* and Δ*porZ* were similar, but Δ*porV* and Δ*porG* lysed more quickly than Δ*porQ* and Δ*porZ* at late death phase. Δ*porP*, Δ*porT* and Δ*porF* were the most defective mutants at logarithmic phase. Δ*porP* showed the most defective growth at each phase, implying that knocking out *porP* may disrupt PorK, PorL, PorM and PorN. Δ*porU*, Δ*porQ* and Δ*porT* reached their stationary phase at similar times, while Δ*porU* lysed more slowly than the other two mutants.

Before reaching the stationary phase, the growth rates of the *porV*, *porU*, *porQ*, *porZ*, *porP*, *porT*, *porG* and *porF* were slower than W50. Furthermore, the growth curve of W50 reached the maximum OD_{600} at 24 hours, but the maximum OD_{600} of the *porV*, *porU*, *porQ*, *porZ*, *porP*, *porT*, *porG* and *porF* occurred later than W50. Thus, at 24 hours, these strains may be in different growth phases. To eliminate the deviations, the student's *t* tests for the maximum OD_{600} of W50 versus Δ*porV*, Δ*porU*, Δ*porQ*, Δ*porZ*, Δ*porP*, Δ*porT*, Δ*porG* and Δ*porF* were calculated and yielded *P* values <0.001, suggesting significant difference between W50 and these T9SS mutants. Also, the high OD bacteria cultures were not diluted, which may lead to deviations of the growth rates. Taken together, these data indicate that the T9SS mutants are defective in growth and supports them having different roles in maintaining the normal growth and death states of *P. gingivalis*.

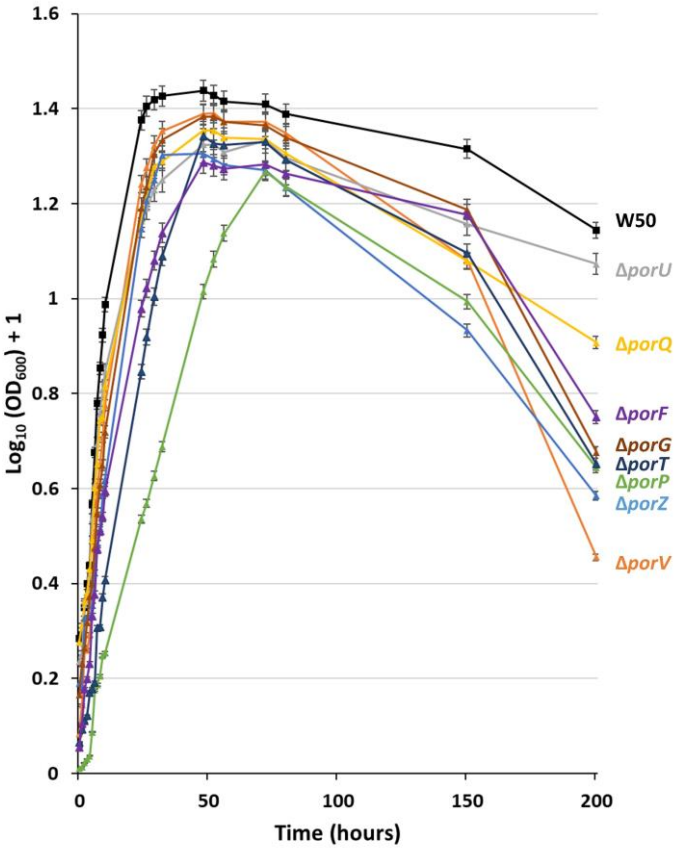

Figure 3.5: Growth curves of *P. gingivalis* W50 and T9SS mutants. Growth curve plotted as [$\log_{10}(OD_{600})$ + 1] versus time for W50, Δ*porV*, Δ*porU*, Δ*porQ*, Δ*porZ*, Δ*porP*, Δ*porT*, Δ*porG* and Δ*porF* grown in BHI broth supplemented with hemin at 37°C in anaerobic cabinet. Samples were withdrawn at each time point under anaerobic condition, and the OD_{600} was measured for 8 days. Three technical repeats of the OD_{600} at each time point were measured. Data are presented as means ± SDs (n = 3). The error bars are shown. Student's *t* test for W50 versus Δ*porV*, Δ*porU*, Δ*porQ*, Δ*porZ*, Δ*porP*, Δ*porT*, Δ*porG* and Δ*porF* at 24 h, 48 h, 72 h, 150 h, and 192 h yielded *P* values <0.001, suggesting significant difference. This assay was replicated, and this is a typical representation.

3.3.3 Enzyme activity analysis

Protease activity on the bacterial cell surface and in the media (soluble factors including OMVs) can be used to assess the ability of the T9SS to export gingipains. Therefore, gingipain protease activity was quantified in these T9SS mutants, and compared with W50 and the *kgp* mutant. Enzyme activity was assesses using substrates which are colourless amide derivatives of nitroanilide, but upon hydrolysis release a yellow free

nitroanilide which absorbs at 405 nm. This was first performed on whole cell samples, reflecting gingipains located in cells or attached to the cell surface, which were obtained by collecting the cell pellet fraction after centrifugation of 20 µl culture. The data suggests that inactivation of either *porF* or *kgp* does not reduce the arginine gingipain (Arg-gingipain) RgpA and RgpB activity in whole cell samples (**Figure 3.6A**). However, significant declines in Arg-gingipain activity were seen in Δ*porU*, Δ*porZ*, Δ*porQ and* Δ*porG*. The results of Arg-gingipain activity in Δ*porV*, Δ*porP* and Δ*porT* were below zero, suggesting that Arg-gingipain activity was completely blocked in whole cells samples of these mutants (**Figure 3.6A**). In whole cell analysis of Δ*porU*, lysine gingipain (Lys-gingipain) Kgp activity was similar to W50 but decreased slightly over the reaction time (**Figure 3.6B**). Lys-gingipain activity in whole cells of Δ*porZ*, Δ*porQ and* Δ*porF* decreased by around 50% of W50. In addition, Lys-gingipain activity in whole cell samples of Δ*porV*, Δ*porP*, Δ*porT*, Δ*porG*, and Δ*kgp* presented flat lines, suggesting no Lys-gingipain activity in these mutants (**Figure 3.6B**).

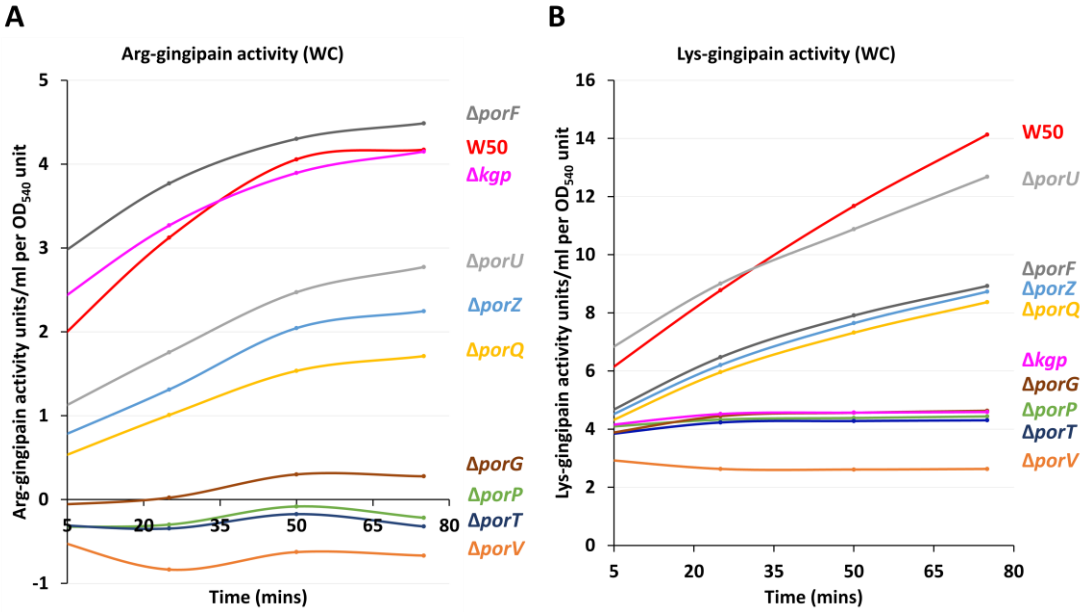

Figure 3.6: Enzyme activity in whole cells of T9SS mutants. Cultures were grown for W50, Δ*porV*, Δ*porU*, Δ*porQ*, Δ*porZ*, Δ*porP*, Δ*porT*, Δ*porG*, Δ*porF* and Δ*kgp* as described in methods. Whole cell (WC) samples were obtained by collecting the cell pellet fraction after centrifugation of 20 µl culture. The optical densities were measured at 540 nm. **A.** Arg-gingipain activity in whole cells of *P. gingivalis* W50, Δ*kgp* and T9SS mutants. Whole cell samples were assayed for Arg-gingipain activity using DL-BRpNA as the chromogenic substrate as described in methods. **B.** Lys-gingipain activity in whole cells of *P. gingivalis* W50, K1A (Δ*kgp*) and T9SS mutants. Whole cell samples were assayed for Lys-gingipain activity using L-AcLyspNA as the chromogenic substrate as described in methods. All the lines were shown in different colours. This data is the average of three technical repeats.

An enzyme activity assay was then performed on culture supernatant samples of these strains, containing OMVs, obtained by collecting the supernatant fraction after centrifugation of 20 µl culture (**Figure 3.7**). Arg-gingipain activity in the supernatant of Δ*porU*, Δ*porF*, and Δ*kgp*, was even higher than that of W50 (**Figure 3.7A**). A decline of Arg-gingipain activity was seen in the supernatant samples of Δ*porQ* and Δ*porZ*. Flat lines were seen in Δ*porV*, Δ*porP*, Δ*porT* and Δ*porG*, suggesting knocking out any of these genes had disrupted Arg-gingipain activity in the supernatant (**Figure 3.7A**). Unexpectedly, Lys-gingipain activity in the supernatant of Δ*porU* was even higher than that of W50 (**Figure 3.7B**). Nevertheless, there were declines in Δ*porZ*, Δ*porQ and*

Δ*porF*, which is in line with the above results of Lys-gingipain activity in whole cells. Similar to the result of Lys-gingipain activity in whole cell samples, no Lys-gingipain activity was detected in supernatant of Δ*porV*, Δ*porP*, Δ*porT*, Δ*porG*, and Δ*kgp* as they all displayed flat lines (**Figure 3.7B**).

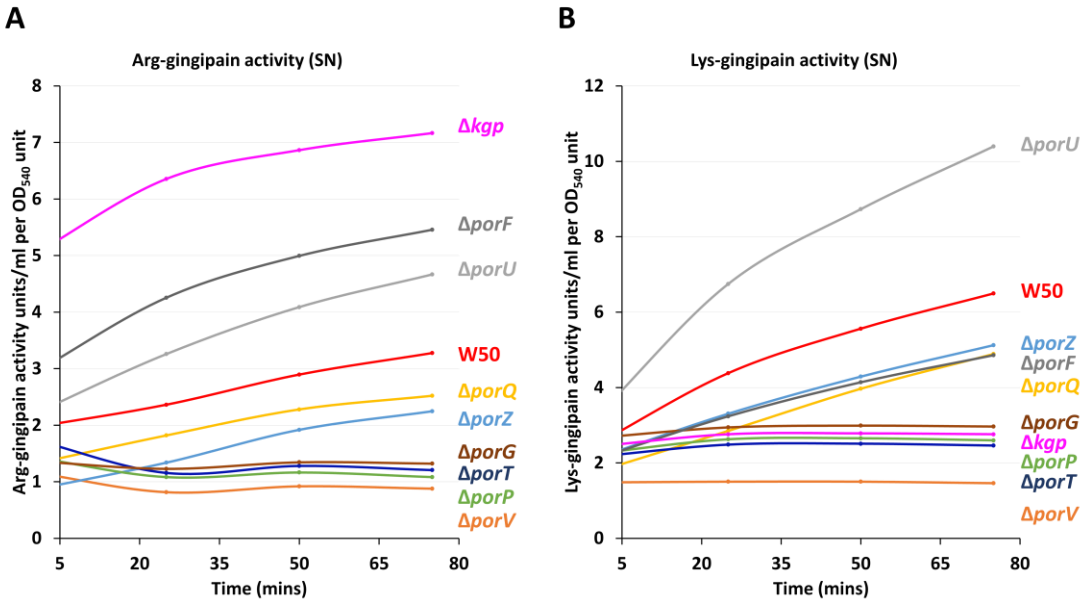

Figure 3.7: Enzyme activity in culture supernatant of T9SS mutants. Cultures were grown for W50, Δ*porV*, Δ*porU*, Δ*porQ*, Δ*porZ*, Δ*porP*, Δ*porT*, Δ*porG*, Δ*porF* and Δ*kgp* as described in methods. Supernatant (SN) samples were obtained by collecting the supernatant fraction after centrifugation of 20 µl culture. The optical densities were measured at 540 nm. **A.** Arg-gingipain activity in culture supernatant of *P. gingivalis* W50, Δ*kgp* and T9SS mutants in culture supernatant. Culture supernatant samples were assayed for Arg-gingipain activity using DL-BRpNA as the chromogenic substrate as described in methods. **B.** Lys-gingipain activity in culture supernatant of *P. gingivalis* W50, K1A (Δ*kgp*) and T9SS mutants. Culture supernatant samples were assayed for Lys-X activity using L-AcLyspNA as the chromogenic substrate as described in methods. All the lines were shown in different colours. This data is the average of three technical repeats.

3.3.4 Secretion analysis

After cleavage of the N-terminal signal peptide by the Sec machinery and translocation into the periplasm, gingipains are composed of the following components: an N-terminal prodomain (NTP), a catalytic domain (CD), an immunoglobulin superfamily-

like domain (IgSF), a hemagglutinin/adhesion (HA) domain and a C-terminal domain (CTD)[98]. Among these proteins, the structure of RgpB is the simplest, as it has no HA domain, while RgpA contains four HA domains ($RgpA_{A1}$-$RgpA_{A4}$) located in the middle of the IgSF and CTD[301]. Kgp also possess three such domains (Kgp_{A1}-Kgp_{A3})[301]. The molecular weight corresponding to each domain is shown in **Figure 3.8**. The effect of these T9SS mutants on the maturation and secretion of gingipains was therefore next analysed by SDS-PAGE and immuno-blotting, monitoring the molecular weight of gingipains, A-LPS and the major proteins RagA and RagB.

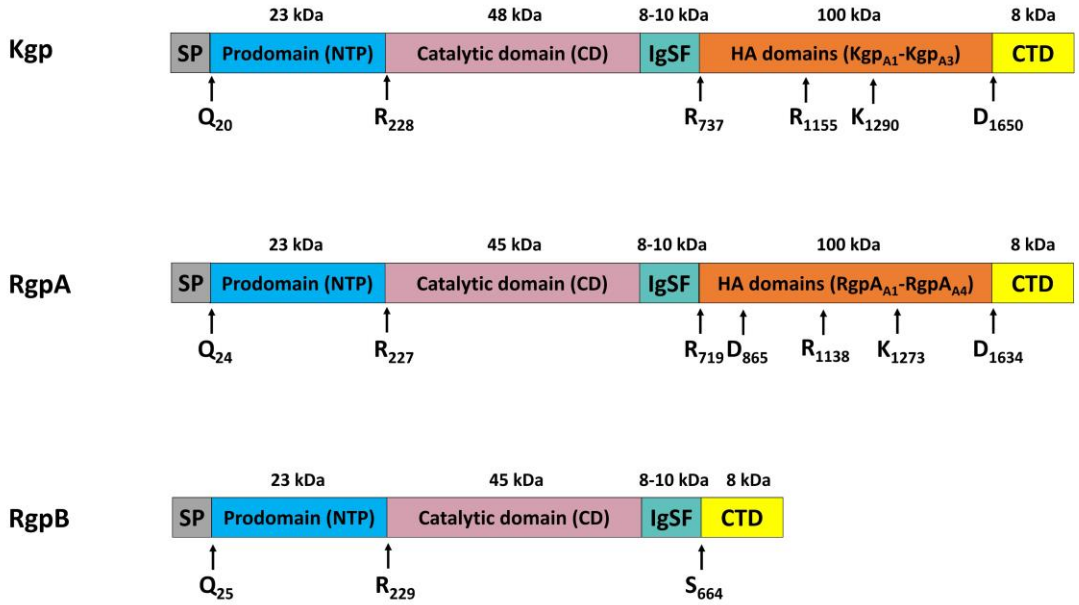

Figure 3.8: Structure of gingipains. The molecular weight of each domain and the internal cleavage sites[302] in Kgp, RgpA and RgpB are shown. Gingipains are made up of the following components: the Sec SP, the N-terminal prodomain (NTP), the catalytic domain (CD), the immunoglobulin superfamily-like domain (IgSF), the hemagglutinin/adhesion (HA) domain, and the C-terminal domain (CTD). The structure of RgpB is the simplest without HA domains. RgpA has four HA domains (named $RgpA_{A1}$ to $RgpA_{A4}$) located in the middle of the IgSF and CTD. Kgp also has such domains (named $KgpA_{A1}$ to $KgpA_{A3}$). Regions of sequence conservation are given the same colouring. Sites of proteolytic processing are indicated with an arrow and residue number.

3.3.4.1 SDS-PAGE of total proteins

Whole cell and supernatant samples of *P. gingivalis* W50 and T9SS mutant strains were collected from overnight growth cultures and first assessed by standard SDS-PAGE to confirm that the total protein amount of the samples was consistent. Proteins in cells or attached to the cell surface were expected to be in the whole cell samples, whereas proteins released in OMVs would be in the supernatant samples. Two major proteins in *P. gingivalis*, RagA and RagB form a peptide importer, where RagA is the barrel channel and RagB acts as the lid[36]. Expected bands for both RagA (110 kDa) and RagB (55 kDa)[303] were present in the whole cells of W50 (**Figure 3.9A**), but RagA was not clearly seen in the supernatant of W50 (**Figure 3.9B**). An expected band for RgpB was evident in either whole cells or supernatant of all the T9SS mutants, however, RgpA was not clearly shown in these mutants. Bands corresponding to the catalytic domain of Kgp (Kgp_{CD} 48 kDa) and the catalytic domains of RgpA ($RgpA_{CD}$ 45 kDa) and RgpB ($RgpB_{CD}$ 45 kDa)[301] were seen in the whole cells of all the mutants. Some unknown bands were also observed either in whole cells or supernatant samples of the T9SS mutants. These indicated that they may be associated with gingipain processing or secretion and were further studied by immunoblot analysis.

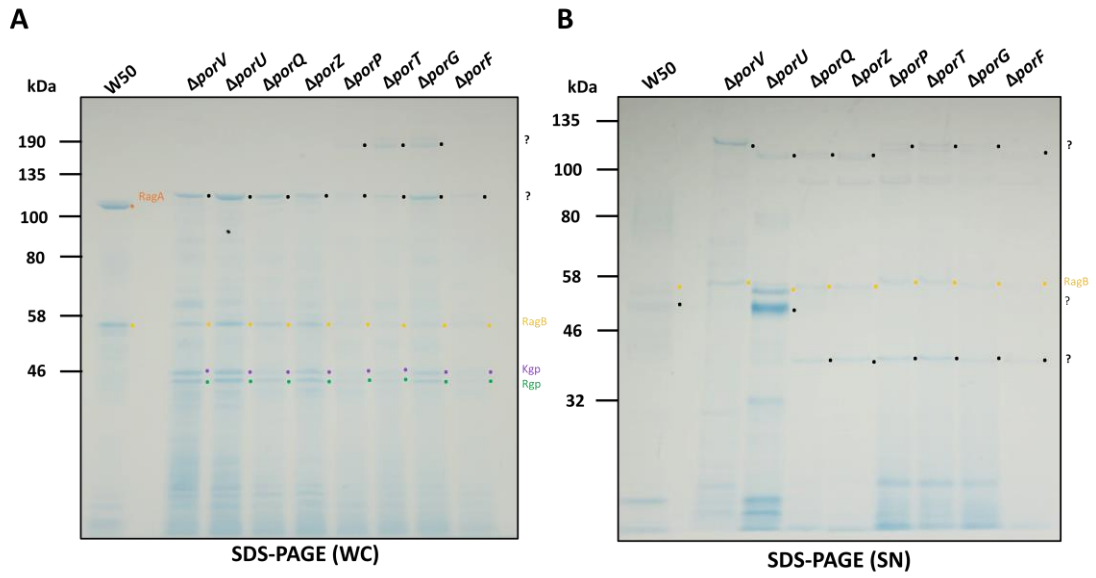

Figure 3.9: SDS-PAGE of total proteins. *P. gingivalis* W50, Δ*porV*, Δ*porU*, Δ*porQ*, Δ*porZ*, Δ*porP*, Δ*porT*, Δ*porG* and Δ*porF* were grown to the same optical density (flask OD_{600} of 1.00). Whole cell (WC) samples were obtained by collecting the cell pellet fraction after centrifugation of 20 µl culture. Supernatant (SN) samples were obtained by collecting the supernatant fraction after centrifugation of 20 µl culture. Based on band size, the designated proteins are dotted in different colour. The unidentified bands are labelled as a question mark. **A.** Whole cell protein profiles of *P. gingivalis* W50 and T9SS mutants. Protein samples from whole cell were normalized to 5µl per lane of 10x dilution of culture and subjected to sample buffer containing reducing agent. **B.** Supernatant protein profiles of *P. gingivalis* W50 and T9SS mutants. Protein samples from culture supernatant were normalized to 5µl per lane of 10x dilution supernatant and subjected to sample buffer containing reducing agent. Number ladders on the left-hand side represent the size of marker proteins in kDa. This assay was repeated twice, and this is a typical representation.

3.3.4.2 Gingipain secretion analysis

To further assess the secretion of cargo proteins in these T9SS mutants, rabbit antiserum Rb7[304], rabbit antiserum Rb3158[305] and mouse monoclonal antibody Mab 1A1[306] were used. Rb7 can recognize the catalytic domains of RgpA and RgpB. Rb3158 and 1A1 can recognize the adhesin domains of RgpA and Kgp. Western blot assays were performed for whole cell and culture supernatant samples of W50 and the T9SS mutants. All band identification was based on band size by comparing with published data.

When probed with Rb7, a 54 kDa catalytic domain form ($Rgp_{CD\text{-}IgSF}$) and 70-90 kDa diffused bands representing glycosylated forms[194] of Arg-gingipains were seen in whole cells and culture supernatant of W50. However, when probing the T9SS mutant strains, many immature forms of Arg-gingipains and non-glycosylated forms of gingipain catalytic domains were detected instead (**Figure 3.10A**). A band corresponding to proRgpB ($RgpB_{NTP\text{-}CD\text{-}IgSF\text{-}CTD}$ ~86 kDa) was present in whole cells of Δ*porV*, Δ*porU*, Δ*porP*, Δ*porT* and Δ*porG*. In addition, proRgpA ($RgpA_{NTP\text{-}CD\text{-}IgSF\text{-}HA\text{-}CTD}$ ~183 kDa) was shown in Δ*porV*, Δ*porU*, Δ*porP*, Δ*porT* and Δ*porG*, and proKgp ($Kgp_{NTP\text{-}CD\text{-}IgSF\text{-}HA\text{-}CTD}$ ~186 kDa) was present in Δ*porV*, Δ*porT* and Δ*porG*. A high molecular weight band referred as proRgpA-Kgp complex[307], was shown in Δ*porV*. In the supernatant blot, a band referred as pro-less RgpA (~115 kDa) and a band referred as pro-less RgpB (~70 kDa)[179] were present in culture supernatant of Δ*porV* (**Figure 3.10B**). The $Rgp_{CD\text{-}IgSF}$ was displayed in culture supernatant of W50, Δ*porU*, Δ*porQ* and Δ*porZ*. However, unlike the other mutants, the Δ*porF* strain produced fully processed mature gingipains in culture supernatant, which was similar to W50.

Rb3158 was used to detect adhesin domains of RgpA and Kgp, and the protein patterns of T9SS mutants were also significantly different from that of W50. Diffused bands that represent mature gingipains were present in both whole cells and culture supernatant of W50, whereas immature gingipain bands were seen in all mutants (**Figure 3.10C**). Moreover, proRgpA and proKgp were detected in whole cells of Δ*porV*, Δ*porU*, Δ*porP* and Δ*porT*. A high MW band corresponding to proRgpA-Kgp complex[307], was shown in Δ*porV*, Δ*porU*, Δ*porP* and Δ*porT*. Two bands referred as Kgp_{A1} and $RgpA_{A1}$[308] were

shown in all the strains. Another two lower bands referred as Kgp_{A3} and $RgpA_{A4}$[308] were not seen in Δ*porU*, Δ*porP* and Δ*porT*, but were shown in the other strains. In the supernatant fractions, a band corresponding to proKgp/RgpA, was seen in Δ*porP*, Δ*porT* and Δ*porG* (**Figure 3.10D**). The high MW band referred as the proRgpA-Kgp complex[307], was present in Δ*porV*, Δ*porP*, Δ*porT* and Δ*porG*. Many lower MW bands representing different subdomains[308] of the HA region were also present in both W50 and the mutants. Interestingly, the overall patterns of Δ*porQ* and Δ*porZ* strains were similar, as were the patterns of Δ*porP*, Δ*porT* and Δ*porG* strains. The pattern of Δ*porU* was unique with many lower and intense bands of HA subdomains present in the supernatant sample.

Mab 1A1 was also used to detect adhesin domains of RgpA and Kgp. The results showed that proRgpA, proKgp and proRgpA-Kgp complex[307] were present in whole cells of Δ*porV*, Δ*porU*, Δ*porZ*, Δ*porP*, Δ*porT* and Δ*porG* (**Figure 3.10E**). Many immature gingipain forms were also observed in these mutants, while the HA subdomains were observed in W50, Δ*porQ*, Δ*porZ*, Δ*porG* and Δ*porF* strains. In the supernatant blot, a band of proRgpA-Kgp complex was only seen in the Δ*porV* sample (**Figure 3.10F**). Kgp_{A1}, $RgpA_{A1}$ and Kgp_{A3} domains were present in culture supernatant of W50 and Δ*porU*, but again the supernatant blot pattern of Δ*porU* was remarkably different from the other T9SS mutants.

Taken together, these Western blot data suggest that all the T9SS outer membrane components play a role in the processing or secretion of gingipains. It appears that PorV, PorP, PorT and PorG are in a functional unit, whereas PorQ and PorZ are in another

functional unit, based on their mutants showing similar blot patterns. PorU is unique as some bands detected in Δ*porU* were also present in W50, which may support PorU functioning at a later stage. Δ*porF* showed less changes compared with W50, which again may suggest that it is involved in the later stages of secretion. However, with this analysis there is still some ambiguity in the identification of these bands, and it would be useful to perform mass spectrometry to validate this.

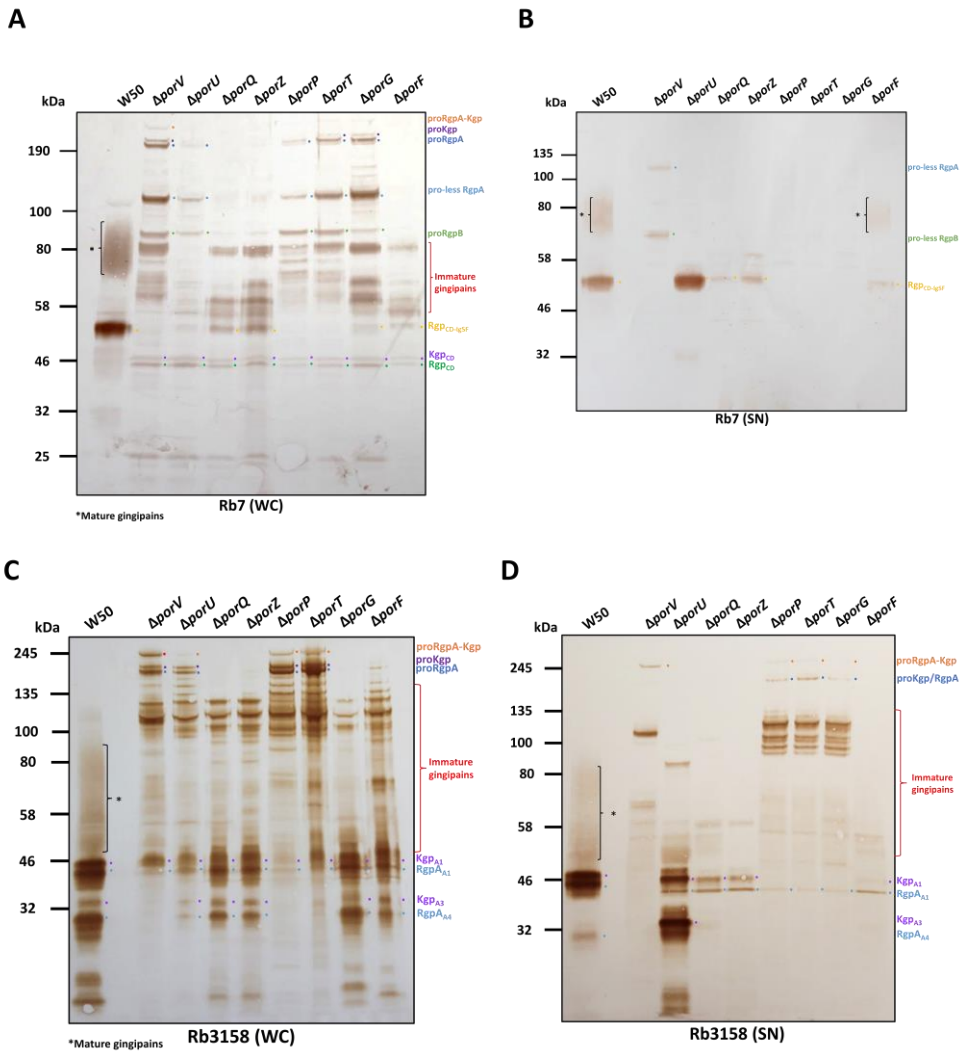

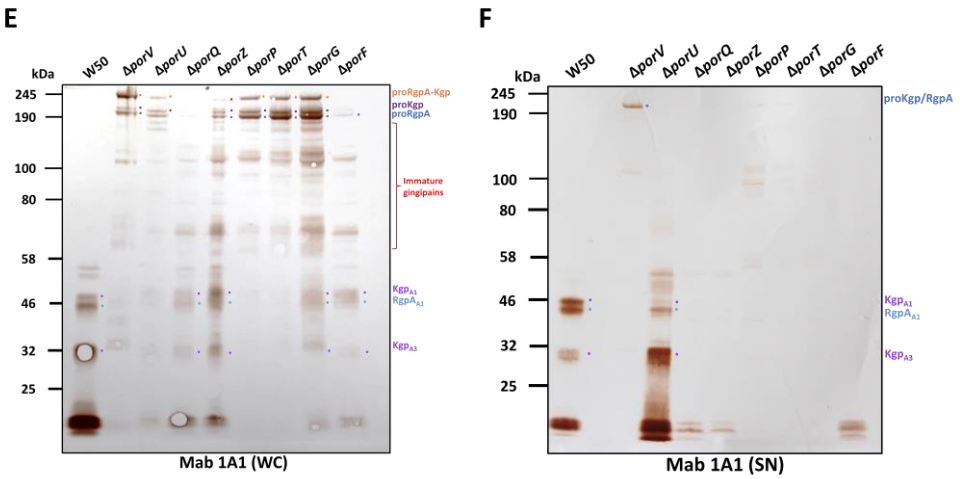

Figure 3.10: Western blot analysis of gingipain secretion. Protein samples were prepared as described above. The immunoblots were probed with rabbit antiserum Rb7 (diluted 1:250) and Rb3158 (diluted 1:500), mouse monoclonal antibody Mab 1A1 (diluted 1:50). Based on band size, the designated proteins are dotted in different colour. **A**, **C, E.** Western blot analysis of whole cell (WC) proteins of *P. gingivalis* W50 and T9SS mutants. **B, D, F.** Western blot analysis of culture supernatant (SN) proteins of *P. gingivalis* W50 and T9SS mutants. Number ladders on the left-hand side represent the size of marker proteins in kDa. This experiment was not repeated due to time restriction.

3.3.4.3 CTD cleavage analysis

Using an RgpB-CTD antibody, Glew *et al.* had previously detected four forms of RgpB in whole cells of a *porU* mutant: RgpB-I (98 kDa) RgpB-II (82 kDa), RgpB-III (70 kDa), and RgpB-IV (56 kDa)[177]. To analyse how these T9SS mutants affect cargo processing and whether the CTD of gingipains is cleaved during the final stage of secretion, additional blots with our own rabbit polyclonal anti-CTD antibody were performed (**Figure 3.11**). This was produced for another lab member, raised against recombinantly expressed and purified RgpB-CTD and its specificity validated against purified RgpB-CTD. The specificity of this antibody has also been validated in another immunoblot assay in Chapter 5 (**Figure 5.13**).

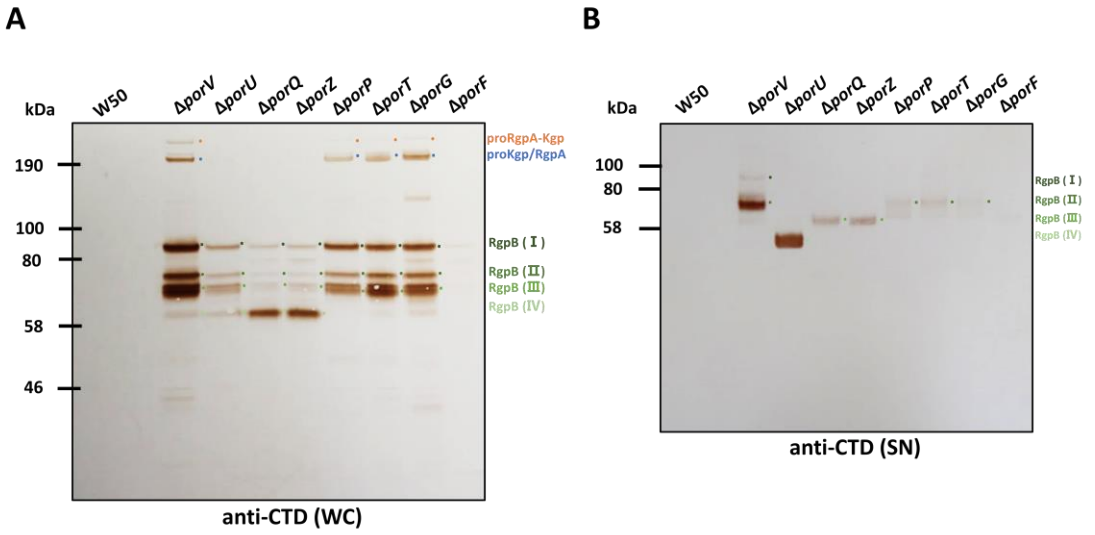

Figure 3.11: Western blot analysis of CTD cleavage. Protein samples were prepared as described above. The immunoblots were probed with rabbit polyclonal antibody anti-CTD (diluted 1:1000). This antibody was raised against recombinantly expressed and purified RgpB-CTD. Based on band size, the designated proteins are dotted in different colour. **A.** Western blot analysis of whole cell proteins of *P. gingivalis* W50 and T9SS mutants. **B.** Western blot analysis of culture supernatant proteins of *P. gingivalis* W50 and T9SS mutants. WC: whole cells. SN: supernatant. Number ladders on the left-hand side represent the size of marker proteins in kDa. This experiment was not repeated due to time restriction.

No CTD band was detected in either the whole cells or supernatant of W50, suggesting that in the majority of gingipains, the CTDs had been cleaved off and processed (**Figure 3.11**). However, four precursor forms of RgpB were detected in whole cells and culture supernatant of the T9SS mutants. All four forms possessed the CTD domain, as they were detected by anti-CTD (**Figure 3.11**). In the whole cell blot, RgpB-II and RgpB-III were mainly present in Δ*porV*, Δ*porU*, Δ*porP*, Δ*porT* and Δ*porG* but RgpB-IV accumulated in Δ*porQ* and Δ*porZ*. No band was detected in Δ*porF*, which was again similar to W50 (**Figure 3.11A**).

Unexpectedly, RgpB-I and RgpB-II were seen in the supernatant of Δ*porV*, suggesting these forms had been released from the cell. Given that PorV is an outer membrane

shuttle that extracts RgpB from the main channel Sov, this could be due to RgpB-II being stuck in Sov, due to the absent of PorV. Overloading of Sov may then cause a leak of this channel, where these RgpB-II forms are released. RgpB-IV accumulated in the supernatant of Δ*porU*, indicating this form had also been released. Likewise, the reason could be that Sov or PorV on the bacterial surface become saturated with RgpB-IV, and the overloading leads to a leaking from Sov or the surface, where these RgpB-IV containing CTD are released. Moreover, traces of RgpB-II were present in the supernatants of Δ*porP*, Δ*porT* and Δ*porG*, and RgpB-III was shown in the supernatants of Δ*porQ* and Δ*porZ*. The explanation here could be that these unprocessed RgpB molecules could be partially packaged into OMVs. Again, no CTD band was detected in the Δ*porF* strain, which was consistent with the whole cell result (**Figure 3.11B**).

Taken together, it appears that maturation of RgpB in the Δ*porV*, Δ*porP*, Δ*porT* and Δ*porG* mutants is stalled at the RgpB-III stage, whereas in the Δ*porQ* and Δ*porZ* mutants it is stalled at RgpB-IV stage. The secreted precursor forms of RgpB in the supernatant suggest that blocking of PorV and PorU may cause a leak in the outer membrane translocon or these unprocessed RgpB were partially packaged into OMVs via an unknow mechanism. High MW bands were also detected in Δ*porV*, Δ*porP*, Δ*porT* and Δ*porG*, which correspond to the expected proRgpA, proKgp or proRgpA-Kgp complex[307], and suggest that these T9SS proteins could be involved in the CTD processing stages of RgpA and Kgp.

3.3.4.4 A-LPS modification analysis

Finally, the mouse monoclonal antibody Mab 1B5[309] was used to detect low molecular weight, non-protein linked forms of A-LPS in *P. gingivalis*. A strong band which represents non-protein linked A-LPS was present in both the whole cells and supernatant samples of W50, weaker bands and/or a change in patterning was observed in whole cells and supernatants of the T9SS mutants (**Figure 3.12**). This suggests that disruption of the T9SS can cause a decline in the levels of A-LPS exported to the outer membrane. It has been shown that A-LPS binds to PorZ which is anchored to the outer membrane through binding to PorQ, and forms part of the T9SS attachment complex[179]. This is reflected in the Δ*porQ* and Δ*porZ* mutants which both show the most defective phenotypes of A-LPS. However, PorZ is also a T9SS cargo protein[109] and knocking out any T9SS outer membrane component could block the secretion of PorZ, which may also lead to a decline of A-LPS. This is again reflected by the less defective A-LPS patterns in Δ*porV*, Δ*porU*, Δ*porP*, Δ*porT*, Δ*porG* and Δ*porF*.

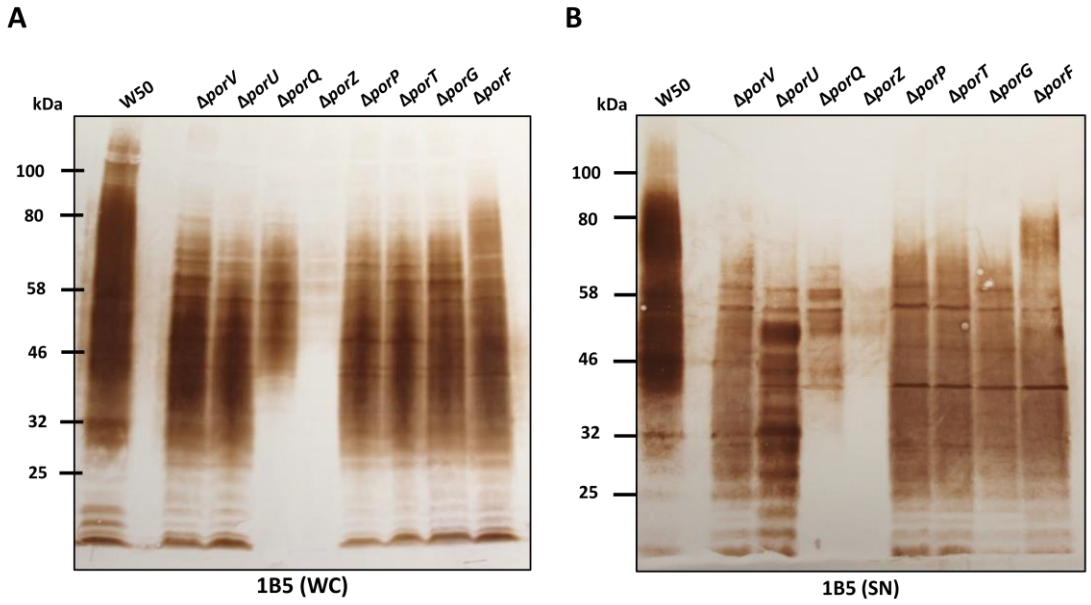

Figure 3.12: Western blot analysis of A-LPS modification. Protein samples were prepared as described above. The immunoblots were probed with mouse monoclonal antibody Mab 1B5 (diluted 1:20). **A.** Western blot analyses of whole cell (WC) proteins of *P. gingivalis* W50 and T9SS mutants. **B.** Western blot analyses of culture supernatant (SN) proteins of *P. gingivalis* W50 and T9SS mutants. Number ladders on the left-hand side represent the size of marker proteins in kDa. This experiment was not repeated due to time restriction.

3.3.5 TEM of T9SS mutants

To investigate OMV formation and morphology in these T9SS mutants, transmission electron microscope (TEM) was applied and showed that OMV blebbing was defective in all the T9SS mutants. While W50 cells produced the expected small and spherical OMVs ~40-50 nm in diameter, all the T9SS mutants formed large and irregular shaped vesicles ~100 nm in diameter (**Figure 3.13A**). Analysis of bacterial and OMV diameters across nine bacterial images for each strain supports that observed cell sizes of W50 and T9SS mutants were similar, but OMV sizes of W50 and T9SS mutants were significantly different (**Figure 3.13B**). This data suggest that these T9SS components

are required for the normal smaller OMV formation in *P. gingivalis*. To assess whether the mutations also influenced the quantity of OMVs formed, OMVs per blebbing cell were also counted (**Figure 3.13C**). Significant differences versus W50 were only shown in Δ*porU* and Δ*porP*, indicating that inactivation of these but not the other T9SS proteins may influence the quantity of OMVs.

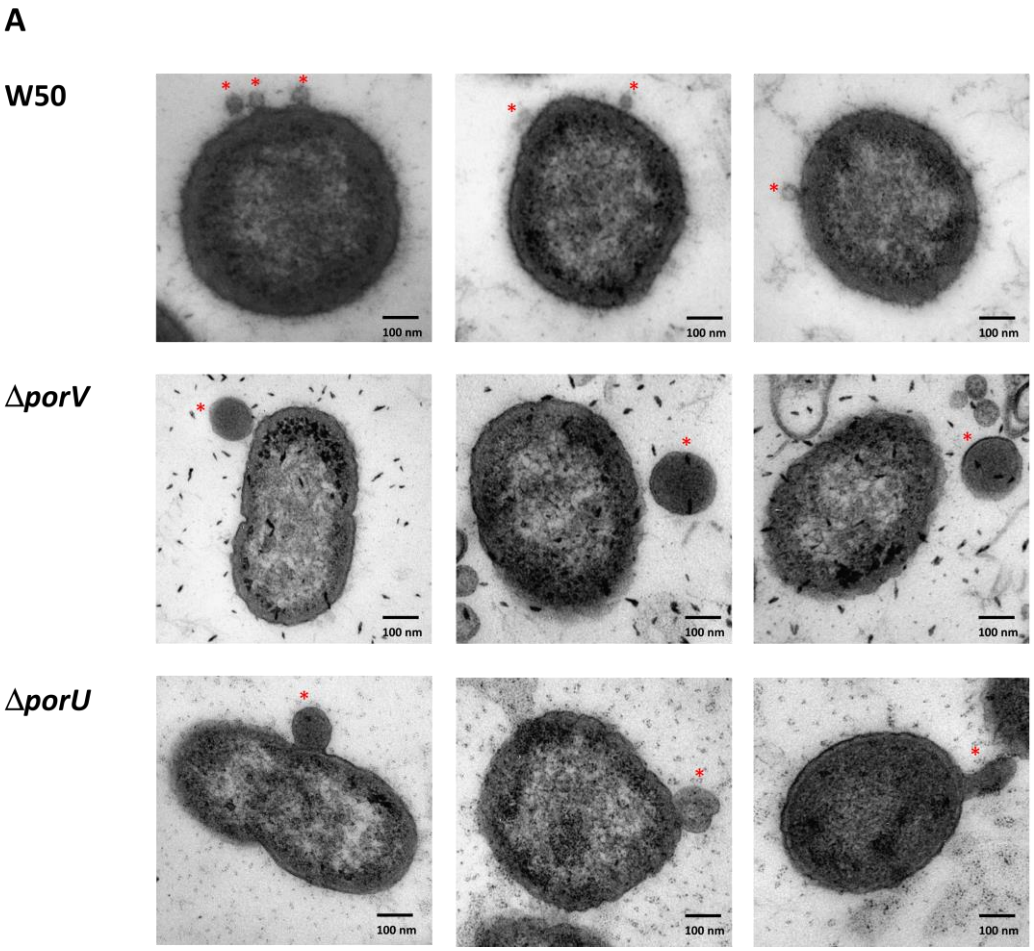

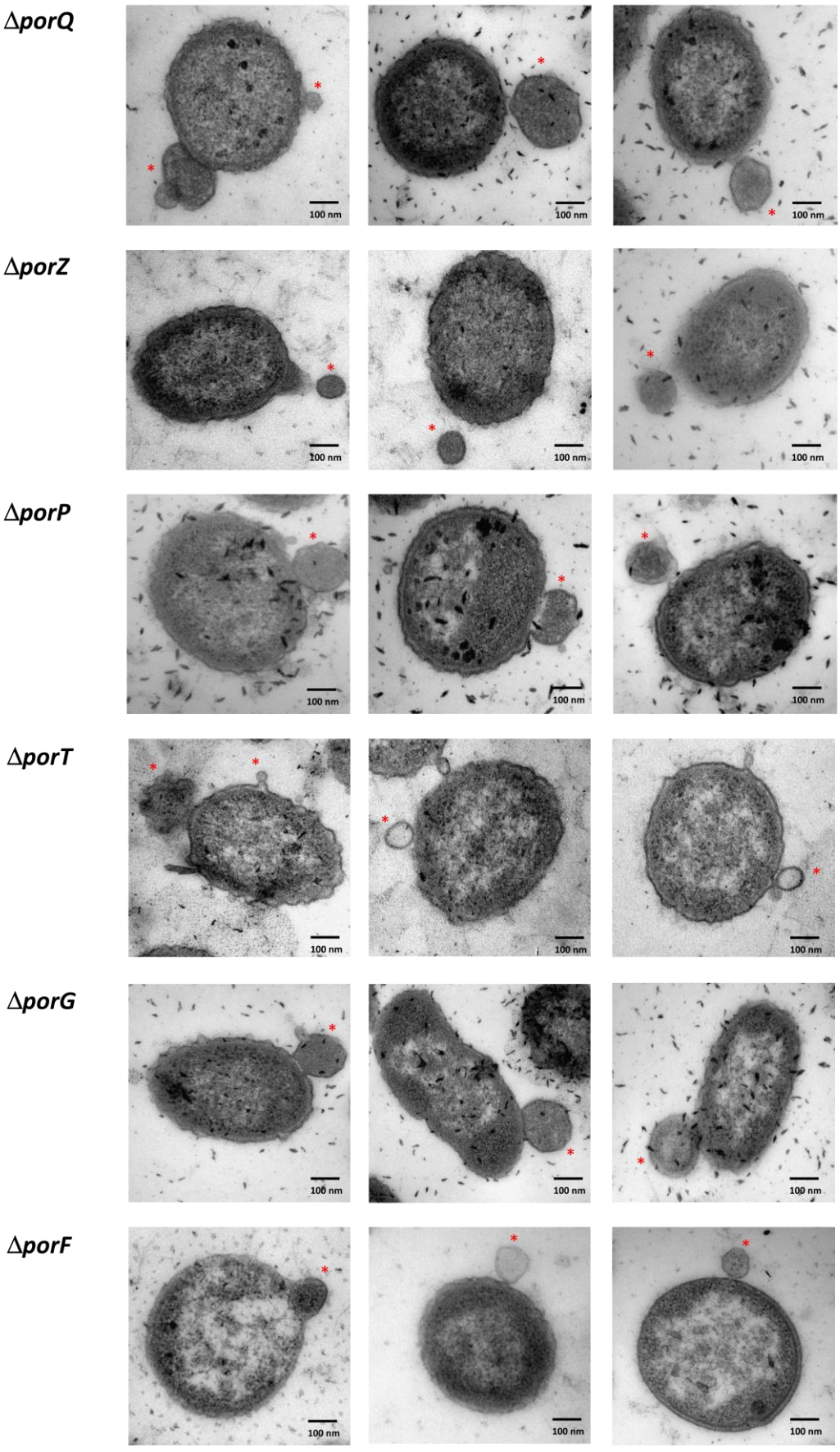
ΔporQ
ΔporZ
ΔporP
ΔporT
ΔporG
ΔporF
100 nm

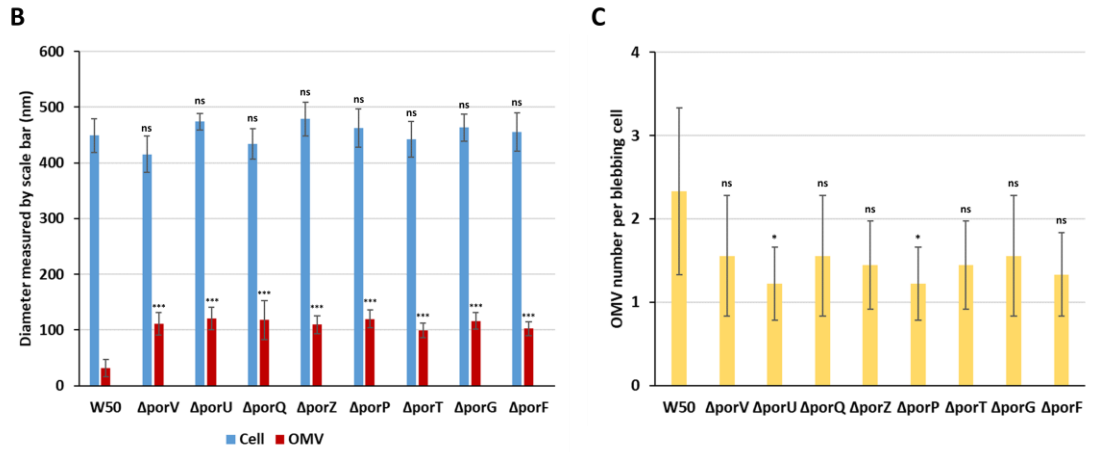

Figure 3.13: TEM of OMV formation in T9SS mutants. A. Transmission electron microscope (TEM) images of *P. gingivalis* W50, Δ*porV*, Δ*porU*, Δ*porQ*, Δ*porZ*, Δ*porP*, Δ*porT*, Δ*porG* and Δ*porF* cells. Samples were prepared using formaldehyde method. Scale bar: 100 nm. The data was collected from random cells which were in an OMV blebbing status. The representative images from three biological repeats were shown. The OMV blebbing was marked as red asterisk. OMV formation in *P. gingivalis* W50 strain was clearly visible as defined structures. The T9SS mutants produced large and irregular vesicles. An electron-dense surface layer (EDSL) in the wild-type was significantly reduced or absent in mutant strains. **B.** Measurements of cell and OMV diameter in each blebbing cell. The blebbing status is defined that OMVs were within 50 nm distance to the cell. Data are presented as means ± SDs (n = 9). Student's *t* test for cell and OMV diameter: W50 versus Δ*porV*, Δ*porU*, Δ*porQ*, Δ*porZ*, Δ*porP*, Δ*porT*, Δ*porG* and Δ*porF* yielded a *P* value. ns: $p > 0.05$, non-significant. ***: $p < 0.001$, significant. **C.** OMV number per blebbing cell. The blebbing status is defined that OMVs were within 50 nm distance to the cell. Data are presented as means ± SDs (n = 9). Student's *t* test for OMV number per blebbing cell: W50 versus Δ*porV*, Δ*porU*, Δ*porQ*, Δ*porZ*, Δ*porP*, Δ*porT*, Δ*porG* and Δ*porF* yielded a *P* value. ns: $p > 0.05$, non-significant. *: $p < 0.05$, significant. These are the representative data of three biological and technical repeats.

3.3.6 NanoSight analysis of T9SS mutants

Nanoparticle tracking analysis (NTA) is a powerful characterisation technique that combines the properties of both laser light scattering microscopy and Brownian motion to obtain size distributions of particles in liquid suspension[310]. As the most widely used instruments for NTA in the extracellular vesicle (EV) field, NanoSight instruments (Malvern, UK) are equipped with one or more lasers and an optical microscope

connected to a digital camera. According to the manufacturer, NanoSight enables characterisation of particles from 10-2000 nm in solution. Particles are visualised by the light they scatter upon laser illumination, and their Brownian motion is monitored. The NTA software enables sizing of single particles by tracking their mean squared displacement and thereby calculating their theoretical hydrodynamic diameter using the Stokes Einstein equation[310]. Although NanoSight has been widely used in studies on eukaryotic EVs, its application in bacteria OMVs is rare, for example, monitoring OMV production in *Neisseria meningitidis*[311]. However, the usage of NanoSight for OMV analysis in *P. gingivalis* has never been reported.

To confirm that NanoSight would be applicable for OMV analysis in *P. gingivalis*, OMV samples of three *P. gingivalis* wild type strains (W50, W83 and ATCC 33277) were prepared from overnight cultures (OD_{600} = 2) and analysed by NanoSight. The TEM data suggested that the diameter of bacteria cell range from 400 nm to 500 nm diameter, while OMVs range from ~50-150 nm diameter (**Figure 3.13B**). Samples were therefore passed through a 0.22-μm filter prior to OMV sample collection to remove the larger cell particles (**Figure 3.14**), and I anticipated that the filtrate would represent a clean OMV sample. The data showed that the OMV size accumulated at 44 nm (5.1 particles/ml) in W50, 22 nm (4.5 particles/ml) in W83 and 35 nm (2.9 particles/ml) in ATCC 33277 with lower concentration of particles larger than ~100 nm also observed in all samples (**Figure 3.14**). This result is in line with published data[173] and my TEM analysis, suggesting that NanoSight is applicable for OMV analysis in *P. gingivalis*.

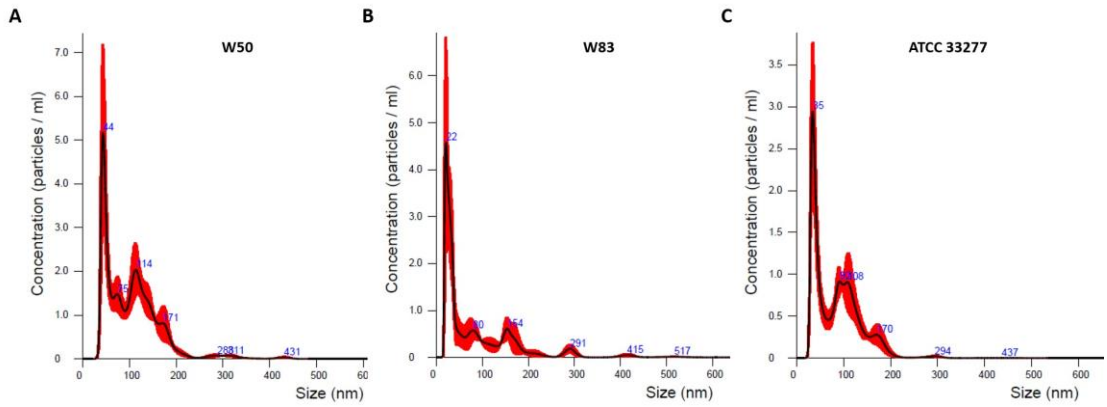

	W50	W83	ATCC 33277
mean (nm)	103	84	85
mode (nm)	44	21	34

Figure 3.14: NanoSight analysis of *P. gingivalis.* **A.** Concentration of OMV size in *P. gingivalis* W50. **B.** Concentration of OMV size in *P. gingivalis* W83. **C.** Concentration of OMV size in *P. gingivalis* ATCC 33277. OMV samples were prepared as described in methods. It appears that W50 and W83 produce similar levels of small OMVs while ATCC 33277 produces ~50% less. Averaged finite track length adjustment (FTLA) concentration and size for experiment were shown. Error bars indicate standard error of the mean. Mean value represents the average size of total OMVs of each sample. Mode value represents the most prominent OMV size of each sample. As overlap of particles may affect the accuracy of size measurement, the samples were diluted 10-fold. These are the representative data of three technical repeats.

Next, NanoSight was also applied for OMV size analysis of the T9SS mutants. The average size of total OMVs of these mutants is ~100 nm, which is similar to W50. The most predominant peaks of Δ*porV,* Δ*porP* and Δ*porT* are 53 nm (2.5 particles/ml), 37 nm (1.7 particles/ml) and 44 nm (3.1 particles/ml), respectively (**Figure 3.15A, E, F**). However, while their predominant size is similar to W50 (44 nm), their particle concentration is much lower than W50 (5.1 particles/ml). The most predominant peaks of Δ*porU,* Δ*porQ* Δ*porZ,* Δ*porG* and Δ*porF* were 108 nm (2.4 particles/ml), 105 nm (1.8 particles/ml), 127 nm (2.2 particles/ml), 117 nm (2.3 particles/ml) and 126 nm (1.8 particles/ml), respectively (**Figure 3.15B, C, D, G, H**). However, the ~50 nm smaller size OMVs decreased to 2 particles/ml in Δ*porU*, 1.7 particles/ml in Δ*porQ*, 0.8

particles/ml in Δ*porZ*, 2.2 particles/ml in Δ*porG* and 1.2 particles/ml in Δ*porF*, compared to 5.1 particles/ml in W50. These data suggest that these T9SS mutants tend to produce the same amount of larger OMVs as W50 does, but they produce much less ~50 nm smaller OMVs than W50. These particle size data imply that knocking out any T9SS outer membrane protein may affect the production of normal smaller OMVs, which is consistent to the TEM data. However, this experiment needs to be biologically repeated to confirm OMV size differences between W50 and these T9SS mutants. Also, due to time restriction, TEM images for these purified OMV samples were not collected, but it would be useful to do this in the future to confirm the OMV samples are consistent with NanoSight data.

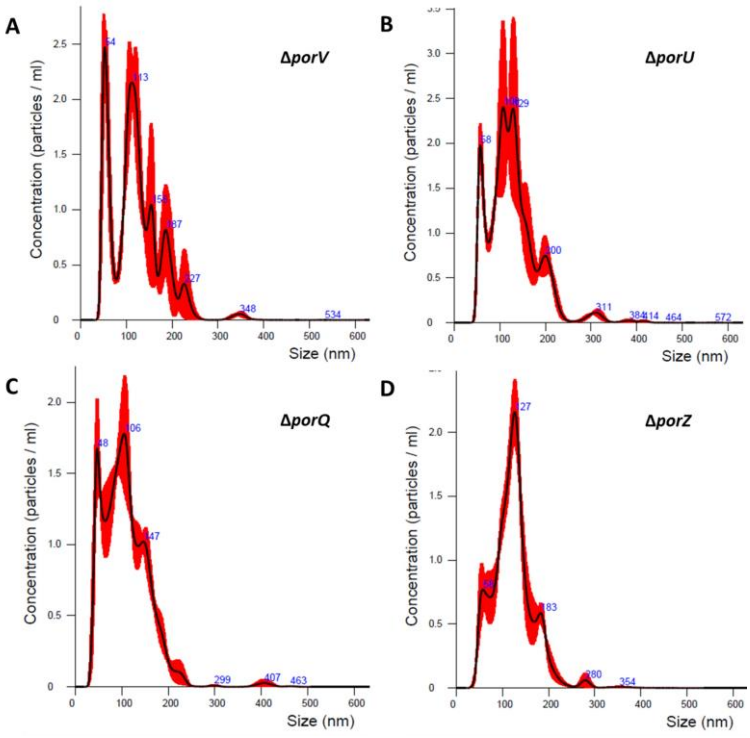

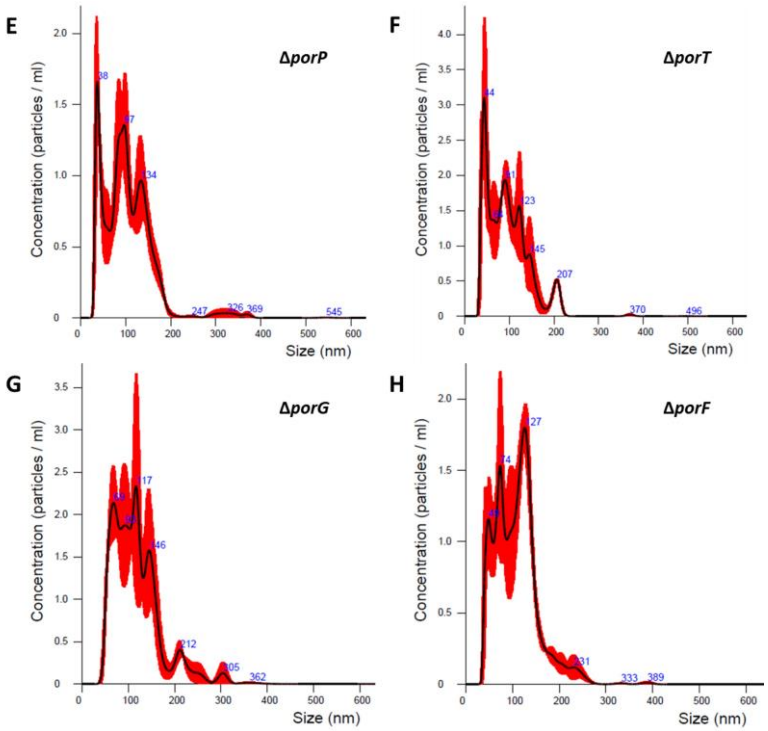

	W50	ΔporV	ΔporU	ΔporQ	ΔporZ	ΔporP	ΔporT	ΔporG	ΔporF
mean (nm)	103	120	128	108	123	102	95	118	109
mode (nm)	44	53	108	105	127	37	44	117	126

Figure 3.15: NanoSight analysis of the T9SS mutants. A-H. Concentration of OMV sizes in the *porV*, *porU*, *porQ*, *porZ*, *porP*, *porT*, *porG* and *porF* mutants. OMV samples were prepared as described in methods. Averaged finite track length adjustment (FTLA) concentration and size for experiment were shown. Error bars indicate standard error of the mean. Mean value represents the average size of total OMVs of each sample. Mode value represents the most prominent OMV size of each sample. These are the representative data of three technical repeats.

3.3.7 Lipid A structure analysis

To understand how the outer membrane of these T9SS mutants is altered and given that lipid A is a key component of Gram-negative bacteria outer membrane, lipid A status in *P. gingivalis* T9SS mutants was investigated. Lipid A from T9SS mutants was purified and matrix-assisted laser desorption ionization time-of-flight mass spectrometry (MALDI-TOF MS) was performed. Lipid A from W50 cells contained bis-P-pentaacyl

(*m/z* 1,768), mono-P-pentaacyl (*m/z* 1,688), mono-P-tetraacyl (*m/z* 1,448), non-P-pentaacyl (*m/z* 1,608), and non-P-tetraacyl (*m/z* 1,368) species (**Figure 3.16A**), which is consistent with reported data[152].

In contrast, lipid A from all T9SS mutants only possessed phosphorylated species; non-phosphorylated species were absent (**Figure 3.16B-I**). The lipid A profiles of Δ*porV*, Δ*porU*, Δ*porQ*, Δ*porZ*, Δ*porP*, Δ*porT*, Δ*porG* and Δ*porF* mutants are similar to that of reported *lpxE* (lipid A 1-phosphatase) mutant in *P. gingivalis* ATCC 33277 strain[290]. As mentioned in the introduction chapter, two lipid A phosphatases LpxE and LpxF, have been identified in *P. gingivalis*. LpxE is responsible for 4-P-pentaacyl, non-P-pentaacyl and non-P-tetraacyl lipid A, while LpxF is responsible for 1-P-pentaacyl and non-P-pentaacyl lipid A. Due to the complete absence of non-phosphorylated lipid A profiles, the activity of LpxE was likely disrupted in all the T9SS mutants. Moreover, the intensity of bis-P-pentaacyl (*m/z* 1,768) is very low in Δ*porQ*, Δ*porT* and Δ*porG* (**Figure 3.16D, G, H**), suggesting that knocking out these proteins may increase expression of LpxF. Taken together, this evidence suggests that correct functioning of the T9SS is required for LpxE activity, and this implies that there is either direct or indirect interplay between the T9SS and the lipid A 1-phosphtase LpxE.

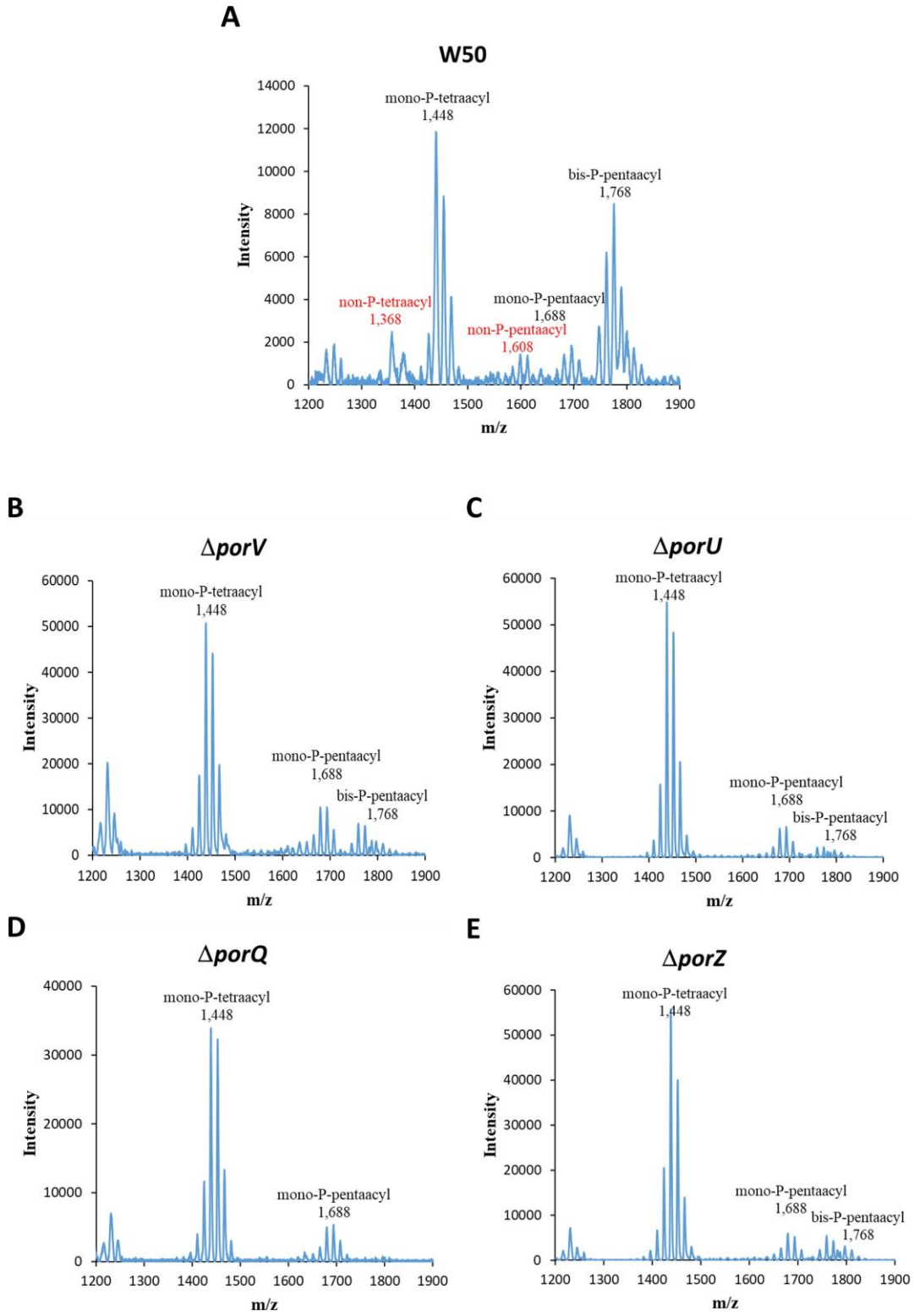
A
W50
mono-P-tetraacyl
1,448
bis-P-pentaacyl
1,768
non-P-tetraacyl
1,368
mono-P-pentaacyl
1,688
non-P-pentaacyl
1,608
Intensity
m/z
B
ΔporV
mono-P-tetraacyl
1,448
mono-P-pentaacyl
1,688
bis-P-pentaacyl
1,768
Intensity
m/z
C
ΔporU
mono-P-tetraacyl
1,448
mono-P-pentaacyl
1,688
bis-P-pentaacyl
1,768
Intensity
m/z
D
ΔporQ
mono-P-tetraacyl
1,448
mono-P-pentaacyl
1,688
Intensity
m/z
E
ΔporZ
mono-P-tetraacyl
1,448
mono-P-pentaacyl
1,688
bis-P-pentaacyl
1,768
Intensity
m/z

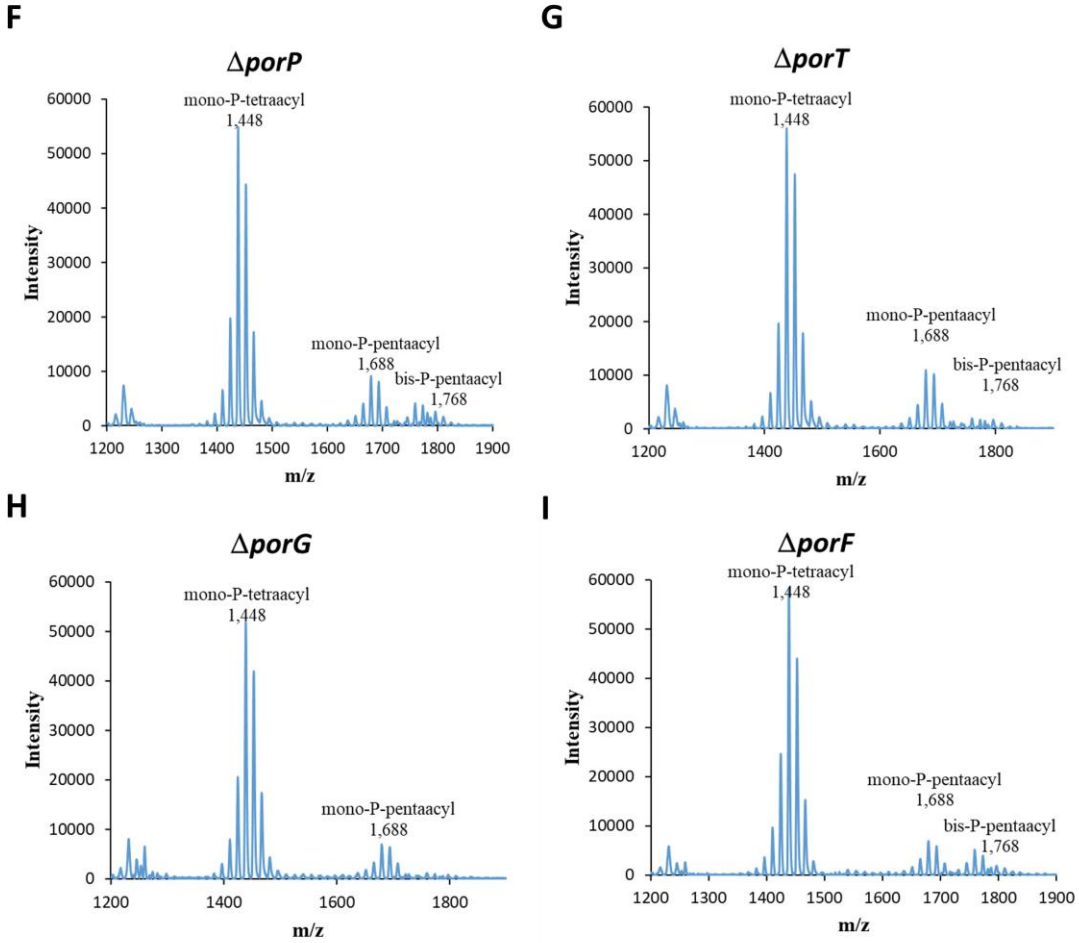

Figure 3.16: MALDI-TOF MS of lipid A from T9SS mutants. Matrix-assisted laser desorption ionization time-of-flight mass spectrometry (MALDI-TOF MS) analysis of lipid A from *P. gingivalis* W50, Δ*porV*, Δ*porU*, Δ*porQ*, Δ*porZ*, Δ*porP*, Δ*porT*, Δ*porG* and Δ*porF* mutant strains. Negative-ion MALDI-TOF MS was performed on lipid A samples with 5-chloro-2-mercaptoben-zothiazole (CMBT) as the matrix as described in materials and methods. Three phosphorylated lipid A clusters (mono-P-tetraacyl, mono-P-pentaacyl and bis-P-pentaacyl) and two non-phosphorylated lipid A clusters (non-P-tetraacyl and non-P-pentaacyl) are labelled. **A.** *P. gingivalis* W50 strain possesses non-P-tetraacyl, mono-P-tetraacyl, non-P-pentaacyl, mono-P-pentaacyl and bis-P-pentaacyl lipid A clusters. **B-I.** Non-phosphorylated lipid A clusters were absent in Δ*porV*, Δ*porU*, Δ*porQ*, Δ*porZ*, Δ*porP*, Δ*porT*, Δ*porG* and Δ*porF* mutants. These are the representative data of three biological repeats.

3.3.8 Detergent inhibition assay

As changes in lipid A structure could affect the stability of the outer membrane, the cell membrane stability of these T9SS mutant strains against Sodium dodecyl sulfate (SDS)

and Triton X-100 was tested using a detergent inhibition assay. SDS is an anionic denaturing surfactant that consists of a 12-carbon tail attached to a sulfate group. Triton X-100 is a non-ionic non-denaturing surfactant that has a hydrophilic polyethylene oxide chain and an aromatic hydrocarbon lipophilic or hydrophobic group. The minimum killing concentration of SDS and Triton X-100 were determined at 8 μg/ml and 35 μg/ml, respectively. The start cultures (OD_{600} = 0.5) were diluted using colony forming unit (CFU) serial dilutions and diluted cultures were spotted on plates with detergents at minimum killing concentration. For the SDS inhibition assay, colonies were not present at the 10^5 dilutions of W50, *porT* and *porG* mutants but were shown at the same dilution of the other strains (**Figure 3.17A**). This indicates that the cell membrane of W50, Δ*porT* and Δ*porG* may be less stable than the other strains, reflecting that PorV, PorU, PorQ, PorZ, PorP and PorF may play a role in destabilizing cell membrane. When treated with Triton X-100, colonies of W50, Δ*porV*, Δ*porQ*, Δ*porT*, Δ*porG* and Δ*porF* were killed at dilution of 10^5 (**Figure 3.17B**). This suggests that the cell membrane of these strains may be less robust than the others, and indicates that PorU, PorZ and PorP may be involved in destabilizing cell membrane.

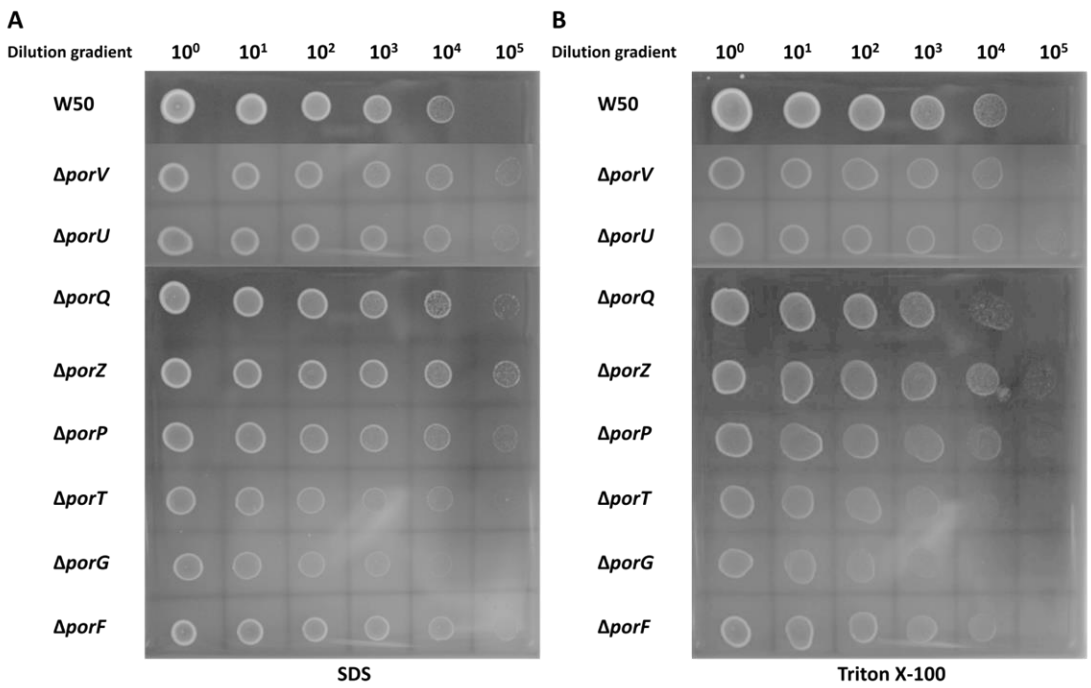

Figure 3.17: Detergent inhibition assay of the T9SS mutants. The detergent inhibition assays were performed on the blood agar plates containing detergent. The OD_{600} of start culture was 0.5 and samples were diluted into different gradients and then dotted on blood agar plates for 4 days growth. **A.** SDS inhibition assay. The applied concentration of SDS was 8 μg/ml. **B.** Triton X-100 inhibition assay. The applied concentration of Triton X-100 was 35 μg/ml. Due to COVID and time restriction, this experiment was not repeated.

3.3.9 Antimicrobial peptide inhibition assay

Antimicrobial peptides (AMPs) target and destabilize bacterial membranes and play an important role in innate host defence against microbial pathogens in many organisms. Therefore, the antimicrobial peptide resistance of the T9SS mutant against two antimicrobial peptides cecropin B and LL-37 was next analysed. Cecropins are a class of antimicrobial peptides that were first described in insects[312], but are also found in mammals[313]. Cecropin B (KWKVFKKIEKMGRNIRNGIVKAGPAIAVLGEAKAL) is one of the best studied AMPs, which assumes a secondary structure that is characterized by the presence of two α-helices[314]. The N-terminal α-helix of cecropin B is highly

amphipathic while the C-terminal α-helix is hydrophobic. The human cathelicidin, LL-37 (LLGDFFRKSKEKIGKEFKRIVQRIKDFLRNLVPRTES), possesses a net positive charge and is amphiphilic, and can eliminate microbes directly via electrostatic attraction to negatively charged bacterial membranes[315].

When treated with cecropin B, colonies did not grow at dilution of 10^5 of W50, *porT* and *porG* mutants but were present at the same dilution of the other strains (**Figure 3.18A**). Similarly, for the LL-37 inhibition assay, colonies were not shown at dilution of 10^5 of the *porT* and *porG* mutants but were present at the same dilution of the other strains (**Figure 3.18B**). This data shows that W50, *porT* and *porG* mutants are more defective to resist AMP killing, and indicates that that PorV, PorU, PorQ, PorZ, PorP and PorF may be required for destabilizing cell membrane.

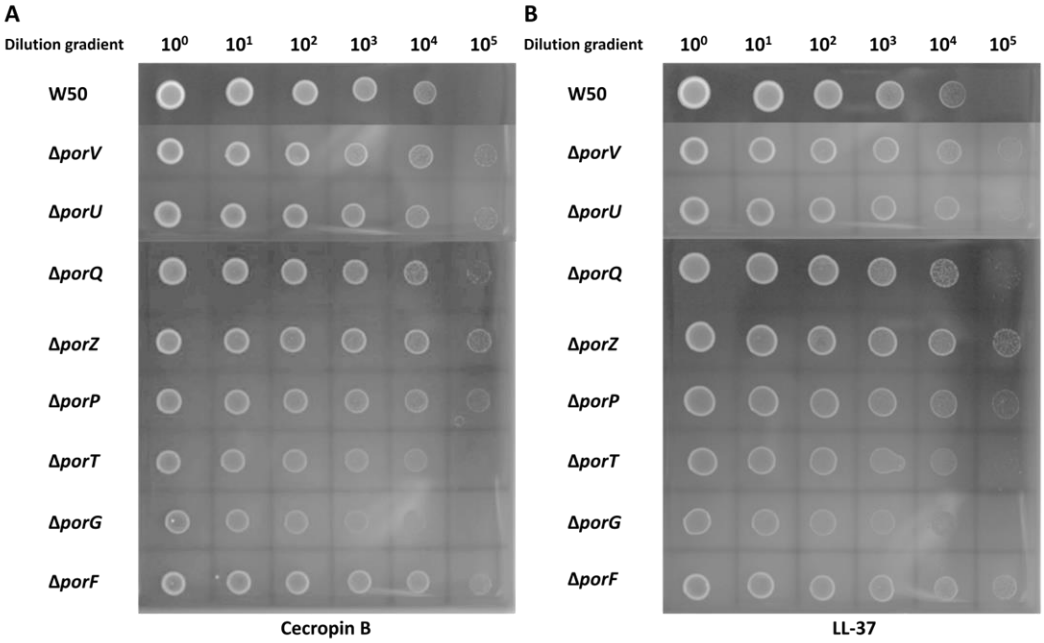

Figure 3.18: Antimicrobial peptide inhibition assay of the T9SS mutants. The antimicrobial peptide inhibition assays were performed on the blood agar plates containing antimicrobial peptides. The OD_{600} of start culture was 0.5 and samples were diluted into different gradients and then dotted on blood agar plates for 4 days growth. **A.** Cecropin B inhibition assay. The applied concentration of Cecropin B was 10 mM. **B.** LL-37 inhibition assay. The applied concentration of LL-37 was 10 mM. Due to COVID and time restriction, this experiment was not repeated.

3.4 Discussion

In recent years, several T9SS outer membrane (OM) accessory components have been identified and many have been shown to be essential for T9SS dependent cargo secretion[174]. However, the precise function of the accessory proteins PorQ, PorP, PorT, PorG and PorF have still not been clarified. This chapter characterized the roles of the T9SS OM accessory proteins PorV, PorU, PorQ, PorZ, PorP, PorT, PorG and PorF, and revealed that they influence OMV biogenesis and lipid A modification. The results of pigmentation and enzyme activity assays suggest that these proteins are required for gingipain secretion and are essential components of the T9SS, and growth rate assays also showed that these proteins are important for promoting bacterial growth. The data of Western blot assays confirmed that these proteins play different roles during cargo secretion, CTD cleavage and A-LPS modification. The detergent and antimicrobial peptide inhibition assays show that PorV, PorU, PorQ, PorZ, PorP and PorF may be involved in cell membrane stability, while PorT and PorG do not appear to be required. The TEM and NanoSight results suggest that these proteins are also required for normal OMV formation. The MALDI-TOF MS analysis revealed that non-phosphorylated lipid A species is absent in the bacterial membranes in these T9SS mutants, and this lipid A phenotype is very similar to a published *P. gingivalis lpxE* mutant[290].

It has been suggested that mutations of T9SS outer membrane proteins (OMPs) PorV and SprT (PorT homologue) result in defective growth in *P. gingivalis*[152] and *Cytophaga hutchinsonii*[316], respectively. Here, my growth rate results support these data and further indicate that all the T9SS OM components are important for bacteria growth. The

reason could be that many T9SS substrates, such as HBP35 and gingipains, are required for nutrients acquisition and import[47].

Previous pigmentation observations have described that the T9SS *porV*, *porU*, *porZ*, *porT* and *porF* mutants are not able to pigment on blood agar, and they form white colonies because they are defective in gingipain secretion[172]. However, in this study presented here, the colony colours of the created T9SS mutants were found to be slightly different. The *porV*, *porP*, *porT* and *porG* mutants presented white colonies, the *porU* and *porF* mutants displayed beige colonies, and the *porQ* and *porZ* mutants showed brown colonies. The results of enzyme activity and Western blot assays also corresponded to this grouping of mutant strains. The difference of colony colours indicates different level of gingipain secretion or activity outside the cell, which implies that these proteins likely play their roles at different stages during type-IX secretion. However, complementation or qPCR would be useful to confirm that these mutations had not resulted in any polar effect.

Among these OM accessory components, PorV is known to have multiple functions and is involved in two complexes: the OM translocon complex (Sov-PorV)[168] and the attachment complex (PorVUQZ)[179]. It is thought to extract cargo proteins from main pore Sov and deliver them to the attachment complex. PorP binds to the PorK/PorN ring[185], and due to similar pigmentation phenotypes, PorT and PorG may also be involved in binding the PorK/PorN ring to maintain the whole OM translocon. Based on this data, it is speculated that PorV, PorP, PorT and PorG play their roles at a relatively early stage of secretion, and therefore the white colonies and the increased

number of unprocessed gingipain bands in Western blots of these mutants could be explained by this. However, in *F. johnsoniae*, only SprT (PorT homologue) is required for substrate secretion[50]. The situation is more complicated for PorV, SprF (PorP homologue) and PorG in *F. johnsoniae*. PorV was thought to shuttle substrates, but secretion of some *F. johnsoniae* T9SS cargos is independent of PorV[317]. SprF is required for T9SS-dependent secretion of SprB in *F. johnsoniae*, but it is not required for secretion of other proteins examined[318]. Mutants lacking PorG have not been examined in *F. johnsoniae*.

As a CTD sortase in the T9SS, PorU is responsible for CTD cleavage[178]. CTD cleavage occurs during the final stages in T9SS-dependent secretion, by which time cargos will have been transported to the OM. This could explain why the colonies present brown pigmentation when *porU* is knocked out. PorF is predicted to be a TonB dependent receptor that is associated with the uptake and transport of large substrates such as iron siderophore complexes and vitamin B12[203]. The phenotypes of the *porF* mutant are similar to the *porU* mutant, indicating that both PorU and PorF may play their roles at later stage. The colony colours of the *porZ* and *porQ* mutants are brown and turn black over time. The reason could be that PorZ is responsible for A-LPS modification of T9SS substrates[198] and PorQ anchors PorZ to the OM. A-LPS modification is the last step of the secretion, which explains the colony colours of the *porZ* and *porQ* mutants are much darker than the other mutants, as cargos have been secreted but might not be anchored. Although the mutants lacking PorU, PorF, PorZ and PorQ have not been studied in *F. johnsoniae*, homologues have been identified, and they are thought to perform similar

function[174,172].

Except in *P. gingivalis*, it has not been reported that inactivation of OM component of bacterial secretory system affects OMV formation in other bacteria. In this chapter, I further verified that not only PorV[152,155], PorT[155] and PorU[177], but also PorQ, PorZ, PorP, PorG and PorF can regulate OMV biogenesis in *P. gingivalis*. The direct evidence is that all these T9SS mutants produce irregular OMVs, and their membrane lipid A phosphorylation status is altered. This implies that a correctly functioning T9SS rather than its individual components is responsible for this regulation. Furthermore, as the structures of lipid A isolated from these T9SS mutants are very similar to published structures of lipid A isolated from a *lpxE* mutant, albeit in ATCC 33277 strain rather than W50 here[290], this implies that the T9SS can either directly or indirectly regulate the activity of LpxE.

Only OM lipoproteins have been suggested to be involved in OMV production in *E. coli*[259,261], but the T9SS OM components are not lipoproteins. In *E. coli*, OmpA is the only well studied β-barrel OMP that is involved in OMV biogenesis. With the aid of lipoprotein Lpp, OmpA can interact with the peptidoglycan layer to maintain the integrity of the cellular envelopes[263]. However, there is no evidence to suggest that any of these T9SS β-barrel OMPs interact with the peptidoglycan layer. Moreover, the MALDI-TOF MS data indicates that inactivation of T9SS OM component altered the phosphorylated status of lipid A, and this has not been reported for any other secretion system. Taken together, these findings imply a novel OMV regulation mechanism may exist in *P. gingivalis* through its T9SS.

In the detergent and antimicrobial peptide inhibition assays, *porV*, *porU*, *porQ*, *porZ*, *porP* and *porF* mutants appeared to be more robust, suggesting they may play a role in destabilizing the *P. gingivalis* OM. Unlike these mutants, an OmpA-like protein deficient *P. gingivalis* strain showed a defect in LL-37 resistance[319]. In the OmpA-like protein mutant, LL-37 accumulated on the bacterial cell surface[319], and resulted in destabilization of the outer membrane. As the differences of T9SS mutants' resistance to detergent and antimicrobial peptide are not conclusive, more dilution gradients of culture and increased concentrations of detergent and antimicrobial peptide would be useful to improve this data.

3.5 Conclusion

This chapter describes the functions of the T9SS outer membrane accessory proteins (PorV, PorU, PorQ, PorZ, PorP, PorT, PorG and PorF) and how are they involved in OMV biogenesis. The results of pigmentation and enzyme activity assays suggest that these proteins are required for gingipain secretion. The result of growth rate assay shows that these proteins are important for bacteria growth. The data of Western blot assays confirmed that these proteins have different influences on CTD cleavage, cargo secretion and A-LPS modification. In the detergent and antimicrobial peptide inhibition assays, it is showed that PorV, PorU, PorQ, PorZ, PorP and PorF are required for destabilizing cell membrane, while PorT and PorG do not appear to be required. The TEM and NanoSight results suggest that these proteins are also required for normal

OMV formation. Using MALDI-TOF MS, there is also clear evidence that the lipid A phenotypes of these T9SS mutants were linked to the *P. gingivalis lpxE* mutant.

Chapter 4 Characterization of *P. gingivalis* Lipid A 1-phosphatase LpxE

4.1 Chapter aims

In Chapter 3, an interplay between the T9SS and LpxE was revealed. The aim of this chapter was to study lipid A 1-phosphatase LpxE in *P. gingivalis* W50 using *in vivo* assays and understand how the T9SS is linked to LpxE activity. It was speculated that the T9SS itself or one of its secreted substrates might regulate the phosphorylation status of lipid A via modulating the activity of LpxE.

4.2 Bioinformatic analysis of LpxE

To acquire homology information about *P. gingivalis* LpxE, a sequence alignment was performed using the Basic Local Alignment Search Tool (BLAST) server. The result indicated that *P. gingivalis* LpxE is composed of an N-terminal signal peptide (SP), which is followed by an N-terminal domain (NTD) and an additional C-terminal region (CTR) (**Figure 4.1**). The NTD is conserved and belongs to the PAP2 (type-2 phosphatidic acid phosphatase)-like superfamily and is therefore likely responsible for the phosphatase activity of LpxE (**Figure 4.1**). However, the sequence of *P. gingivalis* LpxE is much longer than LpxE sequences from other bacteria which do not contain the N-terminal extension or the CTR (**Figure 4.1**). This evidence suggests that *P. gingivalis* LpxE has additional functions. Although LpxE from *Parabacteroides* sp. (Sequence ID: WP_122362166.1 and WP_128135112.1) and *Prevotella pleuritidis* (Sequence ID: WP_021583963.1 and WP_036931304.1) also possess CTRs, these are half the length as in *P. gingivalis* (**Figure 4.1**).

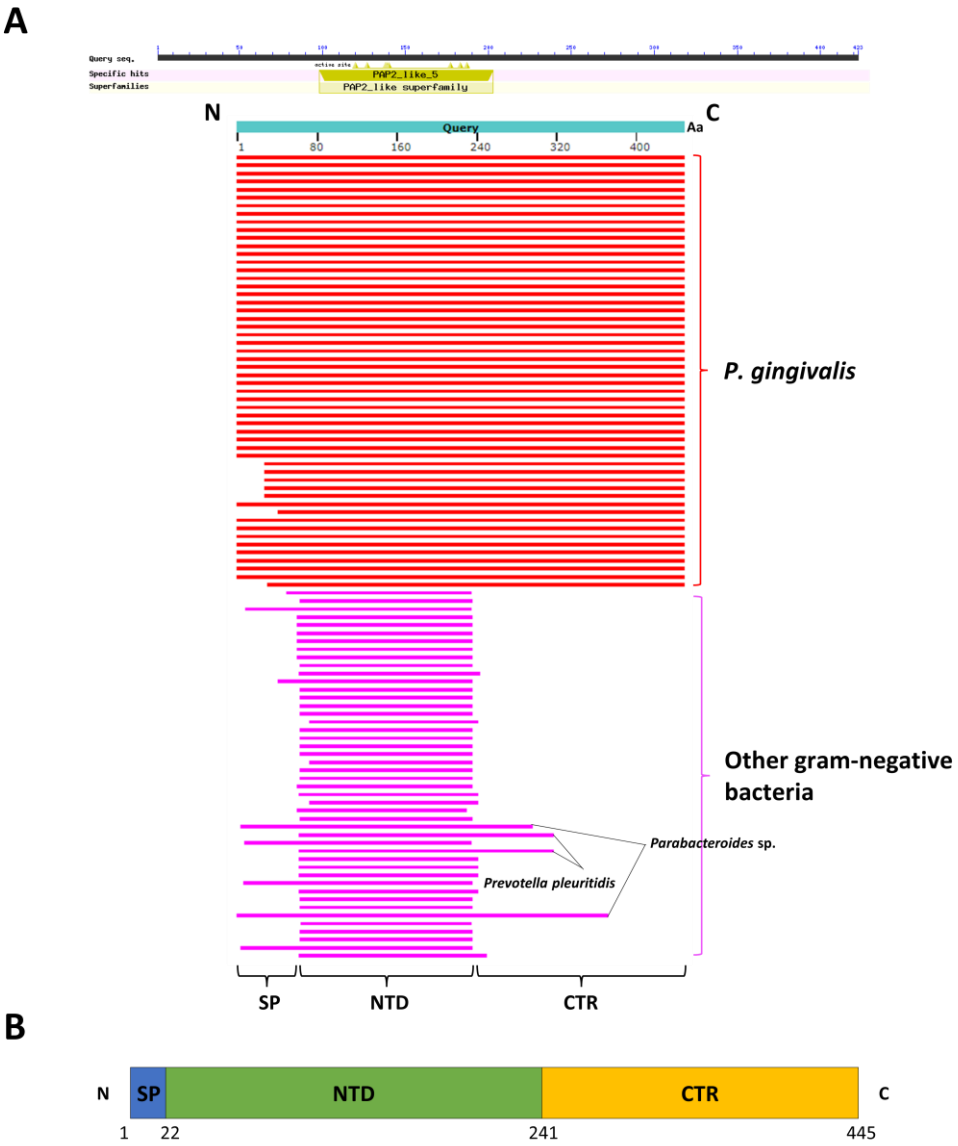

Figure 4.1: Sequence homology alignment of *P. gingivalis* LpxE. A. The sequence homology alignment was performed in PubMed database (www.blast.ncbi.nlm.nih.gov) using default parameters. Distribution of the top 100 Blast hits on 100 bacteria LpxE sequences. The red Blast hits (score ≥ 200) are LpxE from *P. gingivalis* subspecies. The purple Blast hits (score 80-200) are LpxE from other Gram-negative bacteria. The putative conserved N-terminal domain (NTD) belongs to PAP2 (type-2 phosphatidic acid phosphatase)-like superfamily. Only *P. gingivalis* LpxE possesses a signal peptide and the intact C-terminal region (CTR). Both *Parabacteroides* sp. LpxE (Sequence ID: WP_122362166.1 and WP_128135112.1) and *Prevotella pleuritidis* (Sequence ID: WP_021583963.1 and WP_036931304.1) possess signal peptide. *Parabacteroides* sp. Excluding the conserved phosphatase domain, LpxE possesses an N-terminal extension and a partial CTR, but *P. pleuritidis* LpxE only possesses a partial CTR. **B.** Schematic of *P. gingivalis* LpxE with mature sequence numbers and structural features annotated. SP, periplasmic signal peptide, residues 1-22; NTD, N-terminal domain, residues 23-241; CTR, C-terminal region, residues 242-445.

4.3 Structure prediction of LpxE

The above sequence alignment result indicated that *P. gingivalis* LpxE is a novel lipid A 1-phosphatase as it possesses a unique CTR. To investigate the potential function of this unique LpxE sequence, structure predictions were performed using *in silico* tertiary structure prediction software. At the time of carrying out these predictions, the AlphaFold2 program, which now provides highly accurate protein structure predictions based on deep leaning algorithms[320], was not available. The Phyre2 server[321] was instead implemented and these outputs were used to guide further experiments. However, during writing up this thesis, AlphaFold2 was released and *P. gingivalis* LpxE was then reanalysed with this, which is presented in Chapter 5.

The Phyre2 predicted structure of full-length LpxE suggested that the NTD is a typical phosphatase that contains seven α-helices (**Figure 4.2A**), and the two closest hits are an acid phosphatase from *Escherichia blattae* (23% identity, 99.84% confidence score) and a lipid A 1-phosphatase LpxE from *Aquifex aeolicus* (25% identity, 99.79% confidence score). The structures of these (PDB ID code 1D2T, 6EBU)[283,322] has shown them to be integral inner membrane (IM) proteins related to the PAP2-like family. However, although the predicted structure of the *P. gingivalis* LpxE CTR is not shown as it was not possible to acquire a confident structure prediction for this region, secondary structure prediction of this region indicates that it is β-sheet rich and lacks α-helices.

The predicted structure of the *P. gingivalis* LpxE NTD was superposed with the published structure of *A. aeolicus* LpxE[283] (PDB ID code 6EBU) which suggests that

they are conserved, although *P. gingivalis* carries an additional 22 amino acid sequence at the N-terminus. (**Figure 4.2B, C**). The active site of LpxE NTD is defined by a conserved motif specific to the PAP2 enzymes ($K^{120}X_6R^{127}P$---$R^{177}X_5H^{183}X_3D^{187}$) located at the C-terminal end of the α4 helix, α4-α5 loop, α6 helix, α6-α7 loop, and the N-terminus of the α7 helix (**Figure 4.2D)**. In this motif, the catalytically important H183 residue removes the phosphate group from the lipid substrate[283]. Given that the structural homologues of *P. gingivalis* LpxE NTD are integral IM proteins[283,323] and that the surface of LpxE NTD is mainly composed of hydrophobic residues (**Figure 4.2E)**, *P. gingivalis* LpxE is also likely an integral IM protein. However, how the unique CTR in LpxE affects its structure or function is unclear.

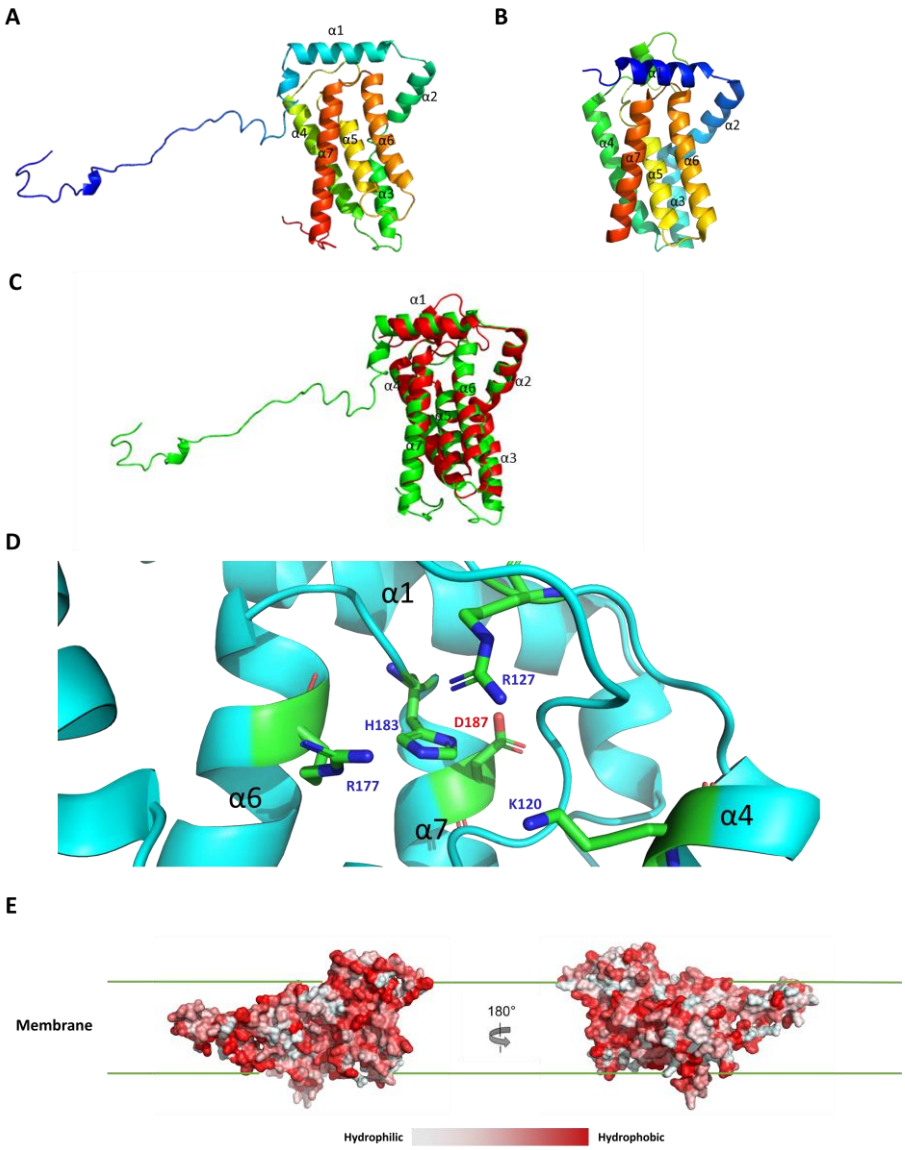

Figure 4.2: Predicted structure of *P. gingivalis* LpxE N-terminal domain. A. Predicted structure of full-length LpxE. The N-terminal domain (NTD) was predicted to be seven helices with an additional N-terminal extended region (22 amino acids). Phyre 2 prediction of C-terminal region (CTR) was disordered and had a very low confident score, and is not shown. **B.** Crystal structure of *Aquifex aeolicus* LpxE^{283} (PDB ID code 6EBU). **C.** Superimposition of predicted LpxE NTD (green) with published structure of *A. aeolicus* LpxE (red). The overall structures superpose very well (25% identity, 99.79% confidence score), although an additional N-terminal region is present at the N-terminus of *P. gingivalis* LpxE NTD. **D.** The active site of LpxE NTD. Side chains of R177, H183 and D187 from the RX_5HX_3D motif and side chains of K120 and R127 from the KX_6RP motif, are shown as sticks. The catalytically important H183 removes the phosphate group of the lipid substrate. **E.** Hydrophobicity of LpxE NTD surface. The more hydrophobic residues are shown in red colour and the more hydrophilic residues are shown in white colour. The structures were predicted by Phyre2 server: www.sbg.bio.ic.ac.uk/phyre2.

Since the *P. gingivalis* LpxE CTR is unusual with no valid model being predicted, and

analysis of the T9SS mutants had suggested that the T9SS may regulate the activity of LpxE, it was possible that this CTR could directly bind to a component of the T9SS. Although the T9SS cargo-CTD is <10 kDa while the *P. gingivalis* LpxE CTR is ~25 kDa, it was speculated that CTR may be acting as a modified CTD secretion motif, and it was therefore compared to sequences of T9SS substrate CTDs. Alignment of the CTDs from the most common T9SS substrates with the LpxE CTR revealed that there are several well-conserved amino acid residues that are scattered around the three conserved motifs (**Figure 4.3A**). However, due to the longer sequence of LpxE CTR, a long internal additional sequence was also observed. In the putative B-motif, 4 of the 9 residues in LpxE CTR (X_2DX_2GKXV) are conserved, however, this motif is not necessary for substrate secretion. For example, the CTD of T9SS substrate HBP35 lacks the motif B[128]. Motif D (G(I/L/V)Y) and motif E (K(VIL)(VIA)(VI)) are thought to be necessary for T9SS dependent secretion[173,223,224]. In the putative D-motif, the second and third sites of LpxE CTR (AVY) are conserved, although LpxE CTR lacks the first Glycine which is present in all known T9SS CTDs. In the putative E-motif of LpxE CTR (KRAT), the first and third residues are conserved, with the first site being completely conserved in all CTDs. Mutational analysis of the CTD from RgpB in *P. gingivalis* has revealed that alanine substitutions of the first, second and third positions in this motif all result in reduced secretion[324]. The phylogenetic analysis of LpxE CTR indicates that it may be close to CTDs of PG2216, PorU and PorZ (**Figure 4.3B**), however, it was not conclusive whether LpxE CTR is a true CTD motif and related to T9SS recognition.

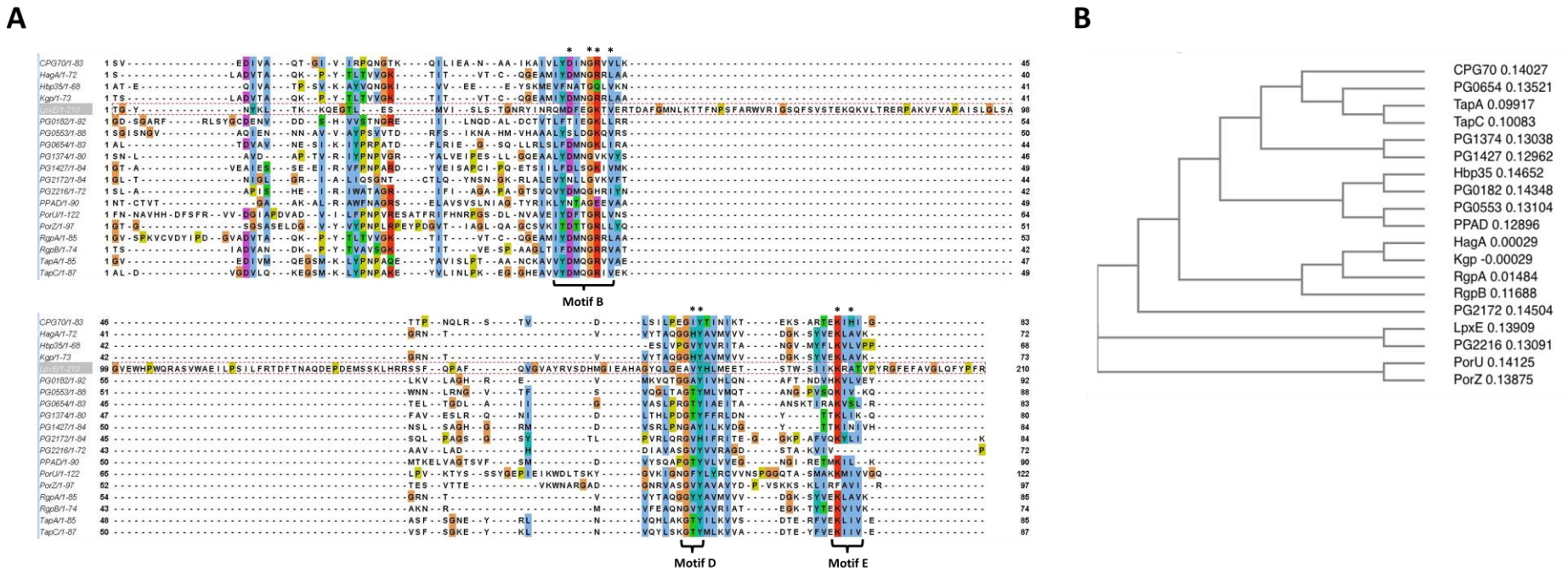

Figure 4.3: Multiple sequence alignment of LpxE CTR and T9SS substrate CTDs. A. Pairwise sequence alignment of *P. gingivalis* LpxE CTR against T9SS substrate CTDs. Conserved residues at three conserved T9SS CTD motifs (motif B, motif D and motif E) were labelled as*. Conservation is defined by Clustal X Colour Scheme[325]. Blue (hydrophobic) - A, I, L, M, F,W,V; Red (positive charge) - K, R; Magenta (negative charge) - E, D; Green (polar) - N, Q, S, T; Orange (glycine) - G; Yellow (proline) - P; Cyan (aromatic) - H, Y; White (unconserved) - any/gap. **B.** Phylogram of LpxE CTR and T9SS substrate CTDs. This is a Neighbour-joining tree without distance corrections. The numbers next to the protein names represent a measure of support for the node. These are numbers between 0 and 1 (1 represents maximal support).

4.1 Mutagenesis of LpxE

To further explore how LpxE could be linked to the T9SS, a *lpxE* mutant in *P. gingivalis* W50 was produced. An *erm* (*ermF-ermAM*) cassette was again used as the positive selector with flanking regions of the gene designed and tagged to the cassette at its 5′ and 3′ ends by PCR. The construct was then targeted to the genomic gene to be modified by electroporation, and then positive colonies were selected by clindamycin resistance on blood agar plates. Finally, correct insertions of the cassette into the coding regions of these genes were identified by colony PCR (**Figure 4.4**). Previous studies have suggested that *P. gingivalis lpxE* is the single gene in an operon[290] and a *lpxE* mutant has been created in ATCC 33277 strain using a similar method[153]. Therefore, the mutation of *lpxE* was not expected to cause any polar issue.

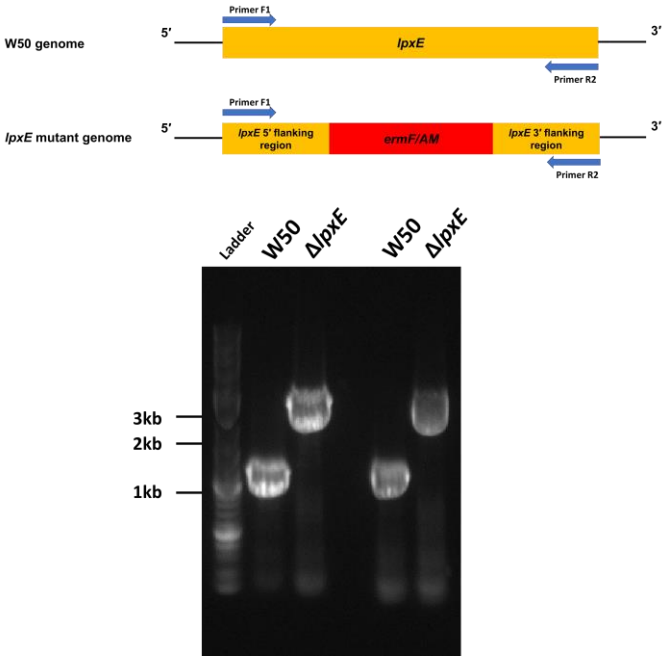

Figure 4.4: Colony PCR of *P. gingivalis* W50 and *lpxE* mutant. Primers at the ends of 5′-region and 3′-region of *lpxE* were used to amplify target DNA fragment. Genomic DNA of W50 and *lpxE* mutant strains were used as colony PCR templates. A significant band shift was seen between W50 and *lpxE* mutant, suggesting that *erm* cassette was successfully inserted into the coding regions of *lpxE* gene. Number ladders on the left-hand side represent the size of marker DNA in kb.

4.2 Construct of *lpxE* HA-tagged complements

Human influenza hemagglutinin (HA) is a surface glycoprotein required for the infectivity of the human influenza virus[326]. The HA-tag is derived from amino acids 98-106 of human influenza hemagglutinin and has been extensively used as a general epitope tag in expression vectors. Many recombinant proteins have been engineered to express the HA-tag, where it does not appear to interfere with the bioactivity or the biodistribution of the recombinant protein. This tag facilitates the detection, isolation, and purification of the protein of interest. To investigate the role of LpxE *in vivo*, a HA-tag was introduced and HA-tagged *lpxE* complement strains were created in *P. gingivalis* W50 strain. It was not known how the HA-tag would interfere with the LpxE folding, thus the plan was to introduce the HA-tag on either the N-terminus or the C-terminus of LpxE (**Figure 4.5A**). At the N-terminus, the HA-tag was designed to be inserted directly after the signal peptide and was expected to remain associated with LpxE, no matter where LpxE localized in the bacteria. At the C-terminus, the HA-tag was designed to be inserted after the last residue in LpxE, however, if the LpxE CTR was functional as a T9SS CTD, the LpxE CTR and the HA-tag may be cleaved off.

Positive colonies of the N-terminal HA-tagged *lpxE* complement (*lpxE*/N-HA) and C-terminal HA-tagged *lpxE* complement (*lpxE*/C-HA) were identified by tetracycline selection and colony PCR (**Figure 4.5B**). Although this suggested that *lpxE* had been complemented back into the *P. gingivalis* genome, mRNA analysis would be needed to confirm gene expression of the two complements. Ultimately, MALTI-TOF mass spectrometry analysis of lipid A was required to quantify the activity of these modified

lpxE products. Unfortunately, due to COVID, this data was not acquired. However, it was still possible to carry out other characterisation of these *lpxE* mutant and HA-tagged strains in relation to OMV formation and protein-protein interaction.

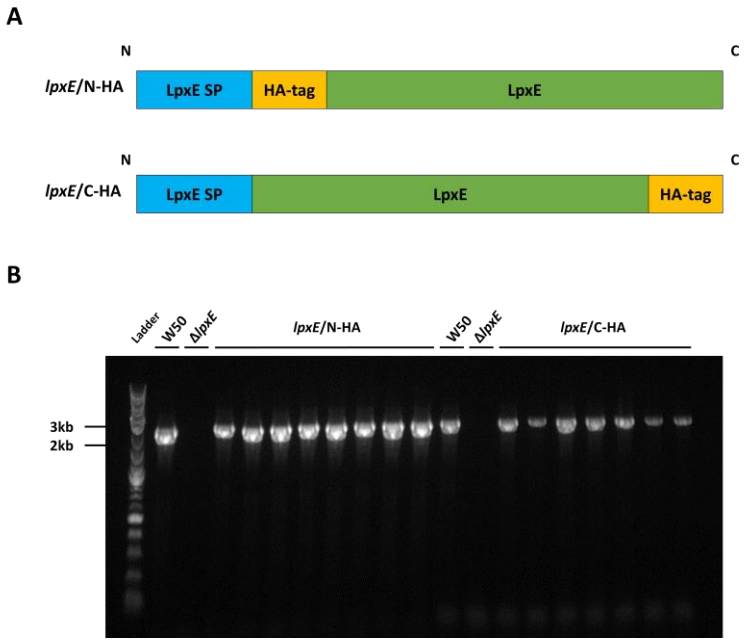

Figure 4.5: Constructs of *P. gingivalis lpxE* complement strains. A. The design of HA-tag complement strains. **B.** Colony PCR of *P. gingivalis* lpxE complement strains. Primers at the ends of 5′-500 bp upstream region and 3′-region of *lpxE* were used to amplify target DNA fragment. Genomic DNA of W50, *lpxE* mutant and two *lpxE* complement strains (*lpxE*/N-HA and *lpxE*/C-HA) were used as colony PCR templates. A band at correct size was amplified in the positive colonies, suggesting that *lpxE* mutant was successfully complemented. Ladder on the left-hand side indicates the size of marker DNA in kb.

4.3 Characterization of LpxE

4.3.1 Pigmentation

Wild-type *P. gingivalis* W50, Δ*lpxE*, *lpxE*/N-HA and *lpxE*/C-HA strains were cultured anaerobically on blood agar plates for 7 days. W50 presented black pigmentation as usual as did the Δ*lpxE*, *lpxE*/N-HA and *lpxE*/C-HA (**Figure 4.6**). This phenotype suggests that LpxE is not required for black pigmentation and therefore is not involved

in the secretion of cargo by the T9SS.

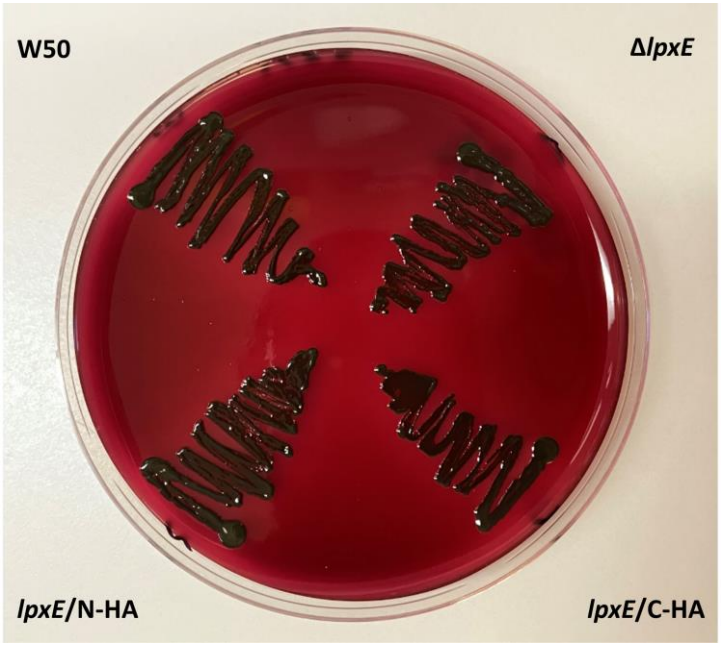

Figure 4.6: Colony morphology of *lpxE* mutant and complement strains. Wild-type *P. gingivalis* W50, *lpxE* mutant and two *lpxE* complement strains grew anaerobically on blood agar plate for 7 days. These four strains presented black pigmentation on blood agar plate.

4.3.2 Growth rate analysis

A growth curve assay was performed next to assess the growth rates of the *lpxE* mutant and two HA-tagged *lpxE* strains. The growth rate of these four strains were very similar with no significant differences observed (**Figure 4.7**). This suggested that these strains were not defective in growth compared to W50.

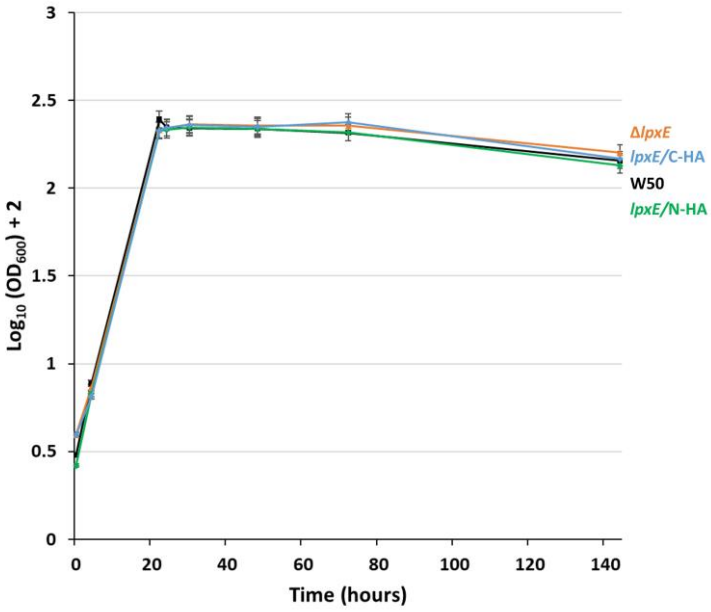

Figure 4.7: Growth curves of *lpxE* mutant and two complement strains. Growth curve plotted as [$\log_{10}(OD_{600})$ + 2] versus time for W50, Δ*lpxE*, *lpxE*/N-HA and *lpxE*/C-HA grown in BHI broth supplemented with hemin at 37°C in anaerobic cabinet. Samples were withdrawn at each time point under anaerobic condition, and the OD_{600} was measured for 6 days. Three technical repeats of the OD_{600} at each time point were measured. Data are presented as means ± SDs (n = 3). The error bars are shown. Student's *t* test for W50 versus Δ*lpxE*, *lpxE*/N-HA and *lpxE*/C-HA at 24 h, 48 h, 72 h and 150 h yielded *P* values > 0.05, suggesting no significant difference. This assay was repeated twice, and this is a typical representation.

4.3.3 Enzyme activity assay

To assess whether LpxE affects gingipain protease activity in T9SS mutants, Arg- and Lys-gingipain activity assays were performed again using whole cell samples and supernatant samples derived from W50, Δ*lpxE*, *lpxE*/N-HA and *lpxE*/C-HA strains. The data showed that knocking out *lpxE* resulted in a decline of both arginine and lysine gingipain activity in whole cell samples (**Figure 4.8**). This phenotype was partially restored in the N-terminal HA-tagged *lpxE* complement, but not in the C-terminal HA-tagged *lpxE* complement.

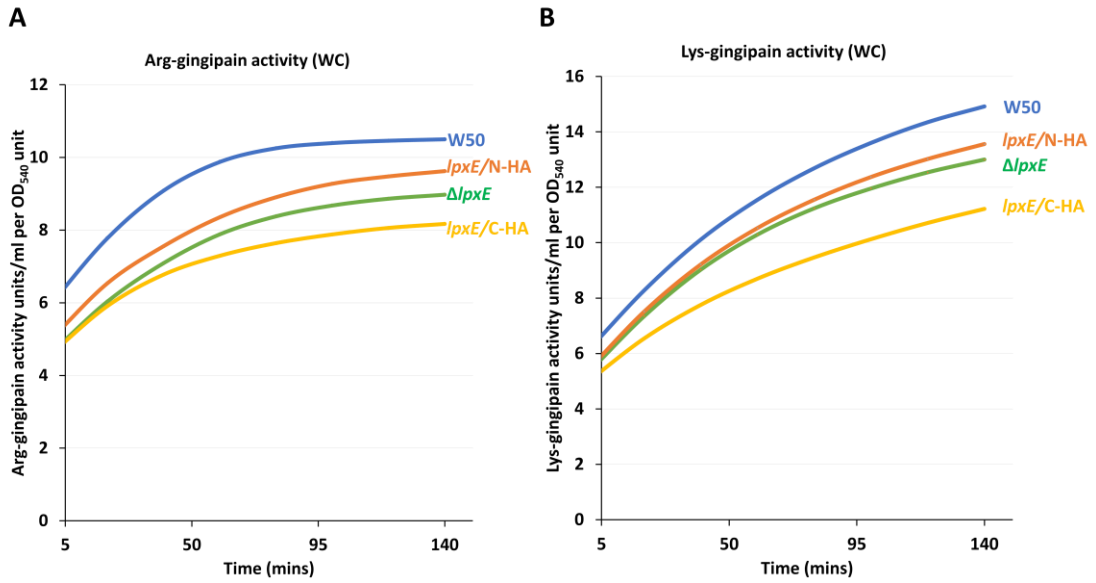

Figure 4.8: Enzyme activity in whole cells of *lpxE* mutant. Cultures were grown as described in methods and whole cell samples were obtained by collecting the cell pellet fraction after centrifugation of 20 µl culture. The optical densities were measured at 540 nm. **A.** Arg-gingipain activity in whole cells (WC) of *P. gingivalis* W50, *lpxE* mutant and two *lpxE* complements. Whole cell samples were assayed for Arg-gingipain activity using DL-BRpNA as the chromogenic substrate as described in methods. **B.** Lys-gingipain activity in whole cells (WC) of *P. gingivalis* W50, *lpxE* mutant and two *lpxE* complements. Whole cell samples were assayed for Lys-gingipain activity using L-AcLyspNA as the chromogenic substrate as described in methods. All the lines were shown in different colours. This data is the average of three technical repeats.

Enzyme activity assays performed on culture supernatant samples of these strains also showed a decline of both arginine and lysine gingipain activity in the *lpxE* mutant compared with W50 (**Figure 4.9**). However, the phenotype was not restored in either the N-terminal HA-tagged or C-terminal HA-tagged *lpxE* complements.

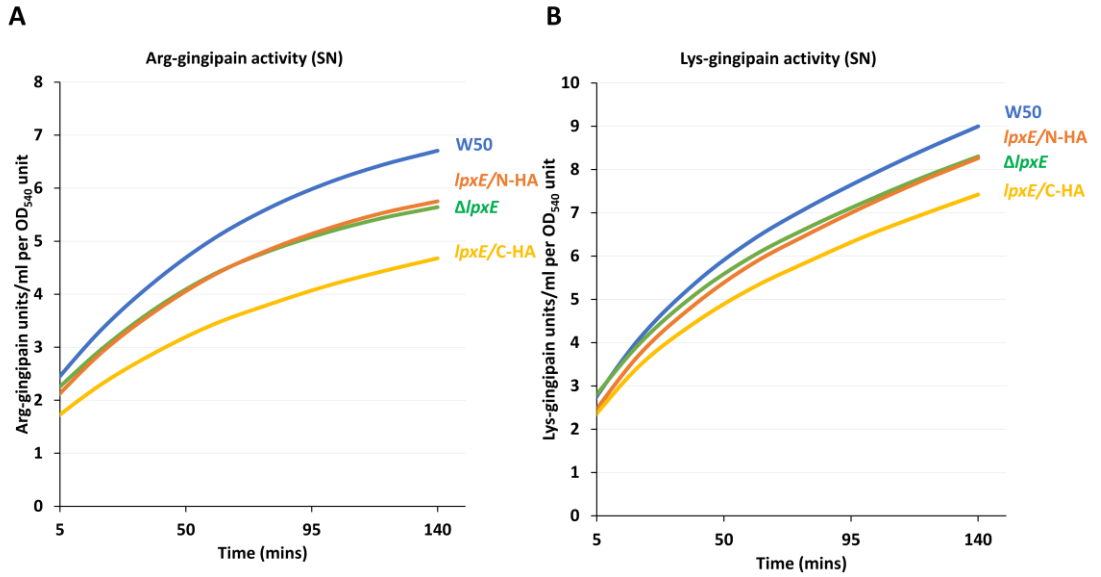

Figure 4.9: Enzyme activity in culture supernatant of *lpxE* mutant. Cultures were grown as described in methods and supernatant samples were obtained by collecting the supernatant fraction after centrifugation of 20 µl culture. The optical densities were measured at 540 nm. **A.** Arg-gingipain activity in culture supernatant (SN) of *P. gingivalis* W50, *lpxE* mutant and two *lpxE* complements. Supernatant samples were assayed for Arg-gingipain activity using DL-BRpNA as the chromogenic substrate as described in methods. **B.** Lys-gingipain activity in culture supernatant (SN) of *P. gingivalis* W50, *lpxE* mutant and two *lpxE* complements. Supernatant samples were assayed for Lys-gingipain activity using L-AcLyspNA as the chromogenic substrate as described in methods. All the lines were shown in different colours. This data is the average of three technical repeats.

As there is no other evidence suggesting that LpxE is involved in secretion through the T9SS, it is difficult to explain why gingipain activity declined in the Δ*lpxE* strain, especially as this mutant formed black pigmentation as W50 does (**Figure 4.6**). Also, this phenotype was not restored in the complements, suggesting that the HA-tag could be interfering with transcription, translation, correct folding and/or membrane localisation of LpxE.

4.3.4 TEM of *lpxE* mutant

In the previous TEM study of the T9SS mutants, the cell samples had been fixed with formaldehyde. However, there was a concern that formaldehyde may be too harsh for these samples, which have different LPS (lipid A) profiles in their outer membrane compared to W50, and the formaldehyde fixation might have led to the abnormal OMV blebbing in these mutants. Thus, a modified and less harsh TEM method was used to investigate OMV formation and morphology of the *lpxE* mutant, through flash-freeze fixation.

The results showed that W50 produced small normal versicles ~40 nm in diameter, whereas the *porV* mutant produced large irregular vesicles ~120 nm in diameter (**Figure 4.10A**). As these phenotypes were consistent with the previous measurements of OMVs from the formaldehyde-TEM, this supported the previous TEM results not being artefacts. The *lpxE* mutant also produced large and irregular vesicles with a diameter of ~170 nm (**Figure 4.10A**) which are similar to the T9SS mutants (**Figure 3.13**). However, the *lpxE*/C-HA complement formed relatively smaller vesicles ~100 nm, indicating that the phenotype was partially restored in the complement. Analysis of bacterial and OMV diameters across nine bacterial images for each strain supports that observed cell sizes of W50, Δ*porV*, Δ*lpxE*, *lpxE*/C-HA strains were similar, but OMV sizes of W50 and Δ*porV*, Δ*lpxE*, *lpxE*/C-HA strains were significantly different (**Figure 4.10B**). Also, the OMV size of Δ*lpxE* was significantly larger than that of Δ*porV*. This data suggests that both PorV and LpxE are required for the normal smaller OMV formation in *P. gingivalis*, while the phenotype was partially restored in the *lpxE*/C-HA

complement. To assess whether the mutations also influenced the quantity of OMVs formed, OMVs per blebbing cell were also counted (**Figure 4.10C**). However, no significant differences versus W50 were present.

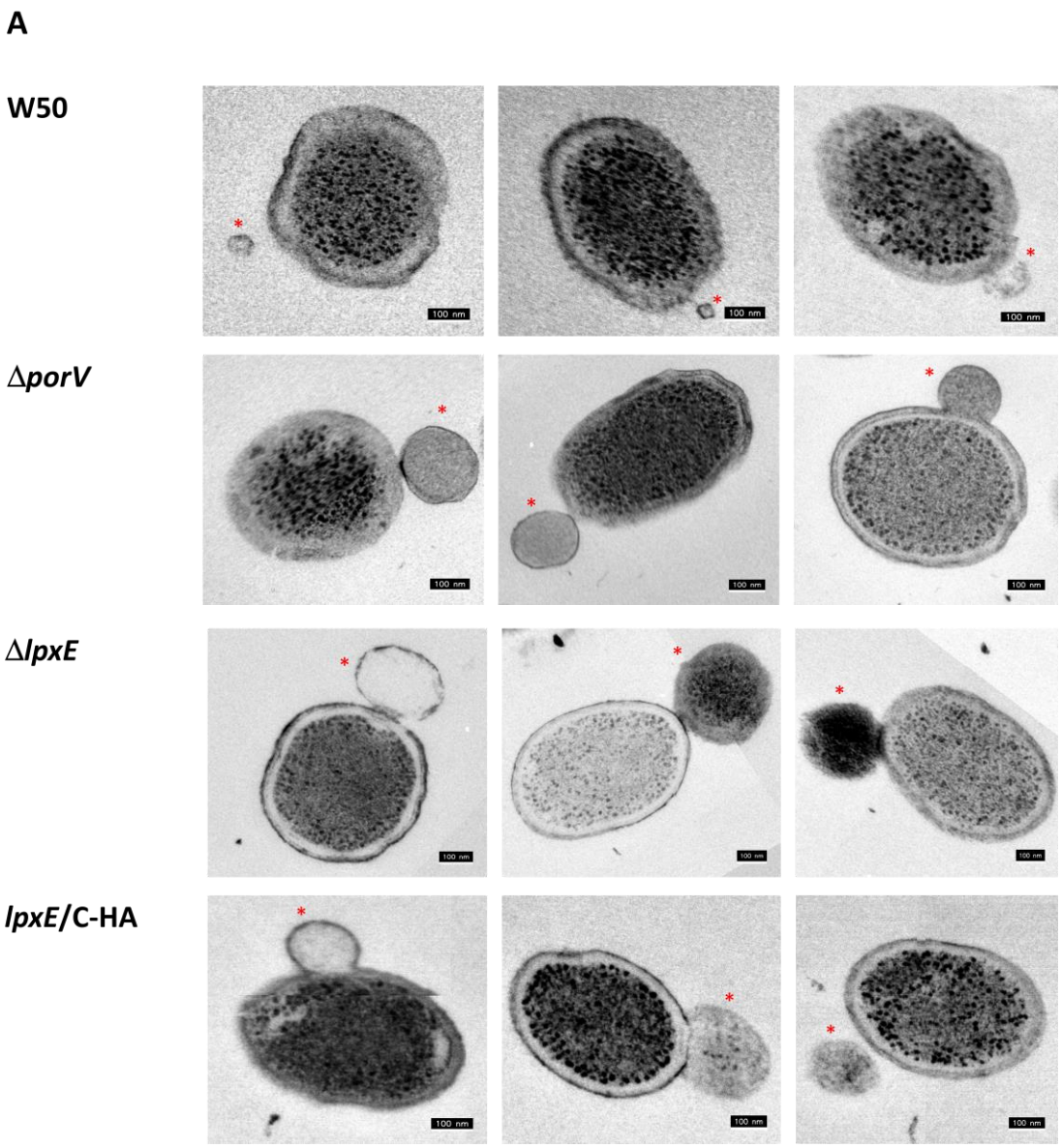

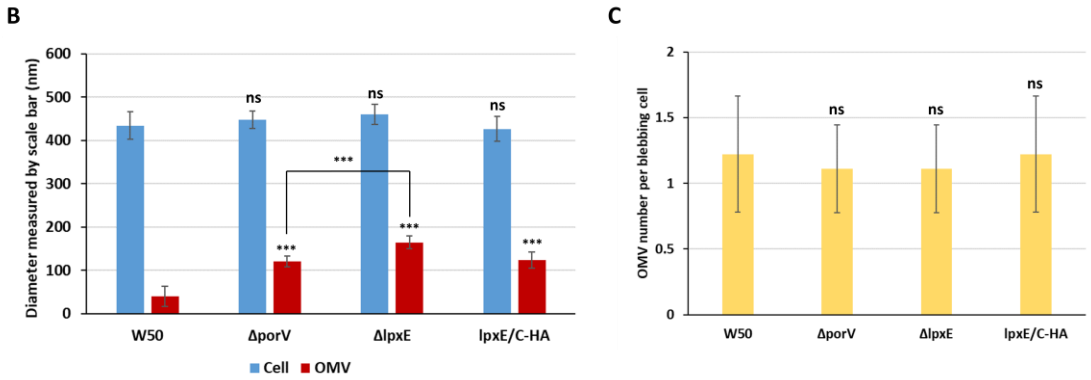

Figure 4.10: TEM of OMV formation in *lpxE* mutant. A. Transmission electron microscope (TEM) images of *P. gingivalis* W50, Δ*porV*, Δ*lpxE* and *lpxE*/C-HA cells. Due to COVID and time restriction, another *lpxE*/N-HA complement strain was not analysed. Samples were prepared using flash-freeze method. Scale bar: 100 nm. The data was collected from random cells which were in an OMV blebbing status. The representative images from three biological repeats were shown. The OMV blebbing was marked as red asterisk. OMV formation in *P. gingivalis* W50 strain was clearly visible as defined structures. Δ*porV*, Δ*lpxE* and *lpxE*/C-HA produced large and irregular vesicles. **B.** Measurements of cell and OMV diameter in each blebbing cell. The blebbing status is defined that OMVs were within 50 nm distance to the cell. Data are presented as means ± SDs (n = 9). Student's *t* test for cell and OMV diameter: W50 versus Δ*porV*, Δ*lpxE* and *lpxE*/C-HA yielded a *P* value. ns: p>0.05, non-significant. ***: p < 0.001, significant. **C.** OMV number per blebbing cell. The blebbing status is defined that OMVs were within 50 nm distance to the cell. Data are presented as means ± SDs (n = 9). Student's *t* test for OMV number per blebbing cell: W50 versus Δ*porV*, Δ*lpxE* and *lpxE*/C-HA yielded a *P* value. ns: p > 0.05, non-significant. These are the representative data of three biological and technical repeats.

4.3.5 NanoSight analysis of *lpxE* mutant

To measure the size of OMV particles produced by the *lpxE* mutant in solution, the Malvern NanoSight LM10 Nanoparticle Characterization was again applied. The average size of total OMVs of Δ*lpxE*, *lpxE*/C-HA and *lpxE*/C-HA strains is ~120 nm, which is close to W50. However, compared to the most predominant peak at 44 nm in W50, the most predominant peaks of Δ*lpxE*, *lpxE*/C-HA and *lpxE*/C-HA are 107 nm (2.5 particles/ml), 140 nm (2.2 particles/ml) and 117 nm (2.1 particles/ml), respectively (**Figure 4.11**). Moreover, the ~50 nm smaller size OMVs decreased to 0.5 particles/ml

in Δ*lpxE*, *lpxE*/C-HA and *lpxE*/C-HA strains, compared to 5.1 particles/ml in W50. These data suggest that these T9SS mutants tend to produce the same amount of larger OMVs as W50 does, but they produce much less ~50 nm smaller OMVs than W50. These particle size data imply that knocking out *lpxE* may affect the production of normal smaller OMVs, which is consistent to the TEM data. However, the phenotype was partially restored in these two complement strains. This experiment needs to be biologically repeated to confirm OMV size differences between W50 and the other strains. Also, it would be useful to do TEM for these purified OMV samples in the future to confirm the OMV samples are consistent with NanoSight data.

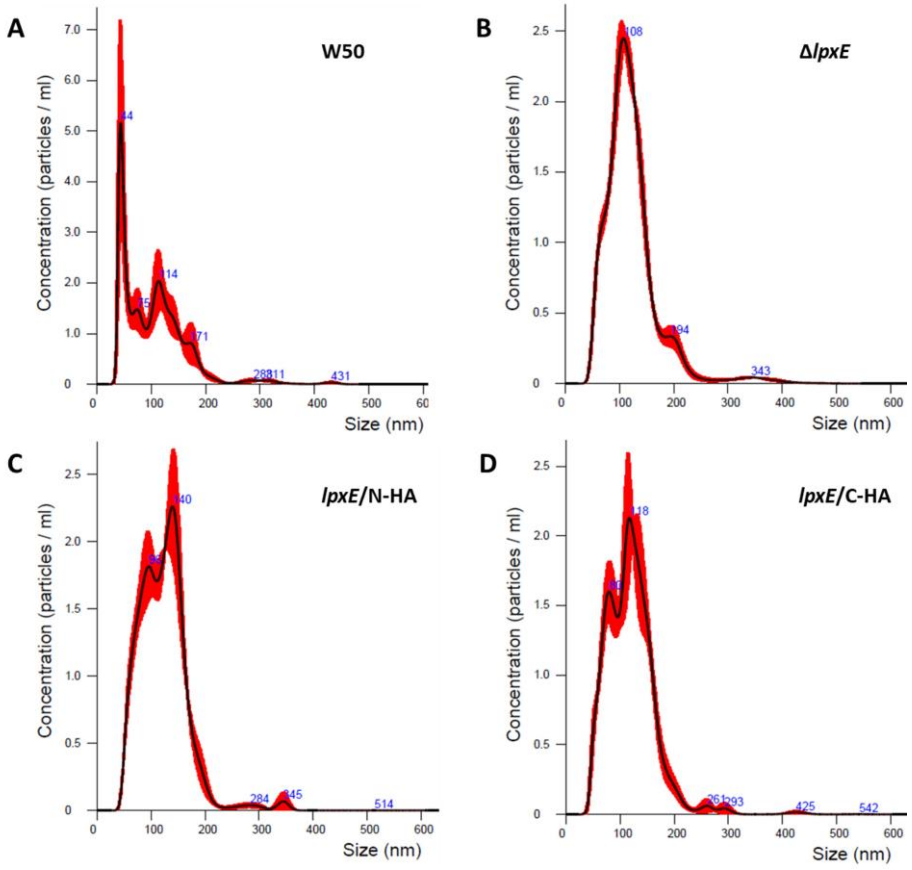

	W50	Δ*lpxE*	*lpxE*/N-HA	*lpxE*/C-HA
mean (nm)	103	122	123	120
mode (nm)	44	107	140	117

Figure 4.11: NanoSight analysis of *lpxE* mutant. A. Concentration of OMV sizes in W50. **B.**

Concentration of OMV sizes in *lpxE* mutant. **C.** Concentration of OMV sizes in N-terminal HA-tagged *lpxE* complement. **D.** Concentration of OMV sizes in C-terminal HA-tagged *lpxE* complement. OMV samples were prepared as described in methods. Averaged finite track length adjustment (FTLA) concentration and size for experiment were shown. Error bars indicate standard error of the mean. Mean value represents the average size of total OMVs of each sample. Mode value represents the most prominent OMV size of each sample. As overlap of particles may affect the accuracy of size measurement, the samples were diluted 10-fold. These are the representative data of three technical repeats.

4.3.6 Dry weight analysis of OMVs

As an additional evaluation of the OMVs produced by the *lpxE* mutant strains, vesicles obtained from 200 ml cultures of W50, Δ*lpxE*, *lpxE*/N-HA and *lpxE*/C-HA strains were purified using ultracentrifugation and their dry weights were measured. The result indicates that the dry weight in the *lpxE* knock-out mutant decreased when compared to W50 (**Figure 4.12**), which is supported by the NanoSight data that shows an overall reduction in the production of smaller particles. However, this reduction in OMV dry weight was restored in both the N-terminal and C-terminal HA-tagged *lpxE* complements (**Figure 4.12**), which is partly supported by the NanoSight results. However, measuring OMV dry mass in this manner is difficult and these need repeating to ensure that these differences are not due to measurement errors.

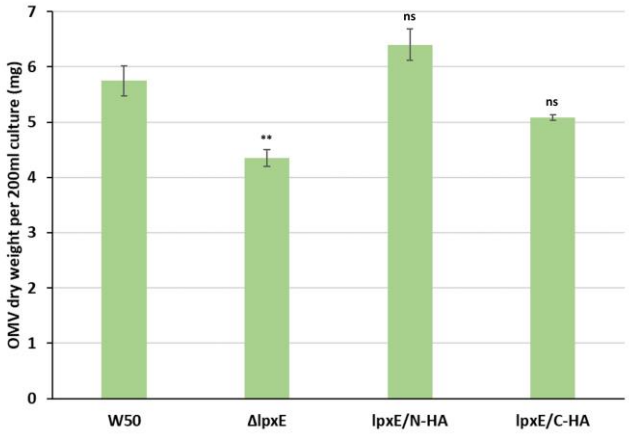

Figure 4.12: Analysis of OMV dry weight. Dried OMV samples were prepared as described in methods. Data are presented as means ± SDs (n = 3). Student's *t* test for dry weight: W50 versus Δ*lpxE*, *lpxE*/N-HA and *lpxE*/C-HA yielded a *P* value. ns: $p > 0.05$, non-significant. **: $p < 0.005$, significant. This data is the average of three technical repeats.

The above analyses of the *lpxE* mutant suggested that OMV production in this strain was abnormal, and OMVs were similar in appearance to those produced by the T9SS mutant strains. To investigate this phenotype further, total protein from the outer membrane (OM) and vesicles of W50 and *lpxE* mutant strains were analysed by SDS-PAGE. The major outer membrane proteins RagA, RagB, Kgp and Rgp^{303} appeared to be present in both OM and OMV samples in all strains. However, two unidentified bands at around 85 kDa and 62 kDa were observed in the OM samples of W50 but not seen in the Δ*lpxE*, *lpxE*/N-HA and *lpxE*/C-HA strains (**Figure 4.13**). Instead, the mutant and HA-tagged *lpxE* strains presented two different bands with slightly lower molecular weight, which were not visible in the W50 lane. These bands could represent the same protein which had been proteolytically cleaved in the modified strains or represent two different proteins displaying different levels of expression. The 85 kDa band was also present in the OMV sample of W50 strain but was again slightly shifted down in the other strains, while the 62 kDa band could not be seen. However, it appears that the

phenotype of the *lpxE* mutant was not restored by the complements in either the OM or OMVs as the protein patterns of Δ*lpxE*, *lpxE*/N-HA and *lpxE*/C-HA were very similar. Nonetheless, inactivation of *lpxE* did appear to have an influence on protein composition of the OM and OMVs and mass spectrometry analysis for the unknown 85 kDa and 62 kDa proteins would be useful to better understand this data.

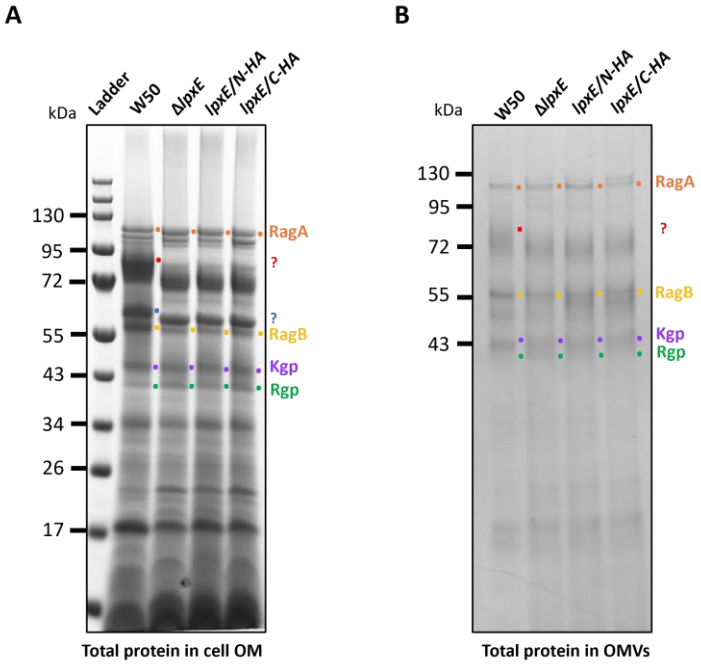

Figure 4.13: SDS-PAGE of total protein in cell OM and OMVs. Bacteria outer membrane and OMV samples were prepared as described in methods. Based on band size, the designated proteins are dotted in different colour. The unidentified bands are labelled as a question mark. **A.** SDS-PAGE of total outer membrane protein of W50, *lpxE* mutant, N-terminal HA-tagged *lpxE* complement and C-terminal HA-tagged *lpxE* complement. **B.** SDS-PAGE of total OMV protein of W50, *lpxE* mutant, N-terminal HA-tagged *lpxE* complement and C-terminal HA-tagged *lpxE* complement. Number ladders on the left-hand side represent the size of marker proteins in kDa. The designations were based on band size by comparing with published data. Due to COVID and time restriction, this experiment was not repeated.

4.3.7 Detergent inhibition assay

To test cell membrane stability of the *lpxE* mutant, the detergent inhibition assay which was performed on the T9SS mutants was repeated. Colonies of the *lpxE* mutant were

observed at a dilution of 10^5 but were not seen at the same dilution of the W50 strain. This suggested that the membrane of *lpxE* mutant was more stable than W50 when treated with SDS (**Figure 4.14A**) or Triton X-100 (**Figure 4.14B**), and that LpxE is required for destabilizing the bacterial membrane. However, colonies were also seen at dilutions of 10^5 in the two complements, which again suggested that the phenotype of these HA-tagged *lpxE* strains were at best only partially restored.

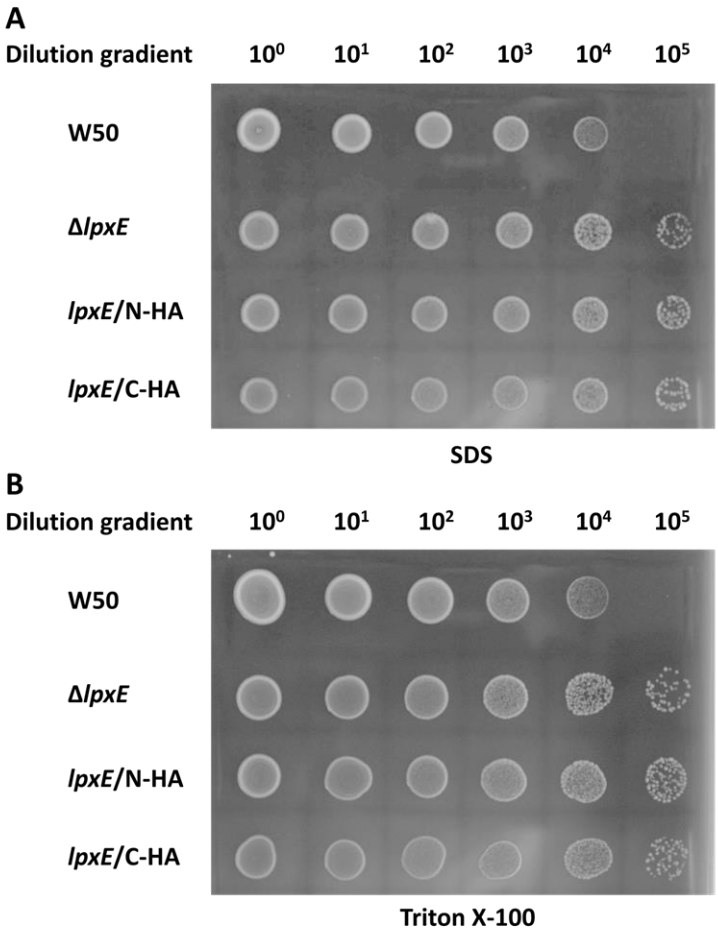

Figure 4.14: Detergent inhibition assay. The detergent inhibition assays were performed on the blood agar plates containing detergent. The OD_{600} of start culture was 0.5 and samples were diluted into different gradients. **A.** SDS inhibition assay. The applied concentration of SDS was 8 μg/ml. **B.** Triton X-100 inhibition assay. The applied concentration of Triton X-100 was 35 μg/ml. Due to COVID and time restriction, this experiment was not repeated.

4.3.8 Antimicrobial peptide inhibition assay

The *lpxE* mutant was next analyzed for its resistance to antimicrobial peptides treating the W50, Δ*lpxE*, *lpxE*/N-HA and *lpxE*/C-HA strains again with the antimicrobial peptides cecropin B and LL-37. As with the detergent inhibition assay, colonies were observed at dilution of 10^5 in the *lpxE* mutant but were not seen at the same dilution in W50 (**Figure 4.15**). This indicated that the *lpxE* mutant was more resistant to cecropin B and LL-37 than W50 and LpxE may be required to destabilize the bacterial membrane.

However, the phenotype was again not restored in two *lpxE* complement strains and the two complement strains appeared to be more resistant to antimicrobial peptides than the *lpxE* mutant (**Figure 4.15**). As outlined previously, this could be due to the HA-tags affecting the folding of LpxE or interfering with other direct interactions such as with the T9SS. On the other hand, the HA-tag could affect *lpxE* transcription, so a clean *lpxE* complement (no HA-tag) and mRNA analysis would be useful to assess this.

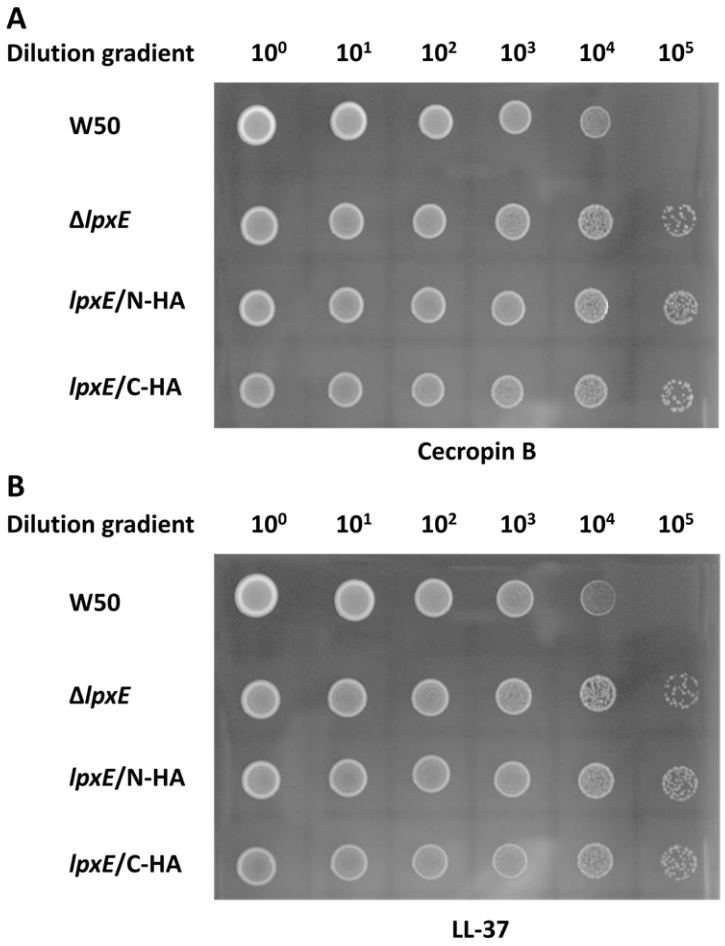

Figure 4.15: Antimicrobial peptide inhibition assay. The antimicrobial peptide inhibition assays were performed on the blood agar plates containing antimicrobial peptides. The OD_{600} of start culture was 0.5 and samples were diluted into different gradients. **A.** Cecropin B inhibition assay. The applied concentration of Cecropin B was 10 mM. **B.** LL-37 inhibition assay. The applied concentration of LL-37 was 10 mM. Due to COVID and time restriction, this experiment was not repeated.

4.3.9 Localization of LpxE

The localization of lipid A 1-phosphatase enzymes has been studied experimentally in several systems, and to date all have been shown to be localized to the inner membrane (IM)[283,327,328]. However, as *P. gingivalis* LpxE is a novel protein that contains an additional N-terminal extension and C-terminal region, it was decided to carry out membrane fractionation analysis of *P. gingivalis* LpxE to confirm whether it was still

targeted to the IM. Although examination of the HA-tagged LpxE complemented strains presented above had at times shown no restoration of wild-type phenotype, some experiments suggested that there was at least a partial recovery. Therefore, in the absence of an LpxE antibody, a HA-antibody was instead used to study LpxE localization.

Whole cell, IM and outer membrane (OM) fractions of W50, Δ*lpxE*, *lpxE*/N-HA and *lpxE*/C-HA strains were prepared, and a fractionated Western blot was probed with HA-antibody. Above non-specific background binding of the antibody, a 48 kDa band which is the predicted molecular weight of LpxE was detected in the purified OM fraction of C-terminal HA-tagged *lpxE* complement but not in the other strains (**Figure 4.16A**). This suggests that LpxE was expressed in the OM of *lpxE*/C-HA but not in *lpxE*/N-HA. However, LpxE was not clearly present in the whole cells of *lpxE*/C-HA, indicating that LpxE could be a naturally low abundant protein as the OM fraction was much more concentrated than the whole cells. However, low abundance could also be explained by the poor restoration of wild-type phenotype in the other studies. Alternatively, it could be an artefact as strong cross-reactivity with the marker was also seen.

To confirm this observation, a biological replicated experiment was performed and the 48 kDa LpxE band was again present, albeit weaker, in the OM of *lpxE*/C-HA but not in the other strains (**Figure 4.16B**). The two consistent results suggest that the 48 kDa band could be LpxE, however, its presence in the OM needs to be confirmed with a specific LpxE antibody or through an alternative method such as mass spectrometry.

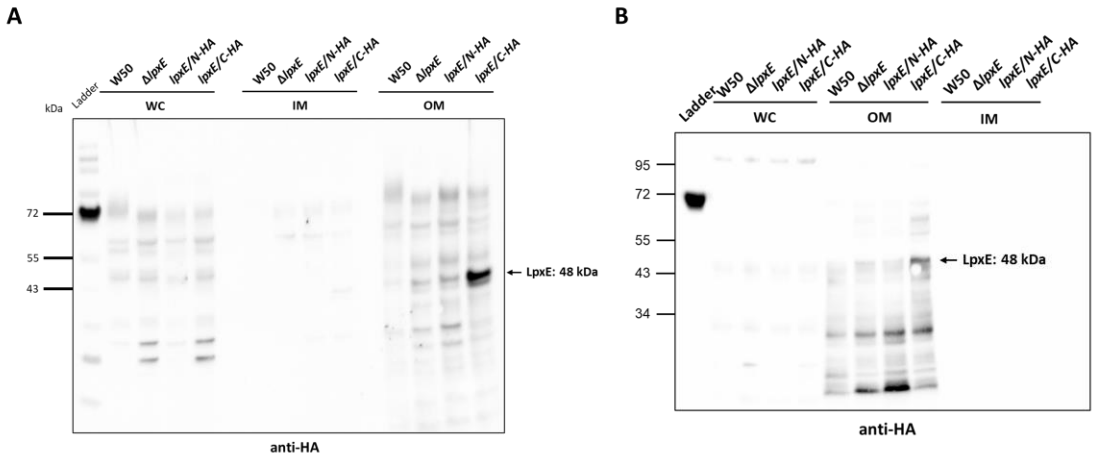

Figure 4.16: Western blot analysis of fractionated protein samples. The fractionated protein samples from whole cells (WC), inner membrane (IM) and outer membrane (OM) were prepared as described in the methods. The immunoblots were probed with anti-HA (diluted 1:1000). **A.** The first fractionated Western blot. B. The repeated experiment. Number ladders on the left-hand side represent the size of marker proteins in kDa. These represent two biological repeats.

Assuming the C-terminally HA-tagged LpxE is at least partially localized to the OM in the *lpxE*/C-HA strain and this is not an artefact, there are several reasons why LpxE may not have been detected in the *lpxE*/N-HA strain. First, it could be due to the additional 22 amino acids at the N-terminus not being stable and resulting in degradation and removal of the HA-tag. Another reason is that the location of this tag does not promote correct membrane targeting and folding. Alternatively, *lpxE* may not have been expressed in this complementation, which should be verified by qPCR in the future. However, since lipid A 1-phosphatases have previously only been reported as IM proteins in other Gram-negative bacteria[283,327,328], this data suggests that *P. gingivalis* LpxE might be the first OM localized lipid A 1-phosphatase. This is a controversial observation and needs to be further thoroughly scrutinized, but while other LpxE structures are fully helical, it is unclear how the additional 25 kDa CTR regions may affect localization of *P. gingivalis* LpxE.

4.3.10 LpxE crosslinking

To complement the membrane fractionation experiments which potential showed location of *P. gingivalis* LpxE in the OM, the next important experiment was to try and identify a protein in *P. gingivalis* that might directly interact with LpxE and could be responsible for regulating its function. Crosslinking is a common method used to identify protein-protein interactions *in vivo* and was therefore implemented. This technique uses a chemical crosslinker to provide a means for capturing protein-protein complexes by covalently binding them together as they interact. The rapid reactivity of the common functional groups on crosslinkers allows even transient interactions to be frozen in place or weakly interacting molecules to be seized in a complex stable enough for isolation and characterization.

For these experiments, two different crosslinker were used: Dithiobis (succinimidyl propionate) (DSP) and formaldehyde. DSP is a homo-bifunctional crosslinker that is lipophilic and cell membrane permeable, so it is useful for studying intracellular and intramembrane interactions. DSP has amine-reactive N-hydroxy succinimide (NHS) esters at both ends of a cleavable, 8-atom (12 Å) spacer arm. DSP contains a reducible disulfide bond in the spacer arm, so the cross-linking can be validated using both reducing and oxidizing conditions[329]. Formaldehyde on the other hand is a chemical cross-linker that is a non-specific with crosslinking space of 2 Å that is suitable for short-distance crosslinking.

As it was not known whether lysis of *P. gingivalis* would display any potential

interactions with LpxE, which would affect crosslinking results, crosslinking was performed before and after lysis, and the crosslinked whole cell samples were then analysed by Western blot with an anti-HA antibody (**Figure 4.17**). In samples that had not been treated with cross-linkers, an additional band was present at around 72 kDa from the *lpxE*/C-HA strain (**Figure 4.17A**), however, this was only observed in the untreated experiment. Moreover, it was expected that any complex would be broken up under these denaturing conditions and this likely represent non-specific binding. No additional bands were seen in the formaldehyde-crosslinked samples except some smearing, which indicates that formaldehyde had caused too many aggregations and was not suitable for this assay. Although strong background was also observed in DSP-crosslinked samples, they could be reduced to analyse captured crosslinked proteins. When the samples were crosslinked before the cell lysis, an intense band was seen at ~85 kDa in the reduced DSP-crosslinked sample of *lpxE*/N-HA (**Figure 4.17B**), but this band was much higher than the anticipated LpxE molecular weight (48 kDa). This indicated that this band was probably due to non-specific binding of the antibody, rather than specific recognition of LpxE, which was supported by a lack of observation of *lpxE*/N-HA in the previous LpxE localization experiment.

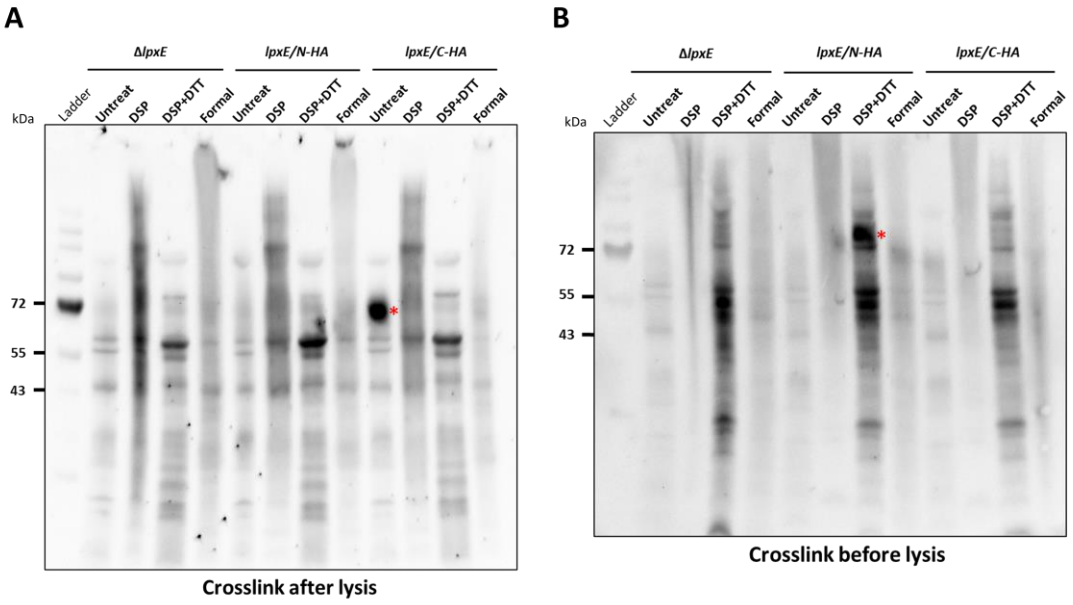

Figure 4.17: Western blot analysis of the crosslinked cell lysate. A. The samples were crosslinked after cell lysis. **B.** The samples were crosslinked before cell lysis. The immunoblots were probed with anti-HA (diluted 1:1000). For each strain, the samples were crosslinked with 2 mM DSP and 1% Formaldehyde. As DSP can be reduced by DTT, the DSP crosslinked samples were also reduced before loaded onto the gel. Untreated samples were the controls. Additional bands (*) were identified in the test samples (*lpxE*/N-HA and *lpxE*/C-HA) compared to the control (Δ*lpxE*). Legend: Δ*lpxE* - cell lysate of the *lpxE* mutant, *lpxE*/N-HA - cell lysate of the N-terminal HA-tagged *lpxE* complement, *lpxE*/C-HA - cell lysate of the C-terminal HA-tagged *lpxE* complement. Number ladders on the left-hand side represent the size of marker proteins in kDa. Due to COVID and time restriction, this experiment was not repeated.

In Western blots for localization of LpxE, LpxE was not seen in whole cells, but was only detected in enriched *lpxE*/C-HA strain outer membranes (**Figure 4.16**). I had supposed that LpxE could be in low abundance in whole cells and therefore decided to first isolate the membranes from these strains and then repeat the crosslinking assay. The cell pellets of these strains were first crosslinked using just DSP, which was then followed by cell lysis, and then the total membrane protein fractions were extracted from the cell lysates and then analysed by Western blot. In addition, as a positive HA-tag control, a HA-tagged RgpB complement strain created by another member of the group was included.

In these experiments, the background was much clearer and detection of HA-tagged RgpB at ~80 kDa confirmed HA-specificity of the antibody. In addition, a high molecular weight band was present in *lpxE*/C-HA, retained in the well, and a high molecular weight smeared band (~130-250 kDa) was also seen in the reduced sample (**Figure 4.18A**). However, when this experiment was repeated, no additional bands were observed in the *lpxE*/C-HA complemented strain (**Figure 4.18B**). Due to the uncertainty of these results, I instead planned to further probe for a potential LpxE interaction using a co-immunoprecipitation (Co-IP) assay.

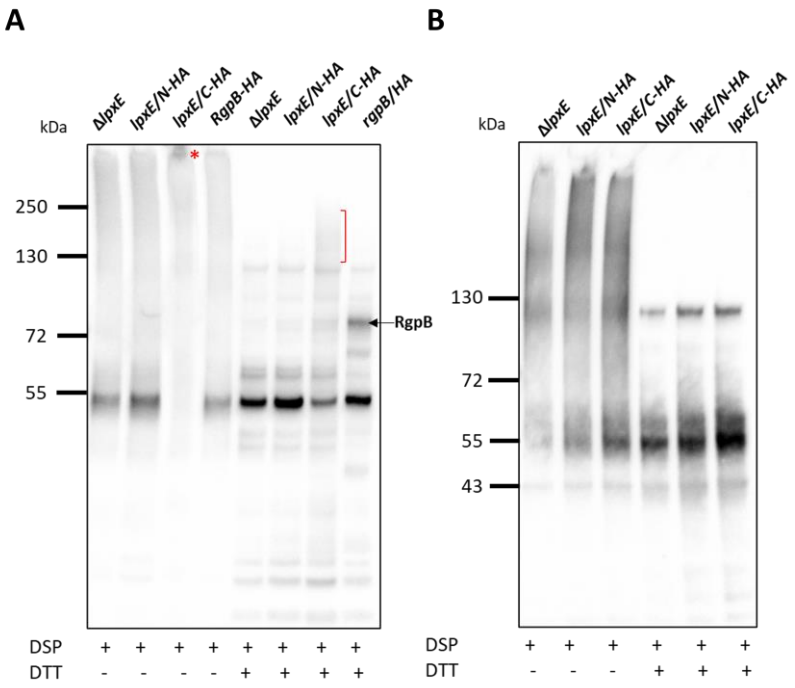

Figure 4.18: Western blot analysis of the crosslinked membrane lysate. A. Analysis of the crosslinked membrane lysate using Western blot probed with anti-HA (diluted 1:1000). **B.** The repeated experiment. The cell pellets were crosslinked with 2mM DSP and the total membrane protein was extracted by 1% DDM. The DSP crosslinked membrane protein samples were also reduced before loaded onto the gel. Additional bands (*) were identified in *lpxE*/C-HA compared to the Δ*lpxE* control. Legend: Δ*lpxE* - membrane proteins of the *lpxE* mutant, *lpxE*/N-HA - membrane proteins of the N-terminal HA-tagged *lpxE* complement, *lpxE*/C-HA - membrane proteins of the C-terminal HA-tagged *lpxE* complement, RgpB/HA - membrane proteins of the HA-tagged *rgpB* complement. Number ladders on the left-hand side represent the size of marker proteins in kDa. Due to COVID and time restriction, this experiment was not repeated.

4.3.11 LpxE co-immunoprecipitation

As the above crosslinking data was not duplicated and LpxE may be natively in low abundance or in low abundance in the complemented HA-tagged strains, a more specific and precise method of Co-IP was applied. Co-IP allows for the indirect capture of interaction partners that are bound to a bait protein recognized by an antibody. These complexes can then be separated by SDS-PAGE and potential interaction partners confirmed with subsequent analysis such as mass spectrometry.

Co-IP reactions were performed using the BioVision Immunoprecipitation Kit using a denaturing lysis buffer. The lysate which was crosslinked with DSP prior to lysis was passed over protein A/G beads alone and beads bound with anti-HA antibody. Protein A/G beads bound to anti-HA antibody with no loading of lysate was used as a negative control. After incubation, the beads were then washed and then eluted using a denaturing method via the addition of SDS-PAGE loading buffer.

The result showed that an additional band at around 65 kDa was present in the reduced DSP-crosslinked sample of *lpxE*/N-HA by SDS-PAGE but not seen in the other strains (**Figure 4.19A**). However, it was not clear if this band was detected by the anti-HA antibody (**Figure 4.19B**). Furthermore, as the localization of LpxE in this strain had not been detected in the above experiments, further verification was needed.

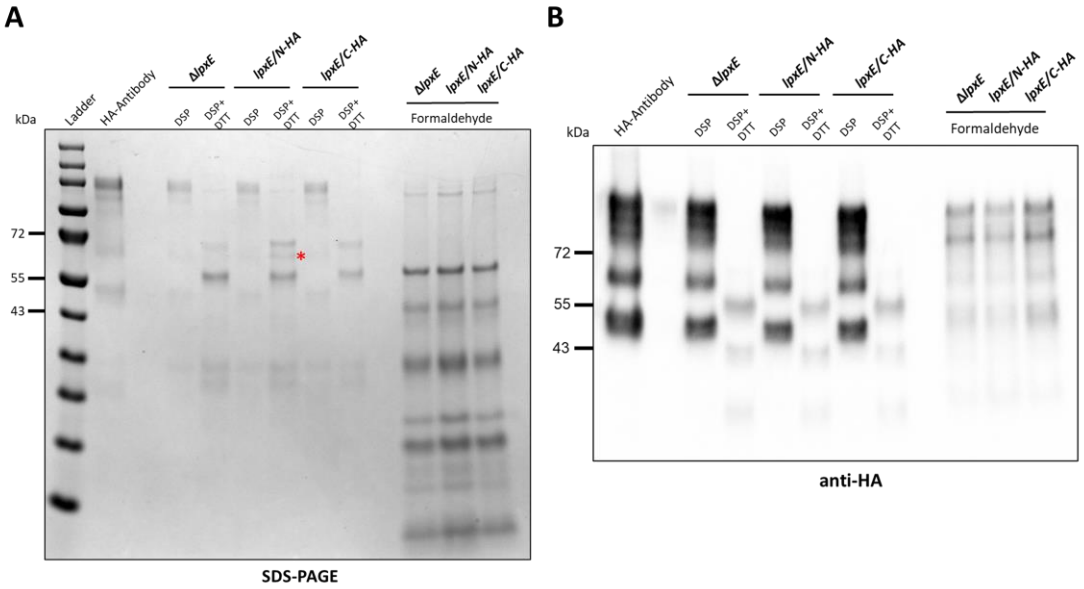

Figure 4.19: Co-immunoprecipitation in the *lpxE* complements. A. SDS-PAGE analysis of co-immunoprecipitation in the *lpxE* complements. An additional band (*) was shown in the reduced DSP-crosslinked sample of *lpxE*/N-HA. **B.** Western blot analysis of co-immunoprecipitation in the *lpxE* complements. The immunoblot was probed with anti-HA (diluted 1:1000). Cells of these strains were crosslinked with DSP and formaldehyde. HA antibody was the negative control. Legend: Δ*lpxE* - the elution sample of Δ*lpxE* lysate, *lpxE*/N-HA - the elution sample of *lpxE*/N-HA, *lpxE*/C-HA - the elution sample of *lpxE*/C-HA. Number ladders on the left-hand side represent the size of marker proteins in kDa.

On repeat of the Co-IP experiment, the ~65 kDa band was not observed in the reduced DSP-crosslinked sample of the *lpxE*/N-HA strain by SDS-PAGE (**Figure 4.20**). However, a faint high molecular weight band ~130 kDa was seen in the reduced DSP-crosslinked samples of *lpxE*/N-HA and *lpxE*/C-HA, but not shown in the *lpxE* mutant (**Figure 4.20**). Due to the lack of reproducibility of this experiment and the issues with reliable complementation of the of *lpxE*/N-HA and *lpxE*/C-HA strains, this was likely another artefact, but this could represent a real interaction partner for LpxE.

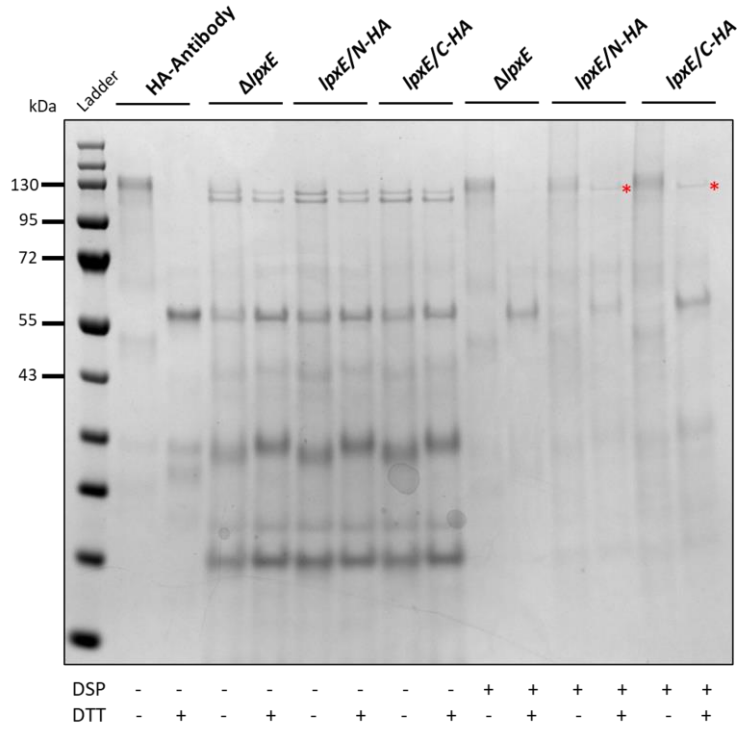

Figure 4.20: Duplication of Co-IP of the *lpxE* complements. SDS-PAGE of the Co-IP duplication. An additional band (*) was shown in the reduced DSP-crosslinked samples of the *lpxE*/N-HA and *lpxE*/C-HA. The eluted samples of non-crosslinked lysate and DSP-crosslinked lysate were used. HA antibody was the negative control. Legend: Δ*lpxE* - the elution sample of Δ*lpxE* lysate, *lpxE*/N-HA - the elution sample of *lpxE*/N-HA, *lpxE*/C-HA - the elution sample of *lpxE*/C-HA. Number ladders on the left-hand side represent the size of marker proteins in kDa.

The above data is ambiguous, and the high background indicates that there is high non-specific binding to the protein A/G beads. Here the anti-HA antibody was a high-affinity mouse IgG_1 monoclonal antibody that recognizes the HA-epitope tag (YPYDVPDYA) derived from the HA-tagged protein and was coupled to the A/G beads during the Co-IP. An alternative approach was to use Pierce® Anti-HA Agarose, which is an immunopurification and immunoprecipitation resin specific for HA-tagged proteins. Thus, the co-immunoprecipitation was modified to HA-tag pull down assay using anti-HA agarose instead. The lysate was directly incubated with anti-HA agarose, followed by wash and elution steps. However, no additional bands were observed in the *lpxE*

complements compared with the *lpxE* mutant (**Figure 4.21**). This further supported no LpxE interaction being observed using Co-IP with these *P. gingivalis* HA-tagged LpxE strains.

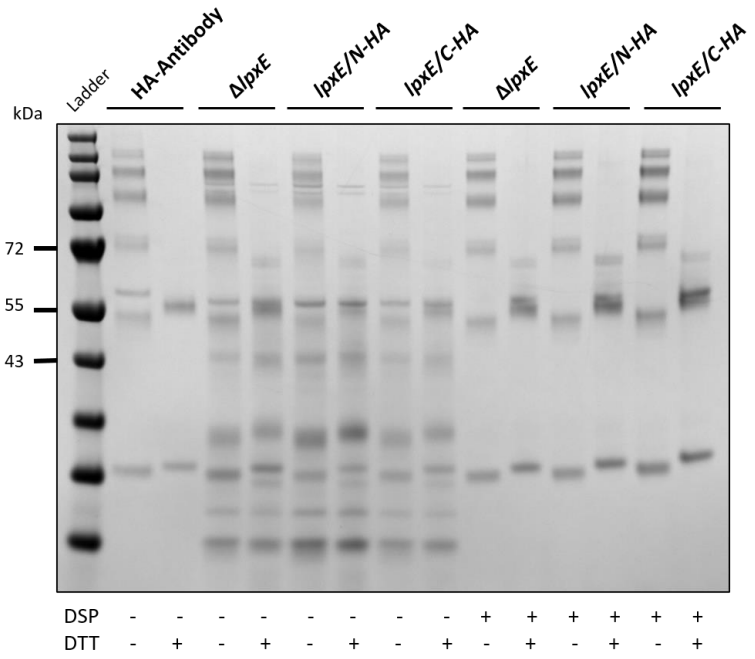

Figure 4.21: HA-tag pull down assay. SDS-PAGE of the pull-down assay. No additional band was shown in the elution samples of the *lpxE* complements. The eluted samples of non-crosslinked lysate and DSP-crosslinked lysate were used. HA antibody was the negative control. Legend: Δ*lpxE* - the elution sample of Δ*lpxE* lysate, *lpxE*/N-HA - the elution sample of *lpxE*/N-HA, *lpxE*/C-HA - the elution sample of *lpxE*/C-HA. Number ladders on the left-hand side represent the size of marker proteins in kDa. Due to COVID and time restriction, this experiment was not repeated.

4.4 Discussion

In Chapter 3, it was proposed that regulation of the lipid A 1-phosphatase LpxE may be linked to the T9SS and its modification of lipid A phosphorylation status in *P. gingivalis*. This chapter characterized the phenotype of LpxE and aimed to understand how this phosphatase is linked to the T9SS. Sequence alignment shows that *P. gingivalis* LpxE is a novel lipid A 1-phosphatase, as it carries an N-terminal signal peptide usually only

seen in periplasmic and outer membrane (OM) targeted proteins, a 22-residue N-terminal extension and an additional C-terminal region. The *lpxE* mutant and two complement strains were created to analyse its molecular mechanism in *P. gingivalis*. The results suggest that LpxE is not required for black pigmentation or normal growth. However, the enzyme activity assays suggested the *lpxE* mutant shows some reduction in gingipain activity and this phenotype is not fully restored in complement strains. The TEM, NanoSight and OMV dry weight data suggest that LpxE is required for normal OMV formation, but again the phenotypes were not fully restored in the complement strains. The detergent and antimicrobial peptide inhibition assays show that LpxE has some role in destabilizing the bacterial membrane, although again the two complements do not restore the wild-type phenotype. Using Western blot assays of fractionated *P. gingivalis* membranes, LpxE was detected in the bacterial OM, which would be the first time this localization has been observed for any other lipid A 1-phosphatase. However, as this was detected using the complement strains that produce HA-tagged LpxE, and there was incomplete restoration of LpxE activity, this could be due to cross-reactivity and this needs to be confirmed by other means. Cross-linking and Co-IP experiments suggest that HA-tagged LpxE may interact with other protein or protein complex, but again the results were not conclusive or reproducible and again the issue with incomplete restoration of LpxE activity in these strains raises concerns.

A main limitation of this Chapter is the complementation of the *lpxE* mutant. Although the mutation of LpxE affects OMV formation and membrane stability, all the data indicate that these phenotypes were not restored in the two complement strains. As

verification of correct genomic insertion is not sufficient to confirm complementation, additional verification such as qPCR to assess correct expression, and mass spectrometry of lipid A to assess correct protein localisation/folding, would be needed to show wild-type phenotype has been correctly restored. However, the issues with the complementation of *lpxE* are likely due to the presence of the HA-tag. This additional sequence may interfere with gene transcription and/or translation, may interfere membrane targeting and correct insertion into the membrane, or could abrogate interactions with other proteins. It would therefore be worthwhile to create a clean *lpxE* complement that does not contain any modification or tag. In the Western blot of LpxE localization, too many non-specific bindings were seen, suggesting that HA-antibody is not specific in *P. gingivalis*. Other tag options such as V5-tag and Flag-tag would be considered and also generating an antibody against LpxE peptides so that localization of LpxE in the wild-type strain could be assessed in the future.

The crosslinking assay did not work well for LpxE. As this was based on recognition of the HA-tag in the *lpxE*/N-HA and *lpxE*/C-HA complemented strains, the above reasons could explain this. However, the reason could also be that the crosslinking system was not appropriate. For example, after the crosslinking step with DSP, the lysed cells formed precipitations that were difficult to solubilize. This suggests that protein and DSP concentrations should be decreased. Another crosslinker such as imidoester crosslinker DMS (dimethyl suberimidate) or N-Hydroxysuccinimide-ester crosslinker BS3 could also be applied to optimize the system. The Co-IP results were not reliable either. For example, an additional band which may interact with LpxE was seen in the

lpxE/N-HA strain, but this result was not repeatable. Despite being a powerful technique for analysing protein interactions, Co-IP is also limited by the availability of antibodies that recognize the bait protein. In some cases, the HA-antibody that recognizes LpxE might bind to the interacting site between LpxE and prey proteins and interfere or disrupt the interaction. So many non-specific bindings can also decrease the availability of HA-antibody that recognizes LpxE.

In *E. coli*, lipid A is a hexa-acylated disaccharide of glucosamine, which is phosphorylated at the 1- and 4′-positions[84,330]. It is synthesized by nine constitutive enzymes in the cytoplasm or on the inner surface of the inner membrane (IM)[84]. Despite having the structural genes for the nine enzymes of the *E. coli* lipid pathway, some other bacteria synthesize lipid A lacking phosphate groups[153,146,331]. The phosphate-deficient lipid A structures were first reported in the plant endosymbionts *Rhizobium leguminosarum*[332] where specific phosphatases LpxE and LpxF remove the 1- and 4′-phosphate residues late in the pathway, respectively[146,147]. LpxE and LpxF enzymes were also discovered in *Francisella tularensis*[327,333] and *Helicobacter pylori*[328,334] where they perform a similar function. These reported LpxE and LpxF belong to the PAP2 (type-2 phosphatidic acid phosphatase)-like superfamily, but do not contain a signal peptide, and have been confirmed as integral IM proteins.

P. gingivalis, similar to other Gram-negative bacteria, synthesizes lipid A that initially contains phosphate moieties at both the 1- and 4′-position of the di-glucosamine backbone[111,151]. *P. gingivalis* also contains lipid A structures lacking phosphates[87], and LpxE and LpxF were identified as being functional here[153]. The *P. gingivalis* LpxF is

similar to lipid A 4′-phosphatases from other bacteria species, as it does not carry a signal peptide and it only contains a phosphatase domain, based on sequence analysis and tertiary structure prediction. Thus, LpxF is thought to be located in the inner membrane as other lipid A 4′-phosphatases. Using BLAST searches, the lipid A 1-phosphatase region of *P. gingivalis* LpxE was found to have high homology with other LpxE sequences; but is novel as it also carries a signal peptide, a 22-residue extension at its N-terminus, and a 200-residue region at its C-terminus, both with unknown function. *P. gingivalis* LpxE may have been detected in the OM by membrane fractionated Western blot, and this would imply that the *P. gingivalis* LpxE may be the first discovered OM bound lipid A 1-phosphatase.

In the BLAST run against the sequence of *P. gingivalis* LpxE using default parameters, two hits were identified for *Prevotella* sp. and two hits were identified for *Parabacteroides* sp., which also possess a signal peptide and a partial C-terminal region (**Figure 4.1**). However, alignment of LpxE from *P. gingivalis*, *Prevotella* sp. and *Parabacteroides* sp. shows high homology in the NTD but not in the CTR (**Figure 4.22**). Moreover, when their CTRs were separately aligned with all bacterial genomes, no new hits were detected.

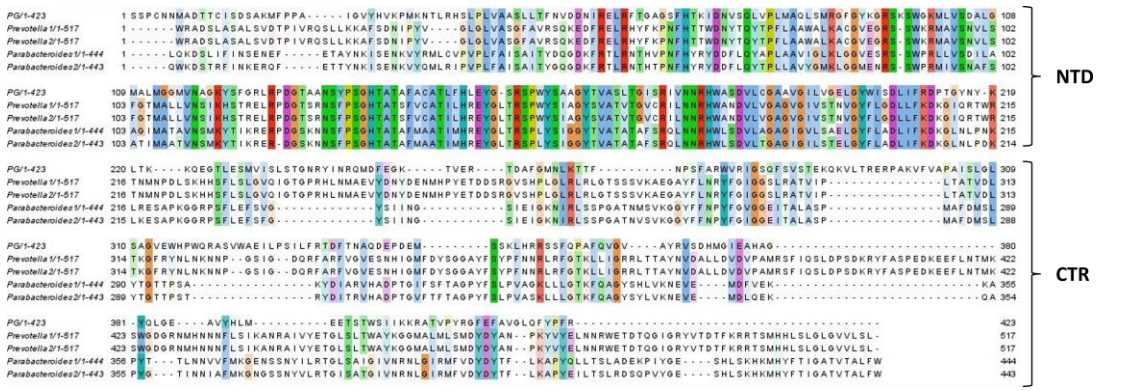

Figure 4.22: Pairwise sequence alignment of LpxE from *P. gingivalis*, *Prevotella* sp. and *Parabacteroides* sp. Conservation is defined by Clustal X Colour Scheme[325]. Blue (hydrophobic) - A, I, L, M, F,W,V; Red (positive charge) - K, R; Magenta (negative charge) - E, D; Green (polar) - N, Q, S, T; Orange (glycine) - G; Yellow (proline) - P; Cyan (aromatic) - H, Y; White (unconserved) - any/gap. NTD: N-terminal domain, 1-219 amino acids; CTR: C-terminal region, 220-423 amino acids.

As lipid A 1-phosphatases have not been reported in other bacteria that utilise a T9SS, such as *F. johnsoniae* and *T. forsythia*, it is unclear whether the unique features of LpxE are correlated to the T9SS. To identify putative lipid A phosphatases in *F. johnsoniae* and *T. forsythia*, the *P. gingivalis* LpxE and LpxF sequences were aligned in these species. The BLAST result of LpxE showed that homologs of *P. gingivalis* LpxE NTD could be present in *F. johnsoniae* (Sequence ID: WP_012024041.1 and WP_012026436.1) and *T. forsythia* (Sequence ID: WP_014224716.1) (**Figure 4.23A**). However, while sequences corresponding to the CTR were absent in *F. johnsoniae*, they were present in the putative in *T. forsythia* LpxE (**Figure 4.23A**). Further BLAST analysis showed that homologs of *P. gingivalis* LpxF were identified in *F. johnsoniae* (Sequence ID: WP_008463839.1 and ABQ06015.1) and *T. forsythia* (Sequence ID: WP_014225991.1 and WP_014226035.1) (**Figure 4.23B**).

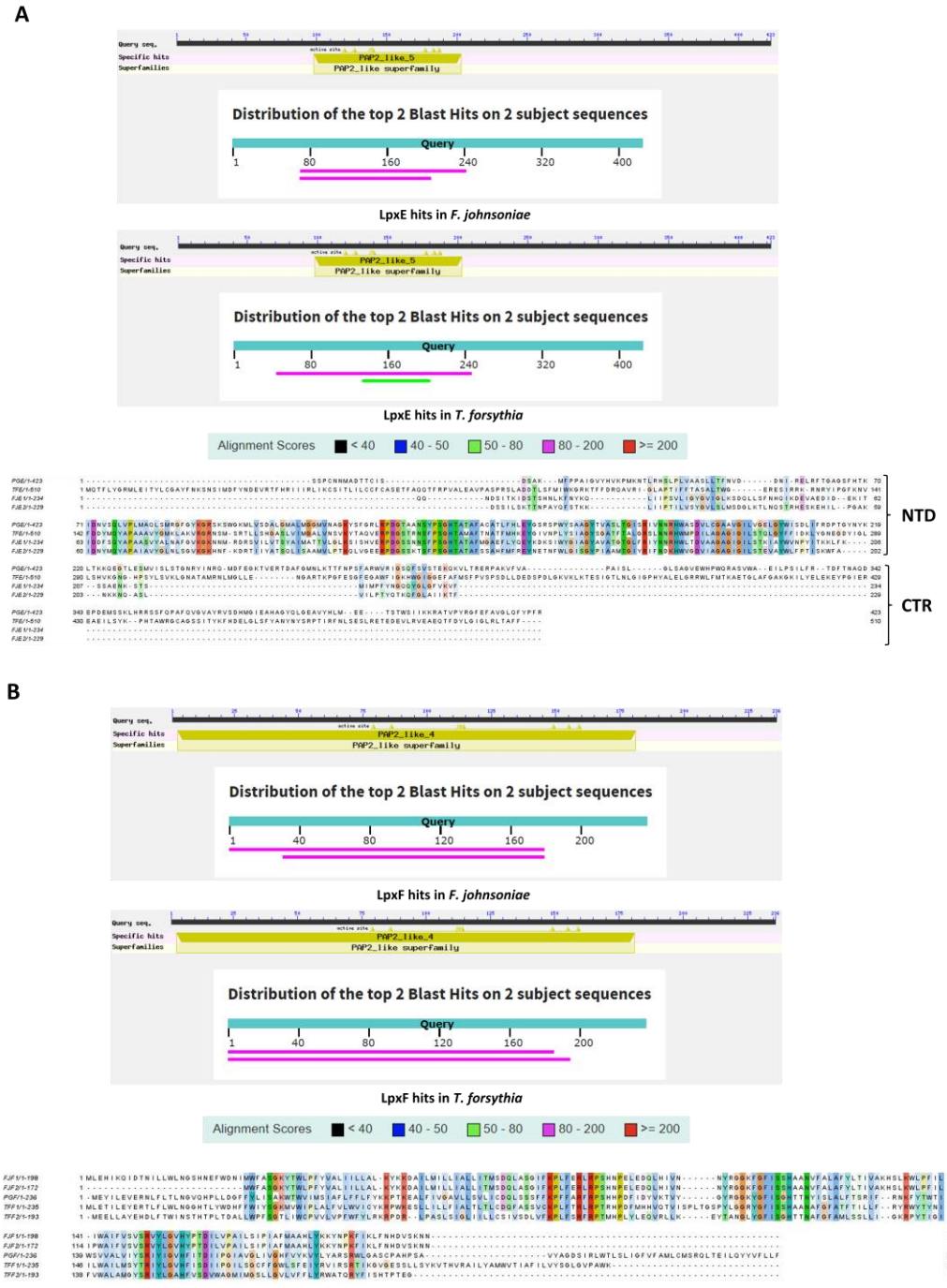

Figure 4.23: Lipid A phosphatase sequence alignment in *F. johnsoniae* and *T. forsythia*. A. LpxE sequence homology alignment in *F. johnsoniae* and *T. forsythia*. Two hits (Sequence ID: WP_012024041.1 and WP_012026436.1) are shown in *F. johnsoniae*. One hit (Sequence ID: WP_014224716.1) was shown in *T. forsythia*. The pairwise alignment of *P. gingivalis* LpxE against all hits suggests that LpxE NTD is conserved but LpxE CTR is not conserved in these bacteria. **B.** LpxF sequence homology alignment in *F. johnsoniae* and *T. forsythia*. Two hits (Sequence ID: WP_008463839.1 and ABQ06015.1) are shown in *F. johnsoniae*. Two hits (Sequence ID: WP_014225991.1 and WP_014226035.1) was shown in *T. forsythia*. The pairwise alignment of *P. gingivalis* LpxF against all hits suggests that LpxF is conserved in these bacteria.

These sequence alignment results suggest that both *F. johnsoniae* and *T. forsythia* possess a LpxF-like lipid A 4′-phosphatase which only contains the PAP2 phosphatase domain. LpxE of *F. johnsoniae* only contains the PAP2 phosphatase domain but LpxE of *T. forsythia* possesses an additional CTR, although it is highly different from the *P. gingivalis* LpxE sequence. This analysis may indicate that bacteria that use a T9SS require both LpxE and LpxF, although whether these are both expressed and active in these bacteria is still to be determined. Furthermore, there has been no studies looking at links between the T9SS, lipid A phosphorylation and OMV formation in *F. johnsoniae* or *T. forsythia*, but it would be interesting to see whether LpxE has any influence here.

4.5 Conclusion

This chapter describes the characterization of the *P. gingivalis* lipid A 1-phophatase LpxE. Sequence alignments show that *P. gingivalis* LpxE is a novel lipid A phosphatase, as it carries a signal peptide, a 22-residue N-terminal extension and an additional CTR. The results of phenotype assays suggest that LpxE is not required for black pigmentation and normal growth. However, the enzyme activity assays showed the *lpxE* mutant is defective in gingipain secretion although this phenotype is not fully restored in complement strains. The TEM, NanoSight and OMV dry weight data suggest that LpxE is required for normal OMV formation. The detergent and antimicrobial peptide inhibition assays show that LpxE is required for destabilizing bacteria membrane.

Using fractionated Western blot assays, LpxE was showed to be in the bacterial outer membrane, but this needs to be confirmed by other methods. The cross-linking and Co-IP experiments suggest that LpxE may interact with other protein or protein complex, but the results were not reproducible and conclusive.

Chapter 5 Recombinant Expression and Purification Studies of the T9SS Outer Membrane Accessory Proteins and LpxE

5.1 Chapter aims

In Chapter 3, it was discovered that LpxE was likely the link between the T9SS and lipid A dephosphorylation. It was thought that LpxE may possess a novel T9SS CTD, or the T9SS or cargo secreted by it may directly bind to and regulate the function of LpxE. Given that LpxE could be a low abundance membrane protein, or the action of combining an affinity tag greatly affects its native function, it was difficult to study its function and interaction *in vivo*. Thus, a new plan was to try to express and purify *P. gingivalis* T9SS outer membrane accessory proteins and LpxE recombinantly in *E. coli*, and study potential interactions *in vitro*.

Over the past decade, cryogenic electron microscopy (cryo-EM) has become a powerful technique in structural biology, and the advantage is that the amount of protein required is low. However, due to the limitation of protein size, it can be difficult to study the structure of small outer membrane proteins <100 kDa using cryo-EM, unless they form higher order complexes and/or display asymmetry. Therefore, the overall aims of this chapter were to produce recombinant T9SS outer membrane accessory proteins and LpxE, to study their interactions *in vitro* and then gain structural insights using cryo-EM, but if not appropriate by X-ray crystallography.

5.2 Expression and purification of PorV in pET28b

As the T9SS outer membrane (OM) protein PorV plays an important role in cargo secretion and is also involved in OMV production, PorV was selected to be the first

membrane protein expressed recombinantly. For the first expression trial of PorV, the expression vector pET28b, a standard vector used in the group for both soluble and membrane proteins, was used with BL21 (DE3) *E. coli* cells.

Selection of an appropriate protein sequence is an important first step in the design of protein constructs for recombinant expression, because this can ensure the expressed protein is in its native state for purification and structural analysis. PorV is a known OM localised β-barrel protein whose structure has been determined from *F. johnsoniae*[168]. Bacterial OM β-barrel proteins are known to possess N-terminal signal peptides for their transfer from the cytoplasm to the periplasm via the Sec system[335]. Therefore, the primary sequence of *P. gingivalis* W50 PorV was assessed by the SignalP-5.0 server for the presence of a signal peptide and its cleavage site prediction[336]. *P. gingivalis* PorV is predicted to contain an N-terminal signal peptide (residues 1-27) for Sec transport with peptide cleavage occurring between residues A27 and Q28 (**Figure 5.1**) and as a β-barrel membrane protein[168], it is not soluble in the cytoplasm.

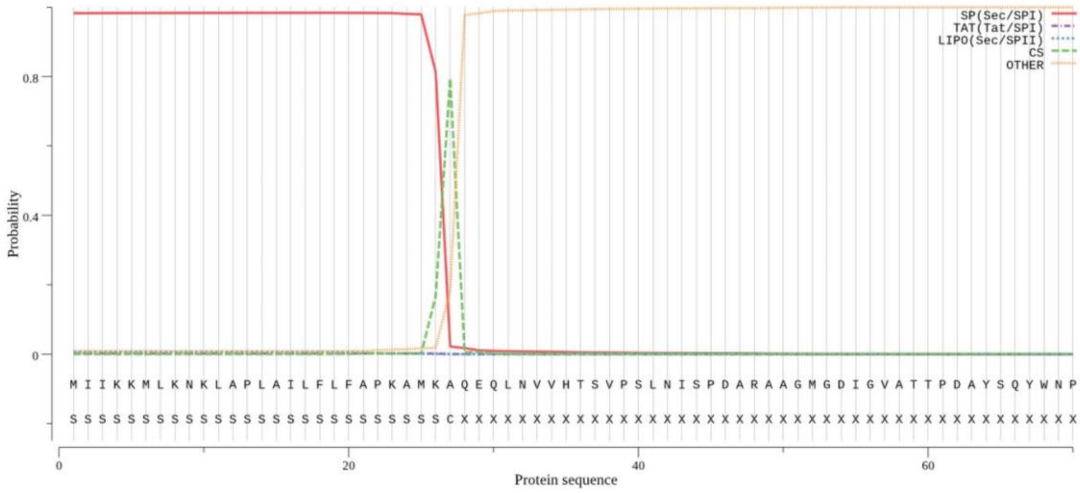

Figure 5.1: Signal peptide prediction of PorV. The prediction showed that PorV contains a Sec signal peptide spanning residues 1-27. Peptide cleavage was predicted to occur between residues A27 and Q28. This prediction was made by the SignalP-5.0 sever[336] which predicted signal peptides based on several different consensus signal sequences. SP (Sec/SPI): "standard" secretory signal peptides transported by the Sec translocon and cleaved by Signal Peptidase I (Lep). TAT (Tat/SPI): Tat signal peptides transported by the Tat translocon and cleaved by Signal Peptidase I (Lep). LIPO (Sec/SPII): lipoprotein signal peptides transported by the Sec translocon and cleaved by Signal Peptidase II (Lsp). CS: cleavage site.

To express PorV in *E. coli*, two constructs pET28b-PorV$_{1\text{-}391}$ and pET28b-PorV$_{28\text{-}391}$ were produced. As pET28b introduces a C-terminal His-tag, PorV would be expressed as PorV$_{1\text{-}391\text{-His}}$ or PorV$_{28\text{-}391\text{-His}}$, respectively. The first construct contained the complete *P. gingivalis* PorV sequence (residues 1-391), including its native signal peptide, and it was expected to be targeted to the *E. coli* OM. Here the native signal peptide PorV$_{1\text{-}27}$ was expected to be recognized by Sec machinery for inner membrane translocation. PorV$_{28\text{-}391\text{-His}}$ would then be inserted and assembled in OM via β-barrel assembly machine (BAM) complex (**Figure 5.2A**). The second construct contained the *P. gingivalis* PorV sequence minus its signal peptide (residues 28-391), and it was expected to be expressed in the cytoplasm and form inclusion bodies, which would be used for refolding experiments (**Figure 5.2B**). Although upon insertion into the OM the

signal sequence would be lost in PorV$_{1\text{-}391\text{-}His}$, to distinguish it from PorV$_{28\text{-}391\text{-}His}$, it will still be referred to as PorV$_{1\text{-}391\text{-}His}$ throughout.

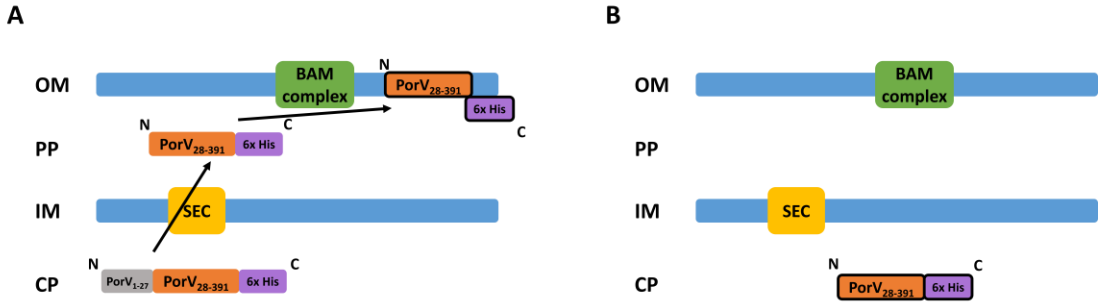

Figure 5.2: Strategies of PorV expression in pET28b. A. Expression of PorV in membrane. When the translated protein PorV$_{1\text{-}391\text{-}His}$ cross through IM, the native SP PorV$_{1\text{-}27}$ would be cleaved off by Sec machinery. The translocated PorV$_{28\text{-}391\text{-}His}$ would be then inserted and assembled in OM under the aid of BAM complex. **B.** Expression of PorV in inclusion bodies. The translated protein PorV$_{28\text{-}391\text{-}His}$ would stay in CP and form inclusion bodies. CP: cytoplasm. IM: inner membrane. PP: periplasm. OM: outer membrane.

5.2.1 Expression of PorV in membrane

BL21 (DE3) is effective at expressing proteins carried by pET vectors under the control of the T7 promoter[337]. The two constructs pET28b-PorV$_{1\text{-}391}$ and pET28b-PorV$_{28\text{-}391}$ were therefore transformed into BL21 (DE3) cells and expression trials were performed (**Figure 5.3**). Expressed PorV$_{1\text{-}391\text{-}His}$ bands were seen in the samples induced with isopropyl β-D-1-thiogalactopyranoside (IPTG) (**Figure 5.3A**), suggesting that PorV$_{1\text{-}391\text{-}His}$ was expressed. BugBuster® is a cell lysis agent which can also act to extract membrane proteins, which remain in the supernatant after centrifugation. However, after cells were lysed with BugBuster®, PorV$_{28\text{-}391\text{-}His}$ was not seen in the supernatant but instead retained in the pellet, suggesting that the PorV$_{1\text{-}27}$ signal peptide was not cleaved and PorV$_{1\text{-}391\text{-}His}$ was expressed in inclusion bodies rather than in the membrane

(**Figure 5.3B**). The reason for this could be that *P. gingivalis* signal peptides may not be efficient in *E. coli*.

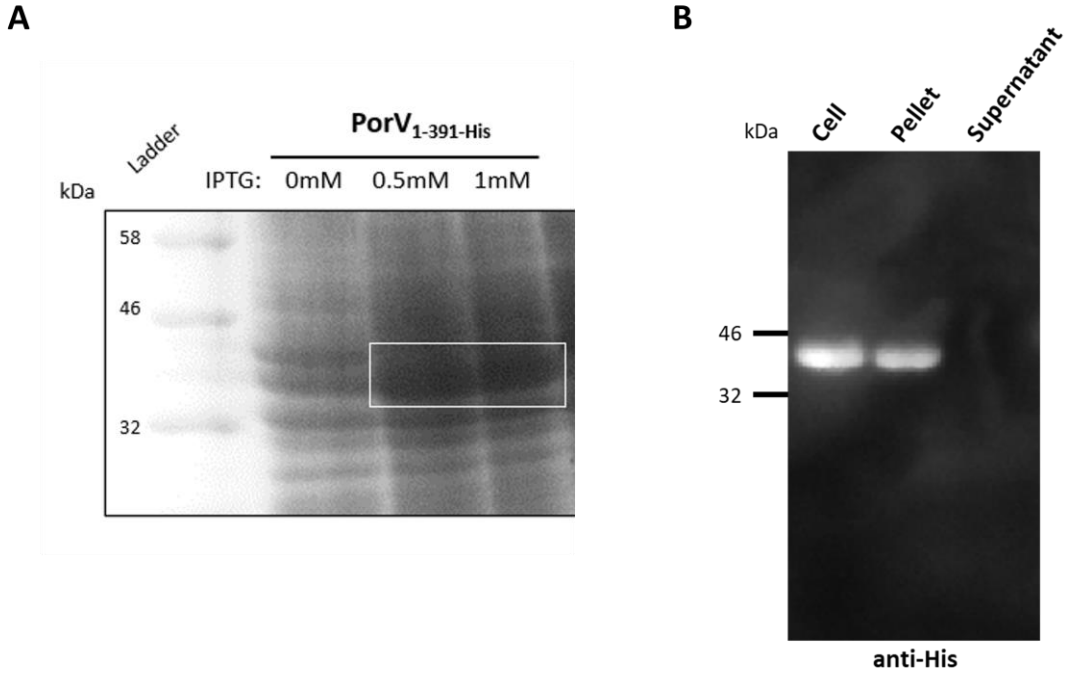

Figure 5.3: PorV$_{1\text{-}391\text{-}His}$ expression trial using pET28b vector. A. SDS-PAGE of PorV$_{1\text{-}391\text{-}His}$ expression in whole cell. Protein expression was induced with 0.5 mM and 1 mM IPTG at 20°C overnight. The molecular weight of PorV$_{1\text{-}391\text{-}His}$ is around 42 kDa. Additional bands at this size were shown. **B.** Western blot of the full-length PorV (PorV$_{1\text{-}391\text{-}His}$) membrane extraction. PorV$_{1\text{-}391\text{-}His}$ was detected in the cell and pellet, but not in the supernatant. The immunoblot was probed with anti-His (diluted 1:1000). Cell, *E. coli* cell; Pellet, pellet of cell lysate; Supernatant, supernatant of cell lysate. Number ladders on the left-hand side represent the size of marker proteins in kDa.

5.2.2 Expression and purification of PorV from inclusion bodies

As PorV$_{1\text{-}391\text{-}His}$ was not expressed in the membrane, another option was to force PorV into inclusion bodies using the pET28b-PorV$_{28\text{-}391}$ construct, then purify it under denaturing conditions and attempt to refold it. Expressed PorV$_{28\text{-}391\text{-}His}$ bands were seen in the samples induced with IPTG (**Figure 5.4A**). To solubilize PorV$_{28\text{-}391\text{-}His}$ from inclusion bodies, 8 M urea was applied to solubilize the pellet. The supernatant containing unfolded PorV$_{28\text{-}391\text{-}His}$ was then loaded onto an equilibrated poly-prep

gravity flow column containing 1 ml nickel-nitrilotriacetic acid (Ni-NTA) agarose resin. The resin was washed using 20 column volumes of Ni-NTA wash buffer and eluted with a series of 2 ml fractions using Ni-NTA elution buffer. The samples of each step were collected and loaded onto the gel for SDS-PAGE analysis (**Figure 5.4B**).

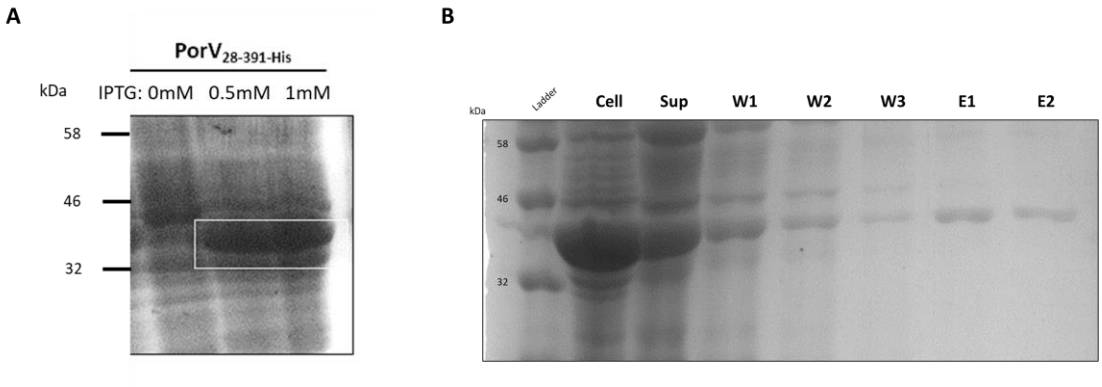

Figure 5.4: Expression and purification of PorV$_{28\text{-}391\text{-}His}$ from inclusion bodies. A. SDS-PAGE of PorV$_{28\text{-}391\text{-}His}$ expression in whole cell. Protein expression was induced with 0.5 mM and 1 mM IPTG at 20°C overnight. The molecular weight of PorV$_{28\text{-}391\text{-}His}$ is around 42 kDa. Additional bands at this size were shown. **B.** SDS-PAGE of PorV$_{28\text{-}391\text{-}His}$ Ni-NTA chromatography purification: Cell, *E.coli* cell; Sup, supernatant of cell lysate; W1, first wash; W2, second wash; W3, third wash; E1, first elution; E2, second elution. Number ladders on the left-hand side represent the size of marker proteins in kDa.

As the purified PorV$_{28\text{-}391\text{-}His}$ was in an unfolded state, the eluted PorV$_{28\text{-}391\text{-}His}$ was subjected to dialysis against buffer containing 4 M urea, followed by 0 M urea to slowly refold it. As the PorV homologue FadL was previously successfully solubilized with the detergent LDAO[338], 1% (vol/vol) LDAO was present in all buffers. The refolded PorV$_{28\text{-}391\text{-}His}$ sample was further purified by size exclusion chromatography to remove contaminant proteins and imidazole. The expected molecular weight of PorV$_{28\text{-}391\text{-}His}$ is ~42 kDa, and so a HiLoad® 16/600 Superdex® 200 pg column was used as it provides good resolution for globular proteins between 10-600 kDa. By calculation of protein standards[339], folded PorV$_{28\text{-}391\text{-}His}$ should have been eluted at ~80 ml on this column.

However, the result showed that the majority of $PorV_{28\text{-}391\text{-}His}$ eluted at ~45 ml (P1) within the void volume (**Figure 5.5**), which indicates that $PorV_{28\text{-}391\text{-}His}$ was largely not refolded. However, a small peak (P2) was observed at the expected molecular weight, but this was not detected by SDS-PAGE.

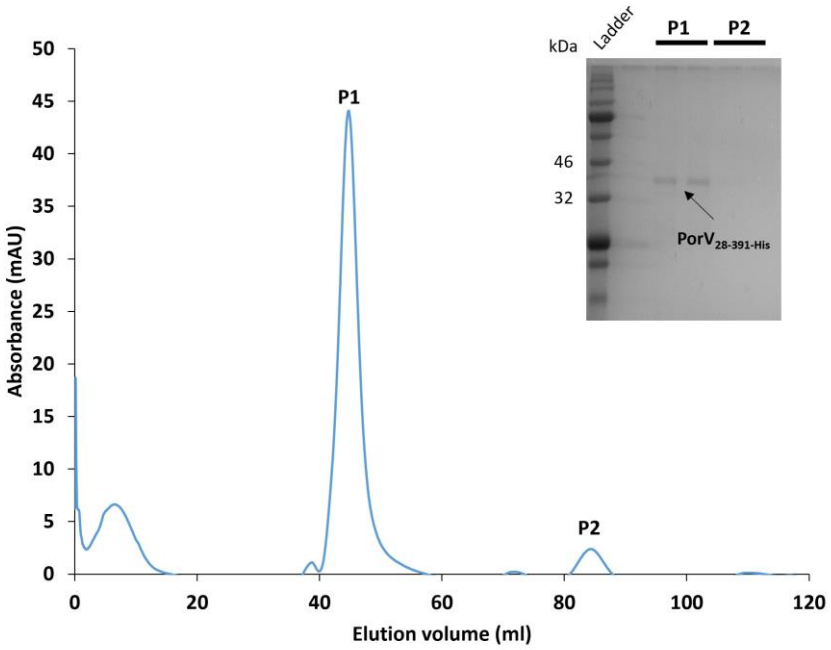

Figure 5.5: Size exclusion chromatography of $PorV_{28\text{-}391\text{-}His}$. Superdex 200 (GE Healthcare) gel-filtration profile of $PorV_{28\text{-}391\text{-}His}$. The elution samples of P1 and P2 were collected and loaded onto SDS-PAGE gel. By calculation of protein standards[339], P1 represents $PorV_{28\text{-}391\text{-}His}$ but it was not refolded. A small peak (P2) was observed at the expected molecular weight, but this was not detected by SDS-PAGE. Number ladders on the left-hand side represent the size of marker proteins in kDa.

5.3 Expression and purification of PorV in pOMPA28

As it was not possible to purify sufficient quantities of PorV for structural studies using the pET28b-$PorV_{1\text{-}391}$ and pET28b-$PorV_{28\text{-}391}$ approaches, it was necessary to re-design the pET28b vector for membrane protein expression in *E. coli*. Here, an OmpA signal peptide originating from *E. coli* was used instead of the native *P. gingivalis* PorV signal

peptide. The *E. coli* OmpA sequence is a highly effective signal peptide that has been extensively used for recombinant expression of periplasmic and membrane proteins in *E. coli*[340]. Thus, the pET28b was modified to contain the OmpA signal peptide and was renamed as pOMPA28 (**Figure 5.6**). An N-terminal 6×His tag was designed to follow the OmpA signal peptide, which allows for protein purification using Ni-NTA chromatography.

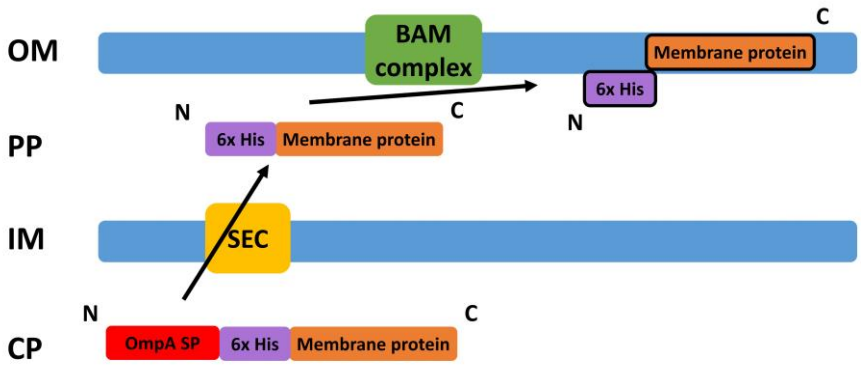

Figure 5.6: Schematic of membrane protein expression using pOMPA28. When the translated protein cross through IM, the OmpA SP would be cleaved off by Sec machinery. The translocated membrane protein with N-terminal His-tag would be then inserted and assembled in OM under the aid of BAM complex. CP: cytoplasm. IM: inner membrane. PP: periplasm. OM: outer membrane.

5.3.1 Expression of T9SS outer membrane accessory proteins

The primary sequences of *P. gingivalis* W50 PorV, PorU, PorQ, PorZ, PorP, PorT, PorG and PorF were uploaded to the SignalP-5.0 server for signal peptide and cleavage site predictions[336]. PorU and PorZ are globular proteins secreted by the T9SS and attached to the OM through interactions with PorV and PorQ, respectively[109,341]. PorV, PorQ, PorP, PorT, PorG and PorF are β-barrel OM proteins. Based on this analysis, PorV residues 28-391 ($PorV_{28\text{-}391}$), PorU residues 24-1158 ($PorU_{24\text{-}1158}$), PorQ residues 38-

345 ($PorQ_{38-345}$), PorP residues 20-313 ($PorP_{20-313}$), PorT residues 29-244 ($PorT_{29-244}$) and PorF residues 37-827 ($PorF_{37-827}$) were identified as mature protein sequences and successfully cloned into the pOMPA28 vector. Because the sequence of $PorG_{29-235}$ contains a restriction enzyme site that was used for cloning, its insertion into the pOMPA28 vector was not taken forward here. PorZ has been expressed and purified from the cytoplasm[109], therefore PorZ was also excluded from this strategy. These constructs pOMPA28-$PorV_{28-391}$, pOMPA28-$PorU_{24-1158}$, pOMPA28-$PorQ_{38-346}$, pOMPA28-$PorP_{20-294}$, pOMPA28-$PorT_{29-244}$ and pOMPA28-$PorF_{37-827}$ were then transformed into *E. coli* BL21 (DE3) cells for expression trials. Except for $PorP_{20-294}$, additional bands at the correct size were seen in the IPTG-induced cells for $PorV_{His-28-391}$, $PorQ_{His-38-346}$, $PorT_{His-29-244}$, $PorU_{His-24-1158}$ and $PorF_{His-37-827}$, suggesting they had been expressed (**Figure 5.7**).

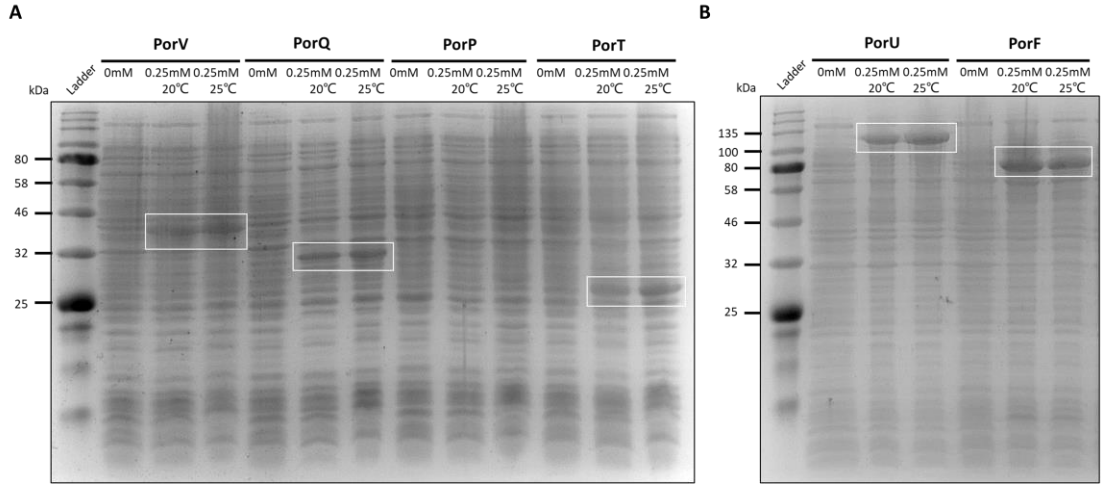

Figure 5.7: Membrane protein expression using pOMPA28. A. Protein expression of PorV, PorQ, PorP and PorT. **B.** Protein expression of PorU and PorF. Each protein was induced with 0.25 mM IPTG at 20°C or 25°C. Highlighted additional bands suggested that $PorV_{His-28-391}$, $PorQ_{His-38-346}$, $PorT_{His-29-244}$, $PorU_{His-24-1158}$ and $PorF_{His-37-827}$ were expressed. Number ladders on the left-hand side represent the size of marker proteins in kDa.

Membrane proteins are notoriously difficult to express and purify in comparison to soluble globular proteins. As the most functionally characterised outer membrane protein component of the T9SS, PorV was selected first for further optimisation. The above data showed that $PorV_{His\text{-}28\text{-}391}$ was expressed, but it was unclear whether it had been targeted to OM or was unfolded in inclusion bodies. Lower speed centrifugation was used to separate membranes and inclusion bodies, as the membranes would stay in the supernatant. The membranes of pOMPA28-$PorV_{28\text{-}391}$ expressed in BL21 (DE3) were next collected by ultra-centrifugation and prepared for SDS-PAGE and Western blot analyses detected with anti-His antibody. $PorV_{His\text{-}28\text{-}391}$ was present in both pellet and membrane samples (**Figure 5.8**), indicating that the majority of $PorV_{His\text{-}28\text{-}391}$ was still in inclusion bodies but part of $PorV_{His\text{-}28\text{-}391}$ was expressed in the membrane.

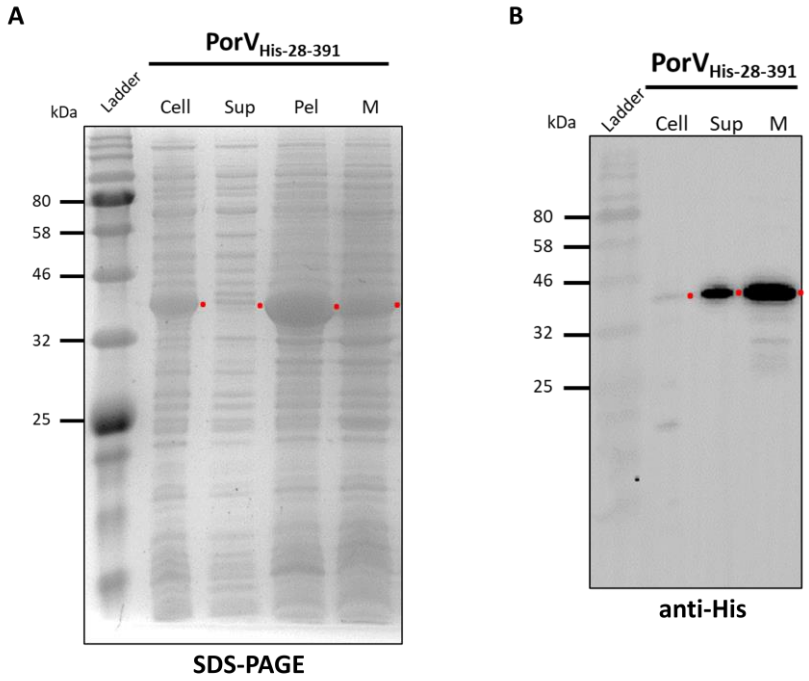

Figure 5.8: Localization of expressed $PorV_{His\text{-}28\text{-}391}$. A. SDS-PAGE of expressed $PorV_{His\text{-}28\text{-}391}$ in fractions. **B.** Western blot of expressed $PorV_{His\text{-}28\text{-}391}$ in fractions. The immunoblot was probed with anti-His (diluted 1:1000). Cell, *E.coli* cell; Sup, supernatant of cell lysate; Pel, pellet of cell lysate; M, membrane. Number ladders on the left-hand side represent the size of marker proteins in kDa.

5.3.2 Optimization of PorV expression using Lemo21 cells

Although ~30% of $PorV_{His\text{-}28\text{-}391}$ was expressed in the membrane, a large amount was in inclusion bodies. To optimize this, a modified version of the *E. coli* cell line BL21 (DE3), Lemo21 (DE3), was used to try and increase the yield of membrane expressed $PorV_{His\text{-}28\text{-}391}$. The Lemo21 (DE3) strain allows more stringent control of the T7 promoter[342]. It carries a pLemo plasmid, containing the *lysY* gene, which encodes lysozyme that is the natural inhibitor T7 RNA polymerase. Lemo21 cells are rhamnose dependent and expression of lysozyme is controlled via the addition of L-rhamnose to the growth media. Therefore, increased concentration of rhamnose results in down regulation and finer control of the T7 system expression system. This can be effective in reducing the formation of inclusion bodies or reductions in cell growth due to protein toxicity by slowing down protein expression. When using Lemo21 competent cells for protein expression, rhamnose is added prior to the IPTG induction.

The construct pOMPA28-$PorV_{28\text{-}391}$ was transformed into *E. coli* Lemo21 (DE3) strain for expression trials. Cultures were then grown at 37°C with various levels of rhamnose followed by normal IPTG induction and incubation at various temperatures. Expression of $PorV_{His\text{-}28\text{-}391}$ was analysed in both cell and supernatant samples. The result of cell samples showed that there was no significant difference of expression level in different rhamnose and temperature conditions (**Figure 5.9A**). However, for the supernatant sample that contains membranes, the best expression band was seen where the condition was addition of 100 μM L-rhamnose and induced at 20°C overnight (**Figure 5.9B**). This condition was then used for large-scale $PorV_{His\text{-}28\text{-}391}$ preparation.

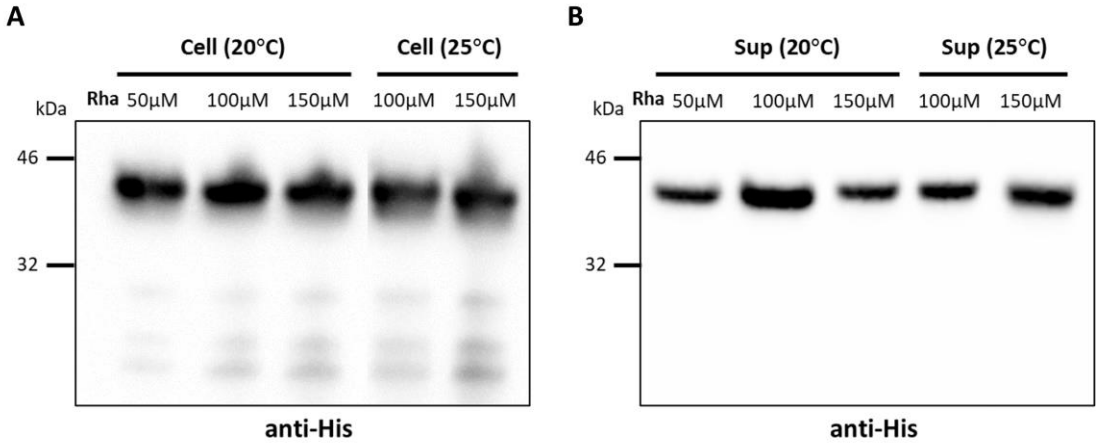

Figure 5.9: PorV expression using Lemo21 competent cells. A. Western blot analysis of $PorV_{His\text{-}28\text{-}391}$ expression in Lemo21 cells. No significant difference was observed within different rhamnose and temperature conditions. **B.** Western blot analysis of $PorV_{His\text{-}28\text{-}391}$ expression in the supernatant that contains membrane fractions. The immunoblots were probed with anti-His (diluted 1:1000). The most significant band was seen where the condition was supplement with 100 μM L-rhamnose and induced at 20°C overnight. The Lemo21 cells were induced with 0.25 mM IPTG at 20°C or 25°C overnight. The $PorV_{His\text{-}28\text{-}391}$ expression was controlled by addition of different concentration of L-rhamnose. Number ladders on the left-hand side represent the size of marker proteins in kDa.

5.3.3 Detergent screening of PorV

Membrane proteins to be extracted from native biological membranes require detergents that mimic the lipid bilayer, disrupting the membrane while surrounding and stabilising the hydrophobic transmembrane portion of the protein. The exact detergent used requires careful selection as they can also cause denaturation of the membrane protein or may fail to correctly solubilise the protein. Furthermore, some harsh detergents can also cause the solubilised protein to lose their functionality.

Most detergents used for the solubilisation of membrane proteins are non-ionic[343] as ionic detergents, such as SDS, are harsher to the membrane and protein. For the solubilisation of $PorV_{His\text{-}28\text{-}391}$, the most common non-ionic detergents C_8E_4

(tetraethylene glycol monooctyl ether), DDM (n-dodecyl-β-D-maltoside), LDAO (lauryldimethylamine N-oxide) and OG (octyl-β-glucoside) were used. As membranes include inner and outer membranes, inner membranes were first isolated using sarcosine. Extracted outer membranes which were anticipated to contain $PorV_{His\text{-}28\text{-}391}$ were then solubilised using C_8E_4 (1% vol/vol), DDM (1% vol/vol), LDAO (1% vol/vol) or OG (1% vol/vol) at 4°C overnight. The samples were then ultracentrifuged to clear the insoluble material. Soluble fractions from each sample were then analysed via Western blot. The result showed that LDAO is more effective at solubilising $PorV_{His\text{-}28\text{-}391}$ than the other detergents (**Figure 5.10**). Therefore, LDAO was selected for solubilisation of $PorV_{His\text{-}28\text{-}391}$ in larger-scale purifications.

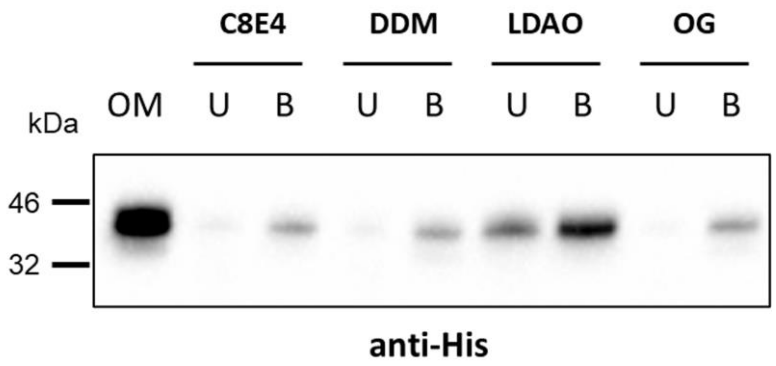

Figure 5.10: Detergent screening and $PorV_{His\text{-}28\text{-}391}$ extraction from outer membrane. Western blot analysis of detergent screening. The immunoblot was probed with anti-His (diluted 1:1000). C_8E_4, C_8E_4 solubilized outer membrane proteins; DDM, DDM solubilized outer membrane proteins; LDAO, LDAO solubilized outer membrane proteins; OG, OG solubilized outer membrane proteins. OM, outer membrane. U, unboiled sample; B, boiled sample. Number ladders on the left-hand side represent the size of marker proteins in kDa.

5.3.4 Purification of PorV

The optimized expression conditions were used for large-scale $PorV_{His\text{-}28\text{-}391}$

purification. Outer membranes were collected using ultracentrifugation and solubilised using 1% (vol/vol) LDAO. After incubation at 4°C overnight, the suspension was ultracentrifuged to clear insoluble material. The resulting supernatant was used for Ni-NTA chromatography (**Figure 5.11**). The solubilised outer membrane suspension was loaded onto an equilibrated poly-prep gravity flow column containing 1 mL Ni-NTA agarose resin. The elution was pooled and concentrated to a volume of 0.5 ml and was further purified by size exclusion chromatography to remove contaminant proteins and imidazole.

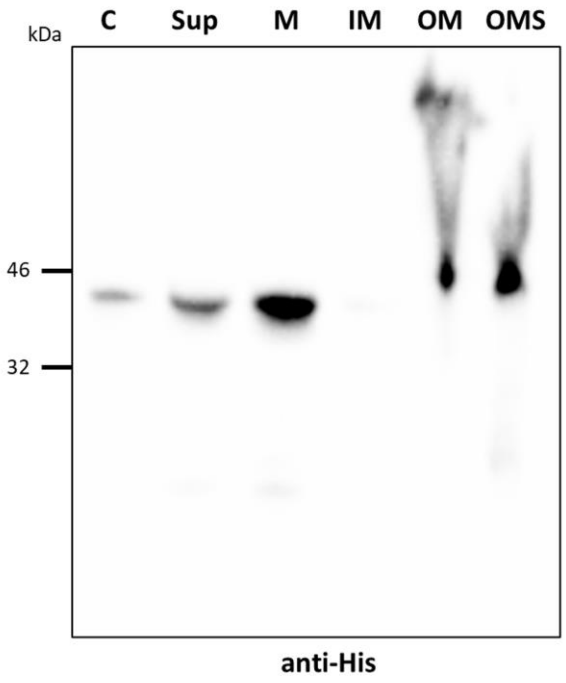

Figure 5.11: PorV$_{His-28-391}$ extraction from outer membrane. Western blot analysis of PorV$_{His-28-391}$ extraction from outer membrane. The immunoblot was probed with anti-His (diluted 1:1000). C, *E. coli* cells; Sup, supernatant of cell lysate; M, membrane; IM, inner membrane; OM, outer membrane; OMS, LDAO solubilized outer membrane proteins. Number ladders on the left-hand side represent the size of marker proteins in kDa.

As the expected molecular weight of PorV$_{His-28-391}$ was ~42 kDa and it was expected to be monomeric, a HiLoad® 16/600 Superdex® 200 pg column was used as it provides

good resolution for globular proteins between 10-600 kDa. By calculation of protein standards[339], folded $PorV_{His\text{-}28\text{-}391}$ should have been eluted at ~80 ml on this column. The result showed that four major peaks were eluted after the void volume of 45 ml (**Figure 5.12A**). To determine which of these peaks corresponded to $PorV_{His\text{-}28\text{-}391}$ an additional purification was performed using Lemo21 (DE3) carrying pOMPA28 vector with no fusion protein. Comparison of the two absorption spectra revealed that there were unique peaks at the void volume (P1) and ~70 ml (P3) in the $PorV_{His\text{-}28\text{-}391}$ purification sample (**Figure 5.12B**). Given that the molecular weight of the void volume was ~42 kDa[339], these could be unfolded $PorV_{His\text{-}28\text{-}391}$. Separation of 2 ml elution fractions representing the peak at 69 ml by SDS-PAGE showed the presence of a major band just above the 43 kDa marker (**Figure 5.12B**). A heat modifiability method has been reported to determine if β-barrel outer membrane proteins are folded properly or not[343]. Unboiled samples generally run more slowly than samples that have been boiled, which is due to the extensive hydrogen bonding network within the β-strands of the barrel, a structural feature that is often resistant to denaturation by SDS alone. A migration difference between the unboiled and boiled states of the P3 was observed, which indicates that $PorV_{His\text{-}28\text{-}391}$ was in a folded form (**Figure 5.12B**). Additional lower bands could also be observed in several fractions which may correspond to partial degradation of the full-length protein (**Figure 5.12B**). The yield of purified PorV is ~ 0.1 mg/L culture.

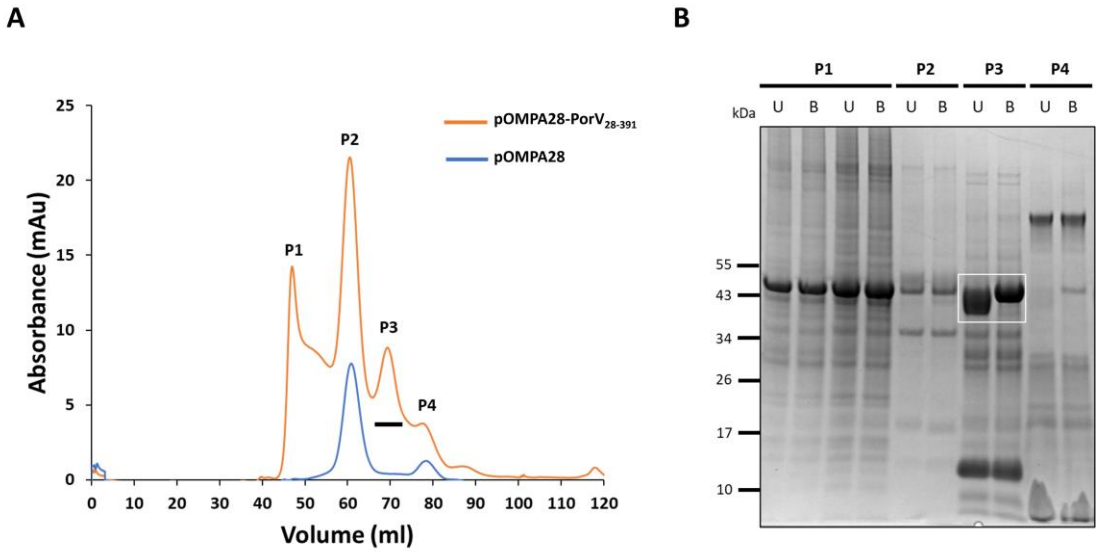

Figure 5.12: Size exclusion chromatography of PorV$_{His-28-391}$. A. UV A280 absorbance chromatogram of the PorV$_{His-28-391}$ and pOMPA28 empty vector purification. P2 and P4 represent contaminant proteins. By calculation of protein standards[339], P1 could be unfolded PorV$_{His-28-391}$. P3 representing folded PorV$_{His-28-391}$ was highlighted. P1, peak 1; P2, peak 2; P3, peak 3; P4, peak 4. **B.** SDS-PAGE of the PorV$_{His-28-391}$ 2 mL fractions from 60 mL to 80 mL. PorV$_{His-28-391}$ ~48 kDa was highlighted. Samples were boiled or unboiled in absence of reducing agent. A band shift between unboiled and boiled samples was observed in P3 elution. U, unboiled sample; B, boiled sample. Number ladders on the left-hand side represent the size of marker proteins in kDa.

5.3.5 Validation of PorV function

To verify that purified PorV$_{His-28-391}$ was functional, a far Western blot assay was performed. Far Western blotting is an effective and efficient technique used to assay interactions that occur between natively, structured proteins. It can be used to specifically detect interactions between the protein of interest and any number of bait proteins immobilized on a solid support membrane, such as nitrocellulose[344]. As PorV has previously been reported to interact with T9SS CTDs[179], its interaction with purified recombinant RgpB-CTD (residues 662-736) created and provided by member of the group was examined. Purified PorV$_{His-28-391}$ was used as a bait protein and was spotted

on a nitrocellulose membrane to detect interactions. BSA was used as a negative control and RgpB-CTD antibody was used as positive control. Afterwards, the nitrocellulose membrane was incubated with the prey protein RgpB-CTD. The results showed that RgpB-CTD bound to $PorV_{His\text{-}28\text{-}391}$ but did not bind to BSA, suggesting that purified $PorV_{His\text{-}28\text{-}391}$ was functional in binding RgpB-CTD (**Figure 5.13**). Due to COVID, I was not able to take this further and I was not able to examine larger scale purification of the other Por proteins.

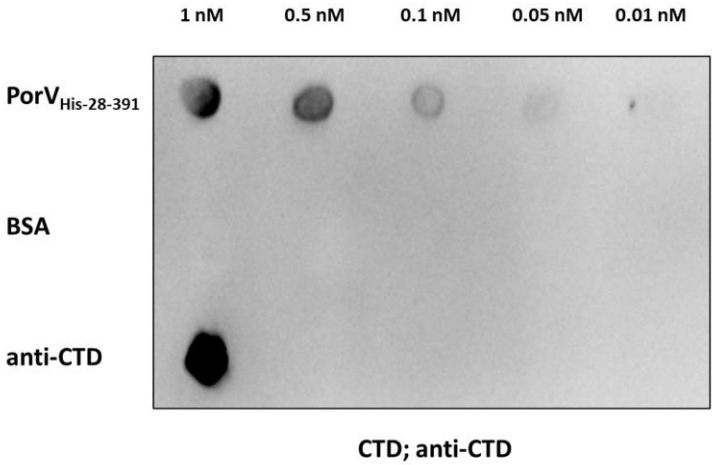

Figure 5.13: Far western blot of interaction between $PorV_{His\text{-}28\text{-}391}$ and RgpB-CTD. $PorV_{His\text{-}28\text{-}391}$, BSA, and RgpB-CTD antibody were spotted in increasing amounts from 0.01 to 1 nmol of monomer on a nitrocellulose membrane. The membrane was incubated with 100 nM purified RgpB-CTD followed by incubation with the primary antibody anti-CTD at a 1:1000 dilution. The membrane was subsequently incubated with the secondary antibody HRP-conjugated anti-rabbit at a 1:2000 dilution.

5.4 Expression and purification of LpxE

Another aim of this chapter was to express and purify *P. gingivalis* lipid A 1-phosphatase LpxE. The primary sequence of *P. gingivalis* W50 LpxE was uploaded to the SignalP-5.0 server for signal peptide and cleavage site predictions[336]. LpxE was predicted to contain an N-terminal signal peptide (residues 1-22) for Sec transport with

peptide cleavage occurring between residues A22 and S23. This is unusual as only *P. gingivalis* LpxE and lipid A 1-phosphatase of *Parabacteroides* carry a signal peptide. According to the Phyre2 predicted model, residues 23-241 are predicted to be the N-terminal phosphatase domain (NTD) and residues 242-445 are predicted to be the novel C-terminal region (CTR) (**Figure 5.14A**). As LpxE NTD was a well characterized inner membrane protein, LpxE residues 23-445 (full-length LpxE) and residues 23-241 (LpxE NTD) were cloned into pOMPA28 and expressed as $LpxE_{His\text{-}23\text{-}445}$ and $LpxE_{His\text{-}23\text{-}241}$ in *E. coli* (**Figure 5.14B, C**). However, the CTR is the most unique region of LpxE and neither Phyre2 or Robetta server[345] could find a homologue or confidently prediction for its structure. The grand average of hydropathicity (GRAVY) index can be used to represent the hydrophobicity value of a protein, which calculates the sum of the hydropathy values of all the amino acids divided by the sequence length[346]. A GRAVY index score below 0 more likely indicates a globular hydrophilic protein, while scores above 0 are more likely membranous hydrophobic proteins[347]. The GRAVY index score of LpxE CTR is -0.397, and it was speculated that the CTR (residues 242-445) could be hydrophilic, and this also supported this region potentially acting as a CTD-like domain. LpxE CTR was therefore cloned into pET46 vector for soluble expression in the cytoplasm as $LpxE_{His\text{-}242\text{-}445}$ (**Figure 5.14D**).

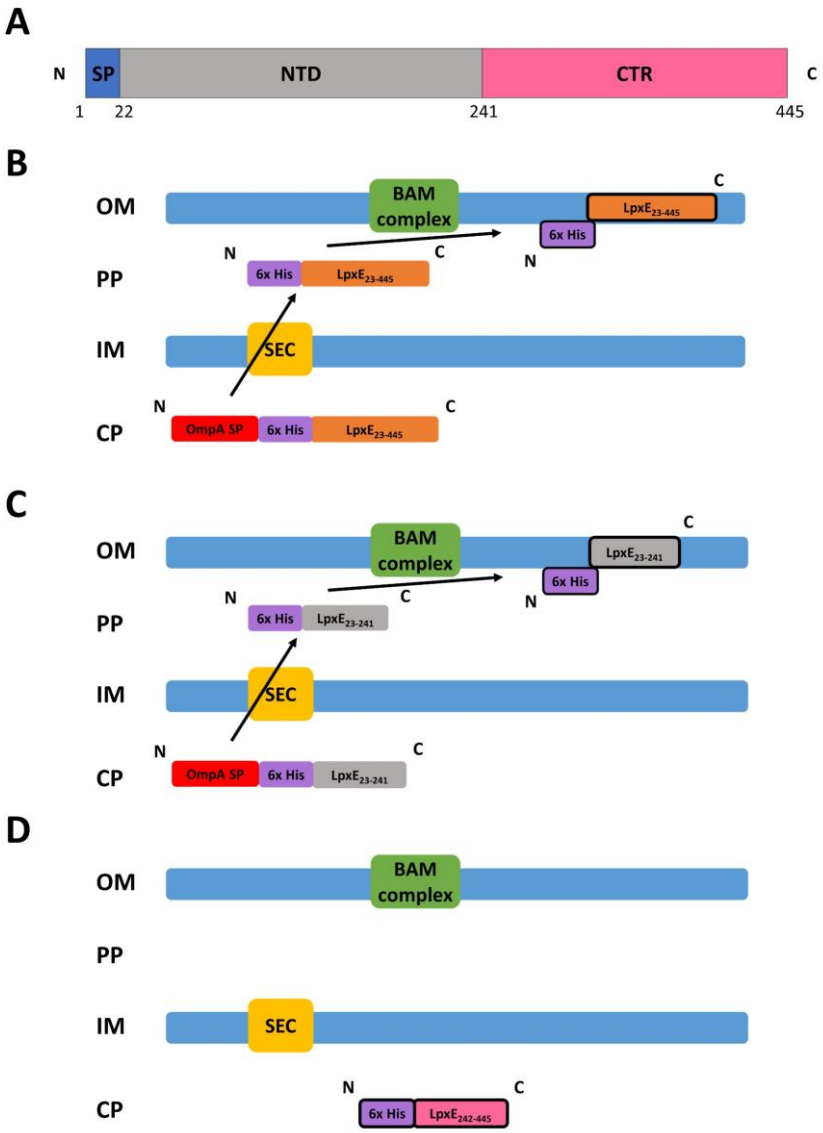

Figure 5.14: Strategies of LpxE expression in *E. coli.* A. Schematic of *P. gingivalis* LpxE with mature sequence numbers and structural features annotated. SP: periplasmic signal peptide, residues 1-22; NTD, N-terminal domain, residues 23-241; CTR, C-terminal region, residues 242-445. **B.** Full-length LpxE is expected to be expressed as membrane protein $LpxE_{His\text{-}23\text{-}445}$, after processed by Sec and BAM machineries. **C.** LpxE NTD is expected to be expressed as membrane protein $LpxE_{His\text{-}23\text{-}241}$, after processed by Sec and BAM machineries. **D.** LpxE CTD is expected to be expressed as soluble protein $LpxE_{His\text{-}242\text{-}445}$ in cytoplasm. CP: cytoplasm. IM: inner membrane. PP: periplasm. OM: outer membrane.

5.4.1 Expression of LpxE

Expression trials of $LpxE_{His\text{-}23\text{-}445}$ were first attempted in BL21 competent cells, although no expression was detected (data not shown). Given that PorV had been

successfully purified from Lemo21 cells, which allows more stringent control of expression of challenging membrane proteins, these cells were next tried. The expression cultures were grown with 50 µM, 100 µM and 150 µM rhamnose, followed by 0.25 mM IPTG induction and 20°C or 25°C overnight incubation. The result showed that $LpxE_{His\text{-}23\text{-}445}$ was expressed in cells (**Figure 5.15A**), but it was not detected in soluble and membrane fraction (**Figure 5.15B**). This suggests that *P. gingivalis* $LpxE_{His\text{-}23\text{-}445}$ was expressed but it may not be correctly targeted to the membrane in *E. coli*. It could be that *E. coli* lacks appropriate molecular chaperones to aid $LpxE_{His\text{-}23\text{-}445}$ folding and insertion into the membrane, or the expression of *P. gingivalis* LpxE in *E. coli* is toxic.

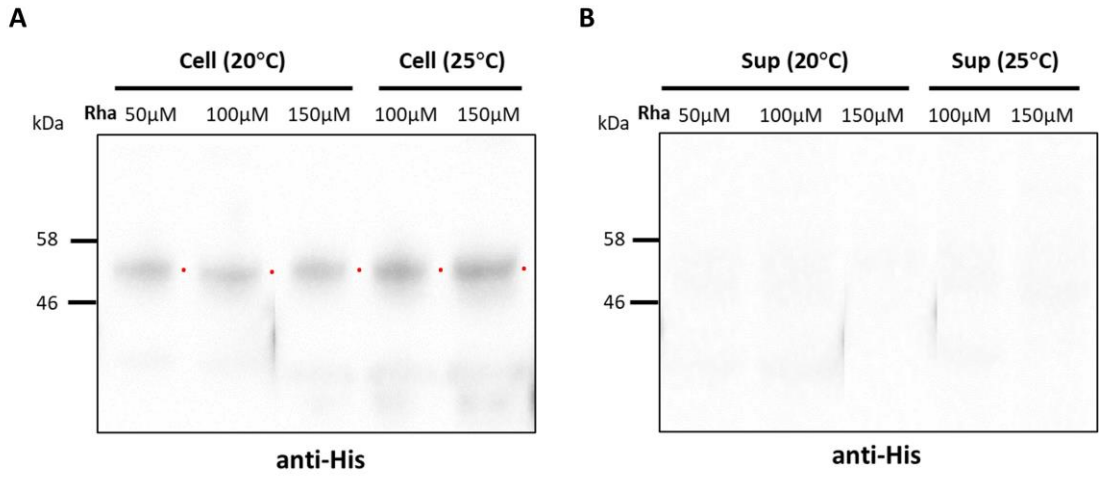

Figure 5.15: $LpxE_{His\text{-}23\text{-}445}$ expression using Lemo21 competent cells. A. Western blot analysis of $LpxE_{His\text{-}23\text{-}445}$ expression in Lemo21 cells. **B.** Western blot analysis of $LpxE_{His\text{-}23\text{-}445}$ expression in the supernatant that contains membrane fractions. The immunoblots were probed with anti-His (diluted 1:1000). The Lemo21 cells were induced with 0.25 mM IPTG at 20°C or 25°C overnight. The $LpxE_{His\text{-}23\text{-}445}$ expression was controlled by the addition of 50 µM, 100 µM and 150 µM L-rhamnose. His-tag antibody was used. Number ladders on the left-hand side represent the size of marker proteins in kDa.

E. coli C41 (DE3) strain is derived from BL21 (DE3), and contains mutations that prevent cell death from the expression of toxic proteins[348]. Although unlike Lemo21,

expression is not tuneable, there are many examples of successful purification of bacterial membrane proteins using C41 cells[348]. The construct pOMPA28-LpxE$_{23-445}$ was therefore transformed into C41 cells for expression trials. LpxE$_{His-23-445}$ was observed to be expressed in the cell membrane fraction with a band visible at ~50 kDa with immunoblot using an anti-His antibody (**Figure 5.16**). However, some lower molecular weight bands (25 and 14 kDa) were also present, which could represent some proteolysis or domain cleavage. A high molecular weight band was also seen at 150 kDa, which indicates that LpxE$_{His-23-445}$ could also form a stable oligomer (**Figure 5.16**).

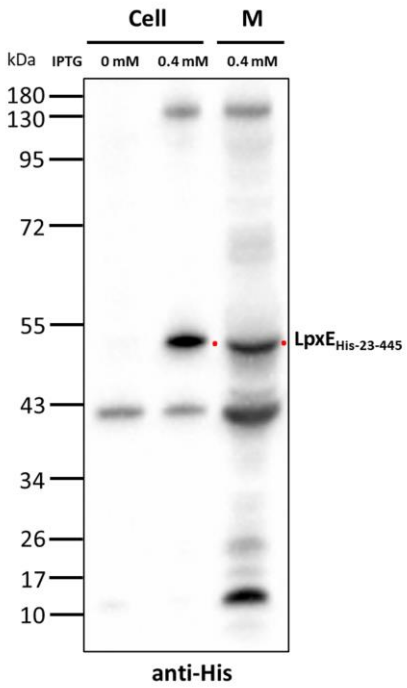

Figure 5.16: Localization of expressed LpxE$_{His-23-445}$. Western blot of expressed LpxE$_{His-23-445}$ in cell and membrane fractions. The immunoblot was probed with anti-His (diluted 1:1000). LpxE$_{His-23-445}$ ~48 kDa was expressed with 0.4 mM IPTG and was observed in membrane. Cell, whole cell; M, cell membrane, was solubilized with 1% DDM. Number ladders on the left-hand side represent the size of marker proteins in kDa.

5.4.2 Purification of LpxE

These optimized expression conditions were next used for large-scale preparation of $LpxE_{His\text{-}23\text{-}445}$. As LpxE from *A. aeolicus* has been successfully purified using DDM detergent[283], membranes were collected using ultracentrifugation and solubilised using 1% (vol/vol) DDM. After incubation at 4°C overnight, the suspension was ultracentrifuged to remove any insoluble material and the resulting supernatant was used for Ni-NTA chromatography (**Figure 5.17**). The solubilised membrane suspension was loaded onto an equilibrated poly-prep gravity flow column containing 1 ml Ni-NTA agarose resin. Purified $LpxE_{His\text{-}23\text{-}445}$ was seen in the elution by Western blot but other lower molecular weight bands were also observed (**Figure 5.17B**). As the His-tag of $LpxE_{His\text{-}23\text{-}445}$ is at the N-terminus, these likely represented the LpxE NTR. The elution was pooled and concentrated to a volume of 0.5 ml and was further purified by size exclusion chromatography to remove contaminant proteins and imidazole.

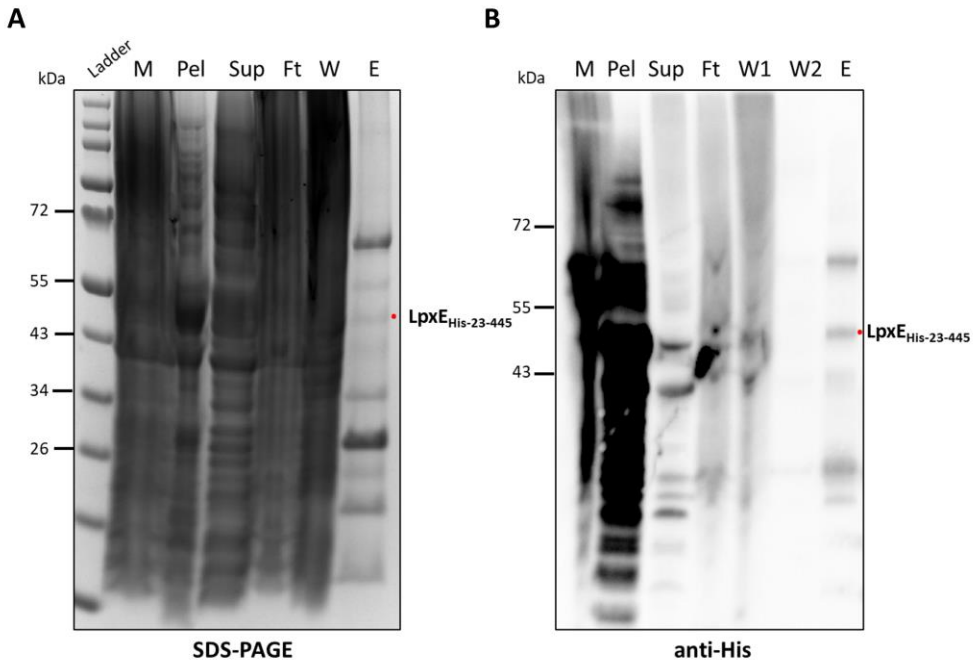

Figure 5.17: Ni-NTA chromatography purification of $LpxE_{His-23-445}$. A. SDS-PAGE analysis of Ni-NTA chromatography purification of $LpxE_{His-23-445}$. **B.** Western blot analysis of Ni-NTA chromatography purification of $LpxE_{His-23-445}$. The immunoblot was probed with anti-His (diluted 1:1000). Purified $LpxE_{His-23-445}$ ~48 kDa was shown. M, membrane; Pel, pellet of solubilized membrane; Supernatant, supernatant of solubilized membrane; Ft, flowthrough of the Ni-NTA column; W1, first wash; W2, second wash; E, elution. Number ladders on the left-hand side represent the size of marker proteins in kDa.

As the expected molecular weight of a $LpxE_{His-23-445}$ was ~48 kDa, a HiLoad® 16/600 Superdex® 200 pg column was used as it provides good resolution for globular proteins between 10-600 kDa. By calculation of protein standards[339], folded $LpxE_{His-23-445}$ should have eluted at ~80 ml on this column. The result showed that four major peaks were eluted (**Figure 5.18A**). SDS-PAGE and immunoblots showed no band of the expected $LpxE_{His-23-445}$ size in peaks P1 and P2. However, in the peaks at ~80 ml (P3) and ~90 ml (P4), a band of the expected molecular weight was seen, but again lower molecular weight degradation was also observed (**Figure 5.18B, C**).

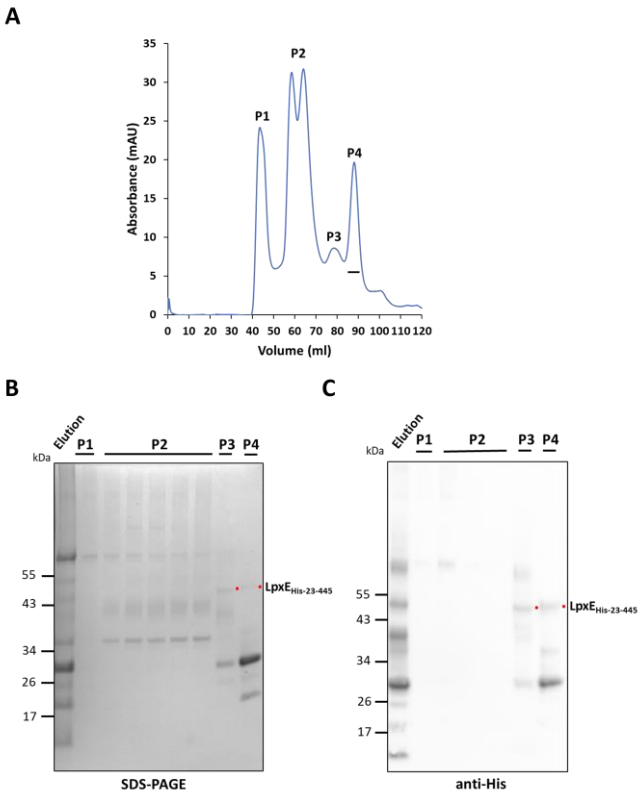

Figure 5.18: Size exclusion chromatography of LpxE$_{His-23-445}$. A. UV A280 absorbance chromatogram of the LpxE$_{His-23-445}$ purification. P1, P2 and P3 represent unknown contaminant proteins. P4 representing purified LpxE$_{His-23-445}$ was highlighted. **B.** SDS-PAGE analysis of the LpxE$_{His-23-445}$ 2 ml fractions from 40 ml to 80 ml. **C.** Western blot analysis of the LpxE$_{His-23-445}$ 2 ml fractions from 40 ml to 90 ml. The immunoblot was probed with anti-His (diluted 1:1000). His-LpxE ~48 kDa was shown. Elution, elution of Ni-NTA chromatography purification; P1, peak 1; P2, peak 2; P3, peak 3; P4, peak 4. Number ladders on the left-hand side represent the size of marker proteins in kDa.

5.4.3 Mass spectrometry identification

To confirm that the purified protein sample was actually LpxE$_{His-23-445}$, a fraction of the P4 sample containing three bands (**Figure 5.18**), was resolved using SDS-PAGE and sent for analysis by high resolution Orbitrap tandem mass spectrometry coupled to liquid chromatography at the Centre of Excellence for Mass Spectrometry (KCL).

Raw mass spectrometry data were processed into peak list files using Proteome Discoverer V2.2 (ThermoFisher Scientific). The data were searched using the Mascot

search algorithm V2.6.0 (MatrixScience) and the Sequest search algorithm[349] against the Uniprot All Taxonomy database (563,552 entries) and a bespoke database containing the LpxE protein sequence only.

In total, 172 proteins were detected across the three sample bands at this stringency with 89 proteins detected in the 50 kDa band, 122 proteins in the 30 kDa band and 45 proteins in the 20 kDa band. However, the protein of interest, lipid A 1-phosphatase, was not detected in any of the sample bands at this stringency when searched against Uniprot All Taxonomy. To allow for less well-matched spectra which may not have achieved the stringent criteria, the protein filter was lowered to 20% and the peptide filter to 0%. This greatly increased the number of identifications per band which have not been assigned at the most confident and stringent assignment filter. It also introduces a greater number of false positive matches which must be manually verified to determine correct database assignment. Even with this drop in stringency the protein of interest was not detected in the data.

As $LpxE_{His\text{-}23\text{-}445}$ had been detected in Western blot, the reasons for the mass spec identification could be the protein concentration was too low or $LpxE_{His\text{-}23\text{-}445}$ had been significantly degraded. Therefore, the strategies were altered to express the LpxE NTD and LpxE CTR domains separately.

5.4.4 Expression and purification of LpxE NTD

To express LpxE NTD, the construct pOMPA28-$LpxE_{23\text{-}241}$ was transformed into

Lemo21 competent cells for expression trials. The expression cultures were grown with various levels of rhamnose, followed by normal IPTG induction. However, no additional band was seen in IPTG induced samples by SDS-PAGE (**Figure 5.19**), which suggests $LpxE_{His\text{-}23\text{-}241}$ was not expressed in these cells. Due to time restriction, pOMPA28-$LpxE_{23\text{-}241}$ was not tested in other cell lines.

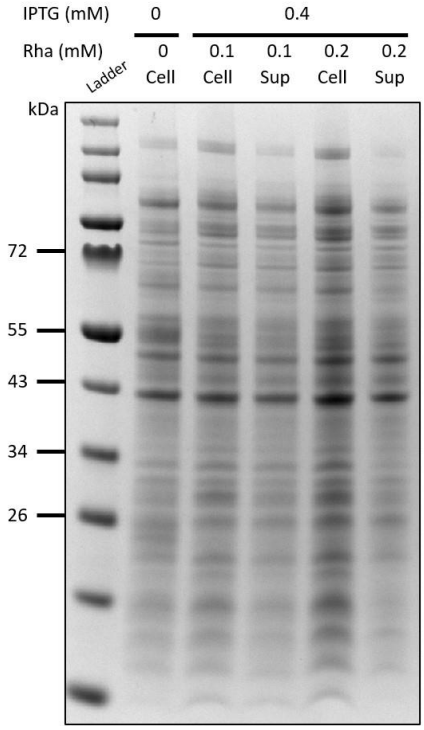

Figure 5.19: Expression of $LpxE_{His\text{-}23\text{-}241}$ using Lemo21. SDS-PAGE analysis of $LpxE_{His\text{-}23\text{-}241}$ expression in cell and supernatant. No additional band was shown in IPTG induced samples. The Lemo21 cells were induced with 0.4 mM IPTG at 20°C overnight. The $LpxE_{His\text{-}23\text{-}241}$ expression was controlled by the addition of 50 μM, 100 μM and 150 μM L-rhamnose. Cell, *E. coli* cells; Sup, supernatant of cell lysate. Number ladders on the left-hand side represent the size of marker proteins in kDa.

5.4.5 Expression and purification of LpxE CTR

As I anticipated that the LpxE CTR may be a soluble domain, the gene of $LpxE_{242\text{-}445}$ was cloned into pET46b Ek/LIC with an N-terminal His-tag for soluble expression in the cytoplasm. The construct pET46-$LpxE_{242\text{-}445}$ was then transformed into BL21

competent cells for expression tests. Although $LpxE_{His-242-445}$ was expressed in cells (**Figure 5.20A**), it was not located in the supernatant, but in inclusion bodies (**Figure 5.20B**). The pellet containing $LpxE_{His-242-445}$ was then solubilized in 8 M urea and attempts were made to refold it. However, after dialysis, $LpxE_{His-242-445}$ was not refolded but formed white aggregation, even over different sodium concentrations and buffer pH. This suggests that the $LpxE_{His-242-445}$ may have membrane protein properties, however, again due to time restrictions, expression of LpxE CTR in *E. coli* membranes was not examined.

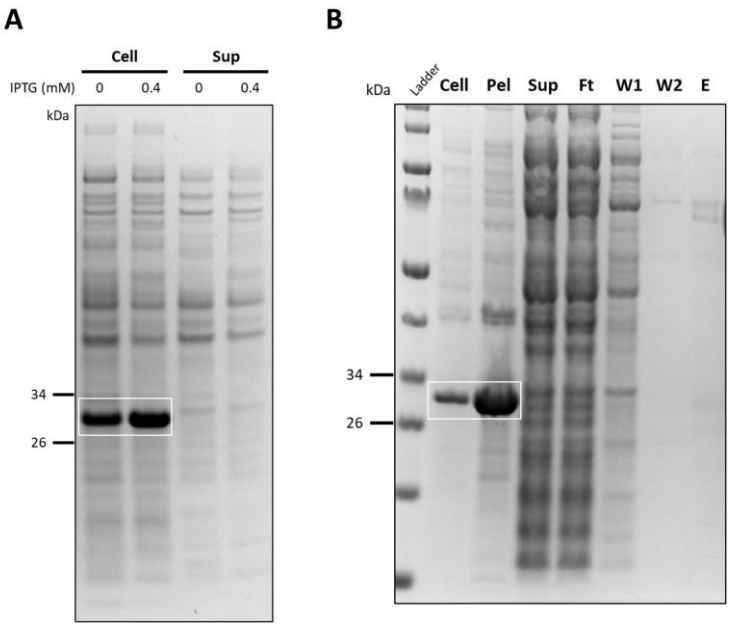

Figure 5.20: Expression and purification of $LpxE_{His-242-445}$. A. Expression of $LpxE_{His-242-445}$ using BL21. Protein expression was induced with 0.4 mM IPTG at 18°C overnight. Expressed $LpxE_{His-242-445}$ was seen in cell samples but was not seen in supernatant samples. **B.** Ni-NTA chromatography purification of $LpxE_{His-242-445}$. $LpxE_{His-242-445}$ expressed in inclusion bodies was highlighted. Cell, *E.coli* cell; Pel, pellet of cell lysate; Sup, supernatant of cell lysate; Ft: flowthrough of the Ni-NTA column; W1, first wash; W2, second wash; E, elution. Number ladders on the left-hand side represent the size of marker proteins in kDa.

5.5 AlphaFold2 model of LpxE

During writing this thesis, the source code for AlphaFold was released and this has allowed a highly accurate protein structure prediction of LpxE to be performed[350]. AlphaFold is an artificial intelligence (AI) system developed by DeepMind that predicts a protein's 3D structure from its amino acid sequence[350]. The latest version of the machine-learning based method AlphaFold2 is powerful as it achieved unprecedented structure prediction accuracy[320]. To get structural insight into *P. gingivalis* LpxE, the sequence minus the predicted signal sequence was uploaded to AlphaFold, which was run on the Google Colaboratory server (https://colab.research.google.com).

The result shows that sequence coverage of LpxE NTD is very high, but it is very low in LpxE CTR (**Figure 5.21A**). The local distance difference test (lDDT) is a superposition-free score that evaluates local distance differences of all atoms in a model[351]. A score above 50 is considered reliable whereas a score under 50 implies inaccuracy or flexibility. Five models of LpxE were generated and the results show that their predicted IDDT score is in general consistent with well folded models, with low values only seen for residues in loop positions (**Figure 5.21B**). The predicted aligned error (PAE) score reports AlphaFold's expected positional error at residue x, when the predicted and true structures are aligned on residue y. For residues x and y drawn from two different domains, a consistently low PAE at (x, y) suggests AlphaFold is confident about the relative domain positions. Consistently high PAE at (x, y) suggests the relative positions of the domains should not be interpreted[320]. The PAE data shows that the lowest consistently PAE at (x, y) was observed in all models within the individual NTR

and CTR regions indicating these were well folded domains (**Figure 5.21C**). However, between domains the PAE at (x, y) was higher, suggesting that the two domains are not rigidly associated with each other.

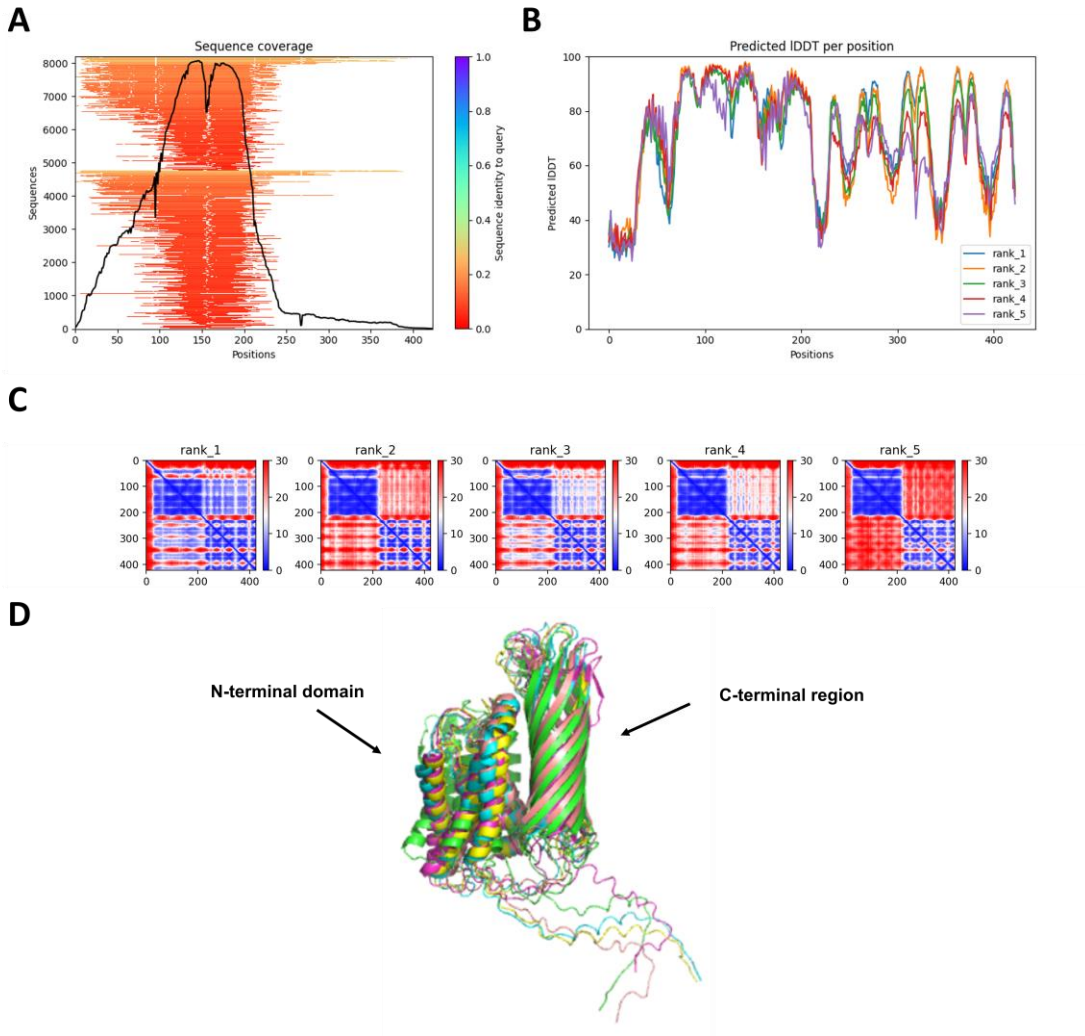

Figure 5.21: Highly accurate LpxE structure prediction with AlphaFold2. A. Sequence coverage analysis of *P. gingivalis* LpxE. **B.** Predicted Local Distance Difference Test (lDDT) per position of LpxE. **C.** Predicted Aligned Error (PAE) of top five ranked LpxE models. **D.** Alignments of top five ranked LpxE structures.

The top five ranked LpxE structures were aligned and shows that they share a similar overall structure and all contains an extended N-terminal region, followed by a α-helical PAP2-family domain and a C-terminal β-barrel domain containing 8 strands (**Figure**

5.21D). The extended N-terminal 22 amino acids could pass back across the membrane and be an additional helix, although this region is quite short, and this is unlikely. Another possibility is that this region could partially insert into the membrane and block access to the active site of LpxE. There are two cystine residues on the extension, suggesting that it could also form intra-or inter-disulphide bonds, which could affect the local conformation of LpxE. The extended sequence has one positive charged residue and two negative charged residues, which may promote interaction with another protein. If this sequence is not membrane embedded and LpxE is localised within the inner membrane, the N-terminal 22 amino acids would be extended into the cytoplasm. If LpxE is in the OM, these would extend into the periplasm.

Further analysis of the LpxE CTR from the first ranked model showed residues with positive or negative charged side chain were distributed on the top, bottom and lumen of the LpxE CTR barrel, but not within an expected external membrane embedded region (**Figure 5.22A**). In contrast, residues with hydrophobic side chains were distributed on the bottom and on the anticipated membrane embedded surface of the LpxE CTR barrel (**Figure 5.22B, C**). This distribution of amino acid type is typical of OM proteins such as OmpA[352], where most hydrophobic residues are on the outside and most charged residues are internal. This strongly supports that LpxE CTR is also an integral membrane protein.

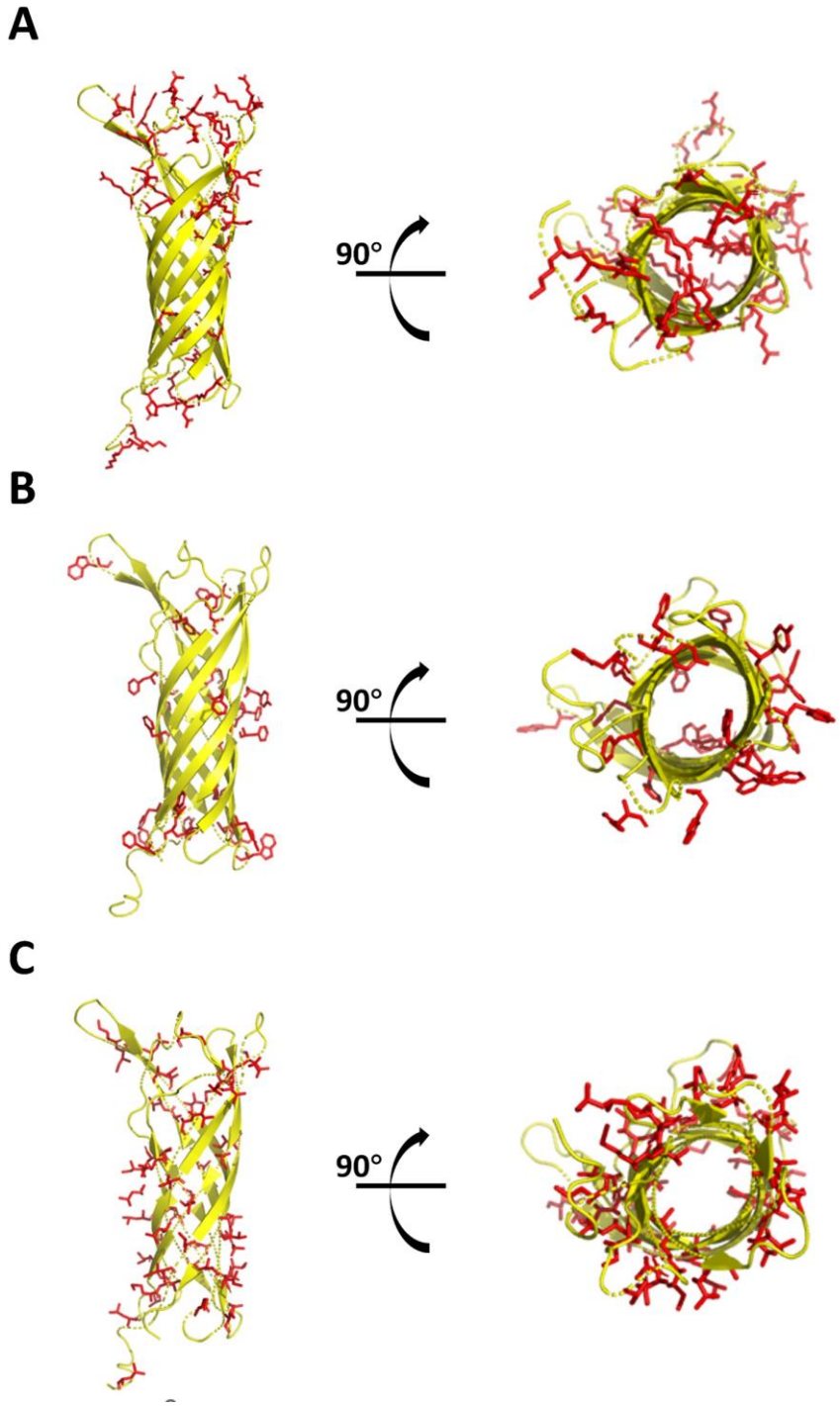

Figure 5.22: Structural analysis of *P. gingivalis* LpxE C-terminal region. A. Residues with electrically positive charged side chain (arginine, lysine) and negative charged side chain (aspartic acid, glutamic acid) are shown as sticks. The charged residues are distributed on the top, bottom and lumen of LpxE CTR. **B.** Residues with aromatic hydrophobic side chain (phenylalanine, tyrosine, tryptophan) are shown as sticks. **C.** Residues with hydrophobic side chain (alanine, valine, isoleucine, leucine, methionine) are shown as sticks. The hydrophobic residues are distributed on the surface and bottom of LpxE CTR.

5.6 Discussion

This chapter describes attempts at recombinant expression and purification of T9SS outer membrane accessory proteins and the lipid A 1-phosphatase LpxE. Using the pOMPA28 vector, PorV, PorU, PorQ, PorT and PorF were expressed in *E. coli* cells. To optimize expression, PorV was then purified from Lemo21 (DE3) competent cells with the detergent LDAO. The far Western blot assay confirms that purified PorV was functional although only low yeilds (~ 0.1 mg PorV/L culture) could be recovered. LpxE was also expressed in *E. coli* and purification was attempted, however the presumed purified protein could not be detected as LpxE by mass spectrometry. Although expression and purification of LpxE NTD and CTR were attempted, the NTD did not express and the CTR was expressed in inclusion bodies. The AlphaFold2 models of *P. gingivalis* LpxE predict that LpxE is composed of an N-terminal phosphatase domain, a C-terminal β-barrel domain and an N-terminal extension carrying two cysteine residues. These unique structural features could explain why it has been difficult to express folded LpxE in *E. coli.*

Although PorV was successfully purified from *E. coli* membranes, the refolding assay of PorV did not work. However, it would be worthwhile to try and refold PorV aggregations with other agents such as guanidinium chloride (GuHCl) which may be better than urea in its solubility and renaturation. LpxE was not successfully purified but with more time, this recombinant expression system could be optimized in the future. Codon optimization is a process used to improve gene expression and increase the translational efficiency of a gene of interest by accommodating codon bias of the

host organism. As previous experience in our lab has shown that *P. gingivalis* proteins can be expressed at high levels without codon optimization, I did not do codon optimization for these recombinant expression constructs, but this might be an option to improve recombinant expression in the future. Likewise, PorP did not express, and this could be improved by using codon optimization. As the OmpA signal peptide may not be suitable for LpxE expression, it would also be worthwhile to test other membrane protein signal peptides such as the PelB signal peptide. Other protein tags such as GST (glutathione S-transferase)-tag, twin-strep-tag or SUMO (small ubiquitin-related modifier)-tag could in addition be tested in different expression systems as they could promote correct folding, solubility and/or assembly in membranes. Due to time restriction, I could not carry out detergent screening for LpxE but chose to solubilize LpxE with DDM, because *A. aeolicus* LpxE whose structure has been determined had been successfully purified with DDM[283]. However, *A. aeolicus* LpxE is only homologous with the *P. gingivalis* LpxE NTD. *P. gingivalis* LpxE is unique as it possesses an additional CTR which might change the property of this phosphatase, so it will be necessary to test more detergents. Alternative protein solubilisation systems such as styrene maleic acid lipid particles (SMALPs) could also be useful. The SMALP method uses an amphipathic polymer, styrene maleic acid co-polymer (SMA), to extract membrane proteins directly from native membranes[353]. In contrast to detergent, the SMA reagent extracts the protein within the portion of membrane that surrounds it, thereby preserving at least some of the native lipid environment[354].

However, the predicted structure of LpxE is unusual because α-helical proteins are more

likely to be localised in the inner membrane (IM), whereas β-barrels are exclusively seen in the outer membrane (OM) of bacteria[355]. Based on my localization data of LpxE in Chapter 4 which indicated that LpxE may be localised to the OM by Western blot analysis, the LpxE model was anticipated to be in the OM. I speculate that the LpxE CTR could be targeted to the OM through the BAM complex, where the NTD would then spontaneously be inserted into OM upon CTR folding. Sequence analysis also suggests that the C-terminus of the LpxE CTR possesses a β-signal motif (FXF) which is recognized by the BAM complex[356] and it could also be possible that some unknown chaperone can aid LpxE to cross the periplasm. In this model, the CTR could act as an OM localisation signal.

If LpxE is in the IM, it would be unusual to have a C-terminal β-barrel because β-barrel proteins are transported and inserted into the OM via the BAM complex[215]. As α-helical proteins are assembled and inserted into the IM via the Sec system[357], the LpxE CTR could be spontaneously inserted into the IM upon correct folding of the NTD. Here the role of the CTR could be to regulate NTD activity. For example, it has been reported that a soluble human phosphatase Ppp5 has an additional CTR and it uses this to regulate its activity by stabilizing the conformation of the phosphatase domain[358].

Here three most likely models were proposed for the location of LpxE (**Figure 5.23**). In the first model, the entire LpxE is thought to be in the OM (**Figure 5.23A**). The LpxE CTR is likely to anchor LpxE NTD to the OM. The two cysteine (Cys) residues Cys4 and Cys12 present on LpxE N-terminus may form a disulphide bond either internally or with other protein. This model is supported by OMV and lipid A data in Chapter 3,

because knocking out any T9SS OM component resulted in the irregular OMV formation and the absent of non-phosphorylated lipid A. Since LpxE is the key enzyme to produce non-phosphorylated lipid A[153] and it has some role in OMV formation (**Figure 4.10**), I speculate that knocking out any T9SS OM component would inactivate LpxE activity. If LpxE is in the OM, it could interact with any number of T9SS OM proteins or T9SS substrates, and the OMV and lipid A data can be explained. Another important evidence is that LpxE was detected in the OM in the Western blot of LpxE localization. Although too many non-specific bindings were seen, the result was observed when repeated. This implies that *P. gingivalis* LpxE may be the first OM bound lipid A 1-phosphatase. However, the limitation of this model is that most α-helical proteins are localised in the IM.

In the second model, LpxE is thought to be in the IM (**Figure 5.23B**). This model is supported by the fact that all the lipid A 1-phosphatases discovered so far are localised to the IM. However, it is uncommon for the C-terminal β-barrel to localise to the IM. Moreover, if LpxE is in the IM, how LpxE is linked to the T9SS is harder to understand. In the third model, LpxE NTD is also thought to be in the IM, but the LpxE CTR is thought to be in the periplasm (**Figure 5.23C**). Given that the structural analysis suggested that LpxE CTR is an integral membrane protein, this last model is not very plausible. The two domains of LpxE could also span between the IM and OM, however, the linker between LpxE NTD and CTR is too short (10 amino acids) and again this is a very unlikely model.

The AlphaFold2 model also implies the reason that LpxE was not identified in Co-IP

assay, as the N-terminal tag may have been cleaved due to the flexibility or affected its correct localization, and the C-terminal HA tag may have been too close to LpxE, affecting its folding and/or being embedded in the membrane.

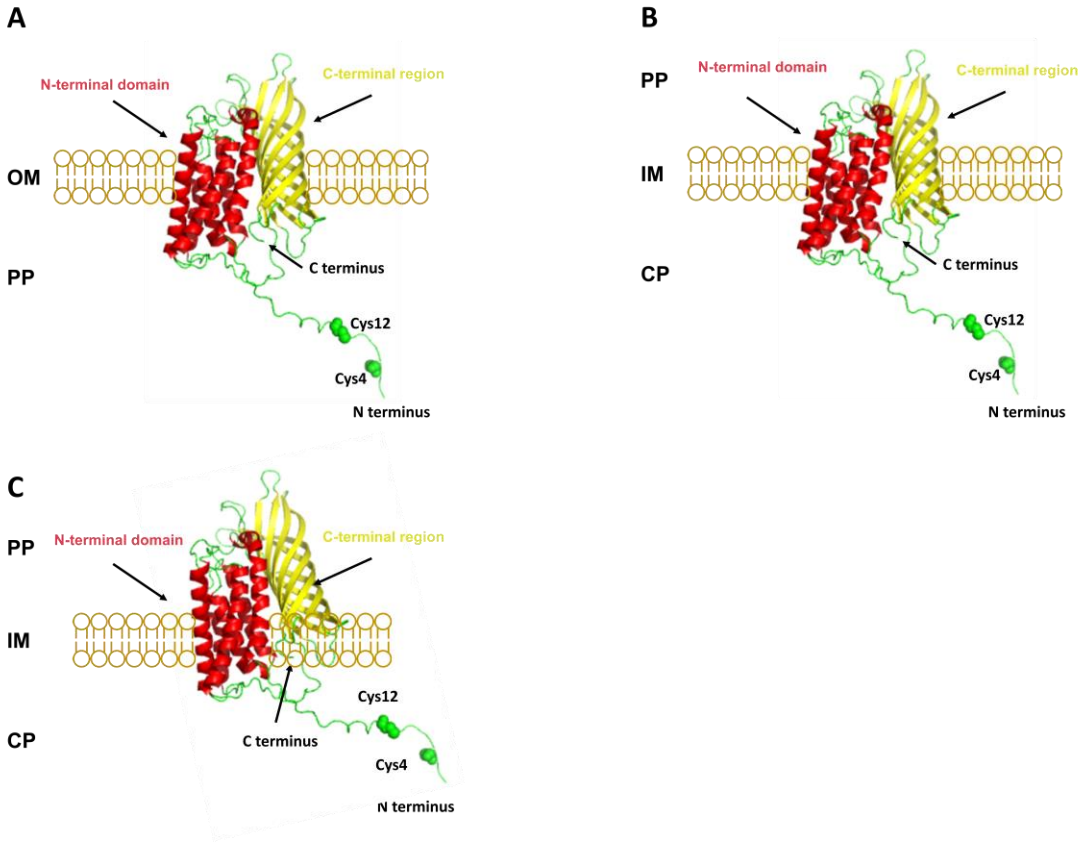

Figure 5.23: Hypothetical models of *P. gingivalis* LpxE localization. A. The LpxE N-terminal domain (NTD) and C-terminal region (CTR) are in the outer membrane (OM). The 22 N-terminal amino acids extend to the periplasm (PP). **B.** The LpxE NTD and CTR are both in the inner membrane (IM). The 22 N-terminal amino acids extend to the cytoplasm (CP). **C.** The LpxE NTD is in the IM, but the CTR is in the PP. The 22 N-terminal amino acids extend to the CP. The NTD is coloured in red and the CTR is coloured in yellow. Two cysteine residues Cys4 and Cys12 are shown on N-terminus extension.

As the CTR of LpxE is also present in *Parabacteroides* sp. and *Prevotella* sp. and *T. forsythia* which all belong to *Bacteroidota*, AlphaFold predictions of LpxE were also performed for these species. Similar to *P. gingivalis* LpxE, the predicted LpxE structures from *Parabacteroides* sp. and *Prevotella* sp. and *T. forsythia* are all composed

of an N-terminal α-helical domain and a C-terminal β-barrel domain containing 8 strands (**Figure 5.24**). While *Prevotella* sp. LpxE was predicted to also contain an unstructured N-terminus, *Parabacteroides* sp. LpxE contained a helical region and in *T. forsythia* this region crossed back across the membrane. However, in the latter case no signal sequence could be identified and therefore this region is longer. Other differences were observed within the surface loops of the CTR β-barrel. These imply that this novel type of LpxE may share a common mechanism in specific bacteria from *Bacteroidota* and deviations in these models may indicate an interaction site for the T9SS or a secreted T9SS cargo protein, which could then somehow regulate activity of the NTD.

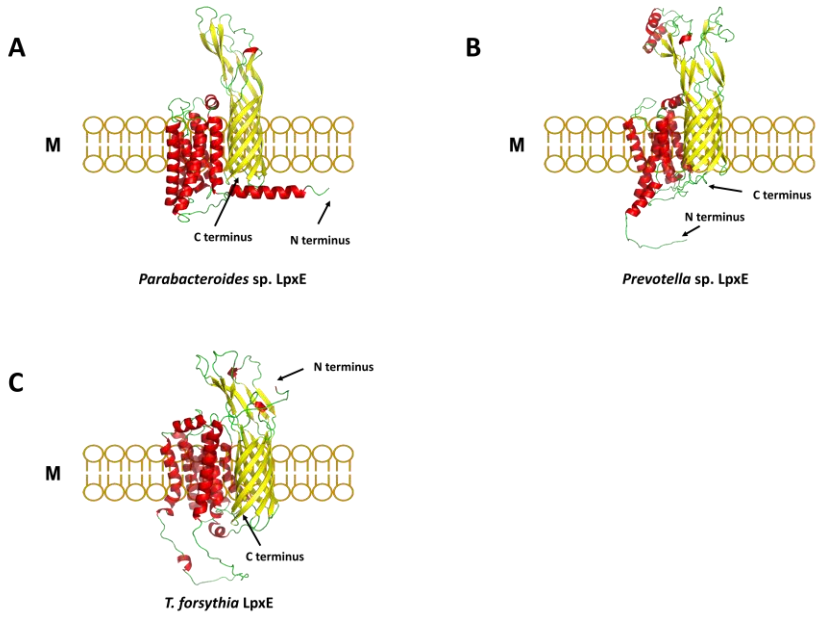

Figure 5.24: AlphaFold2 models of LpxE from other bacteria. A. AlphaFold2 model of *Parabacteroides* sp. LpxE. **B.** AlphaFold2 model of *Prevotella* sp. LpxE. **C.** AlphaFold2 model of *T. forsythia* LpxE. The α-helices are coloured in red and the β-sheets are coloured in yellow.

It has been reported that similar conserved motifs of T9SS CTDs[173] and T9SS

homologues[296] are present in *Parabacteroides* sp.[173,296] and *Prevotella* sp.[172]. *Parabacteroides* sp. colonize the gut but also produce OMVs to cause disease[359]. Increased abundance of *Prevotella* sp. at mucosal sites has been linked to periodontitis, although whether *Prevotella* sp. produce OMVs as a virulence determinant has not been confirmed[360]. As another major pathogen that is associated with periodontitis, *T. forsythia* is also equipped with a T9SS and can export virulence factors such as glycoproteins via OMV formation[361]. Although the mechanism of OMV biogenesis has been not well studied in these bacteria, it could be that the LpxE CTR is an adaptation that links the T9SS to OMV formation bacteria.

5.7 Conclusion

This chapter describes the recombinant expression and purification of T9SS outer membrane accessory proteins and lipid A 1-phosphatase LpxE. Using the pOMPA28 vector, PorV, PorU, PorQ, PorT and PorF were expressed in *E. coli* cells. To optimize expression, PorV was then purified from Lemo21 (DE3) competent cells with detergent LDAO. The far Western blot assay confirms that purified PorV was functional although only low yeilds (~ 0.1 mg PorV/L culture) could be recovered. LpxE was also expressed in *E. coli* and purification was attempted, however the presumed purified protein could not be detected as LpxE by mass spectrometry. Although expression and purification of LpxE NTD and CTR were attempted, the NTD did not express and the CTR was expressed in inclusion bodies. The AlphaFold2 models of *P. gingivalis* LpxE predict

that LpxE is composed of an N-terminal phosphatase domain, a C-terminal β-barrel domain and an N-terminal extension carrying two cysteine residues. The AlphaFold2 models of *Parabacteroides sp. and Prevotella sp.* and *T. forsythia* LpxE imply that this novel LpxE may share a common mechanism in specific bacteria from *Bacteroidetes*.

Chapter 6 Conclusions and Future Perspectives

6.1 Project summary

In this project, I characterized *P. gingivalis* T9SS outer membrane accessory proteins PorV, PorU, PorQ, PorZ, PorP, PorT, PorG and PorF, and revealed that they are involved in OMV biogenesis and lipid A dephosphorylation. At the beginning of this project, it was only known that PorV, PorU and PorT are required for OMV formation and PorV is required for lipid A dephosphorylation. I expanded the understanding of this field because my results suggest that the entire T9SS may regulate OMV biogenesis and lipid A modification in *P. gingivalis*.

The lipid A profiles of these T9SS mutants are linked to a published *P. gingivalis lpxE* mutant. This finding suggests that the T9SS may regulate lipid A status via LpxE. Homologous sequence analysis and protein structure prediction indicate that *P. gingivalis* LpxE is unusual as it possesses an N-terminal SP, a 22-residue N-terminal extension and an additional CTR with unknow function. The characterization of LpxE suggests that this phosphatase is required for OMV production and destabilizing the cell membrane. However, complements of the *lpxE* mutant did not appear to restore the phenotype in many cases. The protein localization analysis suggests that LpxE is in the outer membrane, although this result was dependent on the complements having some restored wild-type activity. Despite attempting many times, the interaction partner of LpxE has not been identified.

The T9SS outer membrane protein PorV was recombinantly expressed and purified from *E. coli*. However, the mass spectrometry showed that LpxE was not purified

successfully. The AlphaFold2 model of LpxE suggests that LpxE is composed of an N-terminal α-helical phosphatase domain and an unusual C-terminal β-barrel domain. I speculated that the C-terminal β-barrel domain may be involved in interaction with the T9SS. Moreover, AlphaFold2 predictions suggest that the C-terminal β-barrel domain is also present in *Parabacteroides* sp. and *Prevotella* sp. and *T. forsythia*. This evidence implies that the LpxE CTR could be the adaption to the T9SS and OMV dependent bacteria.

This project discovered a unique correlation between the T9SS and extracellular vesicle biogenesis, and the connector LpxE has been identified. This could be a general mechanism in T9SS and OMV dependent bacteria. More structural and biochemical studies would be needed to understand the mechanism behind this phenomenon.

6.2 Conclusions

6.2.1 Models of lipid A modifications in *P. gingivalis*

Based on the location of LpxE, two models of lipid A dephosphorylation pathway in *P. gingivalis* are proposed (**Figure 6.1**). In the first model, LpxE is thought to be in the outer membrane (OM) (**Figure 6.1A**). Firstly, the precursor bis-P-pentaacyl lipid A is removed 4′-phosphate by LpxF to generate 1-P-pentaacyl lipid A. Next, the bis-P-pentaacyl and 1-P-pentaacyl lipid A are transported to the OM bound LpxE and deacylase PGN_1123 through a LPS transport pathway. The bis-P-pentaacyl and 1-P-pentaacyl lipid A are removed 1-phosphate by LpxE to generate 4′-P-pentaacyl, non-P-

pentaacyl lipid A. Finally, the non-P-pentaacyl and 1-P-pentaacyl lipid A are deacylated by PGN_1123 to produce non-P-tetraacyl and 1-P-tetraacyl lipid A.

Conversely, LpxE is thought to be in the inner membrane (IM) in the second model (**Figure 6.1B**). Firstly, the precursor bis-P-pentaacyl lipid A is removed 4′-phosphate by LpxF to generate 1-P-pentaacyl lipid A and then removed 1-phosphate by LpxE to generate non-P-pentaacyl lipid A. The precursor bis-P-pentaacyl lipid A is also removed 1-phosphate by LpxE to generate 4′-P-pentaacyl lipid A. Next, the bis-P-pentaacyl, 1-P-pentaacyl, 4′-P-pentaacyl and non-P-pentaacyl lipid A are transported to the OM bound deacylase PGN_1123 through a LPS transport pathway. Finally, the 1-P-pentaacyl and non-P-pentaacyl lipid A are then deacylated by PGN_1123 to produce 1-P-tetraacyl and non-P-tetraacyl lipid A.

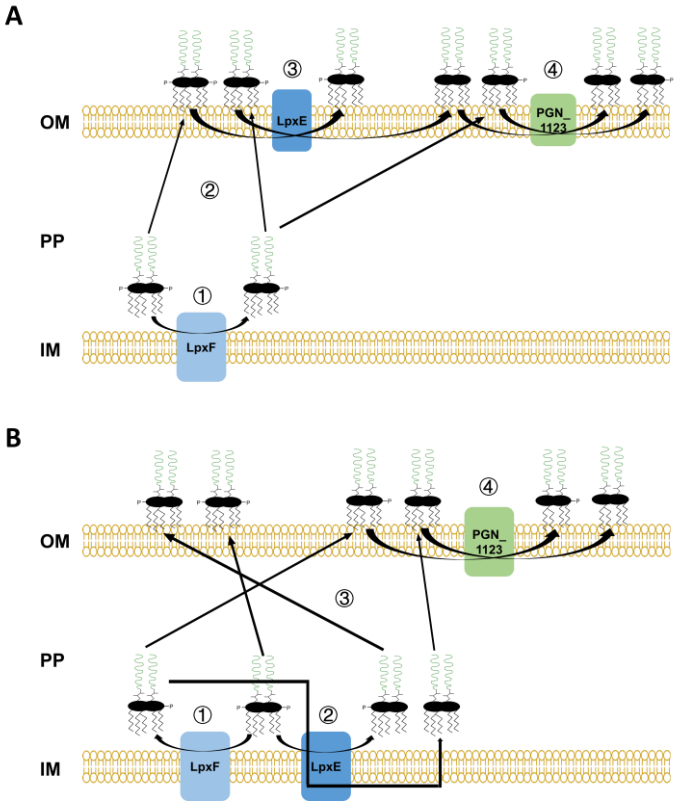

Figure 6.1: Hypothetical lipid A dephosphorylation pathway in *P. gingivalis*. A. LpxE is thought to be in the outer membrane (OM). The lipid A modification pathway includes four steps: 1, the precursor

bis-P-pentaacyl lipid A is removed 4′-phosphate by LpxF to generate 1-P-pentaacyl lipid A; 2, the bis-P-pentaacyl and 1-P-pentaacyl lipid A are transported to the outer membrane bound LpxE and deacylase PGN_1123 through a LPS transport pathway; 3, the bis-P-pentaacyl and 1-P-pentaacyl lipid A are removed 1-phosphate by LpxE to generate 4′-P-pentaacyl, non-P-pentaacyl lipid A; 4, the non-P-pentaacyl and 1-P-pentaacyl lipid A are deacylated by PGN_1123 to produce non-P-tetraacyl and 1-P-tetraacyl lipid A. **B.** LpxE is thought to be in the inner membrane (IM). The lipid A modification pathway also includes four steps: 1, the precursor bis-P-pentaacyl lipid A is removed 4′-phosphate by LpxF to generate 1-P-pentaacyl lipid A and then removed 1-phosphate by LpxE to generate non-P-pentaacyl lipid A; 2, the precursor bis-P-pentaacyl lipid A is also removed 1-phosphate by LpxE to generate 4′-P-pentaacyl lipid A; 3, the bis-P-pentaacyl, 1-P-pentaacyl, 4′-P-pentaacyl and non-P-pentaacyl lipid A are transported to the outer membrane bound deacylase PGN_1123 through a LPS transport pathway; 4, the 1-P-pentaacyl and non-P-pentaacyl lipid A are then deacylated by PGN_1123 to produce 1-P-tetraacyl and non-P-tetraacyl lipid A.

6.2.2 Models of the *P. gingivalis* T9SS-LpxE interplay

Although these T9SS OM accessory proteins have different roles in the secretion process, the TEM and MALTI-TOF MS data presented in this thesis suggest that these proteins are all required for normal OMV formation and lipid A dephosphorylation. The phenotypes are similar to the *lpxE* mutant and therefore an interplay between the T9SS and LpxE is proposed. The AlphaFold model of *P. gingivalis* LpxE suggests that the T9SS may regulate LpxE activity via interaction with the LpxE CTR or the N-terminus extension. According to current knowledge, I hypothesized three models could explain this interplay (**Figure 6.2**).

The first model describes LpxE activation by an unknown T9SS substrate and LpxE is localised to the OM (**Figure 6.2A**). This substrate could bind directly to the LpxE CTR, which could cause conformational change between LpxE NTD and CTR to activate LpxE; or this substrate could form a disulphide bridge with the N-terminal cysteine residues to cause conformational changes within this enzyme. If any T9SS OM

accessory protein is knocked out, this cargo would not cross through the OM translocon or be attached to the cell surface.

The second model describes that LpxE is involved in the T9SS attachment complex and is again located in the OM (**Figure 6.2B**). In this model, LpxE is hypothesized to interact with any T9SS OM protein or protein complex. Given that T9SS components PorU and PorZ possess T9SS CTDs[177,109], they are thought to be transported to cell surface through the T9SS. In that case, only when LpxE is part of the attachment complex, the T9SS-LpxE interplay can be elucidated. The LpxE CTR or the N-terminus extension could directly interact with any component of the attachment complex to maintain phosphatase conformation, and therefore knocking out any T9SS OM components will block LpxE activity.

The third model describes that LpxE is localized to the inner membrane (IM) (**Figure 6.2C**). LpxE may interact with any T9SS IM component such as PorL or PorM. As PorL and PorM can produce proton motive force to drive the whole system[187], inactivating any T9SS component may lead to an inactive system which does not produce proton motive force. This may therefore affect the activity of LpxE. Also, blocking the T9SS may affect regulatory pathways, which could have an indirect effect on LpxE.

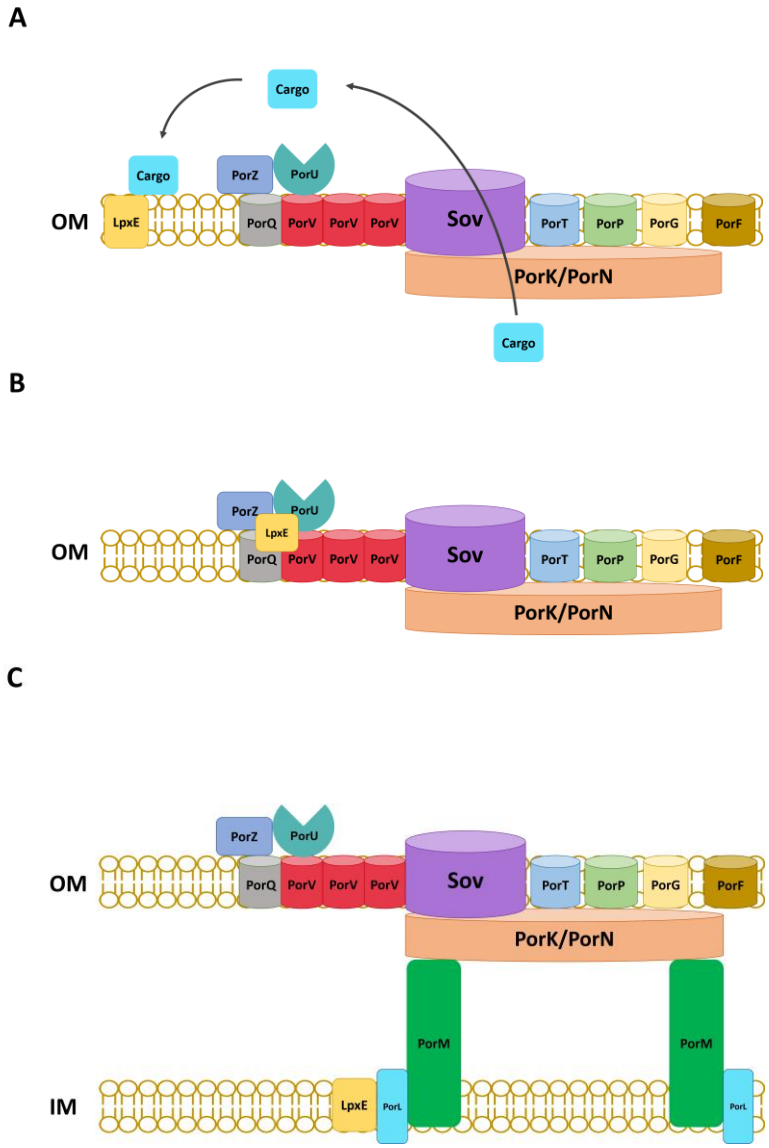

Figure 6.2: Hypothetical models of the *P. gingivalis* T9SS-LpxE interplay. A. The first model describes that LpxE is activated by an unknown T9SS cargo protein. **B.** The second model describes that LpxE is involved in the T9SS attachment complex. The T9SS components and LpxE are shown in different colours. According to reported data, the locations of Sov, PorV, PorU, PorQ, PorZ and PorK/PorN are showed. PorT, PorP and PorG are thought to bind the PorK/PorN ring ,but it is not known are they on the inside or outside (or interact with inside or outside) of the PorK/PorN ring. PorF is thought to be in the OM but no interaction has been identified. **C.** The third model describes that LpxE is in the inner membrane (IM). LpxE may interact with T9SS IM component such as PorL or PorM.

6.2.3 Hypothetical mechanism of *P. gingivalis* OMV biogenesis

Although the biological significance of phosphate-deficient lipid A molecules is

uncertain, LpxE is found to be involved in OMV biogenesis by OMV production analysis. The mutants of T9SS OM accessory proteins showed similar OMV and lipid A phenotypes as the *lpxE* mutant, indicating that there is an interplay between T9SS and LpxE. Moreover, the detergent and antimicrobial peptide inhibition assays suggest that LpxE is required for destabilizing the bacterial membrane. Taken together, a novel mechanism of *P. gingivalis* OMV biogenesis is proposed. The negatively charged phosphate groups in the lipid A are important in forming salt bridges with divalent cations such as Ca^{2+} and Mg^{2+}. The generation of these salt bridges helps to stabilize the OM. The T9SS may regulate LpxE activity via interaction with LpxE CTR to produce non-phosphorylated lipid A that cannot form salt bridges, which can facilitate OMV formation through destabilizing bacteria membrane.

In other T9SS dependent bacteria, the LpxE CTR is absent in gliding bacterium *F. johnsoniae*, but is present in pathogenic and OMV-producible bacteria *T. forsythia*, *Parabacteroides* sp. and *Prevotella* sp.. These may imply that the unusual LpxE CTR is an adaptation that links the T9SS to OMV production. With this novel LpxE, this might represent a more general model for *Bacteroidota* pathogens to regulate OMV production and cargo packaging.

6.3 Future perspectives

6.3.1 Optimization of LpxE expression and purification

Getting structural insight into LpxE would be the key to understand its molecular

mechanism. As recombinant LpxE has not been purified properly, there are many reasons for this. For example, the OmpA signal peptide may not be suitable for LpxE expression. Thus, other membrane protein signal peptide such as PelB signal peptide can be used for expression trials. Moreover, some truncated LpxE constructs may help LpxE express in the membrane rather than express in inclusion bodies.

6.3.2 PorVUQZ and LpxE interaction

The future recombinant work can include purification of the other components in T9SS attachment complex PorVUQZ. This can be used to verify the second T9SS-LpxE interplay model. PorV has been purified, and PorQ has been expressed in the *E.coli* outer membrane. The expression and purification of $PorZ^{109}$ and $PorU^{341}$ have been reported, so it would be possible to assemble the attachment complex *in vitro*. In that case, the interaction between the T9SS attachment complex (~350 kDa) and LpxE could be tested using Cryo-EM.

6.3.3 Reconstruction of *lpxE* complements

The results of LpxE crosslinking and co-immunoprecipitation assays are ambiguous and are not reproducible. One reason could be LpxE is not stable and is in low abundance. To optimize this, a gentler lysis step could be used and more *P. gingivalis* cells could be prepared. Another reason is too much background of Western blot was

seen, which makes it difficult to analyse data. Hence, a clean *lpxE* complement without any tag and a *P. gingivalis* LpxE antibody can be produced to reduce non-specific blotting. Based on the AlphaFold2 LpxE model, new position of tags can also be tested.

6.3.4 Clinical implications

The discovery of the interplay between the T9SS and LpxE shed light on antibacterial treatment. The LpxE could be a novel drug target for inhibitor development. Although LpxE in many other bacteria such as *E. coli* does not possess the CTR, the LpxE targeted inhibitor may also decrease the OMV production in these species. As *P. gingivalis* LpxE has been found to possess a CTR which may interact with the T9SS, a joint inhibitor that targets both the T9SS and LpxE would improve therapeutic effect of periodontal disease. As a similar LpxE structure has also been discovered in *T. forsythia*, *Parabacteroides* and *Prevotella sp*., the joint inhibitor may be developed to treat infection caused by these bacteria.

References

1. Albandar, J. M. & Tinoco, E. M. B. Global epidemiology of periodontal diseases in children and young persons. *Periodontol. 2000* **29**, 153–176 (2002).
2. Pihlstrom, B. L., Michalowicz, B. S. & Johnson, N. W. Periodontal diseases. in *Lancet* 1809–1820 (2005).
3. Kinane, D. F., Stathopoulou, P. G. & Papapanou, P. N. Periodontal diseases. *Nat. Rev. Dis. Prim.* **3**, 1–14 (2017).
4. Nociti, F. H., Casati, M. Z. & Duarte, P. M. Current perspective of the impact of smoking on the progression and treatment of periodontitis. *Periodontol. 2000* **67**, 187–210 (2015).
5. Lalla, E. & Papapanou, P. N. Diabetes mellitus and periodontitis: A tale of two common interrelated diseases. *Nat. Rev. Endocrinol.* **7**, 738–748 (2011).
6. Kinane, D. F. & Marshall, G. J. Periodontal manifestations of systemic disease. *Aust. Dent. J.* **46**, 2–12 (2001).
7. Borrell, L. N. & Papapanou, P. N. Analytical epidemiology of periodontitis. *J. Clin. Periodontol.* **32**, 132–158 (2005).
8. Alpagot, T., Duzgunes, N., Wolff, L. F. & Lee, A. Risk factors for periodontitis in HIV+ patients. *J. Periodontal Res.* **39**, 149–157 (2004).
9. N.J. López, P.C. Smith, J. G. Higher risk of preterm birth and low birth weight in women with periodontal disease. *J. Dent. Res.* **192**, 389–389 (2002).
10. Sanz, M. *et al.* Periodontitis and cardiovascular diseases: Consensus report. *J.*

Clin. Periodontol. **47**, 268–288 (2020).

11. Preshaw, P. M. & Bissett, S. M. Periodontitis and diabetes. *Br. Dent. J.* **227**, 577–584 (2019).

12. Rodríguez-Lozano, B. *et al.* Association between severity of periodontitis and clinical activity in rheumatoid arthritis patients: A case-control study. *Arthritis Res. Ther.* **21**, 1–12 (2019).

13. Dominy, S. S. *et al.* Porphyromonas gingivalis in Alzheimer's disease brains: Evidence for disease causation and treatment with small-molecule inhibitors. *Sci. Adv.* **5**, 1–22 (2019).

14. Michalowicz, B. S. *et al.* Evidence of a Substantial Genetic Basis for Risk of Adult Periodontitis. *J. Periodontol.* **71**, 1699–1707 (2000).

15. Papapanou, P. N. Systemic effects of periodontitis: Lessons learned from research on atherosclerotic vascular disease and adverse pregnancy outcomes. *Int. Dent. J.* **65**, 283–291 (2015).

16. Kamer, A. R., Craig, R. G., Niederman, R., Fortea, J. & de Leon, M. J. Periodontal disease as a possible cause for Alzheimer's disease. *Periodontol. 2000* **83**, 242–271 (2020).

17. Lourenço, T. G. B. *et al.* Microbial signature profiles of periodontally healthy and diseased patients. *J. Clin. Periodontol.* **41**, 1027–1036 (2014).

18. Darveau, R. P. Periodontitis: A polymicrobial disruption of host homeostasis. *Nat. Rev. Microbiol.* **8**, 481–490 (2010).

19. Hajishengallis, G. *et al.* Low-abundance biofilm species orchestrates

inflammatory periodontal disease through the commensal microbiota and complement. *Cell Host Microbe* **10**, 497–506 (2011).

20. Maekawa, T. *et al.* Porphyromonas gingivalis manipulates complement and TLR signaling to uncouple bacterial clearance from inflammation and promote dysbiosis. *Cell Host Microbe* **15**, 768–778 (2014).

21. Wang, M. *et al.* Microbial hijacking of complement-toll-like receptor crosstalk. *Sci. Signal.* **3**, ra11 (2010).

22. Diaz, P. I., Hoare, A. & Hong, B.-Y. Subgingival Microbiome Shifts and Community Dynamics in Periodontal Diseases. *J. Calif. Dent. Assoc.* **44**, 421–435 (2016).

23. Hajishengallis, G. The inflammophilic character of the periodontitis-associated microbiota. *Mol. Oral Microbiol.* **29**, 248–257 (2014).

24. Lamont, R. J., Koo, H. & Hajishengallis, G. The oral microbiota: dynamic communities and host interactions. *Nat. Rev. Microbiol.* **16**, 745–759 (2018).

25. Cugini, C., Klepac-Ceraj, V., Rackaityte, E., Riggs, J. E. & Davey, M. E. Porphyromonas gingivalis: keeping the pathos out of the biont. *J. Oral Microbiol.* **5**, (2013).

26. Hajishengallis, G. & Lamont, R. J. Dancing with the Stars: How Choreographed Bacterial Interactions Dictate Nososymbiocity and Give Rise to Keystone Pathogens, Accessory Pathogens, and Pathobionts. *Trends Microbiol.* **24**, 477–489 (2016).

27. Page, R. C. & Kornman, K. S. The pathogenesis of human periodontitis: an

introduction. *Periodontol. 2000* **14**, 9–11 (1997).

28. Holt, S. C. & Ebersole, J. L. Porphyromonas gingivalis, Treponema denticola, and Tannerella forsythia: The ‘red complex’, a prototype polybacterial pathogenic consortium in periodontitis. *Periodontol. 2000* **38**, 72–122 (2005).

29. Hajishengallis, G., Darveau, R. P. & Curtis, M. A. The keystone-pathogen hypothesis. *Nat. Rev. Microbiol.* **10**, 717–725 (2012).

30. Nakayama, K. Porphyromonas gingivalis and related bacteria: From colonial pigmentation to the type IX secretion system and gliding motility. *J. Periodontal Res.* **50**, 1–8 (2015).

31. Cutler, C. W., Kalmar, J. R. & Genco, C. A. Pathogenic strategies of the oral anaerobe, Porphyromonas gingivalis. *Trends Microbiol.* **3**, 45–51 (1995).

32. Holt, S., Kesavalu, L., Walker, S. & Genco, C. Virulence factors of Porphyrornonas gingivalis. *Periodontol. 2000* **20**, 168–238 (1999).

33. Mayrand, D. & Holt, S. C. Biology of Asaccharolytic Black-Pigmented Bacteroides Species. *Microbiol. Rev.* **52**, 134–152 (1988).

34. Lamont, R. J. & Jenkinson, H. F. Life Below the Gum Line : Pathogenic Mechanisms of Porphyromonas gingivalis. *Microbiol Mol Biol Rev* **62**, 1244–1263 (1998).

35. Potempa J, Banbula A, T. J. Role of bacterial proteinases in matrix destruction and. *Periodontol. 2000* **24**, 153–192 (2000).

36. Madej, M. *et al.* Structural and functional insights into oligopeptide acquisition by the RagAB transporter from Porphyromonas gingivalis. *Nat. Microbiol.* **5**,

1016–1025 (2020).

37. Roper, J. M. *et al.* The enigma of cobalamin (vitamin B12) biosynthesis in Porphyromonas gingivalis: Identification and characterization of a functional corrin pathway. *J. Biol. Chem.* **275**, 40316–40323 (2000).

38. Kusaba, A. *et al.* Cloning and expression of a Porphyromonas gingivalis gene for protoporphyrinogen oxidase by complementation of a hemG mutant of Escherichia coli. *Oral Microbiol. Immunol.* **17**, 290–295 (2002).

39. Smalley, J. W., Briss, A. J., Szmigielski, B. & Potempa, J. The HA2 haemagglutinin domain of the lysine-specific gingipain (Kgp) of Porphyromonas gingivalis promotes μ-oxo bishaem formation from monomeric iron(III) protoporphyrin IX. *Microbiology* **152**, 1839–1845 (2006).

40. Moore, W. E. *et al.* Bacteriology of severe periodontitis in young adult humans. *Infect. Immun.* **38**, 1137–1148 (1982).

41. Hajishengallis, G. & Lambris, J. D. Microbial manipulation of receptor crosstalk in innate immunity. *Nat. Rev. Immunol.* **11**, 187–200 (2011).

42. Darveau, R. P. The oral microbial consortium's interaction with the periodontal innate defense system. *DNA Cell Biol.* **28**, 389–395 (2009).

43. Doungudomdacha, S., Rawlinson, A. & Douglas, C. W. I. Enumeration of porphyromonas gingivalis, prevotella intermedia and actinobacillus actinomycetemcomitans in subgingival plaque samples by a quantitative-competative PCR method. *J. Med. Microbiol.* **49**, 861–874 (2000).

44. Kumar, P. S. *et al.* Changes in periodontal health status are associated with

bacterial community shifts as assessed by quantitative 16S cloning and sequencing. *J. Clin. Microbiol.* **44**, 3665–3673 (2006).

45. Chaves, E. S., Jeffcoat, M. K., Ryerson, C. C. & Snyder, B. Persistent bacterial colonization of porphyromonas gingivalis, prevotella intermedia, and actinobacillus actinomycetemcomitans in periodontitis and its association with alveolar bone loss after 6 months of therapy. *J. Clin. Periodontol.* **27**, 897–903 (2000).

46. Moore, W. E., Moore, L. H., Ranney, R. R., Smibert, R. M., Burmeister, J. A. & Schenkein, H. A. The microflora of periodontal sites showing active destructive progression. 18(10): 729–739 (1991).

47. Smalley, J. W. & Olczak, T. Heme acquisition mechanisms of Porphyromonas gingivalis – strategies used in a polymicrobial community in a heme-limited host environment. *Mol. Oral Microbiol.* **32**, 1–23 (2017).

48. Shoji, M. *et al.* Characterization of hemin-binding protein 35 (HBP35) in Porphyromonas gingivalis: its cellular distribution, thioredoxin activity and role in heme utilization. *BMC Microbiol.* **10**, 152 (2010).

49. Hiratsuka, K., Kiyama-Kishikawa, M. & Abiko, Y. Hemin-binding protein 35 (HBP35) plays an important role in bacteria-mammalian cells interactions in Porphyromonas gingivalis. *Microb. Pathog.* **48**, 116–123 (2010).

50. Sato, K. *et al.* A protein secretion system linked to bacteroidete gliding motility and pathogenesis. *Proc. Natl. Acad. Sci. U. S. A.* **107**, 276–281 (2010).

51. Yilmaz, Ö. *et al.* ATP scavenging by the intracellular pathogen Porphyromonas

gingivalis inhibits P2X7-mediated host-cell apoptosis. *Cell. Microbiol.* **10**, 863–875 (2008).

52. Naito, M. *et al.* Determination of the genome sequence of Porphyromonas glnglvalls strain ATCC 33277 and genomic comparison with strain W83 revealed extensive genome rearrangements in P. glnglvalls. *DNA Res.* **15**, 215–225 (2008).

53. Lunar Silva, I. & Cascales, E. Molecular Strategies Underlying Porphyromonas gingivalis Virulence. *J. Mol. Biol.* **433**, 166836 (2021).

54. Laine, M. L. & Winkelhoff, A. J. van. Virulence of six capsular serotypes of Porphyromonas gingivalis in a mouse model. *Oral Microbiol. Immunol.* **13**, 322–325 (1998).

55. Singh, A. *et al.* The capsule of porphyromonas gingivalis leads to a reduction in the host inflammatory response, evasion of phagocytosis, and increase in Virulence. *Infect. Immun.* **79**, 4533–4542 (2011).

56. Costerton, J. W., Irvin, R. T. & Cheng, K. J. The bacterial glycocalyx in nature and disease. *Annu. Rev. Microbiol.* **35**, 299–324 (1981).

57. Whitfield, C. Bacterial extracellular polysaccharides. *Can. J. Microbiol.* **34**, 415–420 (1988).

58. Whitfield, C. & Valvano, M. A. Biosynthesis and expression of cell-surface polysaccharides in gram-negative bacteria. *Adv. Microb. Physiol.* **35**, 135–246 (1993).

59. Allen, W. J., Phan, G. & Waksman, G. Pilus biogenesis at the outer membrane of Gram-negative bacterial pathogens. *Curr. Opin. Struct. Biol.* **22**, 500–506

(2012).

60. Kuboniwa, M. *et al.* Distinct roles of long/short fimbriae and gingipains in homotypic biofilm development by porphyromonas gingivalis. *BMC Microbiol.* **9**, 1–13 (2009).

61. Enersen, M., Nakano, K. & Amano, A. Porphyromonas gingivalis fimbriae. *J. Oral Microbiol.* **5**, (2013).

62. Shibata, S. *et al.* Structure of polymerized type V pilin reveals assembly mechanism involving protease-mediated strand exchange. *Nat. Microbiol.* **5**, 830–837 (2020).

63. Shoji, M., Shibata, S., Sueyoshi, T., Naito, M. & Nakayama, K. Biogenesis of Type V pili. *Microbiol. Immunol.* **64**, 643–656 (2020).

64. Amano, A. Disruption of epithelial barrier and impairment of cellular function by Porphyromonas gingivalis. *Front. Biosci.* **12**, 3965–3974 (2007).

65. Hajishengallis, G., Wang, M. & Liang, S. Induction of Distinct TLR2-Mediated Proinflammatory and Proadhesive Signaling Pathways in Response to Porphyromonas gingivalis Fimbriae . *J. Immunol.* **182**, 6690–6696 (2009).

66. Park, Y. *et al.* Short fimbriae of Porphyromonas gingivalis and their role in coadhesion with Streptococcus gordonii. *Infect. Immun.* **73**, 3983–3989 (2005).

67. Lee, J. Y. *et al.* Maturation of the Mfa1 fimbriae in the oral pathogen Porphyromonas gingivalis. *Front. Cell. Infect. Microbiol.* **8**, 1–10 (2018).

68. Eichinger, A. *et al.* Crystal structure of gingipain R: An Arg-specific bacterial cysteine proteinase with a caspase-like fold. *EMBO J.* **18**, 5453–5462 (1999).

69. Uitto, V.J., Larjava, H., Heino, J., Sorsa, T. A Protease of Bacteroides gingivalis Degrades Cell Surface and Matrix Glycoproteins of Cultured Gingival Fibroblasts and Induces Secretion of Collagenase and Plasminogen Activator. *Infect. Immun.* **57**, 213–218 (1989).

70. Curtis, M. *et al.* Molecular genetics and nomenclature of proteases of Porphyromonas gingivalis. *J. Periodontal Res.* **34**, 464–472 (1999).

71. Pike, R., McGraw, W., Potempa, J. & Travis, J. Lysine- and arginine-specific proteinases from Porphyromonas gingivalis. Isolation, characterization, and evidence for the existence of complexes with hemagglutinins. *J. Biol. Chem.* **269**, 406–411 (1994).

72. Mikolajczyk, J. *et al.* Sequential autolytic processing activates the zymogen of Arg-gingipain. *J. Biol. Chem.* **278**, 10458–10464 (2003).

73. Nakayama, K. Domain-specific rearrangement between the two Arg-gingipain-encoding genes in Porphyromonas gingivalis: Possible involvement of nonreciprocal recombination. *Microbiol. Immunol.* **41**, 185–196 (1997).

74. Okamoto, K., Kadowaki, T., Nakayama, K. & Yamamoto, K. Cloning and sequencing of the gene encoding a novel lysine-specific cysteine proteinase (Lys-Gingipain) in porphyromonas gingivalis: Structural relationship with the arginine-specific cysteine proteinase (Arg-Gingipain). *J. Biochem.* **120**, 398–406 (1996).

75. Takeuchi, H. *et al.* Porphyromonas gingivalis induces penetration of lipopolysaccharide and peptidoglycan through the gingival epithelium via

degradation of junctional adhesion molecule. *PLoS Pathog.* **15**, 1–26 (2019).

76. Kitamura, Y. *et al.* Gingipains in the culture supernatant of Porphyromonas gingivalis cleave CD4 and CD8 on human T cells. *J. Periodontal Res.* **37**, 464–468 (2002).

77. Glowczyk, I. *et al.* Inactive gingipains from P. gingivalis selectively skews T Cells toward a Th17 Phenotype in an IL-6 dependent manner. *Front. Cell. Infect. Microbiol.* **7**, 1–16 (2017).

78. Yun, P. L. W., DeCarlo, A. A., Collyer, C. & Hunter, N. Modulation of an interleukin-12 and gamma interferon synergistic feedback regulatory cycle of T-cell and monocyte cocultures by Porphyromonas gingivalis lipopolysaccharide in the absence or presence of cysteine proteinases. *Infect. Immun.* **70**, 5695–5705 (2002).

79. Gabarrini, G. *et al.* The peptidylarginine deiminase gene is a conserved feature of Porphyromonas gingivalis. *Sci. Rep.* **5**, 1–8 (2015).

80. György, B., Tóth, E., Tarcsa, E., Falus, A. & Buzás, E. I. Citrullination: A posttranslational modification in health and disease. *Int. J. Biochem. Cell Biol.* **38**, 1662–1677 (2006).

81. Rosenstein, E. D., Greenwald, R. A., Kushner, L. J. & Weissmann, G. Hypothesis: The humoral immune response to oral bacteria provides a stimulus for the development of rheumatoid arthritis. *Inflammation* **28**, 311–318 (2004).

82. Gully, N. *et al.* Porphyromonas gingivalis peptidylarginine deiminase, a key contributor in the pathogenesis of experimental periodontal disease and

experimental arthritis. *PLoS One* **9**, (2014).

83. Nikaido, H. Molecular basis of bacterial outer membrane permeability. *Microbiol. Mol. Biol. Rev.* **67**, 593–656 (2003).

84. Raetz, C. R. H. & Whitfield, C. Lipopolysaccharide endotoxins. *Annu. Rev. Biochem.* **71**, 635–700 (2002).

85. Jain, S. & Darveau, R. P. Contribution of Porphyromonas gingivalis lipopolysaccharide to periodontitis. *Periodontol. 2000* **54**, 53–70 (2010).

86. Shoji, M. & Nakayama, K. Glycobiology of the oral pathogen Porphyromonas gingivalis and related species. *Microb. Pathog.* **94**, 35–41 (2015).

87. Rangarajan, M. *et al.* Identification of a second lipopolysaccharide in Porphyromonas gingivalis W50. *J. Bacteriol.* **190**, 2920–2932 (2008).

88. Paramonov, N. A., Aduse-Opoku, J., Hashim, A., Rangarajan, M. & Curtis, M. A. Structural analysis of the core region of O-lipopolysaccharide of Porphyromonas gingivalis from mutants defective in O-antigen ligase and O-antigen polymerase. *J. Bacteriol.* **191**, 5272–5282 (2009).

89. Paramonov, N., Aduse-Opoku, J., Hashim, A., Rangarajan, M. & Curtis, M. A. Identification of the linkage between A-polysaccharide and the core in the A-lipopolysaccharide of Porphyromonas gingivalis W50. *J. Bacteriol.* **197**, 1735–1746 (2015).

90. Paramonov, N. *et al.* Structural analysis of the polysaccharide from the lipopolysaccharide of Porphyromonas gingivalis strain W50. *Eur. J. Biochem.* **268**, 4698–4707 (2001).

91. Paramonov, N. *et al.* Structural analysis of a novel anionic polysaccharide from Porphyromonas gingivalis strain W50 related to Arg-gingipain glycans. *Mol. Microbiol.* **58**, 847–863 (2005).

92. Beutler, B. Endotoxin, toll-like receptor 4, and the afferent limb of innate immunity. *Curr. Opin. Microbiol.* **3**, 23–28 (2000).

93. Herath, T. D. K. *et al.* Tetra- and Penta-Acylated Lipid A Structures of Porphyromonas gingivalis LPS Differentially Activate TLR4-Mediated NF-κB Signal Transduction Cascade and Immuno-Inflammatory Response in Human Gingival Fibroblasts. *PLoS One* **8**, (2013).

94. Reife, R. A. *et al.* Porphyromonas gingivalis lipopolysaccharide is poorly recognized by molecular components of innate host defense in a mouse model of early inflammation. *Infect. Immun.* **63**, 4686–4694 (1995).

95. Loppnow, H. *et al.* Lipid A, the immunostimulatory principle of lipopolysaccharides? *Adv. Exp. Med. Biol.* 561–566 (1990) doi:10.1007/978-1-4757-5140-6_50.

96. Angus, D. C. *et al.* Epidemiology of severe sepsis in the United States: Analysis of incidence, outcome, and associated costs of care. *Crit. Care Med.* **29**, (2001).

97. Medzhitov, R. Toll-like receptors and innate immunity. *Nat. Rev. Immunol.* **1**, 135–145 (2001).

98. Jia, L. *et al.* Pathogenesis of important virulence factors of Porphyromonas gingivalis via toll-like receptors. *Front. Cell. Infect. Microbiol.* **9**, 1–14 (2019).

99. Poltorak, A. *et al.* Defective LPS signaling in C3H/HeJ and C57BL/10ScCr mice:

mutations in Tlr4 gene. *Science (80-.).* **282**, 2085–2088 (1998).

100. Lien, E. *et al.* Toll-like receptor 4 imparts ligand-specific recognition of bacterial lipopolysaccharide. *J. Clin. Invest.* **105**, 497–504 (2000).

101. Liu, R., Desta, T., Raptis, M., Darveau, R. P. & Graves, D. T. P. gingivalis and E. coli Lipopolysaccharides Exhibit Different Systemic but Similar Local Induction of Inflammatory Markers . *J. Periodontol.* **79**, 1241–1247 (2008).

102. Wang, P.-L. & Ohura, K. Porphyromonas gingivalis lipopolysaccharide signaling in gingival fibroblasts-CD14 and Toll-like receptors. *Crit. Rev. Oral Biol. Med.* **13**, 132–142 (2002).

103. Papadopoulos, G. *et al.* Macrophage-Specific TLR2 Signaling Mediates Pathogen-Induced TNF-Dependent Inflammatory Oral Bone Loss. *J. Immunol.* **190**, 1148–1157 (2013).

104. Hirschfeld, M., Ma, Y., Weis, J. H., Vogel, S. N. & Weis, J. J. Cutting Edge: Repurification of Lipopolysaccharide Eliminates Signaling Through Both Human and Murine Toll-Like Receptor 2. *J. Immunol.* **165**, 618–622 (2000).

105. Hirschfeld, M. *et al.* Signaling by Toll-like receptor 2 and 4 agonists results in differential gene expression in murine macrophages. *Infect. Immun.* **69**, 1477–1482 (2001).

106. Darveau, R. P. *et al.* Porphyromonas gingivalis lipopolysaccharide contains multiple lipid A species that functionally interact with both toll-like receptors 2 and 4. *Infect. Immun.* **72**, 5041–5051 (2004).

107. Triantafilou, M. *et al.* Lipopolysaccharides from atherosclerosis-associated

bacteria antagonize TLR4, induce formation of TLR2/1/CD36 complexes in lipid rafts and trigger TLR2-induced inflammatory responses in human vascular endothelial cells. *Cell. Microbiol.* **9**, 2030–2039 (2007).

108. Jain, S., Coats, S. R., Chang, A. M. & Darveau, R. P. A novel class of lipoprotein lipase-sensitive molecules mediates toll-like receptor 2 activation by Porphyromonas gingivalis. *Infect. Immun.* **81**, 1277–1286 (2013).

109. Lasica, A. M. *et al.* Structural and functional probing of PorZ, an essential bacterial surface component of the type-IX secretion system of human oral-microbiomic Porphyromonas gingivalis. *Sci. Rep.* **6**, 1–22 (2016).

110. Osborn, M. J., Gander, J. E., Parisi, E. & Carson, J. Mechinism of assembly of the outer membrane of Salmonella typhimurium. Isolation and characterization of cytoplasmic and outer membrane. *J. Biol. Chem.* **247**, 3962–3972 (1972).

111. Raetz, C. R. H., Reynolds, C. M., Trent, M. S. & Bishop, R. E. Lipid a modification systems in gram-negative bacteria. *Annu. Rev. Biochem.* **76**, 295–329 (2007).

112. Whitfield, C. & Stephen Trent, M. Biosynthesis and export of bacterial lipopolysaccharides. *Annu. Rev. Biochem.* **83**, 99–128 (2014).

113. Karow, M. & Georgopoulos, C. The essential Escherichia coli msbA gene, a multicopy suppressor of null mutations in the htrB gene, is related to the universally conserved family of ATP-dependent translocators. *Mol. Microbiol.* **7**, 69–79 (1993).

114. Polissi, A. & Georgopoulos, C. Mutational analysis and properties of the msbA

gene of Escherichia coli, coding for an essential ABC family transporter. *Mol. Microbiol.* **20**, 1221–1233 (1996).

115. Zhou, Z., White, K. A., Polissi, A., Georgopoulos, C. & Raetz, C. R. H. Function of Escherichia coli MsbA, an essential ABC family transporter, in lipid A and phospholipid biosynthesis. *J. Biol. Chem.* **273**, 12466–12475 (1998).

116. Doerrler, W. T., Gibbons, H. S., Christian, R. & Raetz, H. MsbA-dependent translocation of lipids across the inner membrane of Escherichia coli. *J. Biol. Chem.* **279**, 45102–45109 (2004).

117. Ward, A., Reyes, C. L., Yu, J., Roth, C. B. & Chang, G. Flexibility in the ABC transporter MsbA: Alternating access with a twist. *Proc. Natl. Acad. Sci. U. S. A.* **104**, 19005–19010 (2007).

118. McGrath, B. C. & Osborn, M. J. Localization of the terminal steps of O-antigen synthesis in Salmonella typhimurium. *J. Bacteriol.* **173**, 649–654 (1991).

119. Whitfield, C. Biosynthesis and assembly of capsular polysaccharides in Escherichia coli. *Annu. Rev. Biochem.* **75**, 39–68 (2006).

120. Cuthbertson, L., Kos, V. & Whitfield, C. ABC Transporters Involved in Export of Cell Surface Glycoconjugates. *Microbiol. Mol. Biol. Rev.* **74**, 341–362 (2010).

121. Greenfield, L. K. & Whitfield, C. Synthesis of lipopolysaccharide O-antigens by ABC transporter-dependent pathways. *Carbohydr. Res.* **356**, 12–24 (2012).

122. Swietnicki, W. & Caspi, R. Prediction of selected biosynthetic pathways for the lipopolysaccharide components in porphyromonas gingivalis. *Pathogens* **10**, 1–18 (2021).

123. Vanterpool, E., Roy, F., Sandberg, L. & Fletcher, H. M. Altered gingipain maturation in vimA- and vimE-defective isogenic mutants of Porphyromonas gingivalis. *Infect. Immun.* **73**, 1357–1366 (2005).

124. Vanterpool, E., Roy, F. & Fletcher, H. M. Inactivation of vimF, a putative glycosyltransferase gene downstream of vimE, alters glycosylation and activation of the gingipains in Porphyromonas gingivalis W83. *Infect. Immun.* **73**, 3971–3982 (2005).

125. Slaney, J. M., Gallagher, A., Aduse-Opoku, J., Pell, K. & Curtis, M. A. Mechanisms of resistance of Porphyromonas gingivalis to killing by serum complement. *Infect. Immun.* **74**, 5352–5361 (2006).

126. Sato, K. *et al.* Lipopolysaccharide biosynthesis-related genes are required for colony pigmentation of Porphyromonas gingivalis. *Microbiology* **155**, 1282–1293 (2009).

127. Yamaguchi, M. *et al.* A Porphyromonas gingivalis mutant defective in a putative glycosyltransferase exhibits defective biosynthesis of the polysaccharide portions of lipopolysaccharide, decreased gingipain activities, strong autoaggregation, and increased biofilm formation. *Infect. Immun.* **78**, 3801–3812 (2010).

128. Shoji, M. *et al.* Por secretion system-dependent secretion and glycosylation of Porphyromonas gingivalis hemin-binding protein 35. *PLoS One* **6**, e21372 (2011).

129. Shoji, M. *et al.* Identification of an O-antigen chain length regulator, WzzP, in

Porphyromonas gingivalis. *Microbiologyopen* **2**, 383–401 (2013).

130. Muthiah, A. S. *et al.* In Porphyromonas gingivalis VimF Is Involved in Gingipain Maturation through the Transfer of Galactose. *PLoS One* **8**, (2013).

131. Shoji, M., Sato, K., Yukitake, H., Naito, M. & Nakayama, K. Involvement of the Wbp pathway in the biosynthesis of Porphyromonas gingivalis lipopolysaccharide with anionic polysaccharide. *Sci. Rep.* **4**, 1–9 (2014).

132. Shoji, M. *et al.* Identification of genes encoding glycosyltransferases involved in lipopolysaccharide synthesis in Porphyromonas gingivalis. *Mol. Oral Microbiol.* **33**, 68–80 (2018).

133. Aruni, A. W., Robles, A. & Fletcher, H. M. VimA mediates multiple functions that control virulence in Porphyromonas gingivalis. *Mol. Oral Microbiol.* **28**, 167–180 (2013).

134. Ruiz, N., Kahne, D. & Silhavy, T. J. Transport of lipopolysaccharide across the cell envelope: The long road of discovery. *Nat. Rev. Microbiol.* **7**, 677–683 (2009).

135. Sperandeo, P., Dehò, G. & Polissi, A. The lipopolysaccharide transport system of Gram-negative bacteria. *Biochim. Biophys. Acta* **1791**, 594–602 (2009).

136. Simpson, B. W., May, J. M., Sherman, David J.Ruiz, N. & Kahne, D. Lipopolysaccharide transport to the cell surface: biosynthesis and extraction from the inner membrane. *Philos. Trans. R. Soc. B Biol. Sci.* **370**, (2015).

137. May, J. M., Simpson, B. W., Sherman, D. J., Kahne, D. & Ruiz, N. Lipopolysaccharide transport to the cell surface: periplasmic transport and

assembly into the outer membrane. *Philos. Trans. R. Soc. B Biol. Sci.* **370**, (2015).

138. Villa, R. *et al.* The Escherichia coli lpt transenvelope protein complex for lipopolysaccharide export is assembled via conserved structurally homologous domains. *J. Bacteriol.* **195**, 1100–1108 (2013).

139. Sperandeo, P. *et al.* Characterization of lptA and lptB, two essential genes implicated in lipopolysaccharide transport to the outer membrane of Escherichia coli. *J. Bacteriol.* **189**, 244–253 (2007).

140. Suits, M. D. L., Sperandeo, P., Dehò, G., Polissi, A. & Jia, Z. Novel Structure of the Conserved Gram-Negative Lipopolysaccharide Transport Protein A and Mutagenesis Analysis. *J. Mol. Biol.* **380**, 476–488 (2008).

141. Okuda, S., Sherman, D. J., Silhavy, T. J., Ruiz, N. & Kahne, D. Lipopolysaccharide transport and assembly at the outer membrane: The PEZ model. *Nat. Rev. Microbiol.* **14**, 337–345 (2016).

142. Dong, H. *et al.* Structural basis for outer membrane lipopolysaccharide insertion. *Nature* **511**, 52–56 (2014).

143. Veith, P. D., Gorasia, D. G. & Reynolds, E. C. Towards defining the outer membrane proteome of Porphyromonas gingivalis. *Mol. Oral Microbiol.* **36**, 25–36 (2021).

144. Freinkman, E., Okuda, S., Ruiz, N. & Kahne, D. Regulated assembly of the transenvelope protein complex required for lipopolysaccharide export. *Biochemistry* **51**, 4800–4806 (2012).

145. Simpson, B. W. & Trent, M. S. Pushing the envelope: LPS modifications and

their consequences. *Nat. Rev. Microbiol.* **17**, 403–416 (2019).

146. Brozek, K. A., Kadrmas, J. L. & Raetz, C. R. H. Lipopolysaccharide biosynthesis in Rhizobium leguminosarum. Novel enzymes that process precursors containing 3-deoxy-D-manno-octulosonic acid. *J. Biol. Chem.* **271**, 32112–32118 (1996).

147. Karbarz, M. J., Kalb, S. R., Cotter, R. J. & Raetz, C. R. H. Expression cloning and biochemical characterization of a Rhizobium leguminosarum lipid A 1-phosphatase. *J. Biol. Chem.* **278**, 39269–39279 (2003).

148. Reynolds, C. M. *et al.* An outer membrane enzyme encoded by Salmonella typhimurium lpxR that removes the 3′-acyloxyacyl moiety of lipid A. *J. Biol. Chem.* **281**, 21974–21987 (2006).

149. Trent, M. S., Pabich, W., Raetz, C. R. H. & Miller, S. I. A PhoP/PhoQ-induced Lipase (PagL) that Catalyzes 3-O-Deacylation of Lipid A Precursors in Membranes of Salmonella typhimurium. *J. Biol. Chem.* **276**, 9083–9092 (2001).

150. Ogawa, T. Chemical structure of lipid A from porphyromonas (bacteroides) gingivalis lipopolysaccharide. *FEBS Lett.* **332**, 197–201 (1993).

151. Kumada, H., Haishima, Y., Umemoto, T. & Tanamoto, K. I. Structural study on the free lipid A isolated from lipopolysaccharide of Porphyromonas gingivalis. *J. Bacteriol.* **177**, 2098–2106 (1995).

152. Rangarajan, M. *et al.* LptO (PG0027) is required for lipid A 1-phosphatase activity in Porphyromonas gingivalis W50. *J. Bacteriol.* **199**, 1–20 (2017).

153. Coats, S. R. *et al.* Human Toll-like receptor 4 responses to P. gingivalis are

regulated by lipid A 1-and 4'-phosphatase activities. *Cell. Microbiol.* **11**, 1587–1599 (2009).

154. Jain, S. *et al.* Identification of PGN_1123 as the Gene Encoding Lipid A Deacylase, an Enzyme Required for Toll-Like Receptor 4 Evasion, in Porphyromonas gingivalis. *J. Bacteriol.* **201**, e00683-18 (2019).

155. Chen, Y. Y. *et al.* The outer membrane protein LptO is essential for the O-deacylation of LPS and the co-ordinated secretion and attachment of A-LPS and CTD proteins in Porphyromonas gingivalis. *Mol. Microbiol.* **79**, 1380–1401 (2011).

156. Costa, T. R. D. *et al.* Secretion systems in Gram-negative bacteria: Structural and mechanistic insights. *Nat. Rev. Microbiol.* **13**, 343–359 (2015).

157. Costa, T. R. D. *et al.* Secretion systems in Gram-negative bacteria: Structural and mechanistic insights. *Nat. Rev. Microbiol.* **13**, 343–359 (2015).

158. Christie, P. J. The Rich Tapestry of Bacterial Protein Translocation Systems. *Protein J.* **38**, 389–408 (2019).

159. Palmer, T., Finney, A. J., Saha, C. K., Atkinson, G. C. & Sargent, F. A holin/peptidoglycan hydrolase-dependent protein secretion system. *Mol. Microbiol.* **115**, 345–355 (2021).

160. Grossman, A. S., Mauer, T. J., Forest, K. T. & Goodrich-Blair, H. A widespread bacterial secretion system with diverse substrates. *MBio* **12**, (2021).

161. Morgan, J. L. W., Acheson, J. F. & Zimmer, J. Structure of a Type-1 Secretion System ABC Transporter. *Structure* **25**, 522–529 (2017).

162. Miletic, S. *et al.* Substrate-engaged type III secretion system structures reveal gating mechanism for unfolded protein translocation. *Nat. Commun.* **12**, 1–14 (2021).

163. Costa, T. R. D. *et al.* Type IV secretion systems: Advances in structure, function, and activation. *Mol. Microbiol.* **115**, 436–452 (2021).

164. Wang, J. *et al.* Cryo-EM structure of the extended type VI secretion system sheath-tube complex. *Nat. Microbiol.* **2**, 1507–1512 (2017).

165. Naskar, S., Hohl, M., Tassinari, M. & Low, H. H. The structure and mechanism of the bacterial type II secretion system. *Mol. Microbiol.* **115**, 412–424 (2021).

166. Leo, J. C., Grin, I. & Linke, D. Type V secretion: Mechanism(S) of autotransport through the bacterial outer membrane. *Philos. Trans. R. Soc. B Biol. Sci.* **367**, 1088–1101 (2012).

167. Goyal, P. *et al.* Structural and mechanistic insights into the bacterial amyloid secretion channel CsgG. *Nature* **516**, 250–253 (2014).

168. Lauber, F., Deme, J. C., Lea, S. M. & Berks, B. C. Type 9 secretion system structures reveal a new protein transport mechanism. *Nature* **564**, 77–82 (2018).

169. Busch, A. & Waksman, G. Chaperone-usher pathways: Diversity and pilus assembly mechanism. *Philos. Trans. R. Soc. B Biol. Sci.* **367**, 1112–1122 (2012).

170. Sato, K. *et al.* Identification of Porphyromonas gingivalis proteins secreted by the Por secretion system. *FEMS Microbiol. Lett.* **338**, 68–76 (2013).

171. McBride, M. J. & Zhu, Y. Gliding motility and por secretion system genes are widespread among members of the phylum bacteroidetes. *J. Bacteriol.* **195**, 270–

278 (2013).

172. Lasica, A. M., Ksiazek, M., Madej, M. & Potempa, J. The Type IX Secretion System (T9SS): Highlights and Recent Insights into Its Structure and Function. *Front. Cell. Infect. Microbiol.* **7**, (2017).

173. Veith, P. D. *et al.* Protein substrates of a novel secretion system are numerous in the Bacteroidetes phylum and have in common a cleavable C-terminal secretion signal, extensive post-translational modification, and cell-surface attachment. *J. Proteome Res.* **12**, 4449–4461 (2013).

174. Veith, P. D., Glew, M. D., Gorasia, D. G. & Reynolds, E. C. Type IX secretion: the generation of bacterial cell surface coatings involved in virulence, gliding motility and the degradation of complex biopolymers. *Mol. Microbiol.* **106**, 35–53 (2017).

175. Li, N., Zhu, Y. & Mcbride, M. J. The Type IX Secretion System Is Required for Virulence of the Fish Pathogen Flavobacterium columnare. *Appl. Environ. Microbiol.* **83**, e01769-17 (2017).

176. Barbier, P., Rochat, T. & Mohammed, H. The Type IX Secretion System Is Required for Virulence of the Fish Pathogen Flavobacterium psychrophilum. *Appl. Environ. Microbiol.* **86**, e00799-20 (2020).

177. Glew, M. D. *et al.* PG0026 is the C-terminal signal peptidase of a novel secretion system of *Porphyromonas gingivalis*. *J. Biol. Chem.* **287**, 24605–24617 (2012).

178. Gorasia, D. G. *et al.* Porphyromonas gingivalis Type IX Secretion Substrates Are Cleaved and Modified by a Sortase-Like Mechanism. *PLoS Pathog.* **11**, 1–31

(2015).

179. Glew, M. D. *et al.* PorV is an Outer Membrane Shuttle Protein for the Type IX Secretion System. *Sci. Rep.* **7**, 1–14 (2017).

180. Ishiguro, I., Saiki, K. & Konishi, K. PG27 is a novel membrane protein essential for a Porphyromonas gingivalis protease secretion system. *FEMS Microbiol. Lett.* **292**, 261–267 (2009).

181. Kadowaki, T. *et al.* A two-component system regulates gene expression of the type IX secretion component proteins via an ECF sigma factor. *Sci. Rep.* **6**, 1–12 (2016).

182. Yang, D., Jiang, C., Ning, B., Kong, W. & Shi, Y. The PorX/PorY system is a virulence factor of Porphyromonas gingivalis and mediates the activation of the type IX secretion system. *J. Biol. Chem.* **296**, 100574 (2021).

183. Gorasia, D. G. *et al.* Structural Insights into the PorK and PorN Components of the Porphyromonas gingivalis Type IX Secretion System. *PLoS Pathog.* **12**, 1–25 (2016).

184. Taguchi, Y. *et al.* Involvement of an Skp-like protein, PGN_0300, in the type IX secretion system of Porphyromonas gingivalis. *Infect. Immun.* **84**, 230–240 (2015).

185. Vincent, M. S. *et al.* Characterization of the Porphyromonas gingivalis type IX secretion trans-envelope PorKLMNP core complex. *J. Biol. Chem.* **292**, 3252–3261 (2017).

186. Gorasia, D. G., Veith, P. D. & Reynolds, E. C. The type IX secretion system:

Advances in structure, function and organisation. *Microorganisms* **8**, 1–9 (2020).

187. James, R. *et al.* Structure and mechanism of the proton-driven motor that powers type 9 secretion and gliding motility. *Nat. Microbiol.* **6**, 221–233 (2021).

188. Leone, P. *et al.* Type IX secretion system PorM and gliding machinery GldM form arches spanning the periplasmic space. *Nat. Commun.* **9**, 1–8 (2018).

189. Saiki, K. & Konishi, K. Identification of a novel Porphyromonas gingivalis outer membrane protein, PG534, required for the production of active gingipains. *FEMS Microbiol. Lett.* **310**, 168–174 (2010).

190. Sato, K. *et al.* Identification of a new membrane-associated protein that influences transport/maturation of gingipains and adhesins of Porphyromonas gingivalis. *J. Biol. Chem.* **280**, 8668–8677 (2005).

191. Nguyen, K. A. *et al.* Verification of a topology model of PorT as an integral outer-membrane protein in Porphyromonas gingivalis. *Microbiology* **155**, 328–337 (2009).

192. Saiki, K. & Konishi, K. Identification of a Porphyromonas gingivalis novel protein sov required for the secretion of gingipains. *Microbiol. Immunol.* **51**, 483–491 (2007).

193. Nelson, S. S., Glocka, P. P., Agarwal, S., Grimm, D. P. & McBride, M. J. Flavobacterium johnsoniae SprA is a cell surface protein involved in gliding motility. *J. Bacteriol.* **189**, 7145–7150 (2007).

194. Saiki, K. & Konishi, K. The role of Sov protein in the secretion of gingipain protease virulence factors of Porphyromonas gingivalis. *FEMS Microbiol. Lett.*

302, 166–174 (2010).

195. Vincent, M. S., Durand, E. & Cascales, E. The PorX response regulator of the Porphyromonas gingivalis PorXY two-component system does not directly regulate the type IX secretion genes but binds the PorL subunit. *Front. Cell. Infect. Microbiol.* **6**, (2016).

196. Heath, J. E. *et al.* PG1058 is a novel multidomain protein component of the bacterial type IX secretion system. *PLoS One* **11**, 1–29 (2016).

197. Trinh, N. T. T. *et al.* Crystal structure of Type IX secretion system PorE C-terminal domain from Porphyromonas gingivalis in complex with a peptidoglycan fragment. *Sci. Rep.* **10**, 1–9 (2020).

198. Madej, M., Nowakowska, Z., Ksiazek, M., Lasica, A. M. & Potempa, J. PorZ, an Essential Component of the Type IX Secretion System of Porphyromonas gingivalis, Delivers Anionic Lipopolysaccharide to the PorU Sortase for Transpeptidase Processing of T9SS Cargo Proteins. *MBio* **12**, e02262-20 (2021).

199. Gorasia, D. G., Glew, M. D., Veith, P. D. & Reynolds, E. C. Quantitative proteomic analysis of the type IX secretion system mutants in Porphyromonas gingivalis. *Mol. Oral Microbiol.* **35**, 78–84 (2020).

200. Yukitake, H. *et al.* PorA, a conserved C-terminal domain-containing protein, impacts the PorXY-SigP signaling of the type IX secretion system. *Sci. Rep.* **10**, 1–17 (2020).

201. Sato, K., Okada, K., Nakayama, K. & Imada, K. PorM, a core component of bacterial type IX secretion system, forms a dimer with a unique kinked-rod shape.

Biochem. Biophys. Res. Commun. **532**, 114–119 (2020).

202. Song, L. *et al.* A unique bacterial secretion machinery with multiple secretion centers. *Proc. Natl. Acad. Sci. U. S. A.* **119**, e2119907119 (2022).

203. Koebnik, R., Locher, K. P. & Van Gelder, P. Structure and function of bacterial outer membrane proteins: Barrels in a nutshell. *Mol. Microbiol.* **37**, 239–253 (2000).

204. Park, Y., Yilmaz, Ö., Jung, I. Y. & Lamont, R. J. Identification of Porphyromonas gingivalis genes specifically expressed in human gingival epithelial cells by using differential display reverse transcription-PCR. *Infect. Immun.* **72**, 3752–3758 (2004).

205. Saiki, K. & Konishi, K. Porphyromonas gingivalis C-terminal signal peptidase PG0026 and HagA interact with outer membrane protein PG27/LptO. *Mol. Oral Microbiol.* **29**, 32–44 (2014).

206. Pugsley, A. P. The complete general secretory pathway in gram-negative bacteria. *Microbiol. Rev.* **57**, 50–108 (1993).

207. Driessen, A. J. M. & Nouwen, N. Protein translocation across the bacterial cytoplasmic membrane. *Annu. Rev. Biochem.* **77**, 643–667 (2008).

208. Zwizinski, C. & Wickner, W. Purification and characterization of leader (signal) peptidase from Escherichia coli. *J. Biol. Chem.* **255**, 7973–7977 (1980).

209. Sklar, J. G., Wu, T., Kahne, D. & Silhavy, T. J. Defining the roles of the periplasmic chaperones SurA, Skp, and DegP in Escherichia coli. *Genes Dev.* **21**, 2473–2484 (2007).

210. Behrens, S., Maier, R., De Cock, H., Schmid, F. X. & Gross, C. A. The SurA periplasmic PPIase lacking its parvulin domains functions in vivo and has chaperone activity. *EMBO J.* **20**, 285–294 (2001).

211. Chen, R. & Henning, U. A periplasmic protein (Skp) of Escherichia coli selectively binds a class of outer membrane proteins. *Mol. Microbiol.* **19**, 1287–1294 (1996).

212. Qu, J., Mayer, C., Behrens, S., Holst, O. & Kleinschmidt, J. H. The Trimeric Periplasmic Chaperone Skp of Escherichia coli Forms 1:1 Complexes with Outer Membrane Proteins via Hydrophobic and Electrostatic Interactions. *J. Mol. Biol.* **374**, 91–105 (2007).

213. Walton, T. A. & Sousa, M. C. Crystal structure of Skp, a prefoldin-like chaperone that protects soluble and membrane proteins from aggregation. *Mol. Cell* **15**, 367–374 (2004).

214. Ge, X. *et al.* DegP primarily functions as a protease for the biogenesis of β-barrel outer membrane proteins in the Gram-negative bacterium Escherichia coli. *FEBS J.* **281**, 1226–1240 (2014).

215. Wu, T. *et al.* Identification of a multicomponent complex required for outer membrane biogenesis in Escherichia coli. *Cell* **121**, 235–245 (2005).

216. Gentle, I. E., Burri, L. & Lithgow, T. Molecular architecture and function of the Omp85 family of proteins. *Mol. Microbiol.* **58**, 1216–1225 (2005).

217. Webb, C. T., Heinz, E. & Lithgow, T. Evolution of the β-barrel assembly machinery. *Trends Microbiol.* **20**, 612–620 (2012).

218. Anderson, D. L. References and notes. *New Theory Earth* 356–374 (2012) doi:10.1017/cbo9781139167291.033.

219. Hagan, C. L., Silhavy, T. J. & Kahne, D. B-Barrel Membrane Protein Assembly By the Bam Complex. *Annu. Rev. Biochem.* **80**, 189–210 (2011).

220. Kulkarni, S. S., Zhu, Y., Brendel, C. J. & McBride, M. J. Diverse C-Terminal Sequences Involved in Flavobacterium johnsoniae Protein Secretion. *J. Bacteriol.* **199**, e00884-16 (2017).

221. De Diego, I. *et al.* The outer-membrane export signal of Porphyromonas gingivalis type IX secretion system (T9SS) is a conserved C-terminal β-sandwich domain. *Sci. Rep.* **6**, 1–17 (2016).

222. Sato, K. *et al.* Immunoglobulin-like domains of the cargo proteins are essential for protein stability during secretion by the type IX secretion system. *Mol. Microbiol.* **110**, 64–81 (2018).

223. Seers, C. A. *et al.* The RgpB C-terminal domain has a role in attachment of RgpB to the outer membrane and belongs to a novel C-terminal-domain family found in Porphyromonas gingivalis. *J. Bacteriol.* **188**, 6376–6386 (2006).

224. Slakeski, N. *et al.* C-terminal domain residues important for secretion and attachment of RgpB in Porphyromonas gingivalis. *J. Bacteriol.* **193**, 132–142 (2011).

225. Vincent, M. S., Chabalier, M. & Cascales, E. Conserved motifs of Porphyromonas gingivalis effector C-terminal secretion signal specify interactions with Type IX secretion subunits. *BioRxiv* (2018).

226. Kulkarni, S. S., Johnston, J. J., Zhu, Y., Hying, Z. T. & McBride, M. J. The Carboxy-Terminal Region of Flavobacterium johnsoniae SprB Facilitates Its Secretion by the Type IX Secretion System and Propulsion by the Gliding Motility Machinery. *J. Bacteriol.* **201**, e00218-19 (2019).

227. Fuchsbauer, O., Silva, I. L., Cascales, E., Roussel, A. & Leone, P. Structural and functional analyses of the Porphyromonas gingivalis type IX secretion system PorN protein. *J. Biol. Chem.* **298**, 101618 (2022).

228. Rangarajan, M., Aduse-Opoku, J., Slaney, J. M., Young, K. A. & Curtis, M. A. The prpR1 and prR2 arginine-specific protease genes of Porphyromonas gingivalis W50 produce five biochemically distinct enzymes. *Mol. Microbiol.* **23**, 955–965 (1997).

229. Haurat, M. F. *et al.* Selective sorting of cargo proteins into bacterial membrane vesicles. *J. Biol. Chem.* **286**, 1269–1276 (2011).

230. McBride, M. J. & Nakane, D. Flavobacterium gliding motility and the type IX secretion system. *Curr. Opin. Microbiol.* **28**, 72–77 (2015).

231. Nakane, D., Sato, K., Wada, H., McBride, M. J. & Nakayama, K. Helical flow of surface protein required for bacterial gliding motility. *Proc. Natl. Acad. Sci. U. S. A.* **110**, 11145–11150 (2013).

232. Shrivastava, A., Johnston, J. J., Van Baaren, J. M. & McBride, M. J. Flavobacterium johnsoniae GldK, GldL, GldM, and SprA are required for secretion of the cell surface gliding motility adhesins sprb and remA. *J. Bacteriol.* **195**, 3201–3212 (2013).

233. Johnston, J. J., Shrivastava, A. & McBride, M. J. Untangling Flavobacterium johnsoniae Gliding Motility and Protein Secretion. *J. Bacteriol.* **200**, e00362-17 (2018).

234. Braun, T. F. & McBride, M. J. Flavobacterium johnsoniae GldJ is a lipoprotein that is required for gliding motility. *J. Bacteriol.* **187**, 2628–2637 (2005).

235. McBride, M. J. Bacteroidetes Gliding Motility and the Type IX Secretion System . *Microbiol. Spectr.* **7**, (2019).

236. Sharma, A. Virulence mechanisms of tannerella forsythia. *Periodontol. 2000* **54**, 106–116 (2010).

237. Narita, Y. *et al.* Lack of a surface layer in Tannerella forsythia mutants deficient in the type IX secretion system. *Microbiol. (United Kingdom)* **160**, 2295–2303 (2014).

238. Tomek, M. B. *et al.* The S-layer proteins of Tannerella forsythia are secreted via a type IX secretion system that is decoupled from protein O-glycosylation. *Mol. Oral Microbiol.* **29**, 307–320 (2014).

239. Kulp, A. & Kuehn, M. J. Biological Functions and biogenesis of secreted bacterial outer membrane vesicles. *Annu. Rev. Microbiol.* **64**, 163–184 (2010).

240. Beveridge, T. J. Structures of gram-negative cell walls and their derived membrane vesicles. *J. Bacteriol.* **181**, 4725–4733 (1999).

241. Mashburn-Warren, L. M. & Whiteley, M. Special delivery: Vesicle trafficking in prokaryotes. *Mol. Microbiol.* **61**, 839–846 (2006).

242. Ellis, T. N. & Kuehn, M. J. Virulence and Immunomodulatory Roles of Bacterial

Outer Membrane Vesicles. *Microbiol. Mol. Biol. Rev.* **74**, 81–94 (2010).

243. Gui, M. J., Dashper, S. G., Slakeski, N., Chen, Y. Y. & Reynolds, E. C. Spheres of influence: Porphyromonas gingivalis outer membrane vesicles. *Mol. Oral Microbiol.* **31**, 365–378 (2016).

244. Kaparakis-Liaskos, M. & Ferrero, R. L. Immune modulation by bacterial outer membrane vesicles. *Nat. Rev. Immunol.* **15**, 375–387 (2015).

245. Nakao, R. *et al.* Outer membrane vesicles of porphyromonas gingivalis elicit a mucosal immune response. *PLoS One* **6**, (2011).

246. Nakao, R. *et al.* Effect of Porphyromonas gingivalis outer membrane vesicles on gingipain-mediated detachment of cultured oral epithelial cells and immune responses. *Microbes Infect.* **16**, 6–16 (2014).

247. Yilmaz, Ö., Watanabe, K. & Lamont, R. J. Involvement of integrins in fimbriae-mediated binding and invasion by Porphyromonas gingivalis. *Cell. Microbiol.* **4**, 305–314 (2002).

248. Zhang, W., Ju, J., Rigney, T. & Tribble, G. D. Fimbriae of Porphyromonas gingivalis are Important for Initial Invasion of Osteoblasts, but Not for Inhibition of Their Differentiation and Mineralization . *J. Periodontol.* **82**, 909–916 (2011).

249. Bélanger, M., Kozarov, E., Song, H., Whitlock, J. & Progulske-Fox, A. Both the unique and repeat regions of the Porphyromonas gingivalis hemagglutin A are involved in adhesion and invasion of host cells. *Anaerobe* **18**, 128–134 (2012).

250. Yuan, L., Rodrigues, P. H., Bélanger, M., Dunn, W. A. & Progulske-Fox, A. Porphyromonas gingivalis HtrA is involved in cellular invasion and in vivo

survival. *Microbiology* **154**, 1161–1169 (2008).

251. Furuta, N., Takeuchi, H. & Amano, A. Entry of Porphyromonas gingivalis outer membrane vesicles into epithelial cells causes cellular functional impairment. *Infect. Immun.* **77**, 4761–4770 (2009).

252. Furuta, N. *et al.* Porphyromonas gingivalis outer membrane vesicles enter human epithelial cells via an endocytic pathway and are sorted to lysosomal compartments. *Infect. Immun.* **77**, 4187–4196 (2009).

253. Ho, M. H., Chen, C. H., Goodwin, J. S., Wang, B. Y. & Xie, H. Functional advantages of Porphyromonas gingivalis vesicles. *PLoS One* **10**, 1–15 (2015).

254. Kou, Y. *et al.* Inflammatory Responses of Gingival Epithelial Cells Stimulated With Porphyromonas gingivalis Vesicles Are Inhibited by Hop-Associated Polyphenols . *J. Periodontol.* **79**, 174–180 (2008).

255. Srisatjaluk, R., Doyle, R. J. & Justus, D. E. Outer membrane vesicles of Porphyromonas gingivalis inhibit IFN-γ-mediated MHC class II expression by human vascular endothelial cells. *Microb. Pathog.* **27**, 81–91 (1999).

256. Haurat, M. F., Elhenawy, W. & Feldman, M. F. Prokaryotic membrane vesicles: New insights on biogenesis and biological roles. *Biol. Chem.* **396**, 95–109 (2015).

257. Zhou, L., Srisatjaluk, R., Justus, D. E. & Doyle, R. J. On the origin of membrane vesicles in Gram-negative bacteria. *FEMS Microbiol. Lett.* **163**, 223–228 (1998).

258. Hayashi, J. I., Hamada, N. & Kuramitsu, H. K. The autolysin of Porphyromonas gingivalis is involved in outer membrane vesicle release. *FEMS Microbiol. Lett.* **216**, 217–222 (2002).

259. Hoekstra, D., van der Laan, J. W., de Leij, L. & Witholt, B. Release of outer membrane fragments from normally growing Escherichia coli. *Biochim. Biophys. Acta* **455**, 889–899 (1976).

260. Silhavy, T. J., Kahne, D. & Walker, S. The bacterial cell envelope. *Cold Spring Harb. Perspect. Biol.* **2**, a000414 (2010).

261. Lee, N. & Inouye, M. Outer membrane proteins of Escherichia coli: biosynthesis and assembly. *FEBS Lett.* **39**, 167–170 (1974).

262. Smith, S. G. J., Mahon, V., Lambert, M. A. & Fagan, R. P. A molecular Swiss army knife: OmpA structure, function and expression. *FEMS Microbiol. Lett.* **273**, 1–11 (2007).

263. Samsudin, F., Boags, A., Piggot, T. J. & Khalid, S. Braun's Lipoprotein Facilitates OmpA Interaction with the Escherichia coli Cell Wall. *Biophys. J.* **113**, 1496–1504 (2017).

264. Lam, J. S., Graham, L. L., Lightfoot, J., Dasgupta, T. & Beveridge, T. J. Ultrastructural examination of the lipopolysaccharides of Pseudomonas aeruginosa strains and their isogenic rough mutants by freeze-substitution. *J. Bacteriol.* **174**, 7159–7167 (1992).

265. Li, Z., Clarke, A. J. & Beveridge, T. J. A major autolysin of Pseudomonas aeruginosa: Subcellular distribution, potential role in cell growth and division, and secretion in surface membrane vesicles. *J. Bacteriol.* **178**, 2479–2488 (1996).

266. Kadurugamuwa, J. L. & Beveridge, T. J. Virulence factors are released from Pseudomonas aeruginosa in association with membrane vesicles during normal

growth and exposure to gentamicin: A novel mechanism of enzyme secretion. *J. Bacteriol.* **177**, 3998–4008 (1995).

267. Sabra, W., Lunsdorf, H. & Zeng, A. P. Alterations in the formation of lipopolysaccharide and membrane vesicles on the surface of Pseudomonas aeruginosa PAO1 under oxygen stress conditions. *Microbiology* **149**, 2789–2795 (2003).

268. Shrivastava, R. & Chng, S. S. Lipid trafficking across the Gram-negative cell envelope. *J. Biol. Chem.* **294**, 14175–14184 (2019).

269. Shrivastava, R., Jiang, X. & Chng, S. S. Outer membrane lipid homeostasis via retrograde phospholipid transport in Escherichia coli. *Mol. Microbiol.* **106**, 395–408 (2017).

270. Chong, Z. S., Woo, W. F. & Chng, S. S. Osmoporin OmpC forms a complex with MlaA to maintain outer membrane lipid asymmetry in Escherichia coli. *Mol. Microbiol.* **98**, 1133–1146 (2015).

271. Malinverni, J. C. & Silhavy, T. J. An ABC transport system that maintains lipid asymmetry in the gram-negative outer membrane. *Proc. Natl. Acad. Sci. U. S. A.* **106**, 8009–8014 (2009).

272. Sutterlin, H. A. *et al.* Disruption of lipid homeostasis in the Gram-negative cell envelope activates a novel cell death pathway. *Proc. Natl. Acad. Sci. U. S. A.* **113**, E1565–E1574 (2016).

273. Roier, S. *et al.* A novel mechanism for the biogenesis of outer membrane vesicles in Gram-negative bacteria. *Nat. Commun.* **7**, 1–13 (2016).

274. Davies, C. *et al.* Sodium Taurocholate Stimulates Campylobacter jejuni Outer Membrane Vesicle Production via Down-Regulation of the Maintenance of Lipid Asymmetry Pathway. *Front. Cell. Infect. Microbiol.* **9**, 1–12 (2019).

275. Chen, S. *et al.* Structural diversity of bacterial flagellar motors. *EMBO J.* **30**, 2972–2981 (2011).

276. Lee, E. Y. *et al.* Global proteomic profiling of native outer membrane vesicles derived from Escherichia coli. *Proteomics* **7**, 3143–3153 (2007).

277. Manabe, T., Kato, M., Ueno, T. & Kawasaki, K. Flagella proteins contribute to the production of outer membrane vesicles from Escherichia coli W3110. *Biochem. Biophys. Res. Commun.* **441**, 151–156 (2013).

278. Aschtgen, M. S. *et al.* Rotation of Vibrio fischeri flagella produces outer membrane vesicles that induce host development. *J. Bacteriol.* **198**, 2156–2165 (2016).

279. Mashburn, L. M. & Whiteley, M. Membrane vesicles traffic signals and facilitate group activities in a prokaryote. *Nature* **437**, 422–425 (2005).

280. Mashburn-Warren, L. *et al.* Interaction of quorum signals with outer membrane lipids: Insights into prokaryotic membrane vesicle formation. *Mol. Microbiol.* **69**, 491–502 (2008).

281. Mashburn-Warren, L., Howe, J., Brandenburg, K. & Whiteley, M. Structural requirements of the Pseudomonas quinolone signal for membrane vesicle stimulation. *J. Bacteriol.* **191**, 3411–3414 (2009).

282. Elhenawy, W. *et al.* LPS remodeling triggers formation of outer membrane

vesicles in salmonella. *MBio* **7**, (2016).

283. Zhao, J. *et al.* The lipid A 1-phosphatase, LpxE, functionally connects multiple layers of bacterial envelope biogenesis. *MBio* **10**, 1–14 (2019).

284. Nelson, K. E. *et al.* Complete genome sequence of the oral pathogenic bacterium Porphyromonas gingivalis strain W83. *J. Bacteriol.* **185**, 5591–5601 (2003).

285. Rangarajan, M., Smith, S. J. M., U, S. & Curtis, M. A. Biochemical characterization of the arginine-specific proteases of Porphyromonas gingivalis W50 suggests a common precursor. *Biochem. J.* **323**, 701–709 (1997).

286. Aduse-Opoku, J. *et al.* Generation of Lys-gingipain protease activity in Porphyromonas gingivalis W50 is independent of Arg-gingipain protease activities. *Microbiology* **146**, 1933–1940 (2000).

287. Rangarajan, M., Aduse-Opoku, J., Hashim, A., Paramonov, N. & Curtis, M. A. Characterization of the α- and ß-mannosidases of Porphyromonas gingivalis. *J. Bacteriol.* **195**, 5297–5307 (2013).

288. Fletcher, H. M. *et al.* Virulence of a Porphyromonas gingivalis W83 mutant defective in the prtH gene. *Infect. Immun.* **63**, 1521–1528 (1995).

289. Yi, E. C. & Hackett, M. Rapid isolation method for lipopolysaccharide and lipid A from Gram-negative bacteria. *Analyst* **125**, 651–656 (2000).

290. Zenobia, C. *et al.* Porphyromonas gingivalis lipid a phosphatase activity is critical for colonization and increasing the commensal load in the rabbit ligature model. *Infect. Immun.* **82**, 650–659 (2014).

291. Veith, P. D., Luong, C., Tan, K. H., Dashper, S. G. & Reynolds, E. C. Outer

Membrane Vesicle Proteome of Porphyromonas gingivalis Is Differentially Modulated Relative to the Outer Membrane in Response to Heme Availability. *J. Proteome Res.* **17**, 2377–2389 (2018).

292. Dam, P., Olman, V., Harris, K., Su, Z. & Xu, Y. Operon prediction using both genome-specific and general genomic information. *Nucleic Acids Res.* **35**, 288–298 (2007).

293. Mao, F., Dam, P., Chou, J., Olman, V. & Xu, Y. DOOR: A database for prokaryotic operons. *Nucleic Acids Res.* **37**, 459–463 (2009).

294. Pertea, M., Ayanbule, K., Smedinghoff, M. & Salzberg, S. L. OperonDB: A comprehensive database of predicted operons in microbial genomes. *Nucleic Acids Res.* **37**, 479–482 (2009).

295. Taboada, B., Ciria, R., Martinez-Guerrero, C. E. & Merino, E. ProOpDB: Prokaryotic operon database. *Nucleic Acids Res.* **40**, 627–631 (2012).

296. Naito, M., Tominaga, T., Shoji, M. & Nakayama, K. PGN_0297 is an essential component of the type IX secretion system (T9SS) in Porphyromonas gingivalis: Tn-seq analysis for exhaustive identification of T9SS-related genes. *Microbiol. Immunol.* **63**, 11–20 (2019).

297. Okamoto, K. *et al.* Involvement of a lysine-specific cysteine proteinase in hemoglobin adsorption and heme accumulation by Porphyromonas gingivalis. *J. Biol. Chem.* **273**, 21225–21231 (1998).

298. Smalley, J. W., Birss, A. J., Szmigielski, B. & Potempa, J. Sequential action of R- and K-specific gingipains of Porphyromonas gingivalis in the generation of

the heam-containing pigment from oxyhaemoglobin. *Arch. Biochem. Biophys.* **465**, 44–49 (2007).

299. Rangarajan, M., Aduse-Opoku, J., Paramonov, N. A., Hashim, A. & Curtis, M. A. Hemin binding by Porphyromonas gingivalis strains is dependent on the presence of A-LPS. *Mol. Oral Microbiol.* **32**, 365–374 (2017).

300. Lewis, J. P., Dawson, J. A., Hannis, J. C., Muddiman, D. & Macrina, F. L. Hemoglobinase activity of the Lysine gingipain protease (Kgp) of Porphyromonas gingivalis W83. *J. Bacteriol.* **181**, 4905–4913 (1999).

301. Yongqing, T., Potempa, J., Pike, R. N. & Wijeyewickrema, L. C. The lysine-specific gingipain of Porphyromonas gingivalis : importance to pathogenicity and potential strategies for inhibition. *Adv. Exp. Med. Biol.* **712**, 15–29 (2011).

302. Li, N. & Collyer, C. A. Gingipains from Porphyromonas gingivalis — complex domain structures confer diverse functions . *Eur. J. Microbiol. Immunol.* **1**, 41–58 (2011).

303. Imai, M., Murakami, Y., Nagano, K., Nakamura, H. & Yoshimura, F. Major outer membrane proteins from Porphyromonas gingivalis: Strain variation, distribution, and clinical significance in periradicular lesions. *Eur. J. Oral Sci.* **113**, 391–399 (2005).

304. Aduse-Opoku, J. *et al.* Identification and characterization of the capsular polysaccharide (K-antigen) locus of Porphyromonas gingivalis. *Infect. Immun.* **74**, 449–460 (2006).

305. Aduse-Opoku, J., Muir, J., Slaney, J. M., Rangarajan, M. & Curtis, M. A.

Characterization, genetic analysis, and expression of a protease antigen (PrpRI) of Porphyromonas gingivalis W50. *Infect. Immun.* **63**, 4744–4754 (1995).

306. Curtis, M. A. *et al.* Characterization of an adherence and antigenic determinant of the ArgI protease of Porphyromonas gingivalis which is present on multiple gene products. *Infect. Immun.* **64**, 2532–2539 (1996).

307. O'Brien-Simpson, N. M., Veith, P. D., Dashper, S. G. & Reynolds, E. C. Antigens of bacteria associated with periodontitis. *Periodontol. 2000* **35**, 101–134 (2004).

308. O-Brien-Simpson, N. M., Veith, P. D., Dashper, S. G. & Reynolds, E. C. Porphyromonas gingivalis gingipains: the molecular teeth of a microbial vampire. *Curr. Protein Pept. Sci.* **4**, 409–426 (2003).

309. Curtis, M. A. *et al.* Variable carbohydrate modifications to the catalytic chains of the RgpA and RgpB proteases of Porphyromonas gingivalis W50. *Infect. Immun.* **67**, 3816–3823 (1999).

310. Vestad, B. *et al.* Size and concentration analyses of extracellular vesicles by nanoparticle tracking analysis: a variation study. *J. Extracell. Vesicles* **6**, (2017).

311. Gerritzen, M. J. H., Martens, D. E., Wijffels, R. H. & Stork, M. High throughput nanoparticle tracking analysis for monitoring outer membrane vesicle production. *J. Extracell. Vesicles* **6**, (2017).

312. Steiner, H., Hultmark, D., Engström, Å., Bennich, H. & Boman, H. G. Sequence and specificity of two antibacterial proteins involved in insect immunity. *Nature* **292**, 246–248 (1981).

313. Lee, J. Y. *et al.* Antibacterial peptides from pig intestine: Isolation of a

mammalian cecropin. *Proc. Natl. Acad. Sci. U. S. A.* **86**, 9159–9162 (1989).

314. Hung, S. C., Wang, W., Chan, S. I. & Chen, H. M. Membrane lysis by the antibacterial peptides cecropins B1 and B3: A spin-label electron spin resonance study on phospholipid bilayers. *Biophys. J.* **77**, 3120–3133 (1999).

315. Kuroda, K., Okumura, K., Isogai, H. & Isogai, E. The human cathelicidin antimicrobial peptide LL-37 and mimics are potential anticancer drugs. *Front. Oncol.* **5**, 1–10 (2015).

316. Gao, L., Tan, Y., Zhang, W., Qi, Q. & Lu, X. Cytophaga hutchinsonii SprA and SprT Are Essential Components of the Type IX Secretion System Required for Ca2+ Acquisition, Cellulose Degradation, and Cell Motility. *Front. Microbiol.* **12**, 1–15 (2021).

317. Kharade, S. S. & McBride, M. J. Flavobacterium johnsoniae PorV Is required for secretion of a subset of proteins targeted to the type IX secretion system. *J. Bacteriol.* **197**, 147–158 (2015).

318. Rhodes, R. G., Nelson, S. S., Pochiraju, S. & McBride, M. J. Flavobacterium johnsoniae sprB is part of an operon spanning the additional gliding motility genes sprC, sprD, and sprF. *J. Bacteriol.* **193**, 599–610 (2011).

319. Horie, T., Inomata, M. & Into, T. OmpA-Like Proteins of Porphyromonas gingivalis Mediate Resistance to the Antimicrobial Peptide LL-37 . *J. Pathog.* **2018**, 1–7 (2018).

320. Tunyasuvunakool, K. *et al.* Highly accurate protein structure prediction for the human proteome. *Nature* **596**, 590–596 (2021).

321. Kelley, L. A., Mezulis, S., Yates, C. M., Wass, M. N. & Sternberg, M. J. Trabajo práctico Nº 13 . Varianzas en función de variable independiente categórica. *Nat. Protoc.* **10**, 845–858 (2016).

322. Ishikawa, K., Mihara, Y., Gondoh, K., Suzuki, E. I. & Asano, Y. X-ray structures of a novel acid phosphatase from Escherichia blattae and its complex with the transition-state analog molybdate. *EMBO J.* **19**, 2412–2423 (2000).

323. Fan, J., Jiang, D., Zhao, Y., Liu, J. & Zhang, X. C. Crystal structure of lipid phosphatase Escherichia coli phosphatidylglycerophosphate phosphatase B. *Proc. Natl. Acad. Sci. U. S. A.* **111**, 7636–7640 (2014).

324. Nguyen, K. A., Travis, J. & Potempa, J. Does the importance of the C-terminal residues in the maturation of RgpB from Porphyromonas gingivalis reveal a novel mechanism for protein export in a subgroup of gram-negative bacteria? *J. Bacteriol.* **189**, 833–843 (2007).

325. Thompson, J. D., Gibson, T. J., Plewniak, F., Jeanmougin, F. & Higgins, D. G. The CLUSTAL X windows interface: Flexible strategies for multiple sequence alignment aided by quality analysis tools. *Nucleic Acids Res.* **25**, 4876–4882 (1997).

326. Field, J. *et al.* Purification of a RAS-responsive adenylyl cyclase complex from Saccharomyces cerevisiae by use of an epitope addition method. *Mol. Cell. Biol.* **8**, 2159–2165 (1988).

327. Wang, X., Karbarz, M. J., McGrath, S. C., Cotter, R. J. & Raetz, C. R. H. MsbA transporter-dependent lipid A 1-dephosphorylation on the periplasmic surface of

the inner membrane: Topography of Francisella novicida LpxE expressed in Escherichia coli. *J. Biol. Chem.* **279**, 49470–49478 (2004).

328. Tran, A. X. *et al.* Periplasmic cleavage and modification of the 1-phosphate group of Helicobacter pylori lipid A. *J. Biol. Chem.* **279**, 55780–55791 (2004).

329. A.J. Lomant & Fairbanks, G. Chemical Probes of Extended Biological Structures : Synthesis and Properties of the Cleavable Protein Cross-linking Reagent [35S] Dithiobis (succinimidyl propionate). *J. Mol. Biol.* **104**, 243–261 (1976).

330. Raetz, C. R. H. Biochemistry of endotoxins. *Annu. Rev. Biochem.* **59**, 129–170 (1990).

331. Vinogradov, E., Perry, M. B. & Conlan, J. W. Structural analysis of Francisella tularensis lipopolysaccharide. *Eur. J. Biochem.* **269**, 6112–6118 (2002).

332. Bhat, U. R., Forsberg, L. S. & Carlson, R. W. Structure of lipid A component of Rhizobium leguminosarum bv. phaseoli lipopolysaccharide. Unique nonphosphorylated lipid a containing 2-amino-2- deoxygluconate, galacturonate, and glucosamine. *J. Biol. Chem.* **269**, 14402–14410 (1994).

333. Wang, X., McGrath, S. C., Cotter, R. J. & Raetz, C. R. H. Expression cloning and periplasmic orientation of the Francisella novicida lipid A 4′-phosphatase LpxF. *J. Biol. Chem.* **281**, 9321–9330 (2006).

334. Tran, A. X., Stead, C. M. & Trent, M. S. Remodeling of Helicobacter pylori lipopolysaccharide. *J. Endotoxin Res.* **11**, 161–166 (2005).

335. Chaturvedi, D. & Mahalakshmi, R. Transmembrane β-barrels: Evolution, folding

and energetics. *Biochim. Biophys. Acta - Biomembr.* **1859**, 2467–2482 (2017).

336. Almagro Armenteros, J. J. *et al.* SignalP 5.0 improves signal peptide predictions using deep neural networks. *Nat. Biotechnol.* **37**, 420–423 (2019).

337. Studier, F. W. & Moffatt, B. A. Use of bacteriophage T7 RNA polymerase to direct selective high-level expression of cloned genes. *J. Mol. Biol.* **189**, 113–130 (1986).

338. Van Den Berg, B., Black, P. N., Clemons, W. M. & Rapoport, T. A. Crystal structure of the long-chain fatty acid transporter FadL. *Science (80-.).* **304**, 1506–1509 (2004).

339. Portlock, T. J. *et al.* Structure, Dynamics and Cellular Insight Into Novel Substrates of the Legionella pneumophila Type II Secretion System. *Front. Mol. Biosci.* **7**, 1–17 (2020).

340. Mergulhão, F. J. M., Summers, D. K. & Monteiro, G. A. Recombinant protein secretion in Escherichia coli. *Biotechnol. Adv.* **23**, 177–202 (2005).

341. Mizgalska, D. *et al.* Intermolecular latency regulates the essential C-terminal signal peptidase and sortase of the Porphyromonas gingivalis type-IX secretion system. *Proc. Natl. Acad. Sci. U. S. A.* **118**, (2021).

342. Wagner, S. *et al.* Tuning Escherichia coli for membrane protein overexpression. *Proc. Natl. Acad. Sci. U. S. A.* **105**, 14371–14376 (2008).

343. Noinaj, N., Kuszak, A. J. & Buchanan, S. K. Heat Modifiability of Outer Membrane Proteins from Gram-Negative Bacteria. *Acta Crystallogr. Sect. F Struct. Biol. Commun.* **1329**, 51–56 (2015).

344. Walsh, B. W., Lenhart, J. S., Schroeder, J. W. & Simmons, L. A. Far western blotting as a rapid and efficient method for detecting interactions between DNA replication and DNA repair proteins. *Methods Mol. Biol.* **922**, 161–168 (2012).

345. Kim, D. E., Chivian, D. & Baker, D. Protein structure prediction and analysis using the Robetta server. *Nucleic Acids Res.* **32**, 526–531 (2004).

346. Kyte, J. & Doolittle, R. F. A simple method for displaying the hydropathic character of a protein. *J. Mol. Biol.* **157**, 105–132 (1982).

347. Magdeldin, S. *et al.* Murine colon proteome and characterization of the protein pathways. *BioData Min.* **5**, 11 (2012).

348. Miroux, B. & Walker, J. E. Over-production of Proteins inEscherichia coli: Mutant Hosts that Allow Synthesis of some Membrane Proteins and Globular Proteins at High Levels. *J. Mol. Biol.* **260**, 289–298 (1996).

349. Jimmy K. Eng, McCormack, A. L. & Yates, J. R. An approach to correlate tandem mass spectral data of peptides with amino acid sequences in a protein database. *J. Am. Soc. Mass Spectrom.* **5**, 976–989 (1994).

350. Jumper, J. *et al.* Highly accurate protein structure prediction with AlphaFold. *Nature* **596**, 583–589 (2021).

351. Mariani, V., Biasini, M., Barbato, A. & Schwede, T. IDDT: A local superposition-free score for comparing protein structures and models using distance difference tests. *Bioinformatics* **29**, 2722–2728 (2013).

352. Pautsch, A. & Schulz, G. E. High-resolution structure of the OmpA membrane domain. *J. Mol. Biol.* **298**, 273–282 (2000).

353. Pollock, N. L., Lee, S. C., Patel, J. H., Gulamhussein, A. A. & Rothnie, A. J. Structure and function of membrane proteins encapsulated in a polymer-bound lipid bilayer. *Biochim. Biophys. Acta - Biomembr.* **1860**, 809–817 (2018).

354. Lee, S. C. *et al.* A method for detergent-free isolation of membrane proteins in their local lipid environment. *Nat. Protoc.* **11**, 1149–1162 (2016).

355. Schulz, G. E. The structure of bacterial outer membrane proteins. *Biochim. Biophys. Acta - Biomembr.* **1565**, 308–317 (2002).

356. Kaur, H. *et al.* The antibiotic darobactin mimics a β-strand to inhibit outer membrane insertase. *Nature* **593**, 125–129 (2021).

357. Xie, K. & Dalbey, R. E. Inserting proteins into the bacterial cytoplasmic membrane using the Sec and YidC translocases. *Nat. Rev. Microbiol.* **6**, 234–244 (2008).

358. Yang, J. *et al.* Molecular basis for TPR domain-mediated regulation of protein phosphatase 5. *EMBO J.* **24**, 1–10 (2005).

359. Zafar, H. & Saier, M. H. Gut Bacteroides species in health and disease. *Gut Microbes* **13**, 1–20 (2021).

360. Larsen, J. M. The immune response to Prevotella bacteria in chronic inflammatory disease. *Immunology* **151**, 363–374 (2017).

361. Friedrich, V. *et al.* Outer membrane vesicles of Tannerella forsythia: Biogenesis, composition, and virulence. *Mol. Oral Microbiol.* **30**, 451–473 (2015).